V-dp/di Droop Control Technique with d^2p/di^2 to Improve Dynamic Performance for Multiple PV Modules in Islanded DC Microgrid

Wing Chun (Dennis) Chan

School of Engineering

Newcastle University

A thesis submitted for the degree of Doctor of Philosophy

January, 2022

Abstract

This thesis proposes the V-dp/di droop control algorithm of an islanded dc microgrid (MG) system with multiple photovoltaic (PV) arrays. A comprehensive literature review on three main coordinated control strategies is carried out, namely centralized, distributed and decentralized control. Decentralized control has some advantages over centralized and distributed control, including plug-and-play capability, easy to implement, and absence of communication agent. The conventional control method implemented in the simulation model is V-dp/dv droop control, which can be used to investigate the dynamic performance of the PV-based dc MG. The simulation results show that the accuracy issue of dp/dv leads to doubling settling time and ±5% power oscillations. Therefore, it is important for a PV generator to perform voltage regulation in a PV standalone mode, in order to continue stabilising the bus voltage of a dc MG. The stability analysis of the proposed V-dp/di control and conventional V-dp/dv method is undertaken based on a PV-based dc MG. The mathematical results show 50% improvements in voltage fluctuations and power ripple during steady state. Compared to conventional V-dp/dv control, the inner loop of the proposed dp/di controller can independently be stabilised without the implementation of outer voltage loop. A comparison between conventional and proposed control schemes is carried out to validate the feasibility and robustness of proposed V-dp/di method, and to present the working principle of the control variable dv/di. This is referred to as incremental-resistance (INR) maximum power point tracking (MPPT) algorithm. The characteristic of a searching MPPT algorithm leads to huge oscillation of the common dc bus voltage, which is the drawback of traditional MPPT schemes. Another contribution of this thesis is the introduction to second differential term of current approach d^2p/di^2. The 2nd derivative is used to minimise the fluctuations of dp/di during steady state. The application of second derivative of power to current yields an improved steady-state performance in a PV-based dc MG. The simulation results present a 30% further improvement in PV power ripple with the help of second differential term.

Acknowledgements

I would like to express my sincere gratitude to my main supervisor Dr Matthew Armstrong for his continuous support and understanding throughout the PhD research. I am also grateful to my second supervisor Dr David Atkinson for sharing his expertise and offering a set of lab equipment to carry out the experiments. I am very grateful to my co-supervisor Prof Volker Pickert for his guidance and support. I am thankful to Dr Petros Missailidis and Dr Haris Patsios for their useful advice.

I am grateful for the full scholarship and funding of the research work provided by the School of Engineering at Newcastle University. I would like to take the opportunity to thank my former personal tutor, Prof Satnam Dlay, for promoting me as the recipient of the full PhD scholarship and for his encouragement and willingness to help to apply for the PhD degree. Many thanks to the academic and administrative staff, in particular Gill Webber, for the administrative assistance throughout my study.

I would like to thank Darren Mackie and Jeffery Warren from the electronics workshop for their advice to develop the test rig and for the patience with me to tackle any challenges I might have during practical experiments. I am grateful to my fellow PhD students working in the PEDM Lab for having a lot of fruitful discussion. I would like to acknowledge James Richardson and Gordon Marshall from the UG Lab for their contributions to the experimental test rig. Many thanks to the technicians from the mechanical workshop for their support with the preparation of the junction box.

I am deeply grateful to my parents for their unconditional love and help with achieving all my goals throughout my life. This thesis would not exist without my parents who support me during the research and writing process. I would like to thank my girlfriend Crystal Wong for being supportive throughout my study and encouraging me during difficult times. I am also thankful to my family and friends for their motivation and support.

Abbreviations

AC	Alternating Current
BESS	Battery Energy Storage System
CC	Central Controller
DBS	DC Bus Signalling
DC	Direct Current
DCLs	Digital Communication Links
DG	Distributed Generation
DSP	Digital Signal Processor
EMI	Electromagnetic Interference
ESR	Equivalent Series Resistance
IGBTs	Insulated-Gate Bipolar Transistors
INC	Incremental Conductance
INR	Incremental Resistance
LBC	Low-bandwidth Communication
LV	Low Voltage
MG	Microgrid
MOSFETs	Metal-Oxide-Semiconductor-Field-Effect-Transistors
MPP	Maximum Power Point
MPPT	Maximum Power Point Tracking
P&O	Perturb and Observe
PI	Proportional-Integral
PID	Proportional-Integral-Derivative
PLC	Power Line Communication
PnP	Plug-and-Play

PV	Photovoltaic
PWM	Pulse-Width Modulation
RES	Renewable Energy Sources
SoC	State of Charge
SSE	Steady-State Error
WiMAX	Worldwide Interoperability for Microwave Access
ZOH	Zero Order Hold

List of Symbols

C	DC-link capacitor
C_{pv}	PV capacitor
dp/di	Derivative of power with respect to current
dv/di	Derivative of voltage to current
d^2p/di^2	Second differential of power with respect to current
dp/dv	Derivative of power with respect to voltage
di/dv	Derivative of current to voltage
$\frac{d\Delta p^{ref}}{d\Delta v}$	Desired first differential of power to voltage in ac variation
D	Duty cycle
D_j	Parallel diode
f_{sw}	Switching frequency
I_c	Capacitor current
I_L	Inductor current
Δi_L	Inductor current variation
ΔI_L	Inductor ripple current
I_{mpp}	PV current at maximum power point
I_{out}^*	Output current reference
I_{out_i}	Output current of converter $\#i$
I_{ph}	PV cell photocurrent
I_{pv}	PV output current
I_{rs}	Reverse saturation current
I_{sc}	Short-circuit current
K_c	Critical gain

K_d	Derivative gain
K_i	Integral gain
K_p	Proportional gain
K_{pv}	Tangent line to linear I-V curve
m_I, m_P	Droop coefficients based on current and power
m_i, m_n	Droop coefficients for the i^{th} and n^{th} PV array
N_s, N_p	Number of PV cells connected in series and in parallel
P_c	Period of oscillation
P_{out_i}	Output power of converter $\#i$
R_j	Parallel diode resistance
R_o	Load resistance
R_s	Series resistance
R_{sh}	Shunt resistance
V_c	Capacitor voltage
ΔV_c	Capacitor ripple voltage
V_{dc}	DC bus voltage
V_{dc}^*	Nominal dc bus voltage
$V_{dc\_i}^*$	Output reference voltage of converter $\#i$
Δv_{dc}	DC-link voltage variation
V_I	Input dc voltage
V_L	Inductor voltage
V_{mpp}	PV voltage at maximum power point
V_{pv}	PV output voltage
V_{oc}	Open-circuit voltage

Table of Contents

List of Figures

List of Tables

Chapter 1. Introduction

1.1 Background

Photovoltaic (PV) system is becoming increasingly important in the distributed generation (DG) networks to tackle key challenges such as global warming and energy crisis. Solar energy is currently one of the dominant sources of renewable energy, providing clean energy to local consumers and feeding excess power into the distribution network. There are many advantages of solar energy, including low maintenance costs, reduction of environmental impacts on energy transportation and noise pollution. According to the Renewables 2022 Global Status Report, it was found that around 12.6% of total global energy consumption in 2021 is supplied by the modern renewable resources, in which hydropower, wind, solar and biomass power are some typical examples [1]. As shown in Figure 1.1, the global PV capacity is increased by almost 24% to 942 gigawatts (GW) in 2021, compared to the cumulative installed capacity in 2020. Meanwhile, solar PV surpassed 30% of total global electricity production from renewable energy sources (RES) in 2021 with a 3% increase compared with the capacity in 2020. The total PV capacity is expected to continue growing after 2021 due largely to cost reductions and technology improvements, reported by Renewable Energy Policy Network for the 21st century (REN21) [1].

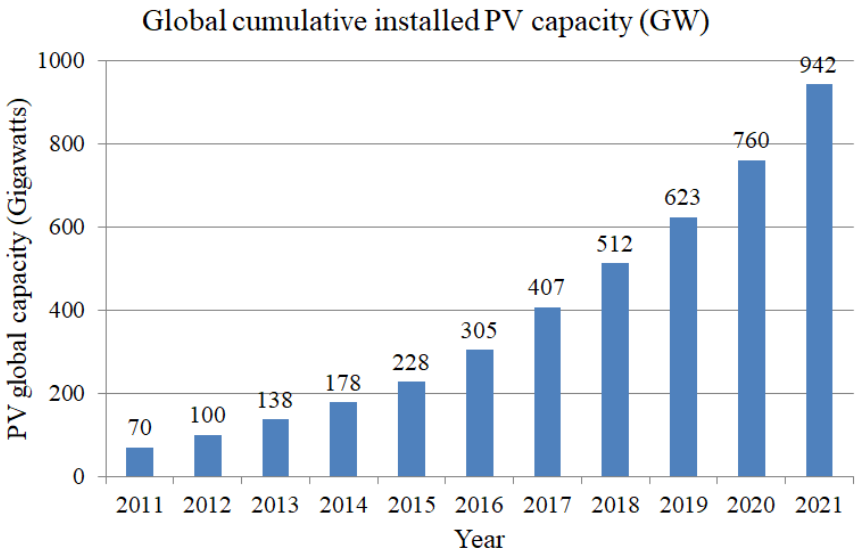

Figure 1.1 Global cumulative PV capacity, 2011-2021.

More importantly, the investments in mini-grid start-ups have more than doubled to USD 113 million in 2019. An estimated USD 468 million in corporate-level investment flows in 2019, down 8.6% from USD 512 million raised in 2018 [2]. The global cumulative capacity of solar

mini-grids is increased to 365 MW, which accounts for 55% of mini-grids [1]. Therefore, the utilisation of embedded generation network is becoming popular worldwide. The term 'embedded' refers to those renewable resources which are directly connected to distribution network rather than traditional high-voltage transmission network.

RES play a vital role in facilitating the development of DG networks. Whilst popular, these sources of renewable energy are intermittent; solar output is low in overcast conditions and negligible during the night; wind brings 24-hour generation to the system, but output is highly variable and unpredictable based on atmospheric conditions [3]. In residential or small-scale commercial systems, multiple sources of renewables, often PV, are integrated alongside various local energy storage systems and consumer loads. The battery energy storage system (BESS) consists of a battery and a bi-directional dc/dc converter. It is capable of supporting and providing backup energy to the distribution network during periods of low, or negligible power generation from renewables, and vice versa. Given the output of PV array and batteries is typically direct current (dc), the concept of employing a common dc bus system approach has been established. It is now regarded as a dc microgrid (MG) [4]. The research conducted by Karlsson and Svensson (2003) demonstrated a typical configuration of a dc MG system with five power converters associated with energy sources or loads [5]. In [6], Kumar et al. (2017) analysed that dc MG is a category of low voltage (LV) power network and thus it is interconnected to the utility grid for the purpose of improved stability of the distribution network. DC MGs have lots of advantages over the alternating current (AC) MGs such as natural interface with dc renewable energy resources and local loads, higher conversion efficiency, compatible with increasing penetration of RES and higher reliability in terms of grid disturbances [6-9]. Both RES and BESS can be integrated in a coordinated control system based on digital signal processor (DSP).

In the event of grid faults, mainly short circuits, the grid-connected converter in a dc MG has to be disconnected from the utility grid as quickly as possible in such a way that it can avoid any risk of further damage [10]. For instance, the renewables might overload the grid infrastructure if the single phase grid-connected inverter is a unique component for voltage restoration in a dc MG. It is mandatory to ensure that a dc MG can operate autonomously. This is commonly referred to as islanded mode. BESS plays a critical role in accommodating the stochastic characteristic and growing penetration of PV arrays [11]. To guarantee a stable dc-link voltage and sufficient load power in a dc MG, the BESS usually offers a two-way power flow to address the problems, particularly in rural areas. State of Charge (SoC) of a

battery is a key concern in literature, which results in shorter lifespan if the cell imbalance issues occur. A number of studies have been published to realise the SoC balancing and precise power distribution [12], [13]. However there is always a possibility for the battery to be fully charged. In other words, the battery could indeed attain certain amount of energy where the BESS is no longer available for RES to charge until the SoC is below the highest level of charge. The classical maximum power point tracking (MPPT) scheme is used to harvest the maximum available power from PV systems or dc renewables. It turns out the disconnection of solar panels from the dc MG is sometimes mandatory for stabilising the MG system. As a consequence, curtailing the power of the PV system at a limited level has been found as an effective approach to overcome the key challenges [10]. Therefore, researchers are encouraged to consider the participation of PV systems in dc bus voltage regulation and power sharing.

1.2 DC MG

In recent years, there are various topologies of dc MG systems published in literature that can typically be divided into three major categories, namely single-bus topology, multibus topology and reconfigurable topology [14]. A general overview of these main topologies can be observed in Figure 1.2. To focus on the scope of this thesis, single-bus topology is introduced and discussed in detail in Chapter 3.

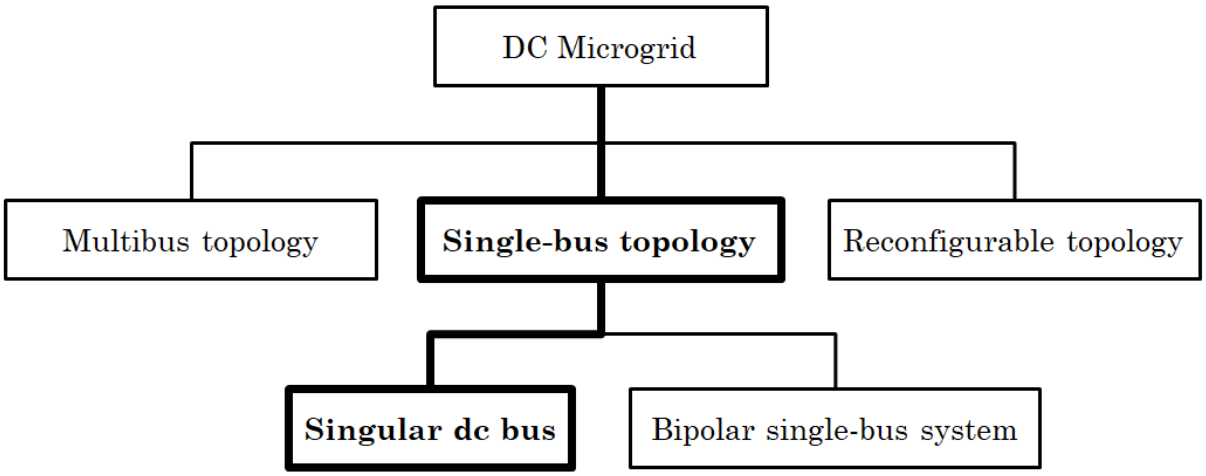

Figure 1.2 Typical topologies of dc MG systems.

Single-bus topology is one of the most widely used topologies in a dc MG. As can be seen from Figure 1.3, it is interconnected with PV systems, BESS, local loads and grid-connected converter based on singular bus structure. A dc bus reference voltage, range of 350 V to 450

V, is the unique dc power link connected to all energy sources and loads simultaneously. In [15], a reference dc bus voltage of 400 V is defined as a common value in a dc MG system, which is usually higher than the peak voltage of grid-connected inverter. The concept of utilising a high dc-link voltage is supported by the study undertaken by Hong et al. [16]. It is noted the power flow direction of BESS and distribution grid is bipolar, which in turn means the surplus energy can be taken from or fed into these sources, respectively. In [17], the fundamental control functions of a grid-connected converter are given for reference. This topology benefits from its simplicity and extendibility, but reliability is lower compared with modern architecture, i.e. reconfigurable topology [14]. In [18], the authors have established a low-voltage bipolar dc bus structure to acquire superior performance of dc distribution network. The dc-dc converter can operate in +170, -170, or 340 V. The bipolar topology is used to avoid single point of failure, due to various selections of dc bus voltage. This is beyond the scope of this thesis and hence will not be further discussed.

The alternative to the above system layout is a multibus dc MG. This is usually achieved by means of expansion of the dc MGs by adding power lines, and thus each dc MG has its own local dc bus to operate [19]. Another typical example of multiple dc links in MG system can be observed in [20]. Besides, this technique can be used for power distribution in the application of aircraft electric power systems, rural areas, telecommunications systems and data centres etc. A detailed hierarchical control algorithm along with multiple dc MGs is presented in [21]. Shafiee et al. (2014) has demonstrated a distributed control method to manage the operations of numerous dc MG clusters. However, the main disadvantage of employing multibus topology is high complexity. In [14], the authors analysed high reliability and compatibility are the merits of using coordinated dc clusters.

Moreover, in case of MG fault detection, the researchers in [14] found that reconfigurable topology is the best available architecture among three main topologies. Since each of the subsystems between nodes in a common dc ring-bus are associated with two intelligent electronic switches, it turns out part of the dc bus can be isolated and therefore fault clearance in the power line is allowed to be carried out during operation [22]. There are a number of configurations proposed in literature, including zonal architecture, multi-terminal dc system and dc ring bus configuration [23]. While these approaches are robust and reliable, it may be difficult to design a dc MG in a reconfigurable topology, and to implement corresponding control strategy.

In terms of dynamic modelling of a dc MG, a dynamic analysis of dc bus voltage control in a microgrid is presented by Li et al. (2021) in [24]. This paper aims to demonstrate the dynamic modelling of a typical dc MG in a reduced-order with commonly used droop control algorithms. This provides a platform to accurately describe the dynamic characteristic of the dc voltage control, particularly the impacts of multiple parallel-connected converters. In [25], a state-space dynamic modelling of a dc MG with a model predictive controller is carried out to evaluate the transient and steady-state performance of the dc MG system. This can be accomplished by calculating the online parameters and tuning the controller gains.

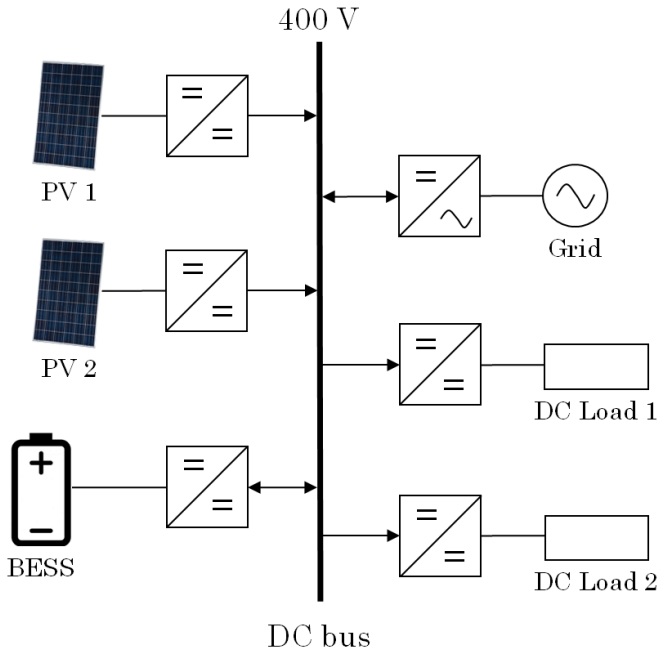

Figure 1.3 Single bus PV-based dc MG with BESS and grid-connected inverter.

Generally speaking, a PV-based dc MG system consists of PV arrays, dc/dc converters, BESS and dc loads. This implies that the system briefly contains power supplies, energy storage component and resistive loads. As shown in Table 1.1, the parameters for simulation study and stability analysis are presented. Two PV sources are implemented in the simulation model to validate the proposed control method, provided that the droop coefficient is used for primary power sharing of PV generators. In the meantime, Table 1.1 details the computed values for each passive element of converters to obtain the desired dynamic response.

The simulation model provides a platform to replicate the conventional V-dp/dv droop control method, and to evaluate the overall performance of the proposed V-dp/di control algorithm. The simulation study introduces three main modes of operation, in which it includes grid-connected mode, battery islanded mode and PV standalone mode. To fully understand the

behaviour of the proposed V-dp/di method in grid-connected mode, a single-phase grid-connected inverter is built to validate its ability to extract the maximum available power from multiple PV arrays. However, in grid-connected mode, the proposed control strategy simply becomes a classical constant voltage MPPT method. It is beyond the scope of the PhD study. The focus on the grid-side operation is thus neglected.

Table 1.1 Specifications of the PV-based dc MG system

Parameter	Value
$PV1$	$2\ kW$
$PV2$	$1.37\ kW$
$Battery\ capacity$	$250\ Ah$
$DC\ Load\ 1$	$9.216\ \Omega$
$DC\ Load\ 2$	$2.304\ \Omega$
C_{PV_input}	$470\ \mu F$
L_{PV1}, L_{PV2}	$1.875\ mH$
C_{PV1}, C_{PV2}	$80\ \mu F$
C_{dc_link}	$2\ mF$
L_{load}, L_{bat}	$0.253\ mH$
C_{load}, C_{bat}	$110\ \mu F$
V_{dc}^{ref}	$400\ V$
$V_{pv_i}(MPP)$	$111.7\ V$
V_{bat}, V_{load}	$48\ V$
m_{PV1}	5
m_{PV2}	5.03
f_{sw}	$20\ kHz$

1.3 Control Principles of a DC MG

The recent developments in advanced control schemes have been crucial for the robust and stable operation of an islanded dc MG system. As shown in Figure 1.4, the control framework can be divided into two levels. In general, local control level provides the following features: 1) primary control functions, e.g. traditional dual loop and droop control; 2) source-dependent functions such as MPPT algorithms for solar panels, battery charging and discharging control,

and estimation of SoC for BESS; 3) decentralized control functions, in particular, adaptive adjustment of droop coefficients, power line communication (PLC) and dc bus signalling (DBS) [8], [26]. PLC aims to transmit the data signals via the distribution network. DC bus signalling refers to the data being transferred on the dc bus, which indicates the direction of power flow. In contrast, coordinated control level is commonly used by modern control strategies to achieve high reliability and stability in a dc MG. For instance, optimal energy storage management, accurate power balancing, proportional load sharing, consensus algorithm and SoC balancing etc. [27], [28]. The term 'coordinated' means the dc MG requires a communication network to obtain local real-time neighbours' data and send them to DSP for data analysis. The control structure is based on digital communication links (DCLs), which usually refers to a centralized or distributed control.

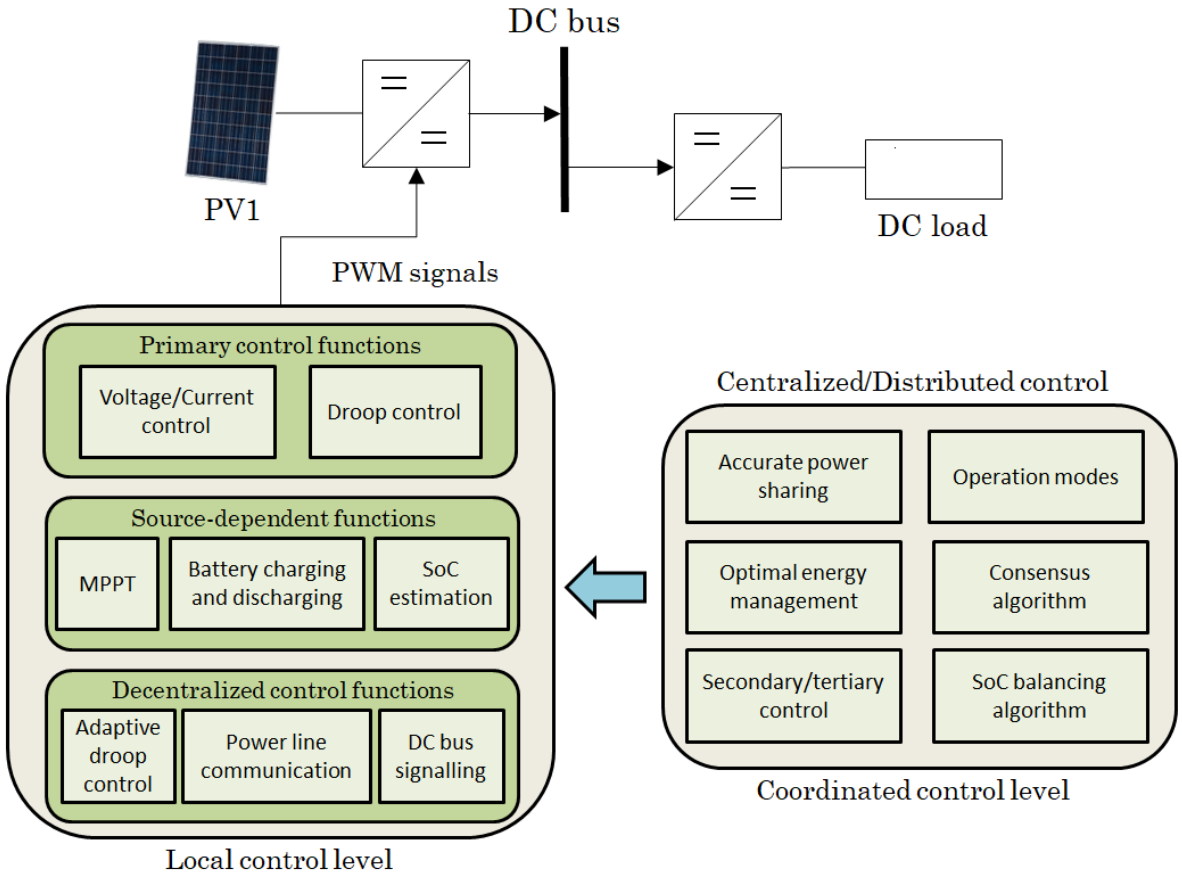

Figure 1.4 Hierarchical control architecture of a dc MG system.

1.3.1 Local Control Functions

In theory, the local control level is made up of primary control functions, source-dependent functions and decentralized control functions. Traditional cascaded loop, as a local control, is generally used by the primary control functions to regulate the dc-link voltage and current of a

power converter, respectively [13]. To realise proportional power balancing, droop control is one of the most prominent solutions for controlling dc MG, particularly in an islanded mode. A thorough literature review on the droop control can be found in Chapter 4. Source-dependent function literally means how the control algorithm can achieve specific objectives, MPPT algorithm, battery charging/discharging and estimation of SoC, are relating to the energy supply installed in a dc MG. On top of the above two fundamental control functions, decentralized control function can be exploited to control the operations of every single unit in a dc MG. In simple words, only local data is received by the controller and thus each of these components in the MG would have a unique controller to operate autonomously, and effectively. Generally speaking, proportional-integral (PI) compensator is the most commonly used controller in a dc MG to eliminate the steady-state error (SSE) and achieve a satisfactory step response. Moreover, researchers may design a proportional-integral-derivative (PID) controller to shorten the rise time and minimise the overshoot/undershoot observed in transient response.

1.3.2 Coordinated Control Functions

Digital communication channels are widely used by secondary and tertiary control functions to realise complex objectives, i.e. accurate power sharing among distributed energy sources, SoC balancing control for BESS and load shedding under extreme conditions [8]. It can be either in centralized or distributed control. One of the main drawbacks of centralized strategy is that it usually suffers from low flexibility since all the local information are required to transfer to the central controller for generating corresponded PWM signals to power converters. Therefore the technique is inapplicable for an extendable dc MG system [29].

In terms of distributed control, DCLs exist in a dc MG where it can be regarded as an independent communication system for exchanging neighbours' data between different distributed controllers. The number of distributed controller mainly depends on the number of power sources, usually RES and BESS. In [12], [13], [30], it is concluded that optimal energy management and SoC balance of BESS are the main goals of implementing coordinated control. To realise accurate power sharing among energy sources in a dc MG, it is essential to apply a coordinated control to the system [4], [13], [31]. Decentralized control is unable to accomplish precise power sharing due to the absence of local neighbours' information. Wang et al. (2016) proposed a distributed control scheme to restore dc bus voltage and minimise the operation costs based on consensus algorithm [28]. Each energy source has its own distributed

controller with exchanged neighbours' information to make the best available decision. To achieve generation costs minimization, the utilization of renewables is maximised under normal circumstances. In [32], the operation cost minimisation was undertaken by incremental cost consensus with the help of distributed controllers among energy sources. However, the cost-effective operation is beyond the scope of this thesis. Furthermore, the researchers in [30] reported that their control strategy relies on the change in operation modes of the dc MG. Fuzzy logic is used to manipulate the adaptive droop resistances for RES and BESS, respectively. However, there is a possibility for the control system to experience a significant dc bus voltage deviation in case of abrupt irradiance change. Such a voltage deviation could actually lead to the dc bus voltage fluctuating around threshold value of the operation mode. In [33], a distributed control strategy based on small-signal model of a dc MG is proposed to enhance the dynamic response performance of the overall system. This is performed by exchanging neighbours' information to calculate the reference power value for each distributed generation, in order to perform accurate power sharing among energy sources.

1.4 Scope and Objectives of the Research

- This work focuses on the decentralized coordination control scheme of a PV-based dc MG system.
- A stability analysis of the control algorithms is conducted and discussed in detail.
- To demonstrate the effectiveness and benefits of implementing the proposed V-dp/di method, transient and steady-state performance of the closed-loop control are examined.

The main aim of this thesis is to investigate the limitations of the conventional coordinated control strategies under abrupt conditions, propose a V-dp/di droop control method to endow fast dynamic response and improved steady-state performance to the PV generators in an islanded dc MG, and to provide new insights into the application of second differential control variable.

The specific objectives of the research are organised as follows:

- To understand the dynamic characteristics of the existing control algorithms and identify the limitations of these techniques.

- To validate and evaluate the proposed droop control scheme under fast changing irradiance and step load change.
- To discuss the impacts of utilising second order derivative of PV power with respect to current under steady-state conditions.

1.5 Thesis Contributions

The following summarise the original contributions of this thesis:

In terms of MPPT algorithm, a comparison of dynamic performances of two droop control methods with incremental conductance (INC) and incremental resistance (INR) algorithms is presented in this thesis to outline the limitations of the conventional V-dp/dv control strategy. The error between calculated value and actual dp/dv is statistically significant, mainly due to steep slope of the P-V characteristics and intrinsic error arising from the non-linear PV relationship. However, this phenomenon does not occur in the proposed algorithm, which refers to slope of power versus current (dp/di).

To address the issue mentioned above, an improved droop control scheme based on incremental resistance (INR) algorithm is introduced to maximise the accuracy of the dv/di which affects the inner control variable dp/di. Thus, the first differential term can be used to represent the PV power level in order to attain solar power curtailment, particularly in battery islanded mode or PV standalone mode.

A novel decentralized droop control scheme with second differential of power to current is proposed to further minimise the PV power fluctuation in a steady state. The second order derivative of power to current (d^2p/di^2) refers to the instantaneous rate of change of the internal control variable (dp/di), where the control term is employed to improve the PV power ripple. The novel control method benefits from better steady-state performance and easy to implement.

1.6 Publications

This thesis is based on the following original publication:

1. W. C. Chan, M. Armstrong, D. Atkinson and V. Pickert, "V-dP/dI droop control technique with d2P/dI2 to improve steady state performance for multiple PV modules in a dc microgrid," 2019 21st European Conference on Power Electronics and Applications (EPE '19 ECCE Europe), Genova, Italy, 2019, pp. P.1-P.10.

1.7 Thesis Outline

The contents of the thesis are described as follows:

Chapter 1 begins by introducing the background of solar energy, gives a brief overview of the recent development of dc microgrids, presents the key functions of a converter controller in a typical dc MG system, and states the aims and objectives of this study. Chapter 1 highlights the main contributions of the thesis and original publication.

Chapter 2 presents a thorough literature review of three major coordinated control strategies in the area of dc MG systems, including centralized, distributed and decentralized control. Chapter 2 analyses the advantages and disadvantages of these approaches, as well as key challenges and limitations. The compromise between decentralized and distributed control schemes is provided in this chapter.

Chapter 3 performs a mathematical modelling of a PV array and demonstrates the design of the dc MG system in islanded mode.

Chapter 4 focuses on the existing decentralized coordination control technique of a PV-based dc MG in literature, which in turn illustrates the research motivation of the thesis. Chapter 4 elaborates the proposed V-dp/di control method and describes how it can be implemented in an islanded dc MG system.

Chapter 5 develops the closed-loop design analysis of the V-dp/di droop control method, focusing on the small-signal model of the control system. Chapter 5 performs a stability analysis to illustrate the characteristics of the novel control variable dp/di. The stability analysis of the conventional V-dp/dv droop control method with a boost converter is undertaken to make a comparison between two control strategies.

Simulation results of V-dp/di droop control method are presented in **Chapter 6**, which is used to verify the feasibility of the proposed control in a dc MG system. The controller parameters on the dynamics of the dc MG such as settling time, voltage overshoot, and power oscillations are assessed and compared with the conventional V-dp/dv control algorithm.

In **Chapter 7,** a summary of the thesis and suggestions for future work are presented.

Chapter 2. Review of Existing Coordinated Control Strategies for DC MG Systems

2.1 Introduction

Researchers have shown continued interest in the field of coordinated control schemes. Previous studies have established three main coordinated control methods for dc MGs to realise local and coordinated control functions, i.e. centralized, distributed and decentralized control. To identify the category of a coordination control strategy, one of the most important factors is the configuration of a communication network used in a dc MG system. Digital communication link is a communication channel that establishes a connection between two independent energy subsystems in a dc MG for the purpose of exchanging useful digital information such as real-time power level of RES and SoC of batteries. Nevertheless, the analog voltage or current output measured by the transducers should be converted to a digital form in order for DSPs to directly process the digital signals. It is noted only decentralized coordination control does not require any DCL to perform coordination control of a dc MG. In contrast, a digital communication network is mandatory for centralized and distributed control schemes to accomplish secondary and tertiary control functions.

Chapter 2 presents a comparison of the existing coordination control methods to outline the key advantages and disadvantages of those techniques. Furthermore, a thorough literature review on three major control strategies is conducted. This should help understand the state-of-the-art control approaches and evolving trends of islanded dc MG. PI controller is the most commonly used controller in control systems due to its ability to eliminate SSE. Section 2.2 provides some background information about PI/PID controller, in addition, some common challenges encountered in conducting this research.

2.2 PI and PID Controllers

A controller usually plays a crucial role in achieving the desired response of a power electronic system. The most widely used controller in industry and academia is a classical PI controller due to effectiveness, simplicity and adaptability. PI controller is a feedback control system that calculates the difference between the desired set-point and output signal, and generates a duty ratio to reduce the error until the desired reference value is obtained. The proportional gain (K_p) produces an output that is directly proportional to the present error, while the integral gain (K_i) accounts for the past errors.

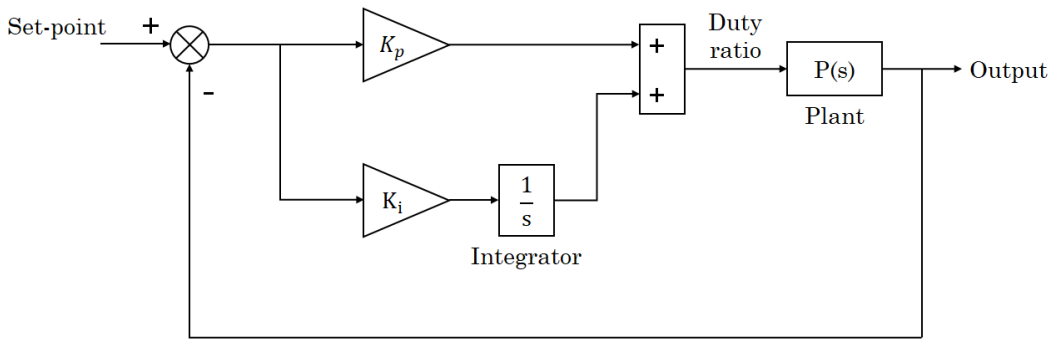

Figure 2.1 Control structure of a PI controller.

It is shown in Figure 2.1 that a block diagram of a PI controller in s-domain is presented. Integral windup is a common phenomenon in designing a PI controller, since the actuator is limited by the physical range for plant. The actuator could have reached its saturated value, but the integral term will continue to rise until further changes. Once the error signal suddenly becomes negative, in which the proportional part is negative, it takes certain amount of time for the integral term to attenuate its impact on the controller. To overcome the windup problem, a simple saturation block is employed in the control loop to limit the overall output of the PI controller.

Table 2.1 Impacts of increasing PID parameters individually

Control Element	Rise Time	Overshoot	Settling Time	Steady-State Error
K_p	Decrease	Increase	Small Change	Decrease
K_i	Decrease	Increase	Increase	Eliminate
K_d	Minor Change	Decrease	Decrease	Minor Change

Last but not least, the derivative gain is a prediction of future errors that aims to improve the overshoot and reduce the settling time. Despite the fact that a PID controller is the full version of the feedback control system, the derivative part often leads to huge oscillations in the process variable. As the measured output signal of voltage/current sensor is always associated with measurement noise, differentiating a noisy signal may create a lot of confusion to the controller. A low pass filter is used to reduce the noise in the derivative term. Table 2.1 summarises the impacts of increasing the above control gains individually. The table above can be used to better understand the effects of increasing each control term. This allows control engineers to apply manual tuning method to optimise the controller, in order to meet

the system requirements. The most commonly recognized tuning method to compute initial PID terms is Ziegler-Nichols tuning algorithm. The proportional gain is expected to moderately increase until it reaches the point of critical stability, in which a continuous diverging oscillation can be observed at the output of the plant. It is regarded as critical gain (K_c). It is noted the period of oscillation (P_c) can be measured. As shown in Table 2.2, the formulas for estimating the P/PI/PID gains are provided.

Table 2.2 Calculations of P/PI/PID terms with Ziegler Nichols method

Controller	K_p	K_i	K_d
P	$0.5K_c$	-	-
PI	$0.45K_c$	$\frac{0.54K_c}{P_c}$	-
PID	$0.6K_c$	$\frac{1.2K_c}{P_c}$	$0.075K_cP_c$
PID1 (some overshoot)	$0.33K_c$	$\frac{P_c}{2}$	$\frac{P_c}{3}$
PID2 (minimal overshoot)	$0.2K_c$	$\frac{P_c}{2}$	$\frac{P_c}{3}$

2.3 Centralized Control

Centralized control is the most commonly used technique implemented in traditional grid operation that makes the best use of a central controller (CC). There are two important features resulting from the control framework, including data analysis for the energy sources and loads as well as generation of PWM signals for each power converter in a dc MG system. The architecture of a centralized control algorithm is presented in Figure 2.2. It can be observed that instantaneous power levels of all sources and loads are fed into the CC so as to compute the power imbalance across the dc bus of the MG system. This is to ensure sufficient power to be transferred to the consumer loads and battery. The desired voltage and power references can eventually be provided by the central controller, following the process of power balancing. A classical single loop or multi-loop control is thus applied to various converters, depending on the specifications of the components. The centralized control

scheme provides the following benefits: i) easy to understand; ii) cost minimization, i.e. only one DSP is employed to control the whole system; iii) precise power balancing.

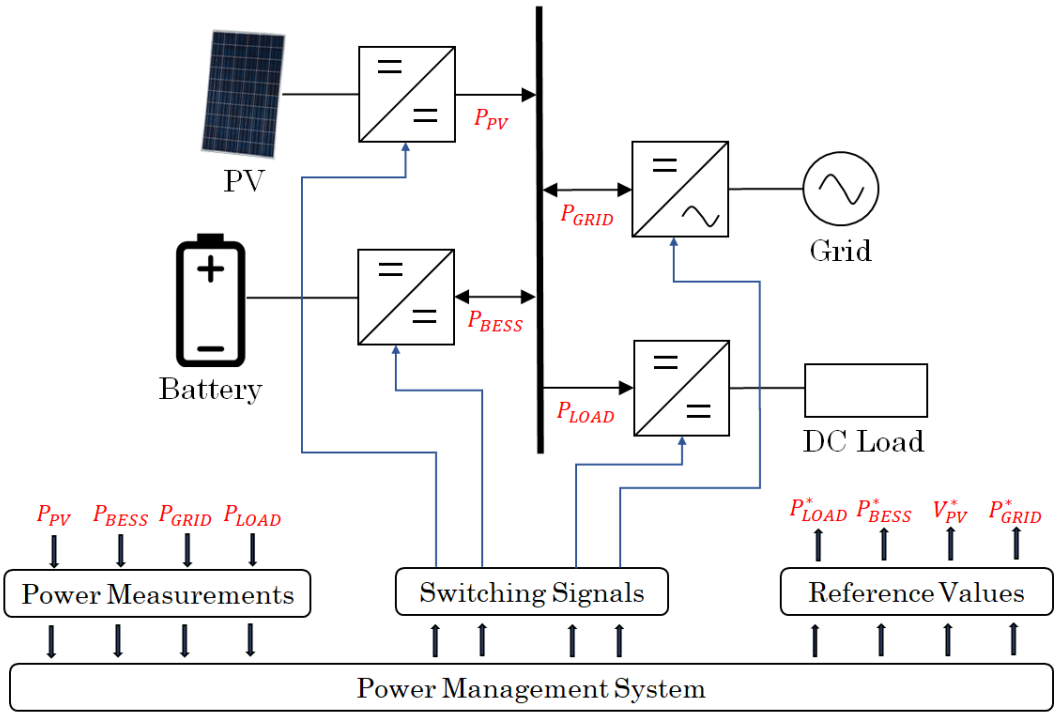

Figure 2.2 Control diagram of a centralized control in a dc MG [34].

In [8] and [28], these studies reported that the dc MG system could cease the operation in the event that a single point of failure occurs, which turns out low reliability compared with the other two coordinated control strategies. Besides, the CC may require a high-performance DSP to shorten the processing time. The minimum switching frequency of a typical power converter would usually be 10 to 20 kHz. Given CC is a unique processing unit in the MG system, it is necessary to complete all the necessary tasks within a short period of time. It is essential for a dc MG system to accommodate the growing penetration of renewables, due to new exciting development of RES technologies. Centralized control is apparently inappropriate for the use of extendable DG networks. To illustrate, the centralized control has the lowest level of flexibility in terms of system architecture. When a new energy source is planned to connect to the system, the main code of DSP has to be modified again to prioritise the computational processes and the data transmission in a digital communication network to avoid any time delay. This is the key disadvantage of centralized control algorithm.

2.4 Distributed Control

Distributed coordination strategy has become the most prominent solution in literature to accomplish multiple objectives such as accurate load power sharing and SoC balancing control for BESS. It is implemented by developing a multi-agent system with DCLs for neighbours' information exchange and a distributed controller for each source and/or load to perform both local and coordinated functions [8], [35]. This highlights every subsystem usually has its own power converter and corresponded digital controller to maintain the functionality. As aforementioned, DCLs are used to obtain real-time information from neighbours in the network. The study in [27] presents the skeleton of a dc MG system with a communication link connected to all power sources and loads, so that energy balancing can be achieved. The key characteristics of this control framework are that dedicated local controller is permitted to collect relevant data from the other energy sources, e.g. PV power generation and battery current, and to share the total power consumption with available sources to significantly reduce the error of current sharing. In [36], to improve the robustness of a dc microgrid, the authors proposed a distributed coordination method to be used in any dc-dc converter. This has validated the effectiveness of a droop control algorithm, which is indeed the most commonly used solution in the field of dc MG system.

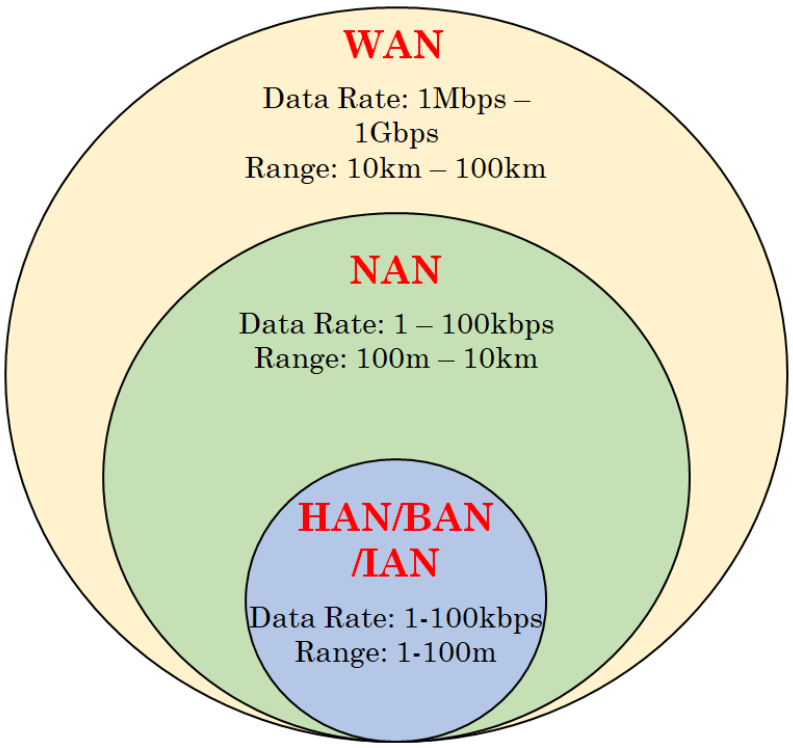

Figure 2.3 Typical standards and technologies of main communication networks [6].

In [6], Kumar et al. (2017) identified the main types of communication networks in a dc MG system: 1) consumer's premises area networks; 2) Neighbourhood area networks; 3) Wide area networks. Figure 2.3 provides some information about the effective coverage range, data transfer rate and some available techniques in three main communication networks for a dc MG system. With reference to local premises, e.g. residential and commercial areas, the coverage range and data rate are up to 100 m and 100 kbps, respectively. Therefore, communication technologies such as local area networks, Wi-Fi and low-bandwidth communication (LBC) are suitable for the use of local premises. LBC network is widely used in a dc MG system for the purpose of transmitting necessary variables to neighbour's unit [4] and [37]. Taking into account only voltage and current data are the common information requested by the local converter, LBC network can significantly reduce data traffic by increasing time period between every data transfer process compared to high-bandwidth communication. In [38], the researchers confirmed there is an impact of communication delay in LBC-based distributed control, but the overall performance of the step response is acceptable with some overshoots and more oscillations.

To develop a communication infrastructure between grid-connected device and consumer load in neighbourhood area network, some advanced techniques are used to cover a wide range of area where the maximum distance can be approximately 10 km. Some examples would be power-line signalling (PLS), Wi-Fi mesh network and Worldwide Interoperability for Microwave Access (WiMAX). PLS refers to the transmission of local data via existing power cables. In [39], the authors suggested PLS can be used to conduct mode transitions. It is different from DBS in which a voltage deviation is compulsory for the controller to determine the mode of operation. Hence this is the main benefit of PLS in distributed control.

Furthermore, in wide area networks, it is essential for dc MG systems to share real-time information with smart grid systems in favour of protection and reliability. This implies available communication technologies have to ensure the device can cover a range of 100 km and attain a high speed data capacity in not less than 100 Mbps, for instance, Fiber optics, PLS and WiMAX [6].

Droop controller, usually based on current feedback signal, is used by the distributed coordination control methods to realise accurate power sharing among parallel connected power converters in a dc MG. This is commonly referred to as adaptive voltage positioning

[38], [40]. The current-based and power-based droop control methods can be defined as follows [8]

$$V_{dc\_i}^{*} = V_{dc}^{*} - m_I \cdot I_{out\_i} \tag{2.1}$$

$$V_{dc\_i}^{*} = V_{dc}^{*} - m_P \cdot P_{out\_i} \tag{2.2}$$

where $V_{dc\_i}^{*}$ is the output reference voltage of the converter $\#i$, V_{dc}^{*} is the nominal value for dc-link voltage, m_I is the droop coefficient for current-based droop control, m_P is droop coefficient for the power-based droop control, I_{out_i} and P_{out_i} are the output current and power of the converter $\#i$, respectively. With reference to current-based droop controller, the droop coefficient is known as virtual output impedance [41], [42]. In the aforementioned equations, line resistance is usually neglected in a classical droop controller to simplify the algorithm where the output dc-link voltages of power converters are assumed to be equal in a dc MG.

In an open-circuit condition, the current of the interface converter in (2.1) is zero and thus the voltage deviation can be neglected. However, an increase in output current for the local converter could lead to an inevitable voltage deviation [38], as can be seen from Figure 2.4. Depending on the calculation of droop coefficient m, higher value of droop coefficient results in greater current sharing accuracy, more damped oscillations and rise in voltage deviation [8]. Given these interface converters are connected in parallel, the difference in line resistances is a main drawback of traditional droop controller which in turn causes a degradation of load current sharing performance [38].

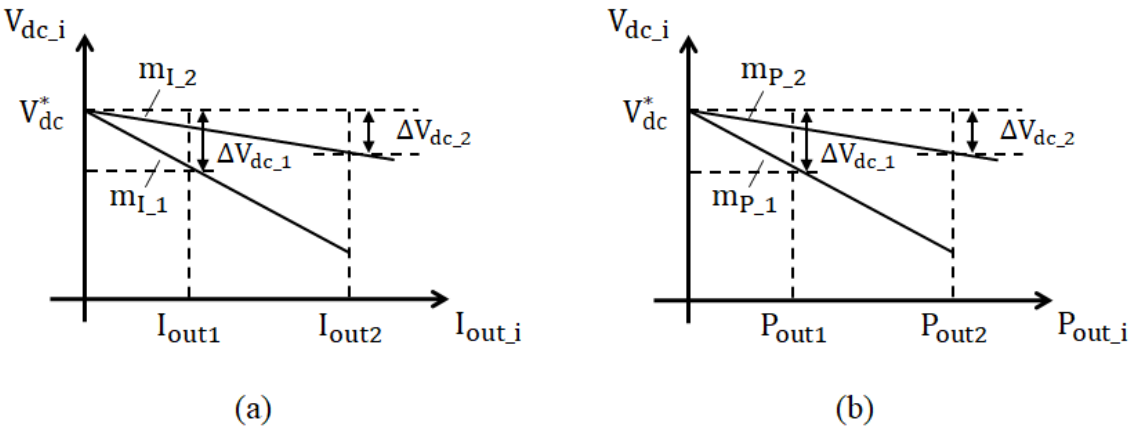

Figure 2.4 Classical droop controllers in a dc MG. (a) Current-based. (b) Power-based.

Moreover, as an alternative method, a distributed droop controller based on output power is commonly used to realise accurate power balancing and dc-link voltage restoration. Line resistance is usually taken into consideration in advanced control algorithm, but not limited to traditional droop control. As described in Figure 2.4, the output power of each DG source can be a feedback signal in a droop controller to calculate a corresponding reference voltage in a dc MG. This strategy is similar to the current-based droop controller, where the determination of droop coefficient is the most crucial factor in a droop control. In [37], the researchers proposed a power distributed control strategy to achieve dc bus voltage restoration and proportional power sharing based on power capacities of all output converters. Besides, by exchanging the neighbours' data, the distributed controller can reassure that output power per unit of each converter is balanced and directly proportional to the available power capacity. The calculation of droop coefficient based on power is expressed as

$$m_P = \frac{V_{dc}^* - V_{dc\_min}}{P_{rated\_i}} \tag{2.3}$$

where V_{dc_min} is the minimum allowable voltage of the dc bus, and P_{rated_i} represents the rated power of the converter $\#i$.

Considering the impacts of the line resistance in a dc MG, the authors in [31] established a distributed control method with SoC balancing and LBC. There is a SoC balancing scheme to balance the SoC levels among BESS with the support of average SoC value. Plus, a compensation term for output power is included in the droop control to ensure accurate power sharing among DG sources. This is achieved by means of virtual power rating. It is beyond the scope of the thesis and therefore detailed explanation can be found in literature. In accordance with the number of battery units, the average per unit power for each element can thus be calculated by a classical PI controller to define a compensation term for the purpose of precise power balancing. Last but not least, the fundamental objective of a dc MG, dc bus voltage regulation, is conducted by computing the average output voltage of battery energy units. Given all compensation terms are identified, a global reference voltage for the dc bus is used by a traditional cascaded loop to manipulate the output voltage and local battery charging/discharging current for each parallel-connected converter in a BESS.

A vast number of distributed control techniques have recently been addressed by researchers to tackle the key challenges of a dc MG system, particularly in an islanded mode. Some typical examples of key challenges in literature are balancing SoC of battery [13], [31], issues

of communication delay [31], [38], accurate load current sharing among energy sources [38], [43], consideration of transmission line impedances [4], [31], [42]. In summary, the distributed coordination control strategy provides the following advantageous features: 1) high reliability; 2) absence of single point of failure; 3) high efficiency; 4) accurate power sharing among parallel-connected energy sources; 5) plug-and-play capability [44]. However, there are a number of existing limitations in relation to distributed control, including communication delay and failure, measurement noise, complex design of digital communication network and difficult to perform stability analysis for non-linear dc MG model [8].

2.4.1 Adaptive Droop Resistance Control

As previously mentioned, the conventional droop control method generally suffers from poor load current sharing performance and significant voltage deviation. To overcome these two key challenges, several advanced control schemes have been proposed in literature. The most commonly used solution for an islanded dc MG system would be distributed adaptive droop control. In principle, droop control is a decentralized control that accounts for output current and voltage of local converters in a MG. In [42], the authors recommended the adaptive droop approach to adjust the global reference voltage in order to mitigate the effects of line impedance and low current sharing accuracy. It can be seen from Figure 2.5 that measured per-unit current and average voltage from its neighbours are transferred to local controller via a sparse communication network. The per-unit current refers to the percentage of load current in a power converter, which helps to achieve proportional load balancing among individual energy sources. In the event of current mismatch, the droop coefficient will accordingly be varied to minimise the current residues with the support of current regulator, as shown in Figure 2.5.

There exists a voltage regulator to reduce the difference between nominal voltage and local voltage set-point. In the first place, an average dc bus voltage is locally estimated at certain node. A dynamic consensus protocol is applied to take neighbours' data into consideration and to determine the average voltage of a dc MG system. Detailed equations can be observed in [42]. By comparing the nominal voltage with the average dc-link voltage, a voltage correction term can be fed into the outer control loop to compute the desired local voltage. In conclusion, this control algorithm is a good representation of distributed adaptive droop control for the use of an islanded dc MG.

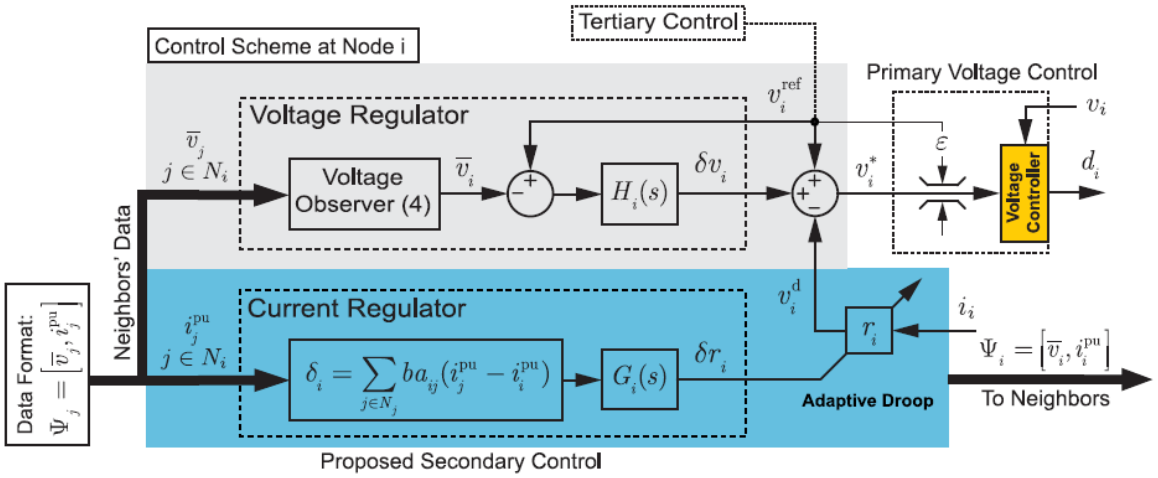

Figure 2.5 Control diagram of a distributed adaptive droop approach [42].

There are a number of ways in which we can enhance the performance of a dc MG. Provided performance degradation is due to unequal cable resistances, a study by Augustine et al. (2015) introduced an adaptive droop control scheme to improve the load sharing accuracy and voltage deviation [43]. Despite the fact that the necessary information requested by this control method is similar to the aforementioned one, it focuses on the adjustment of droop coefficient to simplify the implementation of advanced control. Eventually, Figure 2.6 presents a current-based adaptive droop control which is employed to identify the local reference voltage followed by a classical multi-loop with PI controllers. The voltage variation across the dc MG with the proposed method in [43] is less than ±1% in average. This is one of the key benefits of distributed adaptive droop control. Last but not least, current sharing error is notably decreased as the converter output power losses are evaluated prior to control operations.

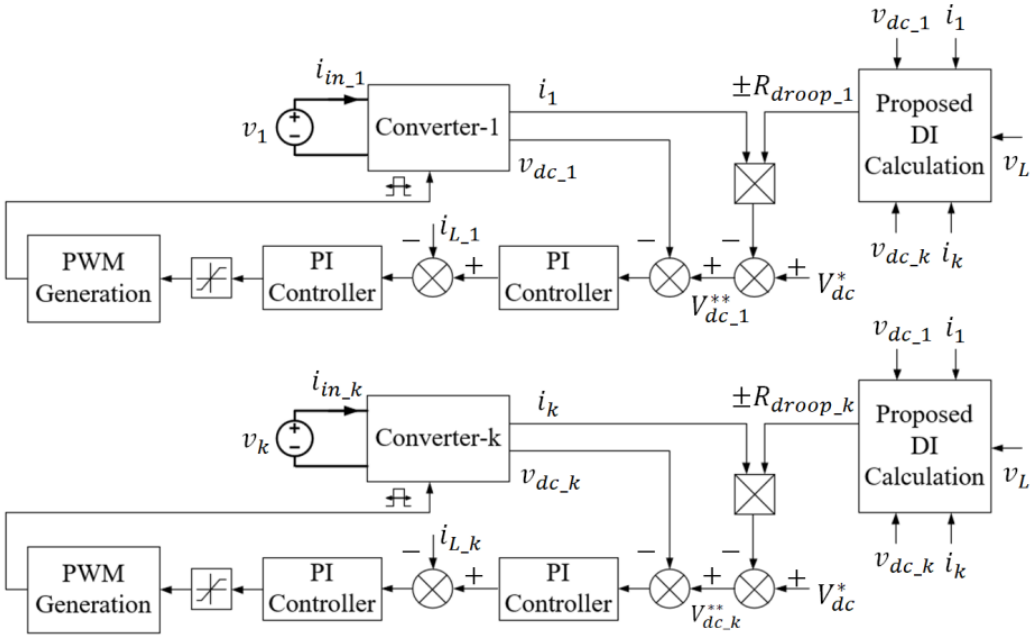

Figure 2.6 Control framework of an adaptive droop control method [43].

2.5 Decentralized Control

Decentralized coordination method is implemented to locally control variables of power electronic converter for RES and BESS, where DCL does not exist in the MG. Therefore, digital communication system can be neglected in this algorithm which indicates the simplicity of fully decentralized approach. Taking the characteristic into consideration, the fundamental control parameter of an islanded dc MG would be dc bus voltage V_{dc}. To clearly signify the present mode of operation, i.e. PV standalone mode or battery islanded mode, it is compulsory for a single dc bus to allow an intrinsic voltage deviation for power transfer of interface converters. The presence of voltage deviation could bring a potential issue to this control scheme in which a conflict between classical controller of BESS and RES' compensator may arise, due to the lack of communication channel. In [3], however, a simulation study was conducted to prove that the settling time for a BESS controller to reach a desired value of dc-link voltage is much shorter than the time for a MPPT control algorithm. The battery current can immediately be computed based on the error of the outer loop to restore the dc bus voltage. Certain period of time required to track the new MPP for a PV array is indispensable in the event of abundant PV generation under high-irradiance conditions. BESS would thus be the dominant energy source in an islanded dc MG system unless the battery cannot maintain full functionality, whilst PV controller continues to maximise the available output power. There are no conflicts of interest in local converters when a dc MG is operated in a battery islanded mode.

Droop control is a well-known strategy adopted by decentralized controller to define a maximum allowable voltage deviation for the purposes of proportional power balancing among renewables, and dc bus voltage regulation. Regarding the droop curve, the adaptive voltage positioning is one of the most widely used methods in which it can be categorised as a current-based droop controller, as mentioned in Section 2.4. In [10], the authors demonstrated the control structure of a traditional $V - I$ droop controller. A mode transition is necessary for the PV-based droop controller to transfer from MPPT mode to voltage restoration mode, and vice versa. Another example of using a mode switching control for a PV boost converter can be found in the study conducted by Liu et al. [45]. There is a single control loop for the MPPT algorithm and an individual loop for dc bus voltage regulation. In [46], the approach of mode transition strategy is utilised in a low-voltage dc MG system for PV arrays, where the MPPT function and voltage regulation are in two different control loops. Accordingly, there is a room for further improvement of classical droop controller, which will be explained in Chapter 4.

Over the past 15 years, Plug-and-Play (PnP) capability is becoming increasingly important in the field of dc MG system due to growing penetration of renewable resources. The term is originated in computer science which could then be utilised in wide variety of applications. In terms of dc MG, it refers to the extendibility of a common dc bus approach without the need for human intervention or physical configuration. In [19], they suggested the following criteria to assess the flexibility of a dc MG: 1) control architecture; 2) topology of dc MG; 3) coordinated control method; 4) centralized versus extendable coordinated controller. There are some attractive reasons to implement decentralized control strategy, including PnP capability, absence of complicated digital communication network, and reduction in implementation costs compared with distributed control. However, some of the most prominent problems existed in decentralized control scheme include adverse effects of inaccurate voltage sensor, inherent voltage deviation and performance degradation of power balancing among local interface converters [8].

DC bus signalling (DBS) is the most commonly used method in decentralized distribution approach [8], [47]. As shown in Figure 1.3, each energy source and BESS are individually connected to the common dc bus. This allows the dc bus to behave as a communication channel. By defining the relationship between voltage deviation and power level via droop curve, the local converter for RES or BESS can inherently be reassured that sufficient power is supplied to the consumer loads [48]. Based on the droop control technique, the generated

power of each interface converter is directly proportional to the maximum capacity of the energy source. Every unit in a dc MG system eventually participates in the voltage restoration to prolong the lifetime of individual sources, i.e. Balanced SoC of battery and proportional power sharing among PV arrays. In DBS approach, a voltage deviation is vital for regulating the dc bus voltage to an acceptable level since this is the key signal to indicate the state of a dc MG [30]. The so-called SSE can usually be observed in a common dc bus, especially in a PV standalone mode. The academics in [49] proposed a mode-adaptive decentralized droop control to identify the operation mode under different circumstances. It introduces three major modes of operation to represent the dominant unit and corresponding actions to be taken. In [10], they argued the continuous oscillations between operation modes could potentially be a downside where an anti-oscillating method may be necessary. Besides, the study aims to unify both MPPT and voltage restoration algorithms to establish a one-off control system which can be applicable to every scenario. A detailed analysis of the conventional PV droop control strategy is presented in Chapter 4.

2.5.1 Adaptive PI Droop Controller

In theory, the traditional droop control is realised by means of virtual impedance to manipulate the output bus voltage and current reference, respectively. To facilitate the development of a decentralized controller for autonomous current sharing, an embedded-virtual-impedance based $I-V$ droop control algorithm is proposed in [50]. Wang et al. (2018) reported poor dynamic response of a droop control method could lead to the issues of low power quality and huge dc bus voltage fluctuations, where the study specifically concentrates on the dynamic characteristics of a decentralized controller for parallel connected dc-dc converter. It can be seen from Figure 2.7 that the control scheme consists of external voltage and internal current loops. An adaptive PI compensator is implemented to perform advanced functions in a decentralized control. Once the error attains an unacceptable level, the proportional term is gradually increased by the adaptive controller to ensure that the system quickly reaches a steady-state condition in a short period of time [50]. To understand the principle of adaptive control, in [51], similar approach of using an adaptive proportional term for PR current controller is presented, where the proportional term depends on the error value of inner current. The SSE can theoretically be eliminated by a small proportional term, following the use of large proportional gain during transients. This is the key advantage of deploying an adaptive PI controller to simultaneously improve the transient response and steady-state performance of a parallel-connected dc converters system.

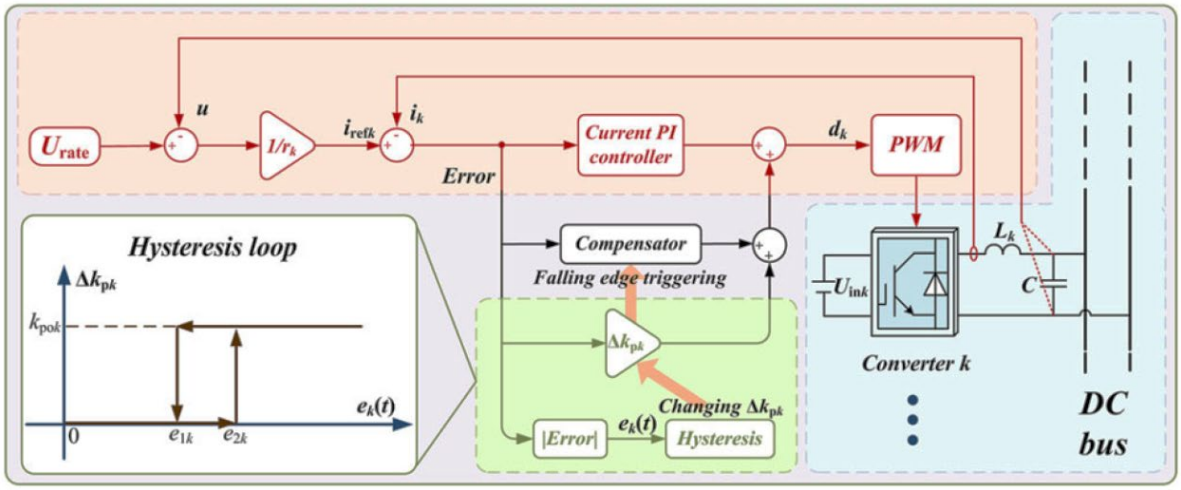

Figure 2.7 Control diagram of an adaptive PI controller with $I-V$ droop control [50].

As shown in (2.1), this is the most common droop characteristic in literature. The $I-V$ droop control in [50] refers to the reverse of the traditional $V-I$ droop control method, which can be written as

$$I_{out}^{*}=\frac{1}{m_I}(V_{dc}^{*}-V_{dc}) \tag{2.4}$$

where I_{out}^{*} is the output current reference and V_{dc} is the dc bus voltage. Relating to the load current of nth parallel-connected dc converters, droop coefficient is re-calculated to achieve proportional power balancing by means of equal maximum voltage deviation of the dc bus.

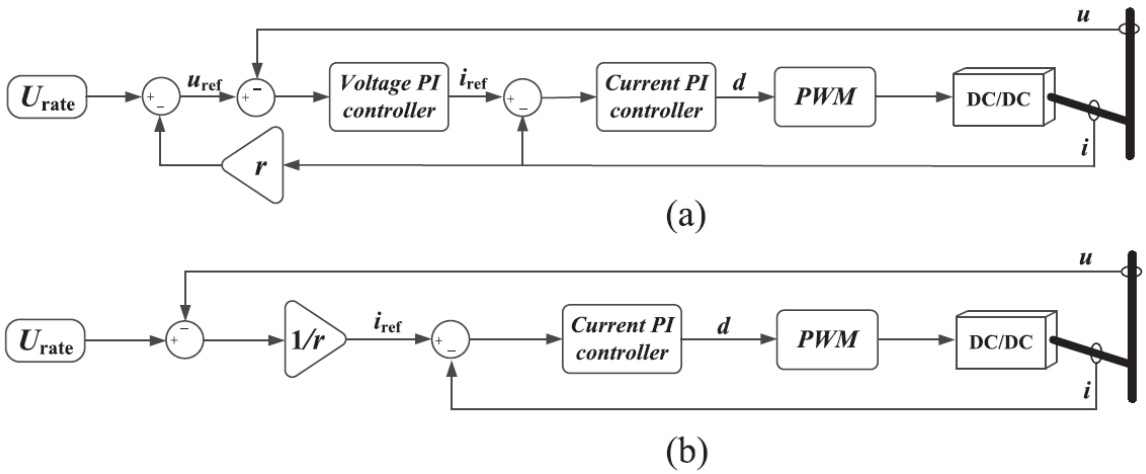

Figure 2.8 Control structures of two droop control strategies. (a) Classical $V-I$ droop control. (b) $I-V$ droop control [50].

It can be observed in Figure 2.8 that the classical droop control requires two separate PI controllers for outer voltage and inner current control, respectively. However, only the current compensator is compulsory for the $I-V$ droop control algorithm. This has highlighted the benefit of implementing the $I-V$ droop method in [50]. The traditional control scheme suffers from slower attenuation in low frequency fluctuation. As a result, the authors concluded that the $I-V$ droop control takes less time to reach the steady-state value than the conventional $V-I$ method where a pole shifting trajectory is presented in [50]. It has become one of the state-of-the-art technologies in which the control structure reduces the number of PI controller to one. In principle, it is usually effortless to manually tune the internal PI compensator rather than two PI controllers in a cascaded loop. The improved $I-V$ droop control has become a promising solution to enhance the dynamic response performance of a dc MG system.

2.6 Comparison of Three Main Coordinated Control Methods

In this chapter, three major coordinated control strategies have been reviewed in terms of implementation, control architecture, dynamic performance and steady-state response. Each of them plays a critical role in the development of dc MG systems such as load current sharing and voltage regulation. Therefore, the selection of coordinated control algorithm depends on the criteria of a dc MG. Centralized control has some advantages over the distributed and decentralized control schemes. Cost minimization and easy to implement are two key benefits of centralized control. However, the centralized control usually suffers from single point of failure which is apparently inappropriate for an extendable dc MG. Decentralized control is capable of independently manipulating the dc-dc converter to achieve voltage regulation and proportional power sharing. PnP capability is one of the advantageous features of utilising decentralized method. Given decentralized control is easy to implement and suitable for dc MGs especially in an islanded mode, this thesis focuses on the improvement of a decentralized controller to enhance the dynamic performance and steady-state response of the PV-based dc MG system. Decentralized approach is subject to certain limitations, including inaccurate load power balancing and inevitable voltage deviation. Most of the researchers are thus keen on the most prominent emerging technology, distributed control, which is realised by means of sparse communication network. High reliability, accurate load current sharing and no single point of failure are the main advantages of distributed control technique. It is noted that distributed control requires complex design of digital communication network to ensure a stable connection between local interface

converters. Last but not least, the researchers in [8] summarises that it is a common challenge for control engineers to undertake a performance analysis of a distributed control.

Table 2.3 Benchmarking of the coordinated control methods

Coordinated Control	PnP Capability	Voltage Deviation	Reliability	DCL Complexity	Control Simplicity
Centralized Control	− −	+	−	−	+
Distributed Control	+ +	+	+ +	− −	− −
Decentralized Control	+ +	− −	+	+ +	+ +

Note: the more +, the higher capability, less voltage deviation, better reliability, less complexity, and simpler.

Eventually, Table 2.3 analyses the characteristics of the main coordinated control strategies for a dc MG system in relation to PnP capability, voltage deviation, reliability, complexity of digital communication network, and simplicity of control algorithm. This has summarised the benefits and drawbacks of implementing various coordinated control schemes for engineers to decide the best control algorithm to accomplish multiple goals in a dc MG system.

2.7 Chapter Summary

In this chapter, the main coordinated control methods of a dc MG system have been reviewed, including centralized, distributed and decentralized control. Some typical examples and fundamental theories of each technique in literature are presented in the previous sections. A comparison of those control algorithms has been presented in terms of various requirements such as PnP capability and reliability, following an introduction to centralized, decentralized and distributed control methods. It summarises the key advantages and disadvantages of the coordinated control schemes, which helps researchers to better understand the trade-offs between them. Plus, it is essential to provide an overview of the PI/PID controllers and to highlight some key concerns like integral windup loop and voltage overshoot issue in this thesis. Researchers can thus decide the best control strategy based on the system requirements.

Chapter 3. Modelling of PV Arrays and DC MG

3.1 Introduction

This chapter presents the mathematical model of a PV array and simulation model of a dc MG using MATLAB/Simulink. In general, there are two common methods of modelling a PV generator which includes mathematical modelling of a PV array and implementation of a built-in PV array block in Simulink. In [52], a mathematical model of a PV generator with necessary procedures was illustrated. The electrical specifications of a solar panel in practice are used by the characteristic equation to represent the behaviour in Simulink. The non-linear characteristics of a PV array such as P-V and I-V curves can be replicated. The mathematical model of PV array provides an extra degree of freedom to design an appropriate PV generator, according to the size of dc MG system. By connecting the PV modules in series and in parallel, the PV output voltage and current are raised, respectively. The total power of the PV array can be calculated. To evaluate the performance of the proposed control algorithm, the mathematical model of PV array is permitted to vary the solar insolation and temperature over time so as to generate some preliminary results under abrupt changes in atmospheric conditions. The model can therefore be implemented in a dc MG with the support of power converter for the use of simulation.

In literature, battery islanded and PV standalone modes have attracted an increasing interest from researchers in the field of dc MG. Provided that grid faults and power outage could often arise, resulting in a temporary disconnection of the single-phase inverter from the utility grid. The mode of operation is regarded as islanded mode. To minimise the disruption to the local consumers, it is essential to build up to an extendable dc MG system and to increase the stability of the distribution network. In this scenario, the dc MG comprises an ESS, PV arrays, dc-dc power converters and local loads. A BESS has become the dominant power source to serve as a finite energy supply to restore the DC-link voltage and to satisfy the needs of the local energy consumption. The BESS can be used for capturing the surplus energy from PV generators, and vice versa.

Due to the intermittent nature of renewable sources, a battery could in turn be fully charged and isolated at a particular time. A PV array plays a crucial role in generating sufficient energy to the loads. Therefore, the dc MG has the capability to operate in a PV standalone mode. These modes of operation will be demonstrated in MATLAB/Simulink. This provides a theoretical framework to understand the key challenges of the established coordination

control strategies in a dc MG system and to validate the devised V-dp/di control system. The details of the design process for a complete dc MG system are given in the following sections.

3.2 PV Array

Photovoltaic (PV) effect is to convert the energy from the sunlight into electric current with the help of semiconductor materials such as mono-crystalline silicon and cadmium telluride. When a photon in the light reaches the semi-conductor, the electrons are excited from the valence band into the conduction band [53]. Correspondingly, the phenomenon creates an electron-hole pair and electrons around the "hole" are allowed to move. This is the basic principle of the conduction process in the semi-conductor material along with the PV effect. In terms of a PV module, it generally comprises 108 solar cells. The equivalent circuit of a solar cell can be observed in Figure 3.1 [12]. I_{ph} represents the photocurrent generated by the solar cell. I_{rs} is the reverse saturation current. V_{pv} and I_{pv} are the output voltage and current of a PV cell. R_s and R_{sh} are the intrinsic series and shunt resistances, respectively. R_o represents the load resistance. D_j is the diode representing the single PV cell and hence R_j is the intrinsic resistance of the diode.

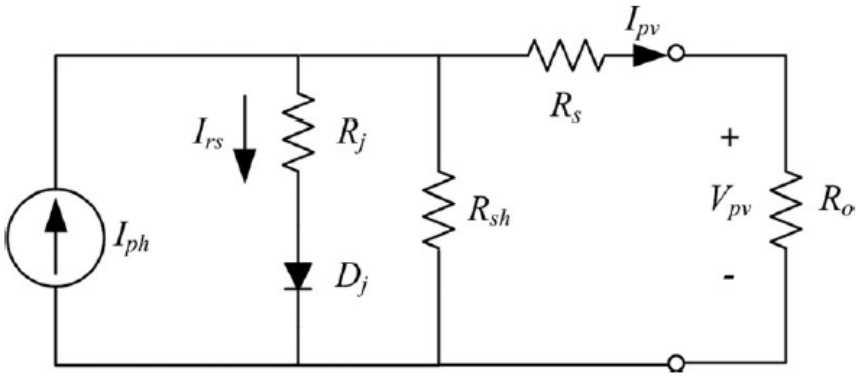

Figure 3.1 Equivalent circuit of a PV cell [12].

Typical voltage of solar cell is about 0.5-0.6 V and the power would be approximately 3.75 W. Therefore, PV cells are always interconnected in series to attain sufficient voltage in a PV system. In [53], the authors highlighted that solar cells in series-parallel configuration allow a PV array to easily stabilise at a range of voltage values. The topology provides a relatively high voltage for the use of power electronics converter to perform various operations. For instance, step up/step down dc-dc conversion and dc-ac conversion. Since the dc bus voltage is set to 400 V in the simulation, it is essential to have a PV generator which can generate more than 100 V to reduce the voltage conversion ratio of the boost chopper. It turns out a

lower voltage stress across the process of power conversion. Taking the highest allowable voltage into account, the PV output power remains small even if a group of solar cells are in series. Another way of raising the overall power is to connect these groups of solar cells in parallel, resulting in an increase in current output to an acceptable level. The above concepts can theoretically be applied to those PV modules so that a PV array is developed based on the requirements in a dc MG system.

In the event of short circuit or faulty wiring, the PV current flows in an opposite direction, leading to severe damage to the PV array. There are two methods of taking safety precautions, including the implementation of blocking diode and use of bypass diode. In accordance with the blocking diode, it is simply a single diode to avoid reverse current flow from the load or battery. In [53], they reported the blocking diode could indeed bring a forward voltage drop and power loss in this scenario. It is the main drawback of utilising blocking diode, given the diode in low power applications in kW may induce a significant power loss. The approach of using blocking diode is uncommon to be adopted by manufacturers. Regarding the bypass diode, it is connected in parallel, but in reverse bias, with a group of series cells. In case of low photocurrent, the diode offers a current path which in turn limits the current to avoid overheating issue. The bypass diode provides an alternative current path in case of failure. To sum up, bypass diode is the most commonly used device in a PV panel to afford protection to partially shaded solar cells.

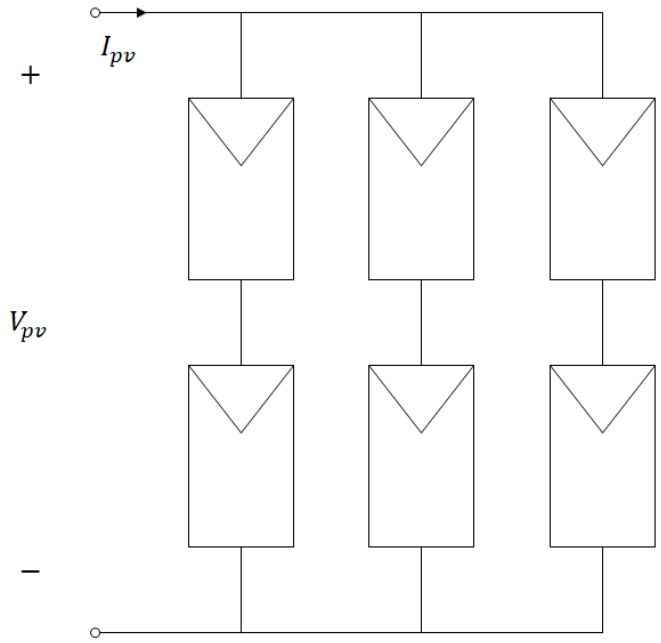

Figure 3.2 Outline of a PV array.

As shown in Figure 3.2, a typical example of a PV array can be observed [53]. The overall PV voltage depends on the number of the solar panels in a series connection. In the meantime, these panels are wired in parallel to increase the total PV output current. Therefore, the specifications of a PV block in MATLAB/Simulink can be varied in accordance with the power dissipation of a local consumer load. In principle, the PV cell is assumed to be at standard test conditions which would be typical cell temperature of 25 °C, air mass 1.5 (AM1.5) spectrum, as well as 1000 W/m^2 of solar insolation.

3.2.1 Mathematical Modelling of PV Array

This section illustrates the design procedure to develop a PV model in order to meet the specifications of the dc MG system. In 1996, Gow and Manning provided a comprehensive mathematical analysis of a PV array which can be used to understand the characteristics of a PV model in accordance with system parameters [54]. The details of basic formulas for a solar cell are provided in Appendix A for reference. In [52], a detailed mathematical model of a PV generator is given. Basically, it consists of four subsystems which include photocurrent, reverse saturation current, module saturation current, and output PV current. As can be seen from Figure 3.3, a layout of the 2 kW PV array is summarised. Provided some of those terms correspond to the specifications of a solar panel, they are kept constant at standard test conditions. Consequently, they are substituted into the formulas given in Appendix A for calculations.

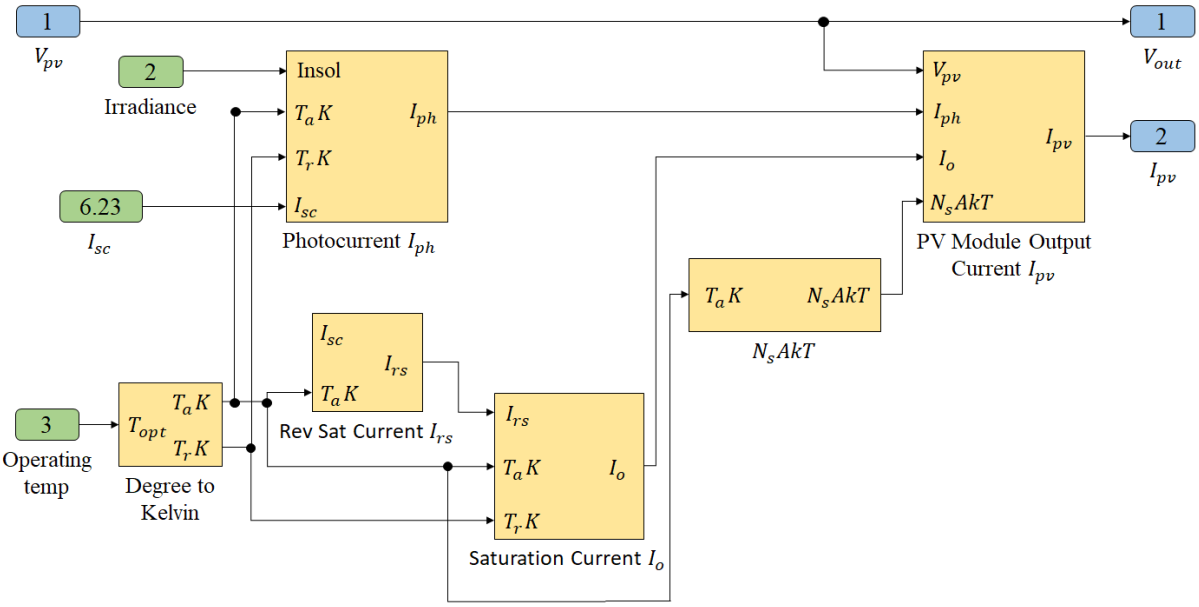

Figure 3.3 Block diagram of mathematical PV array.

The equation for computing the output current of PV model can be observed in (3.1). A mathematical function block is utilised to express the formula for PV current in Simulink library. There is a feedback path with series resistance, since the equation requires the previous value of PV output current to calculate the present value. This key formula can be given by the equation (3.1) [55].

$$I_{pv} = N_p I_{ph} - N_p I_o [e^{\frac{q(V_{pv}+I_{pv}R_s)}{N_s AkT}} - 1] \tag{3.1}$$

Where I_{ph} is the module photocurrent, I_o is the saturation current, A is the ideal factor, q is the charge of electron, k is the Boltzmann constant and T is the cell operating temperature. According to (3.1) and Appendix A, this implies that higher temperature and/or lower irradiance results in lower maximum PV output power, and vice versa. To simplify the analysis of the study, three general test conditions are determined to validate the electrical characteristics of the PV model in terms of irradiance. The effect of varying the temperature is beyond the scope of this study and so the operating temperature is set to a typical value of room temperature throughout the simulation.

To assess the effectiveness of the mathematical model, a PV array based on the solar panels (SPR-X21-335-BLK) is built up to a PV system for simulation. The 2 kW PV generator, i.e. PV1, is used to generate solar power at different levels of irradiance. There are three workspace blocks in this model to store the data of output signals from the PV array which would be PV current, voltage, and output power. Therefore, the electrical characteristics of this PV model can be produced to review the requirements of the dc MG. This is the main benefit of employing a mathematical model for PV array due to its high flexibility for the interaction with the dc MG.

As shown in Figure 3.4, the I-V characteristic curve of the PV array is presented to validate the mathematical model and to understand the effect of fast changing irradiance. It can be analysed the decrease in solar insolation leads to lower short-circuit PV current, as well as the maximum current point. It is undoubted that the P-V characteristics given in Figure 3.5 clearly indicates the maximum PV power dramatically drops from 1996 W to 1212 W, almost 40% of maximum available energy, in accordance with the step change in irradiance. The significant change in solar insolation has provided a challenge to a control system, since the variation results in an inevitable difference between the set-point and feedback value. Indeed, this refers to the error signal in the voltage control loop. To always ensure a high power

conversion ratio during the process, it is compulsory to promptly restore the dc-link voltage and achieve maximum power point tracking in a PV system. Eventually, taking the irradiance change into consideration is one of the most important factors to show the robustness and reliability of the proposed control algorithm.

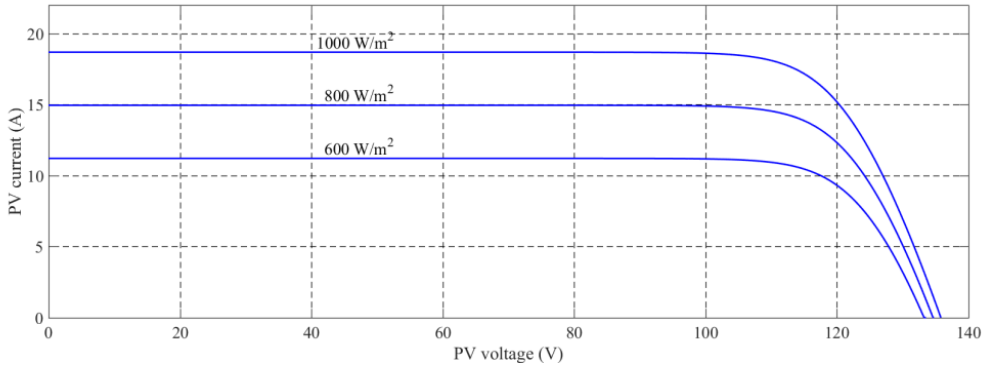

Figure 3.4 I-V characteristics of the 2 kW PV model at three irradiance levels.

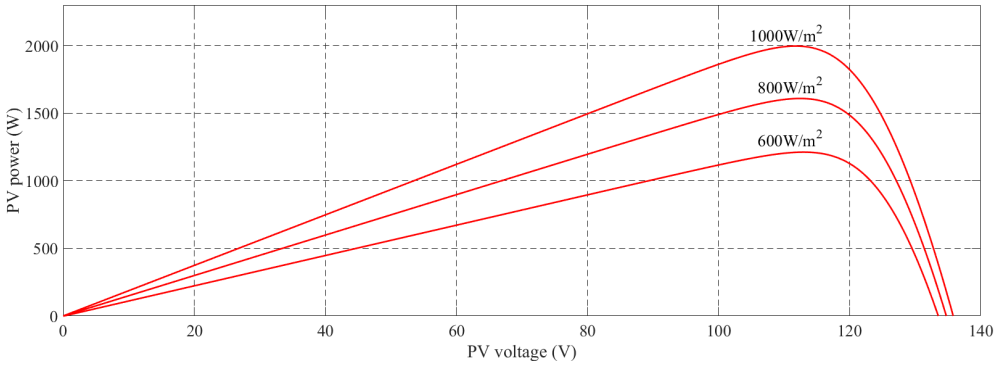

Figure 3.5 P-V characteristics of the 2 kW PV model at three irradiance levels.

3.3 Working Principle of Step-up DC-DC Converter

There are three main categories of DC-DC converters, including buck, boost, and buck-boost converters. They can be used to efficiently step up or down the voltage in relation to the input and output voltages of a power system. In [56], they analysed that the efficiency is in between 80% and 90% which can be the basic standard for evaluating the overall performance. In the past ten years, some researchers have established high efficient dc-dc converter which aims to have an efficiency of more than 90%, up to 99%. It is noted these topologies are usually challenging to be manufactured in a factory. There exists a compromise between efficiency and complexity of converter topology.

An ideal DC-DC converter is assumed to be 100% efficiency. 20 kHz of switching frequency would be recommended as a starting point by the author in [56]. A significant amount of time is required for a MPPT algorithm to search for new MPP. Therefore, the switching frequency is applicable to sample the voltage/current signal and control the power switch in a switching cycle. A power MOSFET is ideal which means it can be switched ON/OFF instantaneously without any delay. In theory, from off (0) to on (1), it is expected to allow a turn-on delay time and a rise time for the MOSFET to be fully on, and vice versa. Plus, the energy storage components, mainly inductor and capacitor, are ideal without any internal parasitic element such as equivalent series resistance (ESR). In practice, the open-loop response of an ideal power converter can remarkably be different from the actual converter. For instance, the overshoot of an ideal converter is always higher than a practical one. Since a notable amount of voltage drops across the ESR, the output voltage can experience an unusual high overshoot in an ideal case. This in turn reduces the stability of a control system but the negative outcome can be prevented by involving the ESRs in front of the inductor and the capacitor in the simulation, respectively. As a consequence, the efficiency of the dc converter in the dc MG system is no longer 100%. The effect of relatively low efficiency in the process of energy conversion can be negligible as it is always true in real-life applications. This provides a platform to easily predict the energy conversion efficiency, and to design a practical dc-dc converter for the purpose of simulation data acquisition.

3.3.1 Design of a PWM Boost DC-DC Converter

Generally speaking, a step-up dc-dc converter is composed of an inductor, a power switch, a diode, a capacitor, and a resistive load [56]. The output voltage of a step-up converter must be larger than its input voltage. Continuous or discontinuous conduction mode can be used to describe the mode of operation of the boost converter in a steady state. During the continuous conduction mode, zero level is never reached by the inductor current since either the switch or diode will be turned ON in any time interval. However, in the discontinuous conduction mode, the switch and diode can both be OFF. The inductor current drops to zero, and remains at zero for a short period of time before the beginning of the next cycle [57]. In the thesis, the step-up converter is assumed to be operated in continuous conduction mode for simplicity.

The LC circuit of the boost converter includes several main features in which it plays a vital role in operating a dc-dc converter. To begin with, an LC circuit refers to an electrical circuit which is composed of two passive elements, inductor L and capacitor C. This low-pass filter is

fully capable of filtering out high switching frequency in a step-up chopper. It is known as a second-order low-pass filter. The term "second-order" represents the number of energy storage elements in a circuit, in which it has 2 passive components in this circuit. In principle, duty ratio D can be in a range of 0 to 100%. However, it is subject to the turn-on and turn-off delay time of a power device. In MATLAB/Simulink, it can be assumed to be an ideal switch and thus the PWM signal always varies from 0 to 1. The dead time of the controlled PWM signal is neglected in the simulation study to simplify the analysis.

When switch is ON,

When the switch is placed in the ON position. In an ideal case, the voltage dropped across the switch is supposed to be zero. It means the current will only flow through the inductor and the switch, but not the diode. This circuit analysis can be undertaken using Kirchhoff's Voltage Law. The equation for the inductance of a common step-up converter can be written as

$$L = \frac{V_I \cdot D}{\Delta I_L \cdot f_{sw}} \tag{3.2}$$

where L is the inductance of the converter inductor, V_I is the input dc voltage, D is the duty ratio of the boost converter, ΔI_L is the inductor ripple current, and f_{sw} is the switching frequency of the converter.

When switch is OFF,

During the OFF-state, a threshold voltage is supplied to the diode for this passive component to be switched on. Again, an ideal diode with a zero forward voltage drop is implemented in the simulation study. The energy is directly transmitted to the dc-link capacitor and the resistive load, respectively. The capacitance of the boost converter can be derived as

$$C = \frac{I_c \cdot (1 - D)}{\Delta V_c \cdot f_{sw}} \tag{3.3}$$

where C is the capacitance of the converter capacitor, I_c is the capacitor current, and ΔV_c is the capacitor ripple voltage.

The above equations (3.2) and (3.3) have given the guidelines on the selections of the converter inductor and capacitor. In [58], a formula for computing minimum capacitance is provided to ensure the desired open-loop response of the boost converter. It should be kept in

mind that the minimum value may not be the best solution to the design of the basic converter. While most of the formulas found in books and studies are suggesting minimum values for the converter inductor and the capacitor, these two equations are capable of defining the sizes of the key components in which the circuit satisfies the general requirements of the boost converter in terms of the ripple current and voltage. To strengthen the simulation study, it is recommended to include the ESRs for the inductor and the filter capacitor, respectively. The overshoot of the step response of a boost converter is usually lower than its ideal case, due to the fact that ESR is capable of absorbing the voltage spike. In other words, the voltage across ESR should be taken into account to reduce the output voltage to a reasonable level. A thorough review on the state-space averaged model and continuous transfer function of a step-up converter is given in Appendix B.

There are three main ways of simulating a step-up converter in MATLAB/Simulink, including Simulink implementation of the circuit, calculation of the open-loop transfer function, and use of boost converter block in Simscape library. The circuit model developed in this study takes advantage of high flexibility. This feature allows the user to effortlessly change the parameter values of the boost converter. One of the key benefits of establishing a simulation model is the lack of converter transfer function derivation. It is highly recommended to implement a simulation model, instead of mathematical analysis, to detail the operating principle of a practical boost converter.

3.4 Battery Energy Storage System

In this section, a SoC-based battery management system using MATLAB/Simulink is introduced to operate the dc MG system in an islanded mode. Compared with supercapacitor, battery benefits from high energy density but low power density and slow dynamic response to abrupt load change [59]. To simulate the behaviour of a BESS, the system is briefly made up of generic battery model, bi-direction dc-dc converter and a charge/discharge cascaded control loop. In [60], a thorough review on the grid-connected inverter interconnected with BESS is provided to summarise the main features of employing a battery management system. There are a number of key characteristics of implementing a BESS:

i. Capable of compensating the power difference between renewables and dc consumer loads.
ii. The ability to deliver adequate energy to the loads during periods of low, or negligible power generation from renewable sources.

iii. The features of load levelling and peak shaving can be achieved.
iv. Improvement of power quality in a dc MG due to lack of ac frequency variations.
v. High response speed to step load change compared with PV system.
vi. Acts as a voltage source to restore dc-link voltage [61] and [62].

A study conducted by Jia et al. (2015) has highlighted the significance of high efficiency and high power density of the bi-directional dc-dc converter [63]. They concluded that there is a compromise between conversion efficiency and power density, in which the selections of switching frequency and passive components' sizes are critical. In case of high switching frequency (>20 kHz), the passive components' volumes tend to be saturated. However, the converter efficiency dramatically reduces which is the key disadvantage of increase in switching frequency. The initial switching frequency of the bi-directional converter is set to 20 kHz in this thesis.

Lithium-ion battery is widely used in many areas such as electric vehicle, portable electronics, and dc MG [62] and [64]. The advantages of a lithium-ion battery include high power density and low self-discharge rate. Provided that the dc MG system in the thesis is specifically designed for residential applications, the power level would thus be low compared to BESS for grid storage applications. As a consequence, a Lithium-ion battery is implemented in the simulation model to behave as a secondary power source during periods of low solar insolation. Energy requirements are usually dictated by the application. Taking the frequency of use of battery into account, the battery stack is meaningless to have a huge amount of capacity due to the fact that it is beyond the scope of this thesis. It is noted the nominal capacity of a BESS depends on the total number of cells, in which the series/parallel combination defines the output voltage and current, respectively. Voltage of the cells is additive in a series connection while parallel connection increases the battery current.

Bi-directional dc-dc conversion has become the most prominent solution to the needs for the implementation of distributed generation with RES, since it is common for lithium BESS to extract power from or feed energy into the dc bus [65]. A circuit diagram of the bi-directional converter can be found in Subsection 3.4.1. The specifications of input and output components have been taken into consideration in the Simulink model, in which the designated values are appropriate to realise the primary function of a BESS without huge amount of power losses.

SoC of a battery is one of the most essential parameters in a BESS, which determines the ratio of present level of charge of battery to the nominal capacity. In [14] and [66], SoC has been employed in a secondary power management control algorithm to ensure the level of charge is maintained in an acceptable range. There are some main drawbacks of neglecting the battery's SoC, which includes battery aging degradation, no protection for overcharge/over-discharge, and unable to estimate the remaining energy of the battery. The SoC is permitted to range from 20%-80%, as a preliminary setting [67]. In the simulation model, to simplify the analysis, the BESS stops charging/discharging if the level of charge is out of the safe range. In other words, the dc MG system in the thesis is expected to operate in PV standalone mode rather than battery mode.

Table 3.1 Technical specifications of the Lithium-ion battery

Parameter	Value
V_{BAT}	$48\ V$
$Battery\ capacity$	$250\ Ah$
$Initial\ SoC$	50%
$Battery\ response\ time$	$30\ s$
$Fully\ charged\ voltage$	$56\ V$
$Cut-off\ voltage$	$36.08\ V$

The system specifications of the BESS are presented in Table 3.1. The nominal voltage of the battery is set to 48 V. Huge battery capacity allows the battery to be discharged at 50 A in 5-hour. This rating is appropriate for the use of stabilising the dc MG during periods of low PV generation. The voltage is increased to 56 V when the battery is fully charged. The cut-off voltage is set to 36.08 V. The generic battery model can be simulated based on the above parameters. It is used to observe the dynamic response performance in islanded battery mode.

3.4.1 Bi-directional DC/DC Converter

Basically, the bi-directional dc-dc converter is used as a power converter in an islanded dc microgrid for integrating the single dc bus alongside storage devices such as BESS and supercapacitor. This circuit comprises two switches (MOSFETs), an inductor, an input capacitor for boost side, and a filter capacitor for buck side [63]. As shown in Figure 3.6, the schematic diagram of this power converter can be observed [65]. The input voltage is the dc-

link voltage, whilst the output dc voltage is exactly the battery voltage. In case of discharging, the input voltage of the converter is now battery voltage, and vice versa. It is capable of transmitting power in both forward and reverse directions, operating in either buck or boost mode.

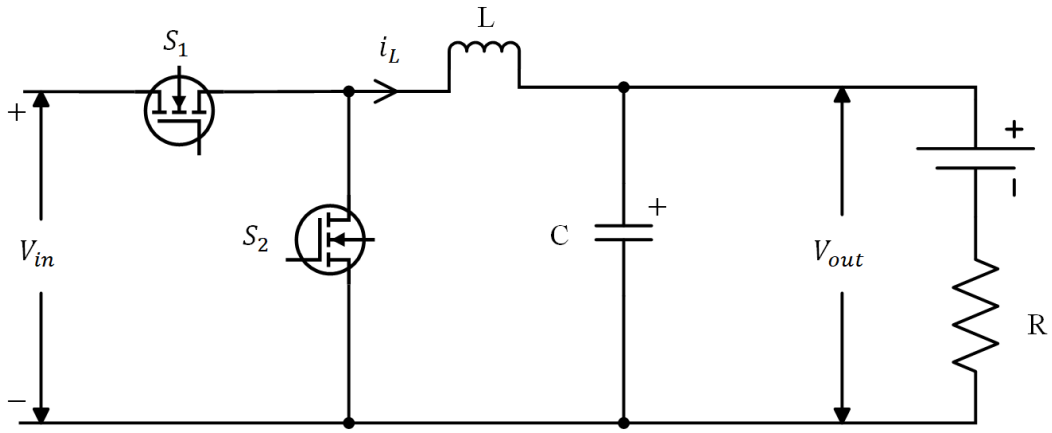

Figure 3.6 Topology of a bi-directional dc/dc converter [65].

It can be assumed that both switches in the simulation model are ideal, which means there is no turn-on or turn-off delay time. This is commonly known as deadband. As mentioned earlier, it is vital to include the impacts of ESRs on the inductor and capacitor to significantly reduce the overshoot of the step response. To generate a duty ratio to control the electrical circuit, a classical cascaded control loop is applied to simultaneously manipulate the dc bus voltage and battery current. The control algorithm would be an outer voltage loop and inner current loop each associated with a PI controller, respectively [65] and [68].

The study in [47] demonstrated the control strategy of a bi-directional dc-dc converter in both charging and discharging mode, as can be seen from Figure 3.7. The key difference of the outer voltage loop would specifically rely on the mode of operation. In charging mode, the battery voltage is the fundamental parameter to be manipulated to prevent overcharging issue as a first step. Outer PI controller strengthens the ability of voltage loop to minimise the error and to compute an appropriate current value for the inner loop to track. A saturation block is implemented to limit the current reference to a tolerated level in relation to the specifications of BESS, following the primary voltage loop. A basic secondary current loop with a PI compensator is used to achieve the desired current. However, in discharging mode, the major objective of the voltage loop is to restore the dc bus voltage to nominal value. It is subject to the maximum available discharging current of the battery and measured battery voltage. As

usual, the outcome of the outer voltage loop would be the reference current. The control algorithm of a bi-directional converter generates a duty cycle to control the ON/OFF operation of the switches, where switch 1 (S_1) applies duty ratio D and switch 2 (S_2) applies complement of duty cycle (1-D).

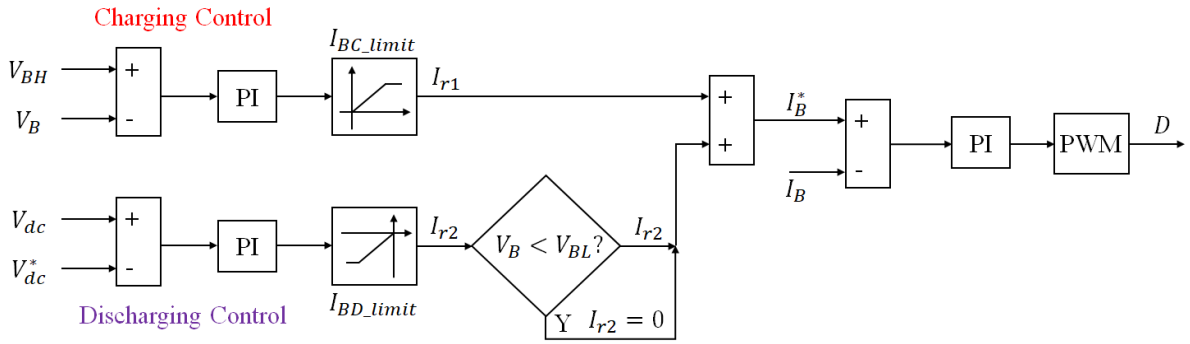

Figure 3.7 Control diagram of a battery's converter in charging/discharging mode [47].

The power flow heavily depends on the deviation of the dc bus voltage in an islanded dc MG. For example, the rise in dc-link voltage representing additional power should be stored by the battery for regulating the dc bus voltage. This in turn states that the multi-loop control technique instantaneously transfers the power to the Lithium-ion battery in buck mode. However, energy can be delivered from battery to the load in which the converter is operated in boost mode [69]. In this scenario, it is usually because of the low electricity supply of PV arrays. An adequate energy can therefore be fed into the consumers' loads to meet the local demands. No communication agent between power sources and loads is required in battery mode, since the primary variable dc-link voltage indicates the present power level of the dc MG system.

There are two modes of operation for the bi-directional converter. In buck mode, when switch S_1 is ON and S_2 is OFF, the energy is transferred from the dc bus to the battery. Switch 2 acts as a diode which is exactly the same as the diode in a step-down dc/dc converter. Therefore, when S_1 is OFF, S_2 is turned on for the inductor to continuously supply power to the dc load. In boost mode, the battery charges up the inductor with the help of S_2. When S_1 is ON and S_2 is OFF, sufficient power can hence be delivered to the dc bus. This in turn behaves as a step-up dc/dc converter. In practice, a deadband for switching operations is implemented to ensure one switch is OFF before turning ON the other switch. Regardless of how the converter operates, a filter-capacitor has to be associated with input side and output side, respectively. This provides a platform for the bi-directional circuit to operate in either buck or boost mode.

To develop a bi-directional dc/dc converter in MATLAB/Simulink, it is mandatory to calculate the capacitance and inductance of the circuit. The value of the inductor can be obtained by (3.2), where the circuit is assumed to be performed in boost mode. The capacitance on the load side is thus computed by (3.3). Similarly, the value of the filter capacitor connected to the battery is obtained in buck mode. The formula is derived as

$$C1 = C_{buck} = \frac{\Delta I_L}{8 \times f_{sw} \times \Delta V_c} \tag{3.4}$$

In order to evaluate the performance of the converter, a fixed duty ratio can be inputted to the switches S_1 and S_2. The characteristics of this system can usually be observed in the step response, for example, overshoot, settling time, and SSE etc. Taking these parameters into account, manual tuning of a PI controller can be undertaken to optimise the controller settings. Eventually, the BESS is interconnected with the dc bus in an islanded dc MG to behave as a dominant energy storage device in battery mode.

3.5 Chapter Summary

This chapter presents a detailed description of the PV-based dc MG system to develop a simulation model to simulate the step response in different scenarios, including PV standalone mode and islanded mode. In the beginning, the mathematical model of a PV array is demonstrated based on the parameters of the real commercial products in industry. This PV model benefits from high flexibility to accommodate with designated load demand. To validate the effectiveness of the proposed V-dp/di method, PV sources with two levels of power have been established to realise proportional power balancing with the support of predefined droop coefficients.

It is compulsory to design a classical dc-dc boost converter to ensure the desired output voltage of the PV system, which simply means voltage reference value in a single-bus dc MG. The design of a step-up converter can be observed in this chapter for reference, following the description of the working principle. The boost chopper is used to deliver the PV power to local loads and/or battery via the dc bus. It is concluded that the implementation of ESRs has a huge impact on the suppression of unusual overshoots in a dc-dc converter.

Last but not least, the importance of a BESS in an islanded dc MG system is critical due to the intermittent nature of PV sources. A lithium battery with a traditional bi-directional dc-dc converter can be observed in this chapter, which implies the capability of absorbing surplus power or providing sufficient energy in a dc MG. A cascaded control loop is compulsory for manipulating the dc-link voltage and battery current simultaneously. SoC of a battery is a key concern of a BESS and therefore the system is assumed to be unavailable when the SoC is over 80%. The BESS is temporarily disconnected from the dc MG system. As a result, this forces the MG to operate in PV standalone mode. The above scenarios are simulated in Chapter 6.

Chapter 4. Comparison of Conventional and V-dp/di Droop Control Methods

4.1 Introduction

DC-DC converters are commonly used in dc MG systems to integrate PV arrays alongside BESS and local consumer loads. A PV system is capable of transmitting solar power to the DG network, which only allows unidirectional flow of current. Recently, the increase in PV penetration has become one of the most critical challenges in the development of islanded dc MGs [2], [10], [70]. There is a purpose for power curtailment and increase in total capacity, however, the implementation of large-scale lithium BESS in an islanded dc MG is cost ineffective and complicated in both residential and commercial uses. The BESS has low capacity, supplying continuous load current for 5-hour, so that the cost of battery storage can be minimised. During periods of high solar PV output, it is crucial for PV sources to take part in constant power generation [71], [72]. The algorithm is to restrict the overall solar PV production to a certain level so that the dc-link voltage can be regulated, regardless of how the supply exceeds demand. In simple terms, this can reassure a stable operation of the islanded dc MG system under significant changes in weather conditions and/or loads, in case of low demand. As aforementioned, dc-link voltage regulation and proportional power sharing among PV arrays are the two main objectives of common decentralized control methods. A decentralized coordination method does not acquire any neighbours' data to calculate the average common bus voltage across the dc MG, and hence the plug-and-play capability is the key advantage of this algorithm.

The major control strategies of PV generators in an islanded dc MG system are reviewed. This contains the traditional MPPT algorithms, conventional droop control strategies, as well as the proposed V-dp/di control in this thesis. The classification and comparison of different MPPT techniques are demonstrated. In the meantime, the benefits and drawbacks of various general approaches will be presented in detail. The selection criteria of an appropriate control method mainly depend on the specifications and requirements of the PV systems. These details will be discussed in the following sections.

4.2 Operating Principle of Traditional MPPT Algorithms

In literature, the traditional control scheme for PV standalone systems is classified into two parts. The first control algorithm usually applies a single loop voltage control method to

restore the voltage, which in turn curtails part of maximum solar power to stabilise the overall system. The second MPPT algorithm is used for maximising the available PV power if applicable. As shown in Figure 4.1, the block diagrams of voltage, current, and direct duty ratio control are presented. PI controller is the most commonly used controller in MPPT algorithms. A typical example of employing a PI controller in MPPT method can be observed in [73]. The operation mode can be determined by the measured dc-link voltage, but the mode adaptive control suffers from rapid fluctuations if the feedback voltage oscillates around the reference value. In the end, this creates confusion for the PI controller to minimise the unpredicted error by incrementing the integral term, resulting in system stability issues. This is commonly referred to as integral windup.

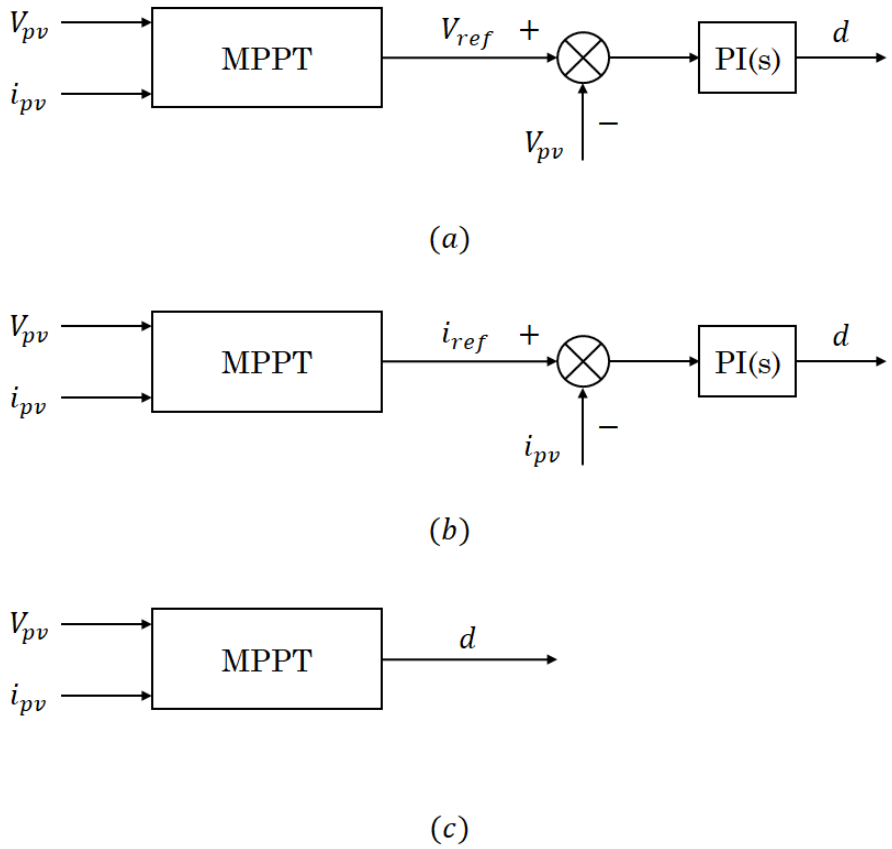

Figure 4.1 Control structure of three P&O MPPT algorithms. (a) PV voltage control. (b) PV current control. (c) Direct duty ratio control.

Furthermore, there are some drawbacks of the traditional MPPT algorithms. In terms of current control, it is incapable of tracking a MPP under significant change in solar insolation. The details of the experiment can be referred to [71]. The authors demonstrated that the short-circuit instability turns out to be a problem of current MPPT control. A possible explanation

for these results might be slow dynamic response of PV arrays. In case of decrease in irradiance, the desired PV current is lower than its feedback value. The PV current would be unable to change instantaneously, however, the P-I characteristics under significant change in irradiance results in lower short-circuit current which is close to array output current.

For the direct duty ratio control, it is one of the perturb and observe (P&O) methods without the need to employ a proper compensator. The duty cycle of the dc-dc converter is used as the primary control parameter to implement a P&O MPPT algorithm. In an islanded PV-based dc MG, the control strategy accommodates with all weather conditions so as to maintain robustness and stability of the system. In [74], they highlighted the confusion of direct duty ratio control during fast changes in solar insolation. Since the dc bus voltage of the MG has a limited range of values to control, this is one of the key characteristics of the direct duty ratio control which should be aware of.

In an islanded dc MG, it is considered as a complicated system in which a PI controller is the minimum requirement for a comprehensive control scheme. Indeed, voltage MPPT control is the most commonly used MPPT algorithm. In this scenario, both dc bus voltage and PV voltage have to be regulated simultaneously. But the fundamental rule of a multi-loop control is that the response speed of inner loop is supposed to be at least ten times faster than the outer loop, so the overall control system works effectively. In [75], they reported that the implementation of P&O algorithm under fast changing irradiance leads to overshoots and additional power losses. Furthermore, the confusion relating to irradiance reduction and system dynamics is found in [76]. These two factors are the top challenges of a dc MG. To conclude, all of these classical MPPT algorithms are inappropriate for the application of a PV-based dc MG system, particularly in an islanded mode. These results of using those traditional MPPT control in a dc MG can be observed in [10].

4.3 Working Principle and Limitations of Conventional Droop Control Techniques

This section describes the principle of operation of some common droop control methods, in which it can be implemented in an islanded dc MG system with multiple PV generators. To realise proportional power balancing and dc bus voltage regulation, Cai et al. established a control scheme for PV arrays to act as a dominant energy source in the PV standalone mode [10]. Solar power generation, in turn, is reduced to a lower level for restoring the common bus voltage of the dc MG. The conventional PV control algorithm benefits from comprehensive multi-loop control without having to define two single loops for different modes of operation.

However, during the simulation phase of the work, there exists some performance issues associated with the mechanism of the traditional PV droop control technique. The details and main limitations are illustrated in the following sub-sections.

Moreover, a comparison between V-I and I-V droop control systems is presented. These methods are intended for the use of a basic dc-dc converter, but the implication of the study has a significant impact on the backbone of the thesis. In theory, the key characteristic of a general cascaded loop is the existence of two PI controllers, one for the primary loop and the other for the secondary loop. In [50], they carried out a stability analysis of these two algorithms, with the help of pole shifting trajectory, to better understand the behaviour of the feedback control systems. The researchers suggested the droop control technique with a single PI controller yields an improved dynamic performance over the traditional cascade control described in literature. Moreover, there is a paper published by the authors in 2017 prior to the publication of conventional PV droop control method. This is a classical cascade control of a PV-based dc MG with two independent PI controllers [77], [78]. They analysed that the conventional control strategy with a single controller results in simplified design and improved transient performance. Therefore, the published works greatly support the preliminary conceptual framework of this thesis, and clearly explains the phenomenon behind the scene.

4.3.1 Classical Droop Control and MPPT Algorithms in a PV-based DC MG

Generally speaking, a traditional droop control system is made up of an outer droop loop and an inner current loop. A current feedback for the inner control loop is the most commonly used variable in power electronic converter. In [79], a decentralized coordination method with inner current control is implemented in a generalised dc MG system. However, this is inappropriate for the application of PV arrays due to poor tracking performance. In a PV-based dc MG system, there exist many limitations of utilising the PV output current to perform a basic MPPT function. As shown in Figure 4.2, an overview of the droop control scheme with inner PV current is presented to describe the traditional way of regulating the dc bus voltage and PV current simultaneously [10].

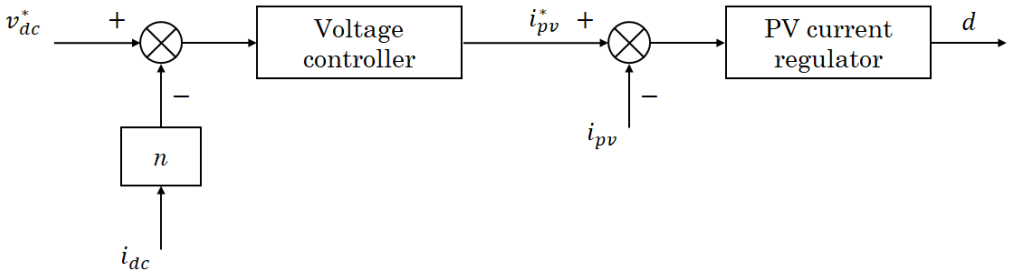

Figure 4.2 Control framework of a classical voltage droop control with inner PV current loop.

This is a combination of the traditional droop control implementation and PV current control algorithm, where n is a droop rate. In [71] and [74], the authors reported that the short-circuit stability issue often occurs during fast changes in solar irradiance. The results concluded that the system may collapse under short-circuit conditions. Furthermore, the study in [80] summarised that the dynamic tracking performance of a P&O MPPT algorithm is poor under abrupt conditions. A P&O current algorithm is developed in the simulation model to maximise the extracted PV power. The PV current could unusually reach the short-circuit value under rapidly changing irradiance, due to incorrect control decision. The variations in PV short-circuit current highly depend on the irradiance change, in which the stability issue occurs if the MPPT regulator response speed is low. In principle, the P&O algorithm takes a significant amount of time in milliseconds to search for the desired power level and its corresponding PV current. Hence, the main drawback of the P&O current MPPT algorithm.

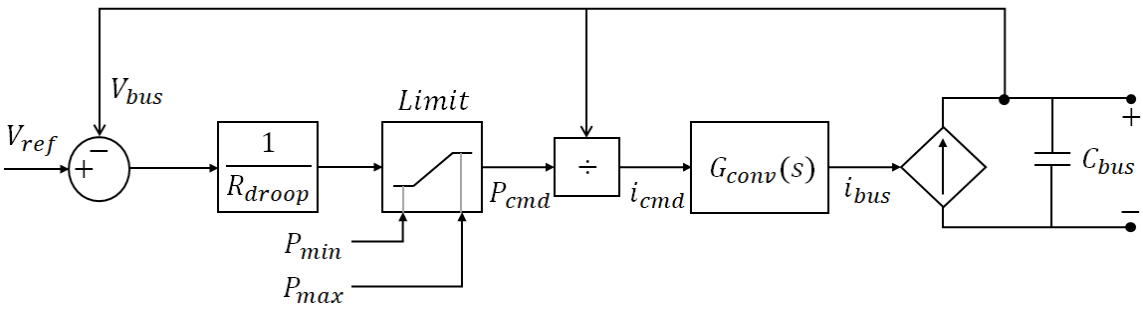

Figure 4.3 Mode-adaptive V-P droop control loop [49].

Indeed, the implementation of P&O MPPT scheme based on PV power could lead to the short-circuit instability, which mainly correlates with PV output current. As shown in Figure 4.3, the control diagram of a mode-adaptive V-P droop control method is present. In [49], the process is identified by the mode of operation, including utility-dominating, storage-dominating and generation-dominating modes. The droop control scheme is applied in a PV standalone mode, when both grid and BESS are unavailable, to produce

sufficient solar power to match the power consumption of a dc MG. In outer voltage loop, a set-point of the PV power is computed with the help of voltage deviation and droop rate. The saturation block is placed in front of the droop coefficient to limit the reference power. Finally, dividing the power by dc-link voltage, a reference current value is obtained to calculate the duty ratio. This in turn behaves as a P&O current MPPT algorithm. The P-I characteristics of a PV array indicate that same amount of solar power can be generated on the left/right of MPP, which means either high current or voltage is measured, and vice versa. In case of PV curtailment, this might fall into a short-circuit condition if it is improperly controlled. In terms of control aspect, this may cause confusion to the controller under abrupt irradiance change in the process of power limitation. In simple words, the MPP could be perturbed at least one step in the opposite direction and hence the mechanism of MPPT is most likely to be interrupted. P&O MPPT algorithm is usually confused by system dynamics and rapidly changing atmosphere conditions [71], [74]. In a dc MG, a promising dynamic response always outweighs the complexity of a feedback control system. As a consequence, it is meaningful to look into the alternatives, for example, INC and INR MPPT algorithms.

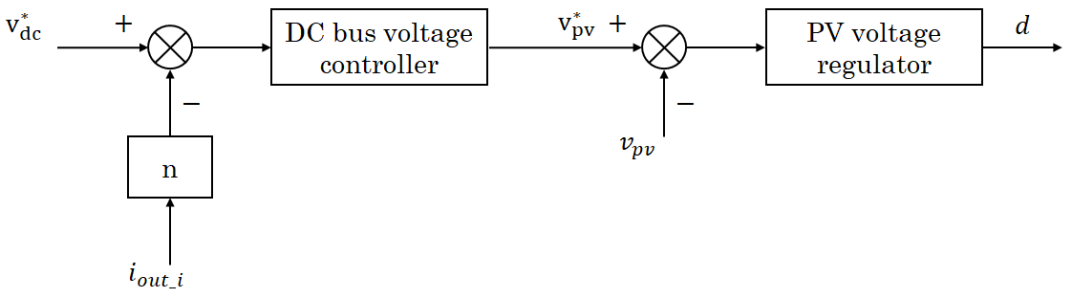

Figure 4.4 Traditional voltage droop controller.

Last but not least, P&O voltage MPPT algorithm is one of the most commonly used control strategies in PV power generation. As can be seen from Figure 4.4, a classical coordinated voltage droop control solution is demonstrated [10]. In case of low power demand, this method is used to restore the dc-link voltage and to produce a desired PV voltage for power curtailment. The output PV power would always be lower than its maximum available power regardless of the atmosphere conditions. The control loop is only activated in PV standalone mode, which is triggered by the feedback value of dc bus voltage. If the dc-link voltage is within an allowable range of values, the operation mode changes back to storage-dominating mode and thus the P&O voltage MPPT algorithm comes into effect. It has the advantages over the current and power MPPT algorithms.

This includes high stability, good stead-state response and ability to work under abrupt change in irradiance [71]. To sum up, the control system shown in Figure 4.4 usually offers a poor dynamic behaviour. All of the classical coordinated droop control techniques are inappropriate for the application of a PV-based dc MG, particularly in islanded mode.

4.3.2 Description of the Conventional V-dp/dv Droop Control Method

In [10], the conventional V-dp/dv droop control strategy was proposed to integrate voltage regulation with INC MPPT algorithm. As shown in Figure 4.5, an overview of the V-dp/dv droop control algorithm is presented [10]. The outer loop would be dc-link voltage regulator, followed by the primary INC MPPT algorithm with a traditional PI controller. The key advantage is no restriction on the type of the power converter.

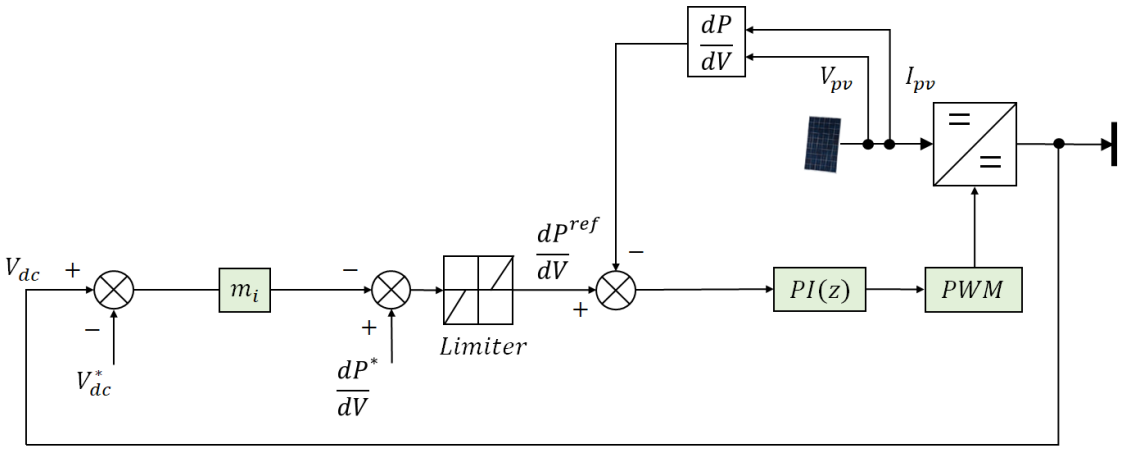

Figure 4.5 Control diagram of the conventional V-dp/dv droop control method [10].

To realise proportional power balancing, a linear droop coefficient is added to the voltage regulator for sharing energy consumption among multiple PV generators. It is the most common technique in decentralized control, in which communication agent is absent from the single-bus dc MG system. The line resistance and voltage drop in line are thus negligible. In grid-connected or battery dominant mode, the error of dc bus voltage is assumed to be zero, given the voltage is regulated by the single-phase inverter and/or BESS. As a result, the nominal dp/dv value at the MPP of P-V characteristics is null. A PI controller is deployed in the inner loop to minimise the difference between desired dp/dv and feedback value. The PV array always operates in a MPPT mode to harvest the maximum solar power under different weather conditions.

In PV standalone mode, for low power consumption, the droop control method acts as a voltage regulator to stabilise the voltage at a level which is higher than the nominal value. In theory, the dc-link voltage tends to increase if there is excess current flowing into the single dc bus. The maximum allowable dc bus voltage is about 5% of the reference value. A range of dp/dv values is equally distributed by the voltage deviation in the droop control. Therefore, the droop rate is used to identify the power required for the dc MG system with regards to the dc-link voltage deviation. A temporary reference voltage is calculated by the droop control equation to operate the MG in PV standalone mode. A seamless MG operation mode transition can hence be assured.

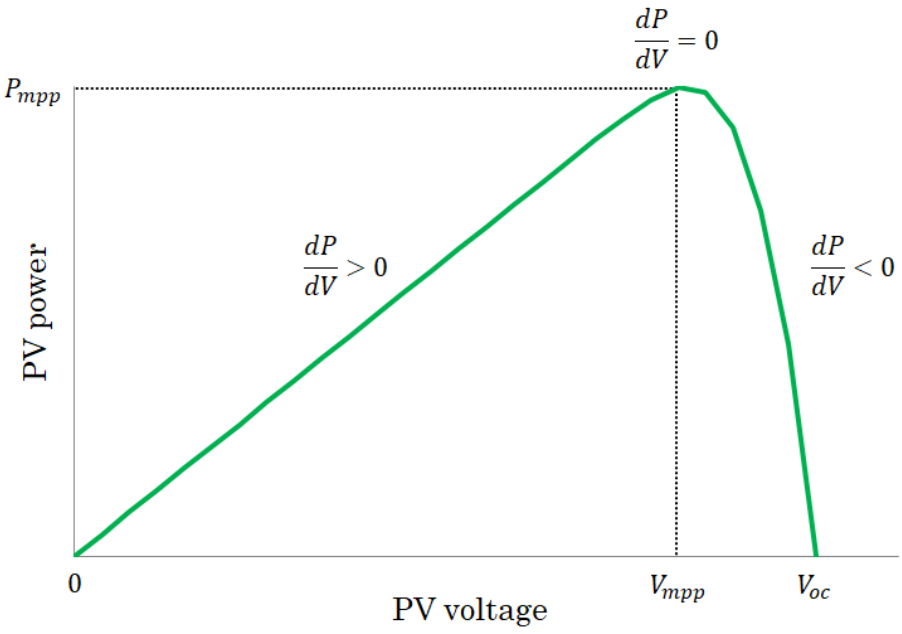

Figure 4.6 P-V characteristics of a PV panel.

Once again, the control framework of the conventional V-dp/dv droop control strategy can be obtained in Figure 4.5. The desired dp/dv value is first computed in the outer loop. In [10], the authors provided the formula to express the dp/dv compensator as

$$\frac{dP^{ref}}{dV} = \frac{dP^*}{dV} - m_i(V_{dc} - V_{dc}^*) \tag{4.1}$$

where $\frac{dP^{ref}}{dV}$ is the set-point of the inner dp/dv loop, $\frac{dP^*}{dV}$ is nominal value (zero) of dp/dv, m_i is droop coefficient of the i^{th} converter, and V_{dc}^* is desired dc voltage of the MG.

As shown in Figure 4.6, the P-V curve of a PV generator can be observed. In mathematical analysis, the curve has only one local maximum point. The maximum power point of the solar panel is found at which the dp/dv is zero. As can be seen from the graph, the power level can be represented by two dp/dv values, one for negative and the other for positive. In principle, a PV array starts to operate at the open-circuit voltage. As previously mentioned, a P&O MPPT algorithm is deployed to search for the MPP if a new value is larger than present value. However, the conventional dp/dv regulator is indistinguishable from INC MPPT method [81]. In principle, the tangent line with a slope of zero at MPP in INC MPPT algorithm is expected. The dp/dv formula is written as

$$\frac{dP_{pv}}{dV_{pv}} = I_{pv} + V_{pv}\frac{dI_{pv}}{dV_{pv}} \tag{4.2}$$

Considering the impact of MPP in the P-V curve, (4.2) can be rewritten as

$$\frac{dI_{pv}}{dV_{pv}} = -\frac{I_{pv}}{V_{pv}} \tag{4.3}$$

Equation (4.3) indicates the main objective of the INC MPPT method, which deduces the possibility of fluctuating around the MPP. By incrementing/decrementing the duty cycle of the dc-dc converter, the MPP can easily be reached. In the conventional dp/dv regulator, the dp/dv parameter is directly manipulated by the inner control loop which correlates to the theory of INC method. To perform the operating principle of the dp/dv controller, it is expected to restrict the range of dp/dv values. The PV array usually works on the right side of the MPP due to the behaviour of a solar panel, in which the value of dp/dv is always less than or equal to zero [10]. This means the desired dp/dv value cannot be positive. In simple words, with the use of traditional PV droop control strategy, the operating point should be on the right side of the curve. To conclude, the conventional method prevents short-circuit issue, as the positive part of the slope of a tangent line to the P-V curve is isolated.

Rearranging the terms of (3.1) it yields

$$Let\ x = \frac{q}{N_s AkT}$$

$$N_p I_o e^{xV_{pv}} e^{xI_{pv}R_s} + I_{pv} = N_p I_{ph} + N_p I_o$$

This is the mathematical equation of PV output current. In [55], the PV current equation includes a specific term to describe the impact of the equivalent parallel resistance on the PV array. However, in a small-scale PV source, the effect is considered to be minor. In the following assumption, this term is hence neglected to simplify the mathematical analysis.

By differentiating both sides with respect to PV output voltage, the equation can be computed as

$$N_p I_o \left(e^{xV_{pv}} \cdot e^{xI_{pv}R_s} \cdot xR_s \cdot \frac{dI_{pv}}{dV_{pv}} + e^{xR_s I_{pv}} \cdot e^{xV_{pv}} \cdot x \right) + \frac{dI_{pv}}{dV_{pv}} = 0$$

The above formula can be rewritten as the following compact form:

$$\frac{dI_{pv}}{dV_{pv}} = -\frac{N_p I_o x e^{x(V_{pv}+I_{pv}R_s)}}{1 + N_p I_o x R_s e^{x(V_{pv}+I_{pv}R_s)}} \tag{4.4}$$

$$where\ x = \frac{q}{N_s AkT}$$

Equation (4.4) can be applied in the dp/dv regulator to calculate the specific value of di/dv, as well as the variable dp/dv. In Subsection 4.3.3, one of the main challenges of deploying the conventional droop control strategy can be illustrated by equation (4.4).

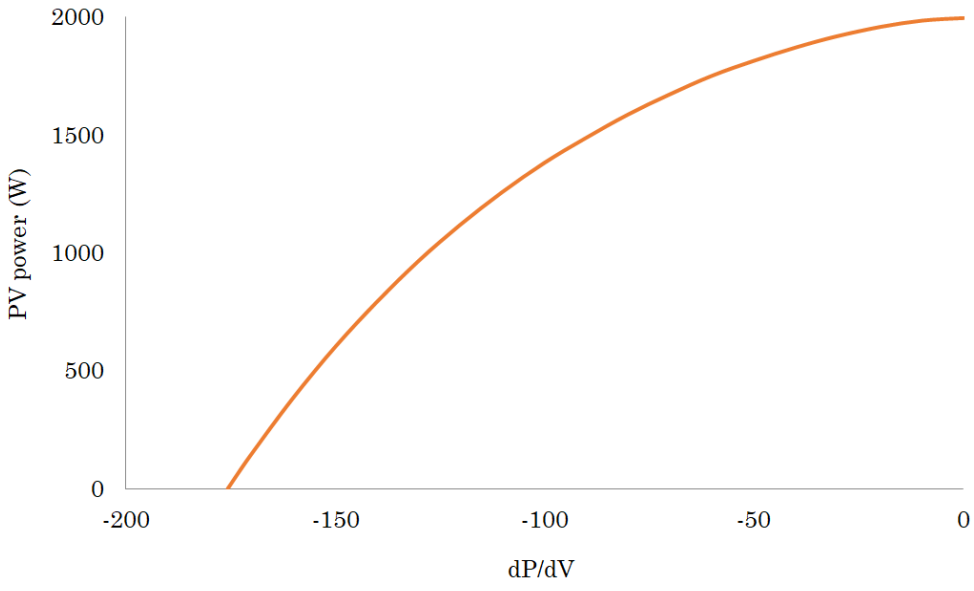

Figure 4.7 P-dp/dv curve of a 2 kW PV source.

The P-dp/dv curve of a 2 kW PV generator is shown in Figure 4.7. The value of dp/dv in different scenarios can be analysed using (4.4) to compute di/dv. By substituting the value of

di/dv into (4.2), the data is used to plot the graph of power versus dp/dv. Figure 4.7 illustrates the non-linear characteristics of a PV model, in which the model is linearized to form a straight line. This is known as droop coefficient. The droop regulator utilises the linearized model of a PV array to accomplish proportional power balancing among PV arrays in a fully decentralized coordination approach.

In [10], it is recommended to linearize the PV source and to calculate a linear droop coefficient, in order to share PV output power in proportion. A detailed elaboration of establishing a droop coefficient for each PV array is provided. However, there is no sharp distinction between droop controller and proportional controller in [10]. In theory, a P controller is implemented to help reduce the SSE and to improve the stability of a system. In a droop controller, however, the deviation is an indicator for the voltage regulator to calculate dp/dv. In case of energy oversupply, a new voltage reference is determined in the droop control loop and thus dc bus voltage always lies within the acceptable spread of values. Despite the fact that the framework of two controllers is exactly the same, having a good understanding of their own tasks ensures a feasible solution to a controller design with multiple objectives.

It can be observed in Figure 4.7 that the P-dp/dv curve can be linearized for the realisation of proportional energy balancing. In [10], an equation for the straight line of the curve is given. Taking the sign of the slope into consideration, the term becomes a negative slope as the open-circuit value of the dp/dv is negative. The straight line of the linearized PV model is arranged into the form $y = mx + c$. The equation can thus be expressed as

$$\hat{P}_{pv,n} = \hat{f}_n\left(\frac{dP}{dV}_n\right) = -\frac{P_{max,n}}{\left.\frac{dP}{dV}\right|_{V_{oc,n}}} \cdot \frac{dP}{dV}_n + P_{max,n} \tag{4.5}$$

where $P_{max,n}$ is the rated power of the nth PV array at standard test conditions, $\left.\frac{dP}{dV}\right|_{V_{oc,n}}$ is the dp/dv of the nth PV source at open-circuit voltage, and $\frac{dP}{dV}_n$ is the value of tangent line for the nth PV model. Hat operator means an estimated value of the power point on a straight line is considered. Subscript n denotes the variables for the nth PV array.

To proportionally share the output power among PV sources, the formula for achieving the main objective is written as

$$\frac{\hat{P}_{pv,1}}{P_{max,1}} = \frac{\hat{P}_{pv,n}}{P_{max,n}} \tag{4.6}$$

Equation (4.6) means the ratio of output power to maximum power for each PV source has to be approximately the same as others. In other words, the desired PV array power heavily depends on its maximum available power under varying atmospheric conditions, as well as the ratio of the present power to the total amount of maximum PV power. By substituting (3.3) into (4.5), it yields

$$\hat{P}_{pv,n} = \frac{P_{max,n}}{\left.\frac{dP}{dV}\right|_{V_{oc,n}}} \cdot m_n \cdot (V_{dc} - V_{dc}^*) + P_{max,n} \tag{4.7}$$

where m_n is a constant droop coefficient of the nth PV array. The maximum allowable voltage should be reached when the value of solar power is zero. The equation for calculating a droop coefficient can be expressed as

$$m_n = -\frac{\left.\frac{dP}{dV}\right|_{V_{oc,n}}}{(V_{dc,max} - V_{dc}^*)} \tag{4.8}$$

where $V_{dc,max}$ is the upper voltage limit of the dc bus in an islanded dc MG. Compared to the equation in [10], a negative sign is included in (4.8) to ensure the value of the droop coefficient is always positive due to negative dp/dv values in the operating range. This is in line with the illustration of (4.5). It turns out that (3.3) calculates a negative reference command for the inner dp/dv regulator to provide adequate solar energy.

4.3.3 Challenges and Limitations of Conventional Droop Control Strategy

Debate continues about the best coordinated control strategies for the power management of an islanded dc MG system. A decentralized control configuration has some advantages over the other two main strategies, namely centralized and distributed control. This includes absence of communication agents, easy to implement, plug-and-play capability, and no transition between two independent control methods. The classical coordinated control is used to produce the preliminary results in [10]. This yields an improved dynamic performance of an islanded dc MG. However, there are some drawbacks associated with the conventional V-dp/dv droop control technique such as poor transients and significant fluctuations in PV output power. In this section, the limitations and key challenges of the conventional V-dp/dv

control method are investigated. The thesis provides new insight into the decentralized coordination control, which indicates some of the theoretical problems occurred in [10].

First, the primary control parameter dp/dv can be described as a category of voltage reference control which is employed in the inner control loop, as shown in Figure 4.5. The PV output voltage has become a dominant variable to participate in proportional power balancing, as well as dc-link voltage regulation. The capacitor voltages are typically regarded as slower variables, compared to the current references in a cascade control system. In a PV standalone mode, the dc-link voltage of the dc MG system is expected to rise at the beginning of the voltage restoration. This is mainly because the conventional V-dp/dv control requires a voltage deviation to identify the correct amount of power to be generated by each PV array. When it comes to the inner control loop, the dp/dv is again a voltage reference signal which fails to comply with the fundamental rule of a general cascaded loop. In theory, the response speed of the inner control loop should be at least ten times faster than the outer loop in such a way that a promising dynamic performance can be achieved. This is the key mechanism of a multi-loop feedback control system. In this scenario, the inner dp/dv regulator takes longer than usual to reach a steady-state value in response to short-term transients. To conclude, it could result in a poor dynamic behaviour such as huge overshoot and long settling time which has an adverse impact on the fluctuations of PV power.

In [10], the results show that there are significant voltage overshoots and undershoots. The maximum overshoot at standard test conditions is around 4% of the dc bus voltage in their experiments. Another possible explanation for these results is that a classical PI controller instead of full PID controller is implemented to calculate the duty cycle of a dc-dc converter. Generally speaking, the derivative gain is mainly used to reduce the overall overshoot of the system dynamic response. In the simulation model, a PID controller is deployed to yield an improved system dynamics of an islanded dc MG. Meanwhile, it offers an opportunity to assess the feasibility of devising a novel control algorithm based on the method in [10].

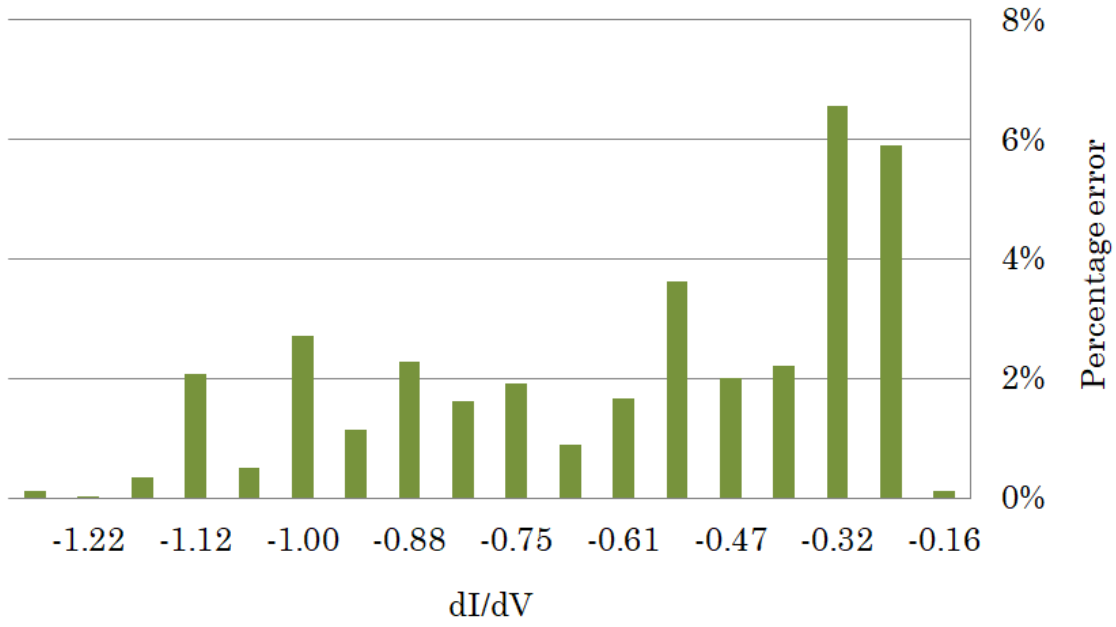

Figure 4.8 The percentage error in the measurement of di/dv.

Plus, it is challenging to calculate the actual value of dp/dv for a PV array, due to the intrinsic error arising from the non-linear relationship between PV array power and output voltage. It is noted that di/dv stands for the derivative of current to voltage. As illustrated in Figure 4.8, the percentage error of measured di/dv values is at an average rate of 2%. This is produced by measuring the di/dv in MATLAB/Simulink, and by calculating the expected di/dv by (4.4). The larger the di/dv, the closer the MPP. Surprisingly, the percentage error of di/dv around the MPP grew 6% on average. This result may be explained by the fact that these values are treated as a part of maximum PV power. The value of di/dv decreased more than 25% in the first 50 W range of a 2 kW PV source. Provided that the di/dv value around the MPP is small, the mode of operation should be MPPT mode where the PV output power is maximally harvested. It is worth to mention the impact of di/dv, since it is the key issue to calculate a precise value of dp/dv.

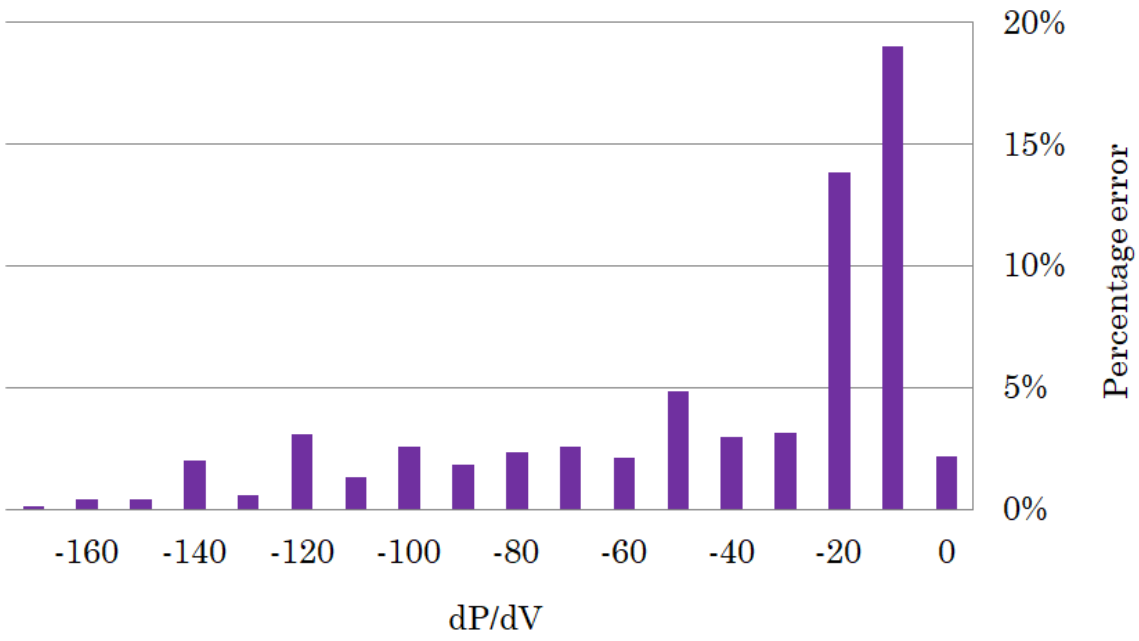

Figure 4.9 The percentage error of measured dp/dv value.

As shown in Figure 4.9, the percentage error between measured and calculated values of dp/dv on the right side of MPP is presented. The percentage error in Figure 4.9 is an absolute value. Zero value of dp/dv represents the MPP of a PV array. Due to the effect of di/dv, the first two values of percentage error of dp/dv dramatically rose 14% and 19%, respectively. The larger the dp/dv, the worse the accuracy. All of the remaining errors fall into a range of 2 to 4%. The parameter dp/dv is incapable of generating sufficient PV power to the load, because of lack of ability to compute a precise value of dp/dv in the feedback loop. It results in excessive power oscillations in the PV system. This is the major drawback of employing dp/dv in a decentralized control system.

To avoid the short-circuit problem, a PV voltage is expected to operate on the right side of the MPP in a P-V characteristics. It can be observed in Figure 4.6 that the PV voltage is in the range of open-circuit value and MPP, given the dp/dv value should be below zero. This can be accomplished by introducing a limiter to restrict the range of dp/dv, in order to ensure it is always equal to or less than zero. A steeper downward tilt to the line can be found in P-V characteristics on the right side of the PV curve. Consequently, the dp/dv is sharply declined with the PV power. This turns out an inevitable error obtained in Figure 4.9. The small variation in dp/dv results in a notable increase in power oscillations and thus a poor PV power quality.

In [81], an investigation into the step size for INC MPPT method was carried out. The rate of change of PV array power versus voltage is normalised in per-unit system. The operating region of the dp/dv regulator is only valid, at which the output voltage of PV source is higher than its voltage at MPP. The range of negative values of dp/dv is significantly varied with a small change in PV array voltage. However, the corresponded PV output power is greatly affected. In Figure 4.9, the graph clearly displays the intrinsic error between measured and actual values of dp/dv. The impact of power oscillations can partially be caused by the inherent error. Besides, in [81], there is a compromise between fast dynamic response and steady-state fluctuation, in which the issue associated with INC MPPT algorithm should be addressed. This implies some improvements can be performed by devising an advanced control scheme to realise fast system dynamics and excellent steady-state response. Sangwongwanich et al. indicated that the values of dp/dv on the right-hand side of the MPP are abruptly changed [71]. Last but not least, they provided the main downsides of implementing dp/dv regulator, including high power loss, huge power oscillations, and low tracking accuracy. The key drawbacks of dp/dv controller are mentioned in [81]. Eventually, this is the focus of the thesis to yield enhanced dynamic characteristics of an islanded dc MG.

A variable step-size Incremental-resistance (INR) MPPT algorithm was proposed in [82]. The traditional INC tracking method is one of the most commonly used MPPT algorithms in literature. Generally speaking, this benefits from high tracking efficiency and simple implementation reported in [82]. However, there is a trade-off between transient response speed and steady-state performance. To further enhance the overall performance of the MPPT method, some studies have suggested a variable step size to accommodate fast changing irradiance. A small step size is used in a steady state to suppress the oscillations. Plus, the maximum step size is employed to increase the dynamic response speed under significant change in ambient conditions. In [82], they conducted simulation and experimental studies to prove that INR method has a faster dynamic response and wider operating range than INC MPPT algorithm, leading to an excellent tracking accuracy during steady state. Given dp/dv can be used as a direct control variable to proportionally share the PV array power in [10], similar control algorithm with INR MPPT method should be able to be implemented.

4.4 Proposed V-dp/di Droop Control Strategy

A common approach to improve the dynamic and steady-state characteristics is adaptive PI control. In [50], Wang et al. proposed an adaptive PI control scheme to offer a substantial

improvement of the response speed in a dc MG system with parallel dc-dc converters. They carried out some experiments to understand the impact of increasing proportional or integral term in closed-loop pole trajectories. The increase in proportional gain leads to reductions in rise time and SSE. However, the research reported that a counter effect on eliminating the error signal with high proportional gain is observed in root locus analysis. The main drawback of a traditional PI controller is the compromise between system dynamics and SSE. Similar experiment to investigate the effects of rising integral term was carried out in [50], following the test of proportional term. Increasing the integral term eliminates the error in a steady state, but it causes huge oscillations of a step response. Besides, it is worth to highlight that an extreme value of proportional and/or integral gain could result in system instability. The adaptive proportional term heavily depends on the error signal of inner current loop. For instance, a large proportional gain is used for those errors above the threshold value, and vice versa. High complexity is the key disadvantage of this solution. Therefore, in the following sections, a novel decentralized control method based on a second differential term is presented to tackle those challenges.

To devise a novel voltage droop control algorithm, several attempts have been made to tackle the key challenges of the conventional droop controller. As previously mentioned, the selection of a primary control parameter should be reconsidered to perform proportional power sharing. The INR MPPT control technique is adopted in the proposed V-dp/di control method to yield an improved dynamic behaviour and steady-state performance of the dc MG system. Equation (4.10) shows that the control variable of dp/di is indeed the dv/di, which is exactly the same control parameter as the one in INR MPPT control.

The V-dp/di droop control method based on a second derivative of power to current is proposed in this study, as shown in Figure 4.10. Basically, the droop control implementation consists of dc bus voltage controller, dp/di regulator, and steady-state compensator. First, with the help of droop coefficient, the voltage restoration can be attained by linearly increasing the desired dc-link voltage, at which the set-point of dp/di rises from zero. The zero value represents the MPP of the PV array. When the load demand is less than the maximum available power generated by PV arrays, the dc bus voltage can be linearly increased in order to output a value of dp/di. This reference value is used to produce sufficient PV power to the load and therefore the new power level should be less than the MPP. During steady state, the second differential term is activated to further minimise the SSE. Eventually, a classical PID controller is used for achieving the desired dynamic response. The key features of the

proposed droop control strategy are absence of digital communication agent, smooth transition between operation modes, and excellent steady-state performance. Similar to the study in [10], a droop coefficient is deployed to linearize the P-I characteristics and control the solar power in proportion under ambient conditions. For simplicity, the power sharing algorithm for multiple PV modules is assumed to be a linear relationship in a decentralized approach, in which a satisfactory transient response is obtained in the results section.

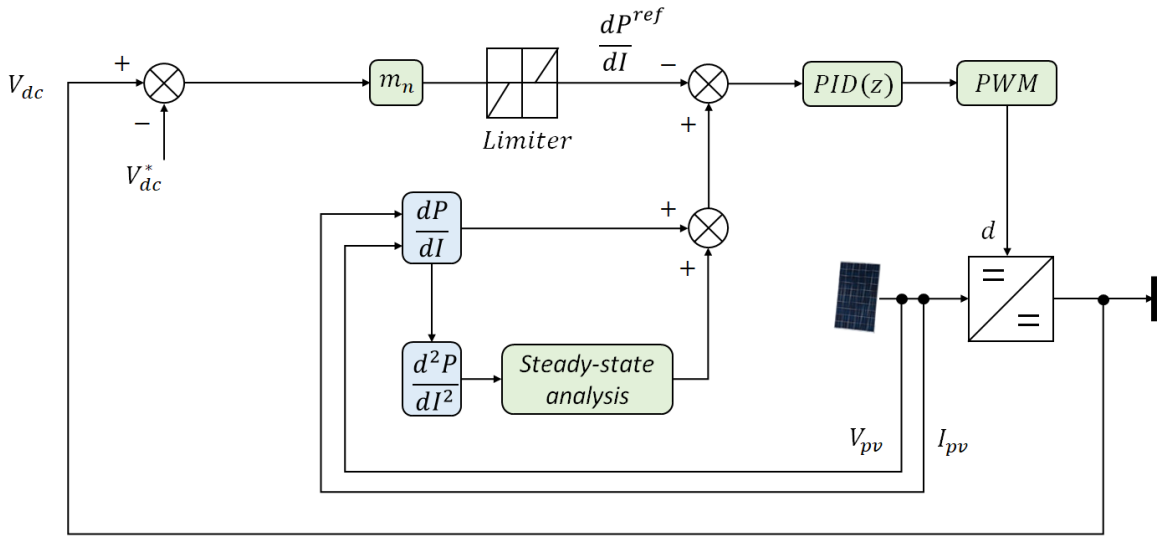

Figure 4.10 V-dp/di droop control strategy based on second differential of current approach.

4.4.1 Working Principle of Control Parameter dp/di

To understand the fundamental theory of dp/di, it is crucial to review the characteristics of PV array and integrate with voltage droop controller and steady-state compensator. The term dp/di stands for the derivative of PV power with respect to current. In contrast to the conventional V-dp/dv droop control, the proposed V-dp/di control strategy is based on a current approach. It would be a good approach for a cascaded loop to ensure the inner loop is at least ten times faster than the outer loop. As can be seen from Figure 4.11, the P-I characteristic curve of a PV source is introduced to illustrate the electrical behaviour. At the beginning of the generation process, the PV current starts from zero at which the PV output voltage is the open-circuit value. It can be observed that the maximum PV array current is reached in which the dp/di is zero. This refers to the local maximum point of a curve. As a result, the operating point of the PV system has to be on the left side of the P-I curve, in which the slope of dp/di grows steadily with a wide range of PV current values. This is known as gentle slope. In a mathematical analysis, compared to the P-V characteristics in Figure 4.6, the change in PV output power is gradually increasing with a broad range of PV current

values. A particular amount of PV power is perfectly represented by the PV current, of which the value of dp/di can be used to manipulate the solar power to supply the consumer load. The dp/di regulator has to match that of the set-point with minimal SSE, in order to produce adequate electrical energy.

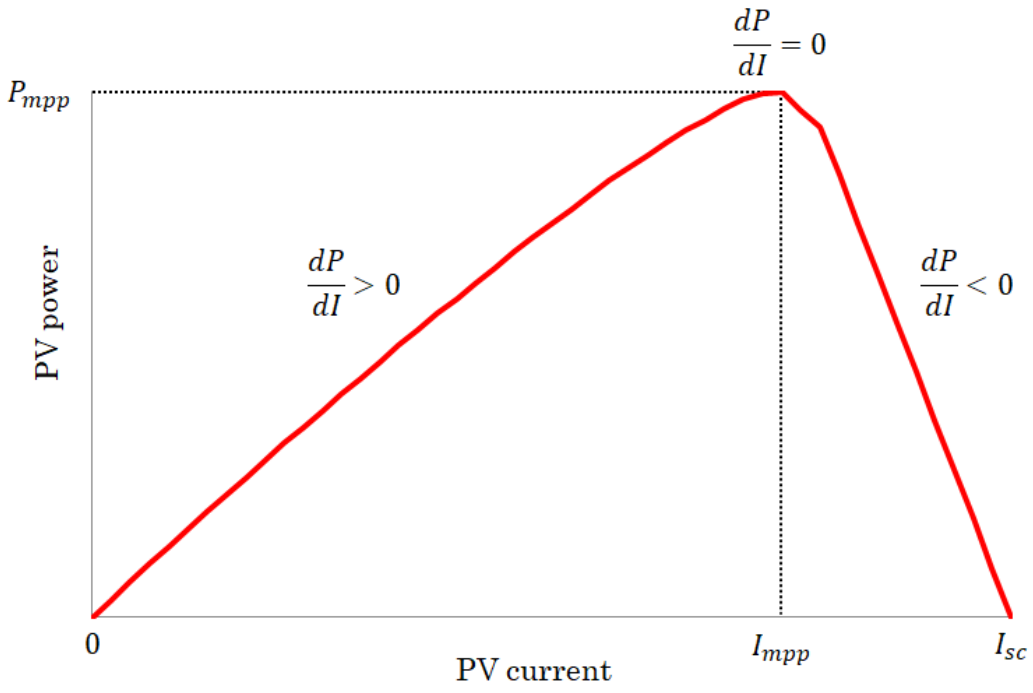

Figure 4.11 P-I characteristics of a PV array.

In [82], the authors summarised that the INR MPPT algorithm has a faster dynamic response speed than INC method. Meanwhile, the variable step size INR MPPT scheme takes advantage of high tracking accuracy to curtail the PV array power. The inner control variable of the proposed V-dp/di method is similar to the design of variable step size. Indeed, the value of dp/di tracks the common bus voltage deviation in every switching cycle, which turns out an improved steady-state performance and better dynamic response with the INR MPPT algorithm.

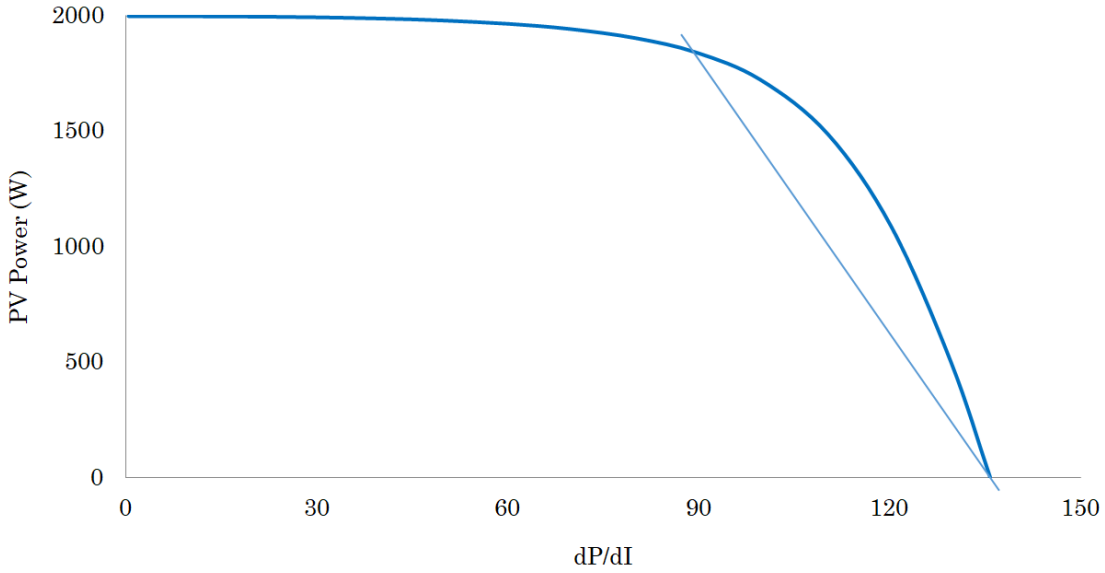

Figure 4.12 P-dp/di characteristics of a PV array.

The P-dp/di characteristics of the 2 kW PV source can be observed in Figure 4.12. The characteristic curve can be expressed as a proportional relationship, at which it has a solar power below approximately 90% of MPP (1.8 kW). There are some inherent power losses in a standalone PV system, including converter losses, measurement errors, and margin of error of MPPT algorithm. Generally speaking, the practical maximum threshold value of PV power over 90% is assumed to be a MPP. The linearized part of the curve benefits from a clear representation of dp/di to a specific PV power level, and thus the system response is less affected by the confusion due to small percentage error. In an islanded dc MG, especially in PV standalone mode, it is of principal importance to enhance the dynamic response performance. The use of a novel control variable dp/di results in a significant increase in MPPT tracking accuracy, in which the results can be observed in Figure 6.19. The graph shows that there is no voltage overshoot under step irradiance change. Meanwhile, the power ripple in V-dp/di method is found to be less than the power fluctuations in conventional V-dp/dv method. The details can be referred to Section 6.4.2.

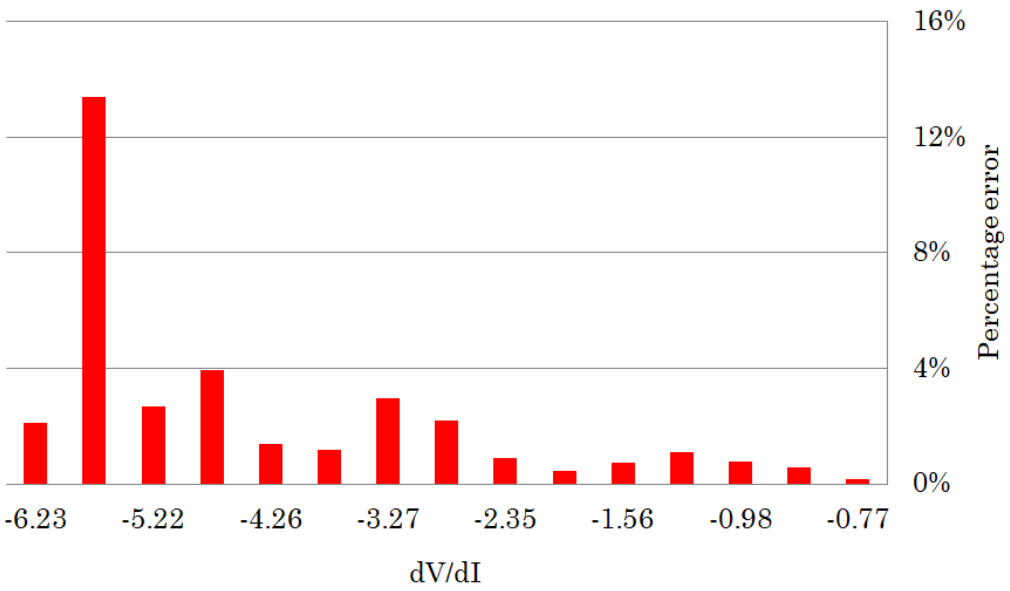

Figure 4.13 The percentage error of measured dv/di value.

To make a comparison of the conventional dp/dv and proposed dp/di methods, this is the first study to investigate the key factors that assess the overall dynamic characteristics of the control systems, to the best of authors' knowledge. One of the major concerns addressed in the conventional V-dp/dv droop control strategy is the effect of percentage error in experimental value. The theoretical value of dp/di is incremented with an interval of 10. Afterwards, the measured value in MATLAB/Simulink can be used to calculate the percentage error between ideal and measured values for each dp/di. As shown in Figure 4.13, the mean percentage error in dv/di drops to a record low of 1.3%, except for two extreme values. The averaged percentage error of di/dv in Figure 4.8 is 2%, which is much larger than proposed dv/di. It could be argued the extreme values may lead to the system stability issues, since the results with a local extremum of 13% are statistically significant. An explanation for this would be that the PV array is operating in MPPT mode at this particular point. The output PV power of these two dv/di values is 0.5% less than its rated power, which evidently shows the present mode of operation. Nevertheless, in the INR MPPT algorithm, the desired value of dv/di at MPP is zero. It is reasonable, therefore, that these extreme values can be negligible in voltage regulation.

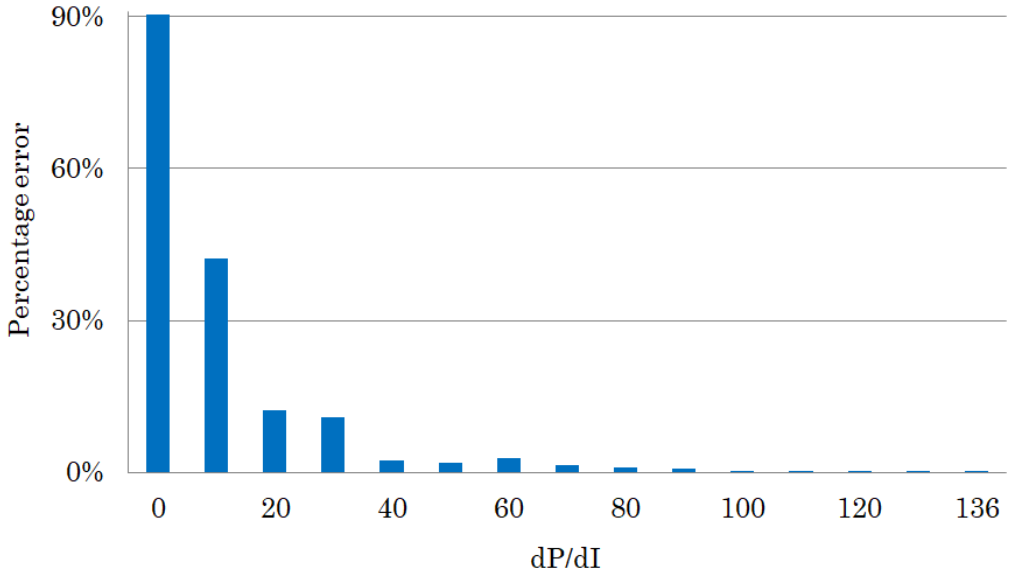

Figure 4.14 The percentage error in the measurement of dp/di.

As can be seen from Figure 4.14, the percentage errors of actual dp/di value by an increment of 10 are presented. Consistent with previous findings, Figure 4.14 confirms that the INR algorithm in MPPT mode can produce enormous percentage errors in measured dp/di. However, it is undoubted that the power ripple of PV generator remains at a low level of around 5% in the worst scenario. The larger the dp/di, the better the accuracy. The average percentage error of dp/di falls down 1 percentage point to average 1.1%, and a target of a 50% reduction in error have been met. Surprisingly, the control term dp/di performs much better than conventional dp/dv in voltage restoration mode. It is effortless to calculate the correct value of the inner loop variable due to the negligible error in the non-linear P-I curve. The devised V-dp/di control strategy is capable of reducing the PV power oscillations. The proposed droop control method takes advantage of low percentage error. This is the main reason why dp/di has become a new representation of PV output power to be employed as the primary closed-loop variable.

4.4.2 Calculations of dp/di and Droop Coefficient

This subsection introduces, in detail, the mathematical model of the proposed V-dp/di control algorithm. As described in Section 4.3, in [10], a detailed modelling of the conventional V-dp/dv control is illustrated. In principle, the proposed control strategy can be analysed in a similar approach to fully understand the design and theories. In Section 4.3.2, the formula for PV array current is differentiated with respect to PV voltage in order to obtain (4.4). To

reduce the computational complexity, the reciprocal of (4.4) is the exact representation of dv/di. The equation can be rewritten as

$$\frac{dV_{pv}}{dI_{pv}} = -\frac{1 + N_p I_o x R_s e^{x(V_{pv}+I_{pv}R_s)}}{N_p I_o x e^{x(V_{pv}+I_{pv}R_s)}} \tag{4.9}$$

$$where\ x = \frac{q}{N_s A k T}$$

The term dv/di is the most complicated part in the mathematical expression of the devised variable, as the conventional dp/dv method suffers from huge SSE. In [10], a note of caution is due since the equation is inconsistent with the simulation model. For this reason, (4.9) is validated by the simulation study to confirm the feasibility of the mathematical analysis. As shown in Figure 4.13 and Figure 4.14, these outcomes support the idea of implementing dp/di. Therefore, the expression for calculating dp/di of a PV array can be obtained as

$$\frac{dP_{pv}}{dI_{pv}} = V_{pv} + I_{pv}\frac{dV_{pv}}{dI_{pv}} \tag{4.10}$$

Equation (4.10) is implemented in Simulink to conduct a simulation study, in which the form of this equation is validated in [83]. The feedback value of dp/di should be computed in every duty cycle, according to the designated switching frequency, for the purpose of generating adequate PV power. Taking signal processing into consideration, a piece of code can be written in this form to calculate dp/di. Another definition of dv/di would be the slope of line tangent of P-I curve. It implies, by subtracting the previous value from the present value, the PV power derivative is comfortably obtained. When it comes to the experimental study, it is important to reduce the number of steps of the compilation process for accelerating the control algorithm. There are two critical factors associated with (4.10) to affect the steady-state performance of the dc MG system, including measurement errors and quality of dv/di. The concern is, when the inner loop parameter is manipulated, the PV output power does not comply with the desired amount if dp/di contains enormous error. Hence, the issue of power oscillations may arise. Provided that the dv/di measurement is accurate, it has become the most prominent control variable for the decentralized control algorithm to implement.

Droop control is the most commonly used solution in a decentralized coordination method to realise proportional power sharing among PV arrays, with the help of droop coefficient. In the event of power surge, an overvoltage exceeding the dc-link voltage reference value usually

occurs in a PV standalone system. Eventually, curtailing the PV array power is mandatory to match with the local load demand. The mechanism is that the use of dc bus voltage deviation computes the set-point for dp/di, which in turn represents the PV power. As can be seen from Figure 4.10, the droop coefficient is multiplied by the voltage deviation to calculate the desired value of dp/di. The equation is obtained as

$$\frac{dP^{ref}}{dI} = m_n(V_{dc} - V_{dc}^*) - \frac{dP^*}{dI} \tag{4.11}$$

where $\frac{dP^{ref}}{dI}$ is the reference value of dp/di, m_n is the droop coefficient for n^{th} PV module, and $\frac{dP^*}{dI}$ is the rated dp/di. Figure 4.11 highlights the zero slope of P-I characteristics at MPP, which is exactly the nominal value of dp/di.

The non-linear characteristic of a PV module can be described by a linear equation to reduce the computational complexity of the mathematical function. In [84], the writers introduced some key terms to elaborate the meaning of a linearized model. Literally, second or higher order ac variation terms are eliminated in the process of linearization, in which it is left with dc terms and first order variation terms. All the non-linear terms are neglected to make the mathematical operations more accessible. A straight line is used in P-dp/di curve to express the linear relationship. Considering the standard form of a straight line (y = mx + c), it yields

$$\hat{P}_{pv,n} = \hat{f}\left(\frac{dP}{dI}_n\right) = -\frac{P_{max,n}}{\left.\frac{dP}{dI}\right|_{V_{oc,n}}} \cdot \frac{dP}{dI}_n + P_{max,n} \tag{4.12}$$

where $\left.\frac{dP}{dI}\right|_{V_{oc,n}}$ is the dp/di value at open-circuit voltage of the n^{th} PV source, and $\frac{dP}{dI}_n$ is the value of dp/di for the n^{th} PV array.

Substituing the open-circuit voltage of the PV array into (4.10), one obtains

$$\left.\frac{dP}{dI}\right|_{V_{oc,n}} = V_{oc,n} \tag{4.13}$$

Compare (4.13) with (4.2), it can be summarised that the mathematical operations of the proposed V-dp/di method are simpler. Equation (4.13) is critical for computing the linear droop coefficient for the PV curve. The issue of measuring dp/dv is explained in Section 4.3.

However, the initial droop coefficient for dp/di is effortlessly achieved in (4.15). By substituting (4.11) into (4.12), the equation can be rewritten as

$$\hat{P}_{pv,n} = -\frac{P_{max,n}}{\left.\frac{dP}{dI}\right|_{V_{oc,n}}} \cdot m_n(V_{dc} - V_{dc}^*) + P_{max,n} \tag{4.14}$$

Taking the initial operating state into account, the PV open-circuit voltage would be the maximum threshold voltage of the system. The formula for computing the droop coefficient is expressed as

$$m_n = \frac{\left.\frac{dP}{dI}\right|_{V_{oc,n}}}{V_{dc,max} - V_{dc}^*} \tag{4.15}$$

Equation (4.15) is the standard form for the computation of a reference droop coefficient. However, control engineers should always attempt to manually tune the droop rate in order to achieve optimal dynamic response. This is due to the fact that the calculated droop coefficient is a linear variable. It is similar to the prediction of a proportional gain in control theory and so manual tuning is usually found to be useful in optimising the voltage regulator. Moreover, a trade-off between the system stability and voltage deviation is seen as a challenge for engineers. The idea is supported by the papers in [10] and [70]. An increase in droop coefficient results in a reduction in voltage deviation, but an overall degradation of the system stability, and vice versa. It is vital to bear in mind that the upper limit of the dc-link voltage is usually restricted. This is always the first priority to be taken into consideration, since the dc-link voltage is indispensable for operating an islanded dc MG.

To begin with, the system dynamics of the cascaded loop depend largely on the inner dp/di regulator. Initially, the traditional PID controller computes the error value between the desired dp/di and feedback values. This error is processed by the compensator to calculate a duty ratio to drive the power MOSFET of the boost converter. It is noted that the second differential term is only included in the control loop during steady state. There exists a conditional signal to autonomously enable/disable the function of enhancing the steady-state performance, which is described in detail.

The second derivative of power to current is proposed to remarkably minimise the SSE, following the concern raised in the PV power fluctuations. During the steady state, it is

assumed that the SSE between final desired output and feedback value is eliminated with the support of PID controller. However, oscillatory response usually occurs due to the switching operation of a power converter. This is known as control fluctuations. The influence of voltage oscillations is a serious problem to a single-bus dc MG, as the voltage deviation is crucial for droop control. The oscillatory response of dp/di is affecting the dc bus voltage, given the inner loop usually reacts ten times faster than outer loop. The islanded dc MG system may collapse if the value of dp/di continues to fluctuate under steady-state condition. To provide a high quality steady-state performance of the entire system, it is essential to propose an advanced controller to significantly reduce the oscillations of dp/di, so that the overall quality of PV power and dc-link voltage can be improved. As shown in Figure 4.10, the equation for describing the error signal of dp/di is derived as

$$\frac{dP^{error}}{dI} = \frac{dP}{dI} - \frac{dP^{ref}}{dI} + \frac{d^2P}{dI^2} \tag{4.16}$$

where $\frac{dP^{error}}{dI}$ is the error signal of inner PID controller, and $\frac{d^2P}{dI^2}$ is the second differential of PV current to power.

The proposed dp/di regulator performs the basic function of manipulating the control variable, as well as the second differential term. In a steady state, the error of dp/di is supposed to be close to zero. Afterwards, the PID controller focuses on the further reduction in the change of dp/di, which is known as second derivative of PV power to current. If the line tangent of dp/di is regulated, then the steady-state performance of the dc MG will be improved, in particular the oscillatory response. There is a conditional signal to activate the second differential approach during steady state. Otherwise, it may slow down the transient response of the system. In the worst scenario, the use of second differential term leads to system instability. First, it is crucial to ensure that the system is in a steady state. Comparing the previous value with present feedback, any difference less than 0.125% can be analysed as steady-state oscillations. Meanwhile, the continuous low ripple should always be smaller than 0.5 V to represent the end of dynamic process. As can be summarised in Figure 4.14, the absolute error of dp/di is disappeared when the PV output power is below 25%. Therefore, the application of second differential approach is subject to a limited range of values, which is in between rated value and 25% of maximum power. This is the normal operating range for the dp/di regulator, at which the error value of dp/di is becoming significant to the controller.

4.4.3 Analysis of Operation Modes

This section introduces three key modes of operation in a PV-based dc MG, namely grid-connected mode, battery islanded mode and PV standalone mode, to understand how the proposed V-dp/di control scheme handles these challenging situations in the power management of solar energy. In [49], an adaptive decentralized control method is established to control various electrical elements based on the dc bus voltage. They defined some operation modes to give a detailed explanation of the dominant energy sources. However, the main drawback of implementing the control scheme is voltage fluctuations around threshold values. To prevent the inconsistency of the control strategy, the study mitigates the impact by avoiding voltage oscillations around the threshold value. In contrast, the proposed V-dp/di algorithm takes advantage of all-in-one control system, in which the solution accommodates with each operation mode. No mode switching is required in the proposed V-dp/di control strategy. If the dc bus voltage is less than or equal to 400 V, then the operation mode will be either grid-connected or islanded mode depending on the grid and battery. Otherwise, it is operating in PV standalone mode when the dc bus voltage is higher than reference value.

One of the most commonly used operation modes in a dc MG is grid-connected mode. In [49], it is summarised that the grid-connected converter would be the dominant energy source. In other words, a grid-connected single-phase inverter is the only component of the PV-based dc MG to maintain the dc-link reference voltage in grid-connected mode, regardless of how the battery or PV array behaves. The common bus voltage is always kept constant with the help of bi-directional grid-connected inverter. For the BESS, it may provide or store energy depending on the SoC and voltage of the battery. For instance, the battery is charged up once the SoC reaches an upper safety limit of 80%. The multi-loop in the grid-connected inverter adjusts the converter current to maintain the dc-link reference voltage. As a result, BESS is irresponsible for the dc bus voltage regulation in this case. A cascaded loop is suitable for extracting the surplus power from the PV source and grid, in which the outer loop controls the dc bus voltage and inner loop controls the battery current. In battery mode, a PV system harvests the maximum available power from the solar panels under the ambient conditions. The solar power generation is undertaken by implementing a traditional INC or P&O MPPT algorithm.

In an islanded mode, where connection to the utility grid is unavailable, BESS plays a critical role in restoring the common dc-link voltage at certain level, and balancing the load demand

and energy supply. The disconnection from the main grid results in a temporary loss of the most reliable voltage regulator. This is the key reason to install a BESS in a PV-based dc MG system to tackle the issues related to power outage. The study in [49] analysed that the BESS has become the major energy source of the dc MG system. The battery is capable of absorbing excess renewable power in case of low demand. Besides, it can supply adequate energy to the load during periods of low, or negligible power production from RES. The task of the PV array is exactly the same as usual, which harvests the maximum solar energy from the Sun. The function of voltage restoration in a PV system is disabled at this stage. As can be observed in Figure 4.10, when the feedback value is equal to the reference voltage, the value of dp/di is always zero. A horizontal tangent line represents the MPP of a PV array, and hence the framework of the proposed V-dp/di control algorithm for PV module remains unchanged in the battery islanded mode.

It can be assumed that the battery can be charged up in an islanded mode when the upper safe limit is reached, i.e. 80% of SoC level. This is commonly referred to as PV standalone mode. Both grid and BESS are unavailable to support the dc MG. The PV standalone system is made up of solar panels, power electronic converters, and individual consumer loads. As a result, the PV array has to act as a dominant power source in the PV standalone mode to participate in dc bus voltage regulation. The voltage deviation, with the support of droop control algorithm, is used to represent the desired amount of power generated by a PV array. In case of low load demand, curtailing the PV output power is the best available solution to ensure the stable operation of a dc MG in battery islanded or PV standalone mode. However, during periods of low, the proposed controller switches back to the inner dp/di regulator to harvest the maximum electrical energy under ambient conditions. Once the battery capacity drops below the upper boundary, the cascaded loop of BESS is re-activated to support the dc MG with seamless transition between operation modes. The BESS has become the dominant energy source and reacted to voltage deviation. Therefore, the PV arrays can be operated in MPPT mode without the need to regulate the dc bus voltage. This is the key benefit of implementing the proposed V-dp/di control.

4.4.4 Digital Control System

In recent years, researchers have shown an increasing interest in the field of digital control system. The concept of implementing the cascade control in a DSP has many advantages over the analogue control, including high flexibility, visible control panel, cost effective, advanced

adaptive control, and easy to upgrade. The skeleton of a digital control loop can shortly be reconfigured in the platform such as Code Composer Studio™. In practice, the test rig of this thesis is monitored by a DSP in real-time, in which the digital control system is coded and implemented. Besides, the real-time information of the test rig can be displayed on the user interface established in MATLAB, which is regarded as graphical user interface. This allows the discrete control system to show the status of the plant and control loop, which is easier for engineers to locate possible errors in the system. On the other hand, some typical disadvantages of digital control could be complex to design and signal loss issue. Sampling the input signal is the key step for a discrete-time system, in which some information of the analogue signal is lost during the sampling process. However, by increasing the frequency of sampling, the effect of signal loss is usually mitigated. The recommended frequency for recovering a continuous signal would be at least ten times larger than the signal frequency. The benefits of digital control, therefore, far outweigh the downsides.

In a digital system, it is critical for the DSP to sample the feedback input signal in signal processing. The block for sampling a signal is known as zero order hold (ZOH). It is applied to sample and hold the signal in discrete-time domain. The sizes of passive power elements can greatly be reduced by a high switching frequency. A saturation block is used as an actuator to limit the output of the control loop. This enables the control system to output a duty ratio to drive the power converter. Considering the impact of ZOH, the equation for including the ZOH effect and taking z-transform of a transfer function is written as

$$H(z) = (1 - z^{-1})Z\left\{\frac{H(s)}{s}\right\} \tag{4.17}$$

where $H(z)$ is the z − transform of the plant $H(s)$ including the effect of ZOH.

It is vital to calculate the present value of second derivative of power to current. The application of unit delay block results in a second derivative of the line tangent at the output of the sum block. As highlighted in Subsection 4.4.4, the second differential term is included in the inner loop at which the dc MG is in a steady state. There are two conditions suggested by the proposed V-dp/di method to identify the state of the dc MG. The assumption of the inner dp/di regulator is that the error of dp/di is around zero, which means the steady-state value has been reached. First, the value of dp/di has to be less than or equal to 130. The limit 130 refers to 500 W of PV array power. The reason for setting up this minimum limit is that the absolute error of dp/di for the output power less than 500 W is only about 0.01%. It means

the accuracy of dp/di in low power range is almost perfect, and hence it is unnecessary to enable the second differential term to reduce the SSE. Second, the dc-link voltage fluctuations between present and previous values should be less than 0.5 V to confirm the system is stable. The AND gate is used to output '1' to the conditional signal, so that the second derivative of power to current is permitted to be included in the primary loop. The introduction to the 2nd differential term further enhances the steady-state performance of the dc MG. It will not become a disturbance signal to the controller in the process of electrical transient state, since the 2nd derivative control can autonomously be terminated.

The formula for expressing a traditional discrete-time PID controller can be written as

$$PID(z) = K_p + \frac{K_I}{1 - z^{-1}} + K_d(1 - z^{-1}) \tag{4.18}$$

where K_p is the proportional gain, K_I is the integral gain, and K_d is the derivative gain of a classical PID controller. The z-domain represents the discrete-time domain of the controller, in which it is applied in a DSP for processing digital signals. The error of dp/di regulator is fed into the digital PID controller for calculating a duty cycle. Afterwards, a PWM signal is generated for driving the ON/OFF operations of the switch in a boost converter.

4.5 Chapter Summary

In this chapter, the proposed V-dp/di control algorithm is illustrated in detail to outline the working principle of droop coefficient and dp/di regulator. The conventional V-dp/dv droop control method is discussed to list the key challenges and limitations, including poor dynamic performance, enormous measurement error of inner control variable, and low PV power quality. In terms of the classical control scheme, this may require two individual feedback control loops for PV standalone and MPPT modes, respectively. Therefore, the proposed V-dp/di droop control strategy benefits from all-in-one topology, promising dynamic performance and high quality of PV output power. In the meantime, it is capable of sharing load demand among multiple PV sources in proportion, according to their rated powers.

To facilitate the development of droop control method, the inner control variable (dp/di) is devised to manipulate the desired power level of PV arrays. The application of dp/di regulator has a significant impact on the measurement accuracy of the inner variable, in which the control term remarkably enhances both dynamic and steady-state performance. A complete PID controller is implemented to particularly suppress the overshoots and undershoots of the common bus voltage. The mathematical analysis of the proposed V-dp/di control algorithm is demonstrated to fully understand the calculations of droop coefficient and its control parameters.

A novel second derivative of PV power to current approach is proposed in this thesis to improve the steady-state characteristics of the system. Two conditions applied in the conditional signal are the key factors to identify the present status of a dc MG. The second differential term is enabled during steady state and will be immediately deactivated if there is a dramatic change in system dynamics. The overall variation in dp/di is mitigated and thus the quality of the corresponding PV power is notably promoted. Furthermore, an analysis of the three main operation modes is presented to show the robustness and effectiveness of the proposed V-dp/di method in an islanded dc MG system with multiple solar panels.

Chapter 5. Stability Analysis of Proposed V-dp/di and Conventional Methods

5.1 Introduction

Stability analysis is critical for control engineers to understand the steady-state characteristics of a control algorithm implemented in a power system. In [10], [70], the approach of employing the conventional V-dp/dv method in a buck converter is presented. The main benefit of using a buck converter is easy to control. However, the nominal voltage of a PV array in a rural area is usually less than the common bus voltage of an islanded dc MG system. A boost converter is commonly used in a dc MG to step up the voltage, after which the output voltage is always higher than the input voltage. In [85], a system identification of a step-up dc/dc converter is carried out. There is a right-half-plane (RHP) zero contained in the transfer function. It exists in the pole-zero map for boost converter, but not buck converter [86]. This is referred to as non-minimum phase system. The step response of a boost converter first moves towards the opposite direction of the steady-state value, which results in a voltage sag at the beginning of dynamic process. In literature, there has been little quantitative analysis of boost converter in a PV-based dc MG system, particularly in a decentralized control approach.

The stability analysis presented in this thesis is essential to validate the system parameters of a PV-based dc MG, and to examine the stability of the proposed V-dp/di control algorithm. The comprehensive stability analysis of proposed and conventional methods for a PV system with boost converter in frequency domain is introduced. The line tangent of the PV characteristics is linearized about the quiescent operating point to describe the small-signal PV model. Considering the linear first-order ac variations, the small-signal equivalent circuit of a boost converter is illustrated in the analysis. It is assumed that the boost converter is ideal in the calculations, neglecting the effect of ESR. The open-loop duty ratio-to-PV voltage transfer function of the PV system is derived in this thesis. A classical PI controller is deployed in the control algorithm. The closed-loop transfer function of the inner control loop can be obtained. There are three key parameters for analysing the steady-state performance, including phase margin, gain margin, and bandwidth. Phase margin refers to the amount of phase that the system is marginally stable. Gain margin is defined as the required amount of change in gain to make the system unstable. A typical system with greater gain margin and/or phase margin results in greater stability. Bandwidth is a gain crossover frequency in which the

magnitude of bode plot does not fall below 0 dB point or -3 dB in theory, and this is known as cutoff frequency. Taking droop coefficient into account, an overall transfer function of decentralized control method is derived. The transfer function is then implemented in MATLAB to investigate the proposed and conventional control strategies, respectively. Afterwards, the second set of outcomes are produced by the simulation model and compared with the stability analysis. The results obtained in Simulink model validate the feasibility of the stability analysis on the steady-state performance evaluation of the proposed V-dp/di method. The comparison study between them for a PV-based dc MG system in a PV standalone mode is provided to have a deep understanding of the novel control algorithm. To maximise the performance of the dc MG system, various controller tuning criteria for the proposed V-dp/di method are given in detail.

5.2 Stability Analysis of Conventional V-dp/dv Control Method

In [10], they have reported the tangent line to a linear I-V curve of a PV array, one obtains

$$K_{pv1} = \frac{\Delta i_{pv}}{\Delta v_{pv}} \tag{5.1}$$

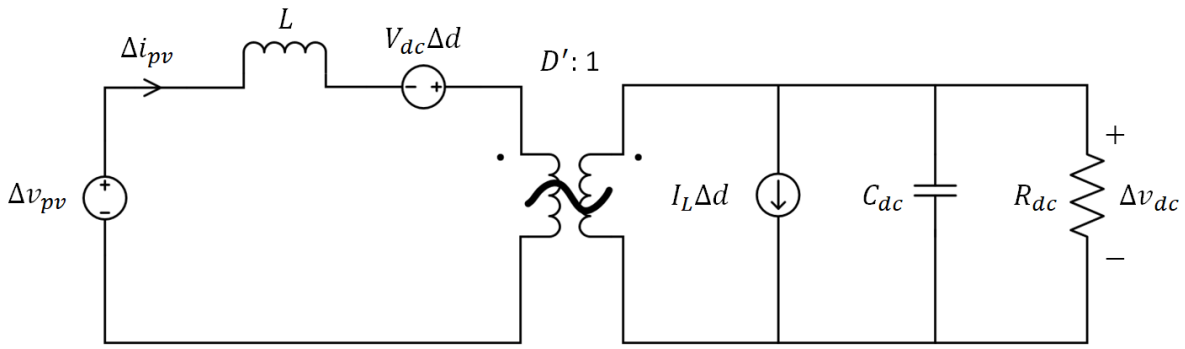

Figure 5.1 Small-signal model of an ideal step-up converter.

The small-signal model in this study is linearized about the quiescent operating point, in which all dc terms and second-order non-linear ac terms are neglected. As shown in Figure 5.1, the small-signal ac equivalent circuit for an ideal boost converter is presented [84]. The input side of the circuit would be the PV output voltage. Overall, the PV array power is transferred from the solar panels to the resistive load via the dc bus. The small-signal dynamics can be expressed in the following linear first-order averaged equations.

$$L\frac{d\hat{\imath}_L(t)}{dt} = \hat{v}_{in}(t) + V_{out}\hat{d}(t) - D'\hat{v}_{out}(t)$$

$$L\frac{d\Delta i_L}{dt} = \Delta v_{pv} + V_{dc}\Delta d - D'\Delta v_{dc} \tag{5.2}$$

$$C\frac{d\hat{v}_{out}(t)}{dt} = D'\hat{\imath}_L(t) - I_L\hat{d}(t) - \frac{\hat{v}_{out}(t)}{R_o}$$
$$C\frac{d\Delta v_{dc}}{dt} = D'\Delta i_L - I_L\Delta d - \frac{\Delta v_{dc}}{R_o} \tag{5.3}$$

where L is the inductance of the boost converter, I_L is the input current of the inductor, D' is the complement of the duty ratio (1-D), C is the dc-link capacitance, and R_o is the load resistance. A capital letter represents the steady-state value of a variable. The symbol Δ refers to the ac variations of the small-signal model.

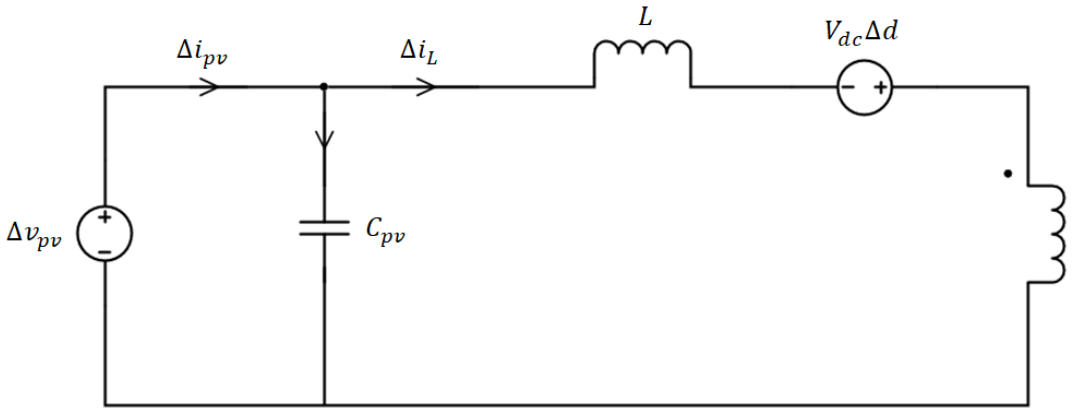

Figure 5.2 Small-signal ac equivalent circuit of boost converter on the input side.

As can be seen from Figure 5.2, the average small-signal ac model of a step-up converter is present to describe the input circuit and derive the formula using Kirchhoff's Current Law (KCL). As a result, the ac variations in the PV voltage are given by

$$C_{pv}\frac{d\Delta v_{pv}}{dt} = \Delta i_{pv} - \Delta i_L$$
$$C_{pv}\frac{d\Delta v_{pv}}{dt} = K_{pv1}\Delta v_{pv} - \Delta i_L \tag{5.4}$$

where C_{pv} is the capacitance of the PV capacitor in parallel with the PV array, K_{pv} is the slope of the linear I-V curve. The first order derivative of the PV power with respect to voltage in terms of ac variations can be linearized and defined as

$$\frac{d\Delta p}{d\Delta v} = K_{pv1}\Delta v_{pv} + \Delta i_{pv} = 2K_{pv1}\Delta v_{pv} \tag{5.5}$$

Equation (5.5) is clearly unexpected in the analysis. This is due to the fact that the calculation of dp/dv is complicated, in which the value of di/dv has to be precise to obtain a practical outcome. This is one of the reasons why the value of dp/dv in conventional control method is found to be inaccurate. Given the ac variation of dc bus voltage can be neglected in the inner dp/dv loop, taking the Laplace transform of (5.2) and (5.4) yield

$$\overset{LT}{\Rightarrow} sL\Delta i_L(s) = \Delta v_{pv}(s) + V_{dc}\Delta d(s)$$

$$\overset{LT}{\Rightarrow} sC_{pv}\Delta v_{pv}(s) = K_{pv1}\Delta v_{pv}(s) - \Delta i_L(s)$$

Rearranging the above two expressions, the small-signal control-to-output transfer function can be written as

$$G_{v_{pv}d}(s) = \frac{\Delta v_{pv}(s)}{\Delta d(s)} = -\frac{V_{dc}}{s^2 LC_{pv} - sLK_{pv1} + 1} \tag{5.6}$$

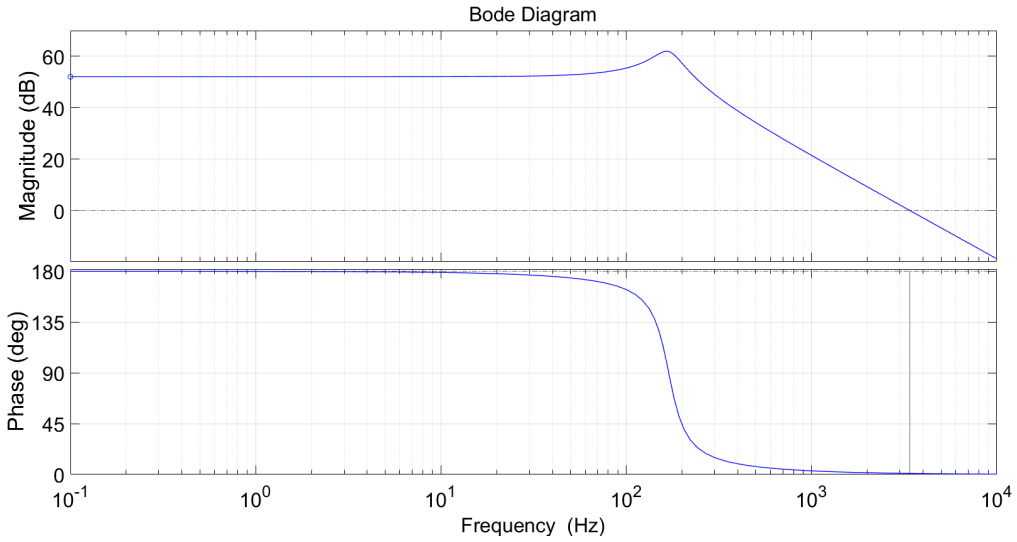

Figure 5.3 Bode plots of the open-loop transfer function of PV system without compensation.

As shown in Figure 5.3, bode plots of the open-loop transfer function of a PV system with boost converter can be observed. One of the most commonly used switching frequencies in PV applications is 20 kHz, which turns out to be the best starting point. In the inner dp/dv regulator, the settling time should be extremely short in order to reduce the error as quickly as possible. Eventually, the ripple of the common bus voltage in the open-loop transfer function is set to zero for simplification. The phase margin is -179 °, in which a negative value implies that it will never reach a steady state. In the meantime, the gain margin of the open-loop system is -52 dB. It is considered to be unstable, if any of these two values is negative on

bode plots. The measured bandwidth of the system response is about 3.4 kHz. Considering a switching frequency of 20 kHz, the cutoff frequency at zero amplitude is huge in the open-loop response. To enhance the stability performance of the PV system, it is mandatory to implement a traditional controller such as PI/PID controller to obtain the desired step response. The derived transfer function shows the ideal relationship between the PV voltage and duty cycle variations. A classical PI controller is deployed to act as a unique controller of the conventional V-dp/dv control algorithm and thus it is given by

$$PI_1(s) = \frac{K_{p1}s + K_{i1}}{s} \tag{5.7}$$

The control framework of the conventional inner dp/dv loop can be observed in Figure 5.5. It is summarised that the structure is a negative feedback path. Equation (5.7) introduces the transfer function of a PI controller, where K_{p1} and K_{i1} refer to proportional gain and integral gain, respectively. The feedback value of the line tangent can be computed in (5.5). The closed-loop transfer function of the inner loop can be defined as [10]

$$H_1(s) = \frac{\Delta v_{pv}(s)}{\frac{d\Delta p}{d\Delta v}^{ref}(s)} = \frac{PI_1(s)G_{v_{pv}d}(s)}{1 + PI_1(s)G_{v_{pv}d}(s)2K_{pv1}} \tag{5.8}$$

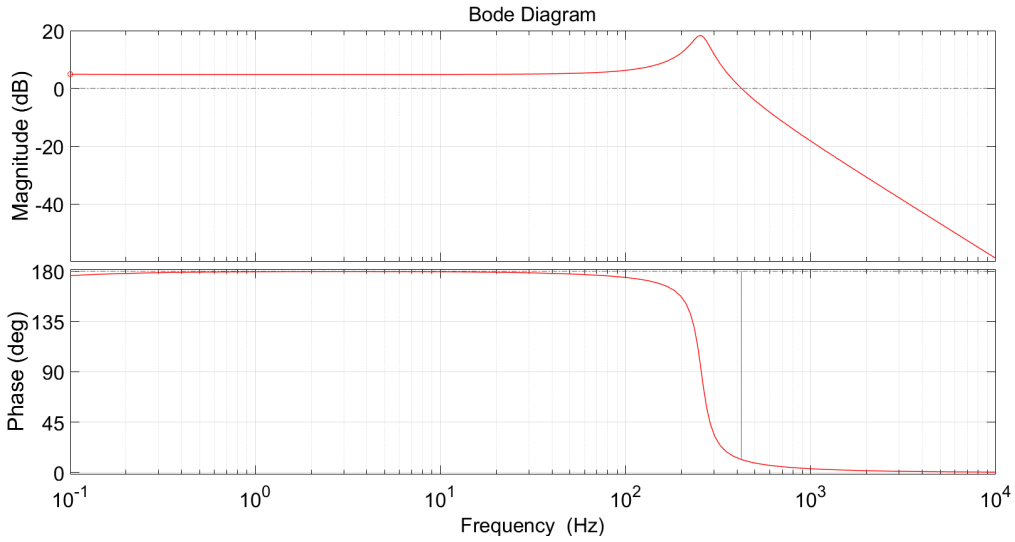

Figure 5.4 Bode plots of the closed-loop dp/dv regulator with PI control in MPPT mode.

Figure 5.4 presents the closed-loop system of dp/dv regulator with a PI controller. The proportional and integral gains of the PI control are set to 0.01 and 0.001, respectively. The switching frequency for the controller is fixed at 20 kHz. The measured phase margin is -

168 °. It has been slightly improved by the PI control, but the negative value indicates that the feedback system is unstable. In terms of gain margin, it is found to be 0.32 dB. This is far away from the criterion of marginally stable, in which gain margin is not equal to phase margin. In this case, the bandwidth is 422 Hz. This cutoff frequency is considered reasonable, compared with the previous frequency value in open-loop PV system. In [10], the authors suggested that the conventional V-dp/dv method with PI controller in a buck converter is always stable. They claimed that the conventional method is applicable for step-up converter. However, this thesis analyses that the dp/dv cannot precisely represent the correct level of PV power in MATLAB simulation, resulting in a stability issue. The inner loop system with a boost converter in MPPT mode is always unstable, regardless of its controller gains. This is the key challenge of implementing the conventional control strategy in a step-up dc/dc converter.

It is shown in Table 5.1 that the simulation results for closed-loop transfer function of the inner loop are present. Overall, none of these PI control settings meets the requirements and stabilises the system of the primary loop. The data for phase margin with different PI settings is always negative, ranged from -48.2 ° to -177 °. The minus sign indicates that the system is unstable. The gain margin is always -9.86 dB, regardless of how the PI controller terms vary. Once again, these outcomes mean the inner feedback loop is an unstable system. The simulation results for conventional V-dp/dv method with PI control are unexpected. In [10], a traditional PI controller is implemented to minimise the error for generating sufficient amount of PV power. However, the results above highlight that the conventional V-dp/dv strategy with PI controller is inapplicable for a PV system with boost converter. Gain and phase margins must be positive in a stable feedback system, while the phase margin is always greater than gain margin. As previously stated, the low accuracy of dp/dv leads to stability issues. The dp/dv produces unnecessary errors to the PI controller and hence the system will never reach a steady state.

Table 5.1 Magnitude and phase data of conventional control with various PI gains

Gains of PI controller	Gain Margin (dB)	Phase Margin (deg)	Bandwidth (Hz)
$K_p = 0.1, K_i = 0.1$	-9.86	-177	1240

$K_p = 0.1, K_i = 0.01$	-9.86	-177	1240
$K_p = 0.1, K_i = 0.001$	-9.86	-177	1240
$K_p = 0.01, K_i = 0.1$	-9.86	-169	422
$K_p = 0.01, K_i = 0.01$	-9.86	-168	422
$K_p = 0.01, K_i = 0.001$	-9.86	-168	422
$K_p = 0.001, K_i = 0.1$	-9.86	-50.2	156
$K_p = 0.001, K_i = 0.01$	-9.86	-48.4	157
$K_p = 0.001, K_i = 0.001$	-9.86	-48.2	157

On the other hand, a step-down dc/dc converter was used in [10] to examine the steady-state performance of conventional control. Compared to step-up converter, a RHP zero does not exist in a classical buck converter. This could be a reason why the outcomes in [10] are totally different. In literature, the dynamic response of buck converter usually shows a promising performance of the system even if there is a significant step change. To conclude, the conventional V-dp/dv method implemented in a PV system with boost converter is always unstable in MPPT mode.

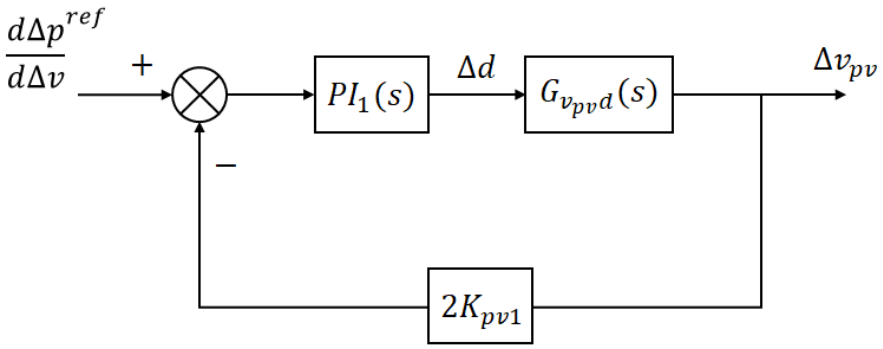

Figure 5.5 Control diagram of the conventional inner loop with PI feedback controller [10].

As can be seen from Figure 5.5, the error signal can be eliminated with the help of PI controller. This turns out two formulas in relation to the ac variation of duty ratio. The increment of duty cycle can be obtained as follows.

$$\Delta d(s) = \Delta d_p(s) + \Delta d_i(s)$$

$$\Delta d(s) = \left(\frac{d\Delta p^{ref}}{d\Delta v}(s) - 2K_{pv1}\Delta v_{pv}(s) \right) K_{p1} + \Delta d_i(s) \tag{5.9}$$

$$\Delta d_i(s) = \left(\frac{d\Delta p^{ref}}{d\Delta v}(s) - 2K_{pv1}\Delta v_{pv}(s) \right) \frac{K_{i1}}{s} \tag{5.10}$$

where Δd_p and Δd_i are the small ac variations of the proportional and integral parts of the controller, respectively. The implementation of the PI controller offers an independent control of two elements, which is the most commonly used controller in control engineering. In frequency-domain, by applying the Laplace transform to (5.2)-(5.4), the averaged small-signal ac model of the boost converter can be rewritten as

$$\overset{LT}{\Rightarrow} sL\Delta i_L = V_{dc}\left[\left(\frac{d\Delta p^{ref}}{d\Delta v} - 2K_{pv1}\Delta v_{pv} \right) K_{p1} + \Delta d_i \right] + \Delta v_{pv} - D'\Delta v_{dc} \tag{5.11}$$

$$\overset{LT}{\Rightarrow} sC\Delta v_{dc} = D'\Delta i_L - \frac{\Delta v_{dc}}{R_o} - I_L\left[\left(\frac{d\Delta p^{ref}}{d\Delta v} - 2K_{pv1}\Delta v_{pv} \right) K_{p1} + \Delta d_i \right] \tag{5.12}$$

$$\overset{LT}{\Rightarrow} sC_{pv}\Delta v_{pv} = K_{pv1}\Delta v_{pv} - \Delta i_L \tag{5.13}$$

Rearranging terms of (5.12), one obtains the following equation

$$\Delta i_L = \frac{sC\Delta v_{dc}}{D'} + \frac{\Delta v_{dc}}{D'R_o} + \frac{I_L}{D'}\left[\left(\frac{d\Delta p^{ref}}{d\Delta v} - 2K_{pv1}\Delta v_{pv} \right) K_{p1} + \Delta d_i \right] \tag{5.14}$$

The above formula is an expression of the small-signal ac variation of the inductor current. Considering (3.14) and (5.11) can be rewritten as

$$sL\left\{ \frac{sC\Delta v_{dc}}{D'} + \frac{\Delta v_{dc}}{D'R_o} + \frac{I_L}{D'}\left[\left(\frac{d\Delta p^{ref}}{d\Delta v} - 2K_{pv1}\Delta v_{pv} \right) K_{p1} + \Delta d_i \right] \right\}$$
$$= V_{dc}\left[\left(\frac{d\Delta p^{ref}}{d\Delta v} - 2K_{pv1}\Delta v_{pv} \right) K_{p1} + \Delta d_i \right] + \Delta v_{pv} - D'\Delta v_{dc}$$

$$\Delta v_{dc}\left[s^2LC + s\frac{L}{R_o} + (D')^2\right] = (V_{dc}D' - sLI_L)\left[\left(\frac{d\Delta p^{ref}}{d\Delta v} - 2K_{pv1}\Delta v_{pv}\right)K_{p1} + \Delta d_i\right] + D'\Delta v_{pv} \tag{5.15}$$

Substituting (5.10) into (5.15) and rearranging these terms, this yields

$$\Delta v_{dc}\left[s^2LC + s\frac{L}{R_o} + (D')^2\right] = (V_{dc}D' - sLI_L)\left[\left(\frac{d\Delta p^{ref}}{d\Delta v} - 2K_{pv1}\Delta v_{pv}\right)K_{p1} + \left(\frac{d\Delta p^{ref}}{d\Delta v} - 2K_{pv1}\Delta v_{pv}\right)\frac{K_{i1}}{s}\right] + D'\Delta v_{pv}$$

$$\Delta v_{dc}\left[s^2LC + s\frac{L}{R_o} + (D')^2\right] = \Delta v_{pv}\big(sLI_L2K_{pv1}K_{p1} + LI_L2K_{pv1}K_{i1} + D' - V_{dc}D'2K_{pv1}K_{p1} - V_{dc}D'2K_{pv1}\frac{K_{i1}}{s}\big) + \frac{d\Delta p^{ref}}{d\Delta v}\left(V_{dc}D'K_{p1} + V_{dc}D'\frac{K_{i1}}{s} - sLI_LK_{p1} - LI_LK_{i1}\right) \tag{5.16}$$

Rearranging terms of (5.16), the equation can be rewritten as

$$\Delta v_{dc}[s^3LCR_o + s^2L + s(D')^2R_o] = \Delta v_{pv}\big(s^2LR_oI_L2K_{pv1}K_{p1} + sLR_oI_L2K_{pv1}K_{i1} + sD'R_o - sV_{dc}D'R_o2K_{pv1}K_{p1} - V_{dc}D'R_o2K_{pv1}K_{i1}\big) + \frac{d\Delta p^{ref}}{d\Delta v}\left(sV_{dc}D'R_oK_{p1} + V_{dc}D'R_oK_{i1} - s^2LR_oI_LK_{p1} - sLR_oI_LK_{i1}\right) \tag{5.17}$$

Substituting (5.10) and (5.14) into (5.13), this equation can be rewritten as

$$sC_{pv}\Delta v_{pv} = K_{pv1}\Delta v_{pv} - \frac{sC\Delta v_{dc}}{D'} - \frac{\Delta v_{dc}}{D'R_o} - \frac{I_L}{D'}\left[\left(\frac{d\Delta p^{ref}}{d\Delta v} - 2K_{pv1}\Delta v_{pv}\right)K_{p1} + \left(\frac{d\Delta p^{ref}}{d\Delta v} - 2K_{pv1}\Delta v_{pv}\right)\frac{K_{i1}}{s}\right]$$

$$\Delta v_{pv} = \frac{sC\Delta v_{dc} + \frac{\Delta v_{dc}}{R_o} + I_LK_{p1}\frac{d\Delta p^{ref}}{d\Delta v} + I_L\frac{K_{i1}}{s}\frac{d\Delta p^{ref}}{d\Delta v}}{K_{pv1}D' + I_L2K_{pv1}K_{p1} + I_L2K_{pv1}\frac{K_{i1}}{s} - sC_{pv}D'} \tag{5.18}$$

By substituting (5.18) into (5.17) and rearranging these terms, one obtains an expression of the small-signal ac model with desired dp/dv and dc-link voltage

$$\Delta v_{dc} h_1 = \Delta v_{dc} h_2 + \frac{d\Delta p^{ref}}{d\Delta v} h_3 + \frac{d\Delta p^{ref}}{d\Delta v} h_4 \tag{5.19}$$

$$h_1 = (s^3 LCR_o + s^2 L + s(D')^2 R_o)\left(K_{pv1} D' + I_L 2K_{pv1} K_{p1} + I_L 2K_{pv1} \frac{K_{i1}}{s} - sC_{pv} D'\right)$$
$$= s^3 LCR_o K_{pv1} D' + s^3 2LCR_o I_L K_{pv1} K_{p1} + s^2 2LCR_o I_L K_{pv1} K_{i1} - s^4 LCR_o C_{pv} D'$$
$$+ s^2 LK_{pv1} D' + s^2 2LI_L K_{pv1} K_{p1} + s2LI_L K_{pv1} K_{i1} - s^3 LC_{pv} D'$$
$$+ sR_o K_{pv1} (D')^3 + s2R_o I_L K_{pv1} K_{p1} (D')^2 + 2R_o I_L K_{pv1} K_{i1} (D')^2 - s^2 R_o C_{pv} (D')^3$$

$$h_2 = \left(sC + \frac{1}{R_o}\right)\left(s^2 LR_o I_L 2K_{pv1} K_{p1} + sLR_o I_L 2K_{pv1} K_{i1} + sD' R_o\right.$$
$$\left. - sV_{dc} D' R_o 2K_{pv1} K_{p1} - V_{dc} D' R_o 2K_{pv1} K_{i1}\right)$$
$$= s^3 LCR_o I_L 2K_{pv1} K_{p1} + s^2 LCR_o I_L 2K_{pv1} K_{i1} + s^2 CR_o D' - s^2 CV_{dc} R_o 2K_{pv1} K_{p1} D'$$
$$- sCV_{dc} R_o 2K_{pv1} K_{i1} D' + s^2 LI_L 2K_{pv1} K_{p1} + sLI_L 2K_{pv1} K_{i1} + sD' - sV_{dc} 2K_{pv1} K_{p1} D'$$
$$- V_{dc} 2K_{pv1} K_{i1} D'$$

$$h_3 = \left(I_L K_{p1} + I_L \frac{K_{i1}}{s}\right)\left(s^2 LR_o I_L 2K_{pv1} K_{p1} + sLR_o I_L 2K_{pv1} K_{i1} + sD' R_o\right.$$
$$\left. - sV_{dc} D' R_o 2K_{pv1} K_{p1} - V_{dc} D' R_o 2K_{pv1} K_{i1}\right)$$
$$= s^2 LR_o {I_L}^2 2K_{pv1} {K_{p1}}^2 + sLR_o {I_L}^2 2K_{pv1} K_{p1} K_{i1} + sR_o I_L K_{p1} D' - sV_{dc} R_o I_L 2K_{pv1} {K_{p1}}^2 D'$$
$$- V_{dc} R_o I_L 2K_{pv1} K_{p1} K_{i1} D' + sLR_o {I_L}^2 2K_{pv1} K_{p1} K_{i1} + LR_o {I_L}^2 2K_{pv1} {K_{i1}}^2 + R_o I_L K_{i1} D'$$
$$- V_{dc} R_o I_L 2K_{pv1} K_{p1} K_{i1} D' - V_{dc} R_o I_L 2K_{pv1} \frac{{K_{i1}}^2}{s} D'$$

$$h_4 = \left(sV_{dc} D' R_o K_{p1} + V_{dc} D' R_o K_{i1} - s^2 LR_o I_L K_{p1} - sLR_o I_L K_{i1}\right)\left(K_{pv} D' + I_L 2K_{pv1} K_{p1}\right.$$
$$\left. + I_L 2K_{pv1} \frac{K_{i1}}{s} - sC_{pv} D'\right)$$
$$= sV_{dc} R_o K_{pv1} K_{p1} (D')^2 + V_{dc} R_o K_{pv1} K_{i1} (D')^2 - s^2 LR_o I_L K_{pv1} K_{p1} D' - sLR_o I_L K_{pv1} K_{i1} D'$$
$$+ sV_{dc} R_o I_L 2K_{pv1} {K_{p1}}^2 D' + V_{dc} R_o I_L 2K_{pv1} K_{p1} K_{i1} D' - s^2 LR_o {I_L}^2 2K_{pv1} {K_{p1}}^2$$
$$- sLR_o {I_L}^2 2K_{pv1} K_{p1} K_{i1} + V_{dc} R_o I_L 2K_{pv1} K_{p1} K_{i1} D' + V_{dc} R_o I_L 2K_{pv1} \frac{{K_{i1}}^2}{s} D'$$
$$- sLR_o {I_L}^2 2K_{pv1} K_{p1} K_{i1} - LR_o {I_L}^2 2K_{pv1} {K_{i1}}^2 - s^2 V_{dc} R_o C_{pv} K_{p1} (D')^2 - sV_{dc} R_o C_{pv} K_{i1} (D')^2$$
$$+ s^3 LR_o C_{pv} I_L K_{p1} D' + s^2 LR_o C_{pv} I_L K_{i1} D'$$

Rearranging those terms of (5.19), the small-signal dp/dv-output transfer function can therefore be computed as

$$\frac{\Delta v_{dc}}{\frac{d\Delta p}{d\Delta v}^{ref}} = \frac{h_3 + h_4}{h_1 - h_2}$$

where

$$h_3 + h_4 = s^3\left(LC_{pv}R_oI_LK_{p1}D'\right) + s^2(LC_{pv}R_oI_LK_{i1}D' - C_{pv}V_{dc}R_oK_{p1}(D')^2$$
$$-LR_oI_LK_{pv1}K_{p1}D') + s(R_oI_LK_{p1}D' + V_{dc}R_oK_{pv1}K_{p1}(D')^2 - LR_oI_LK_{pv1}K_{i1}D'$$
$$-C_{pv}V_{dc}R_oK_{i1}(D')^2) + R_oI_LK_{i1}D' + V_{dc}R_oK_{pv1}K_{i1}(D')^2$$

$$h_1 - h_2 = -s^4\left(LCC_{pv}R_oD'\right) - s^3\left(LC_{pv}D' - LCR_oK_{pv1}D'\right) - s^2(CR_oD' + C_{pv}R_o(D')^3$$
$$-LK_{pv1}D' - 2CV_{dc}R_oK_{pv1}K_{p1}D') - s(D' - 2V_{dc}K_{pv1}K_{p1}D' - 2CV_{dc}R_oK_{pv1}K_{i1}D'$$
$$-R_oK_{pv1}(D')^3 - 2R_oI_LK_{pv1}K_{p1}(D')^2) - (-2V_{dc}K_{pv1}K_{i1}D' - 2R_oI_LK_{pv1}K_{i1}(D')^2)$$

The overall closed-loop transfer function of inner dp/dv regulator in the PV-based dc MG system can be expressed as

$$H_1(s) = \frac{\Delta v_{dc}}{\frac{d\Delta p}{d\Delta v}^{ref}} = \frac{b_0s^3 + b_1s^2 + b_2s + b_3}{a_0s^4 + a_1s^3 + a_2s^2 + a_3s + a_4} \tag{5.20}$$

where

$$b_0 = -LR_oC_{pv}I_LK_{p1}$$
$$b_1 = R_oC_{pv}D'V_{dc}K_{p1} + LR_oI_LK_{pv1}K_{p1} - LR_oC_{pv}I_LK_{i1}$$
$$b_2 = LR_oI_LK_{pv1}K_{i1} + R_oC_{pv}D'V_{dc}K_{i1} - R_oI_LK_{p1} - R_oD'V_{dc}K_{pv1}K_{p1}$$
$$b_3 = -R_oI_LK_{i1} - R_oD'V_{dc}K_{pv1}K_{i1}$$
$$a_0 = LR_oCC_{pv}$$
$$a_1 = LC_{pv} - LR_oCK_{pv1}$$
$$a_2 = R_oC + R_oC_{pv}(D')^2 - LK_{pv1} - 2R_oCV_{dc}K_{pv1}K_{p1}$$
$$a_3 = 1 - 2V_{dc}K_{pv1}K_{p1} - 2R_oCV_{dc}K_{pv1}K_{i1} - R_o(D')^2K_{pv1} - 2R_oD'I_LK_{pv1}K_{p1}$$
$$a_4 = -2V_{dc}K_{pv1}K_{i1} - 2R_oD'I_LK_{pv1}K_{i1}$$

To calculate the inductor current in a steady state, in time-domain, the averaged model of (5.3) is used to express the relationship between capacitor ripple voltage and inductor current. By rearranging the equation, the inductor current can be computed for the use of (5.20). In the conventional V-dp/dv control method, the calculations of the inductor current are excluded

from the paper due to simplicity. Eventually, in this thesis, the formula is defined for the use of stability analysis to compensate for the deficiency.

$$C\frac{dV_{dc}}{dt} = D'I_L - \frac{V_{dc}}{R_o}$$
$$\therefore I_L = \frac{C\Delta V_{dc} f_{sw}}{D'} + \frac{V_{dc}}{D'R_o} \tag{5.21}$$

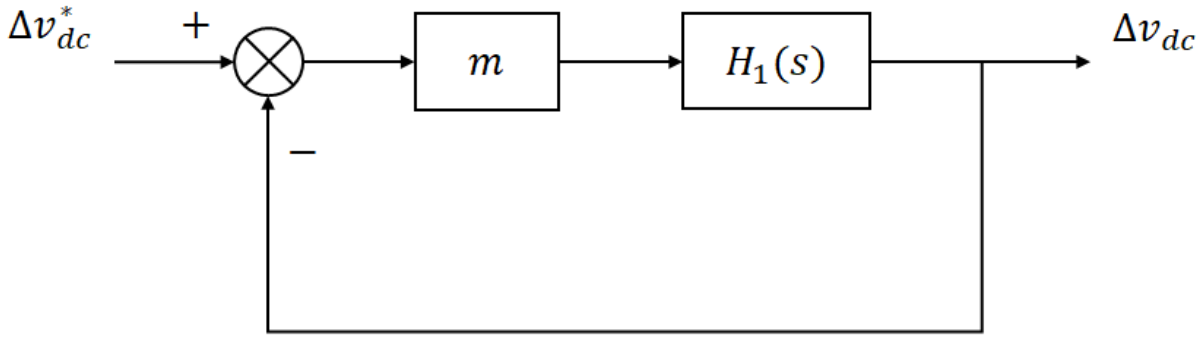

Figure 5.6 Block diagram of cascade control system in conventional approach.

The control framework of the overall closed-loop transfer function, including the implementation of outer loop, is presented in Figure 5.6. The desired value of dp/dv is the multiplication of dc bus voltage error and droop coefficient. The P-V characteristic curve of the PV array is linearized by the droop control, which achieves proportional power sharing among multiple PV generators in a stand-alone operation. The droop coefficient m in the stability analysis is set to 1.7 for MPPT mode. The droop rate is small enough to minimise the effect of the droop control in grid-connected or battery mode. In [10], the authors summarise that there is a trade-off between stability and voltage deviation. Basically, the increase in droop coefficient results in stability issues. When it comes to larger droop coefficient, the response speed of the system is higher and the voltage deviation is dramatically suppressed. The open-loop transfer function of the entire system is the multiplication of overall inner loop transfer function and droop coefficient. The output signal of the transfer function is ac variation of common bus voltage, which is fed into the outer control loop to perform voltage regulation.

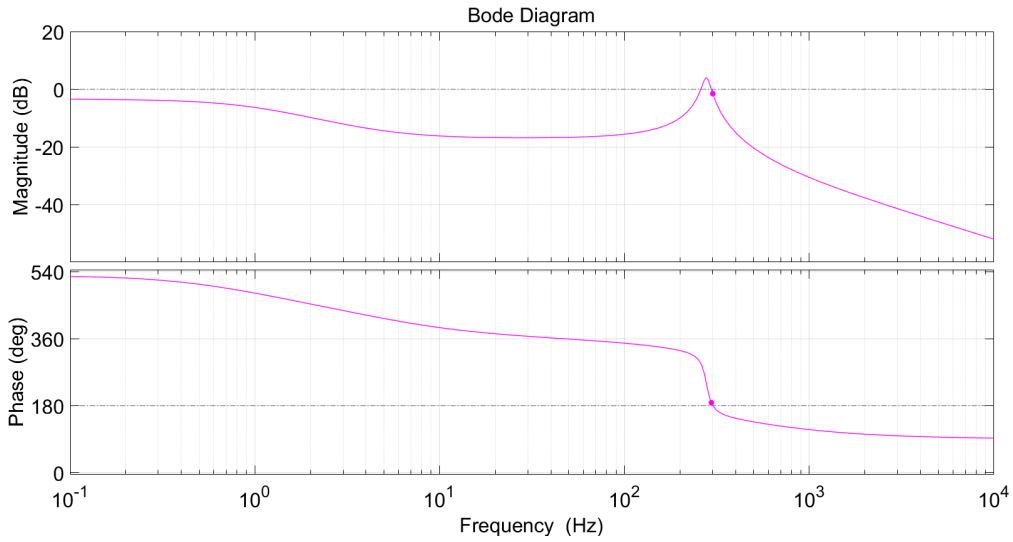

Figure 5.7 Bode plots of overall closed-loop transfer function of conventional method in MPPT mode.

The magnitude and phase data for the cascaded loop of conventional V-dp/dv control strategy are shown in Figure 5.7. The gain margin is 1.54 dB which is considered as critically stable, due to positive value near zero. In terms of phase margin, this is measured as 7.65 °. Since the gain crossover frequency is slightly higher than phase crossover frequency, the overall system is unstable. The bandwidth of the outer loop is about 295 Hz. In [10], the study reported that the bandwidth of the outer loop is roughly ten times less than the bandwidth of inner loop. However, in the simulation, the bandwidth of outer control loop in Figure 5.7 is similar to the one in primary loop. The dc MG system is operating in MPPT mode, where the dc bus voltage error in the control loop is assumed to be zero. As a consequence, the outer voltage loop is disabled in MPPT mode for the purpose of maximising the PV output power. This is the main reason why the bandwidth difference in cascaded loop is lower than expected. The droop control method in battery mode or grid-connected mode is a single dp/dv control loop, which aims to extract the maximum power from PV arrays. It can be summarised that high bandwidth of outer voltage loop in MPPT mode is the key advantage of droop control algorithm. The bandwidth indicates how fast the PV array reaches the MPP in grid-connected and battery modes, which shows how the conventional V-dp/dv control improves the steady-state performance of a dc MG system.

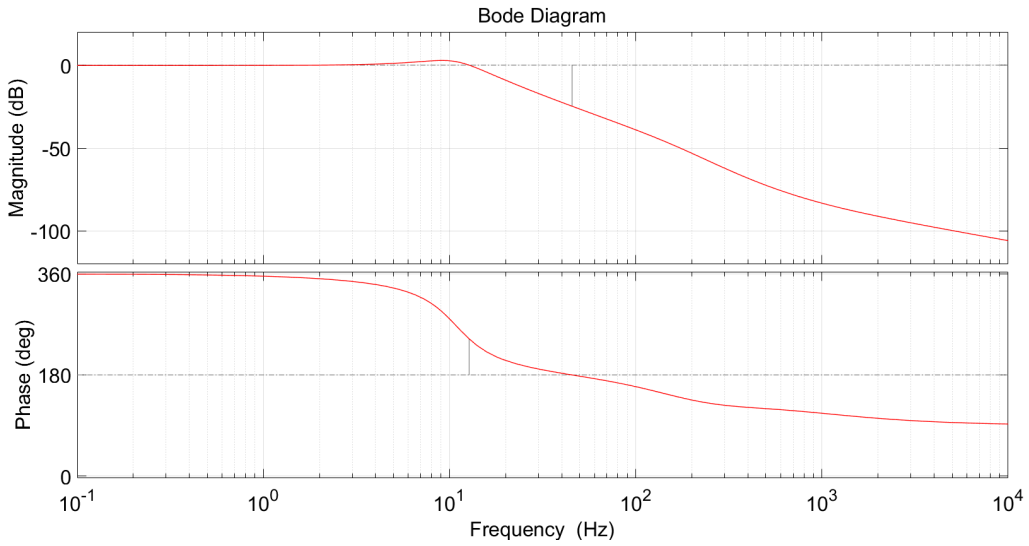

Figure 5.8 Bode plots of outer voltage loop of conventional method in PV standalone mode.

To examine the steady-state performance of dc MG system in a stand-alone mode, some critical specifications in the stability analysis have been adjusted. In this scenario, the dc MG is supposed to draw 1.5 kW from PV arrays. The droop coefficient is set to 5, which corresponds to the simulation model in the next chapter. Accordingly, the desired dc-link voltage can be computed in the analysis. The proportional and integral gains of the controller are 0.00001 and 0.02, respectively. As shown in Figure 5.8, in terms of outer loop, the overall closed-loop system is stable with a gain margin of 24.8 dB, a phase margin of 64.2 °, and a bandwidth of 45.4 Hz. In a voltage regulation mode, the secondary voltage loop plays a critical role in restoring the dc bus voltage to certain value. Therefore, the cascade control is fully functional where the inner loop is reacting almost ten times faster than the outer loop.

In principle, an inevitable error only exists in the outer voltage loop when the dc MG is working in PV standalone mode. This generates a desired dp/dv term by the multiplication of the voltage deviation and droop coefficient. In other words, the aim of a droop controller is to calculate a temporary reference voltage value for the use of energy balancing across PV sources. This implies that the voltage error cannot be eliminated unless the dc MG transfers back to battery or grid-connected mode. The droop coefficient can be treated as a proportional gain of an outer controller. In a droop control system, this is similar to a pure proportional controller but a sustained error is maintained for any load conditions in voltage restoration mode. Given a maximum allowable dc bus voltage is defined in advance, there is always a limit to the voltage variation in order to protect the circuit from overvoltage conditions.

The conventional V-dp/dv control strategy is incapable of obtaining a satisfactory steady-state performance of the inner dp/dv regulator. The accuracy issue of dp/dv has a significant impact on the stability of the feedback control system. In Chapter 4, this thesis shows that there is a major difference between desired and actual dp/dv values, resulting in unnecessary continuous error existed in the primary dp/dv regulator. The simulation model in Chapter 5 analyses that the dc MG system is stable, in which a classical PID controller must be implemented. The steady-state response characteristics of conventional V-dp/dv method can be improved by an advanced controller. To tackle the stability issue, this thesis proposes a V-dp/di control algorithm to remarkably enhance both the dynamic and steady-state performance of PV arrays in a dc MG system.

5.3 Stability Analysis of Proposed V-dp/di Control Strategy

The stability analysis of the proposed V-dp/di control algorithm is presented. There are some differences between two droop control methods in this analysis. For instance, the inner control variable, PI settings, droop coefficient, and atmospheric conditions may vary from the analysis in Section 5.2. In the first place, the small-signal ac equivalent circuits of step-up dc/dc converter and P-I characteristic curve of the PV array are derived to understand the steady-state behaviour. These equations can be rearranged to obtain the closed-loop transfer function of the inner loop. The small-signal ac model of inner dp/di regulator is then defined to calculate the overall $V_{dc} - \frac{dp}{di}$ transfer function. The comparison between two control methods is present in this analysis to highlight the main benefits of employing the proposed V-dp/di droop control algorithm in a dc MG system.

The small-signal dynamics of the PV model are linearized about the dc quiescent point. The $I - V$ characteristic curve can be described by a tangent line. Compared with Section 5.2, the definition of the slope of line tangent would be the same as (5.1). The formula for expressing the I-V characteristics of a PV array can be written as

$$K_{pv2} = \frac{\Delta i_{pv}}{\Delta v_{pv}} \tag{5.22}$$

where K_{pv2} is the tangent line of the linearized PV model for the proposed V-dp/di method.

Considering the P-I characteristics of the PV array, (5.22) can be expressed as

$$h = N_p I_o \frac{q}{N_s AkT} e^{\frac{q(V_{pv}+I_{pv}R_s)}{N_s AkT}}$$

$$K_{pv2} = -\frac{h}{1+hR_s} = -\frac{N_p I_o \frac{q}{N_s AkT} e^{\frac{q(V_{pv}+I_{pv}R_s)}{N_s AkT}}}{1+N_p I_o \frac{qR_s}{N_s AkT} e^{\frac{q(V_{pv}+I_{pv}R_s)}{N_s AkT}}} \tag{5.23}$$

where N_p is the number of solar cells connected in parallel, and N_s is the number of solar cells connected in series. It is noted that the impact of parallel resistance R_p is neglected due to simplification. The primary control variable of the proposed control method is dp/di. As a result, the formula for calculating the tangent line of P-I characteristics is written as

$$\frac{d\Delta p}{d\Delta i} = \Delta v_{pv} + \Delta i_{pv} \frac{\Delta v_{pv}}{\Delta i_{pv}} = 2\Delta v_{pv} \tag{5.24}$$

Compared to (5.5), (5.24) clearly shows that the equation for describing the novel control term dp/di is simpler to calculate. The equation in [10] requires some steps to obtain the value of dp/dv, however, the PV voltage ripple is the only variable required for dp/di to be computed in each loop. The results in Chapter 4 summarise that the value of dp/di is accurate, particularly in voltage regulation. It could be argued that the computed value of dp/di is almost perfect in the phase of simulation study, which should achieve better results from the control point of view. The reduced error of inner loop in a steady state results in fewer fluctuations, as well as lower overshoots and undershoots.

As stated in Section 5.2, the small-signal dynamics of the boost converter without ESR are derived in (5.2) and (5.3). Due to the new definition of the control variable dp/di, it is compulsory to modify part of the equivalent circuit equations. The slope of line tangent for the conventional V-dp/dv control scheme can be reconsidered as an inner control parameter for the proposed V-dp/di method. As shown in Figure 5.2, a detailed circuit diagram at the input side can be observed. Taking the PV capacitor into account, the formula for expressing the input PV capacitor of the power electronic converter can be rewritten as

$$C_{pv} \frac{d\Delta v_{pv}}{dt} = \Delta v_{pv} K_{pv2} - \Delta i_L \tag{5.25}$$

Taking the Laplace transformation of (5.2) and (5.25), it yields

$$\overset{LT}{\Rightarrow} sL\Delta i_L(s) = \Delta v_{pv}(s) + V_{dc}\Delta d(s)$$

$$\overset{LT}{\Rightarrow} sC_{pv}\Delta v_{pv}(s) = \Delta v_{pv}(s)K_{pv2} - \Delta i_L(s)$$

The small-signal ac variations around the steady dc component are supposed to be null, since the dc-link voltage is expected to be constant in a steady state. This assumption helps eliminate the ac variations corresponding to the dc bus voltage. Rearranging the above two equations, the averaged small-signal control-to-output transfer function of the boost converter with proposed V-dp/di control scheme can be written as

$$G_{v_{pv}d}(s) = \frac{\Delta v_{pv}(s)}{\Delta d(s)} = -\frac{V_{dc}}{LC_{pv}s^2 - K_{pv2}Ls + 1} \tag{5.26}$$

The open-loop transfer function of the inner dp/di loop illustrates the small-signal properties of an ideal step-up chopper, given the effect of the tangent line is considered. This presents the plant of a PV standalone system to make full use of a mathematical analysis. To demonstrate the overview of the inner dp/di regulator, (5.7) is used by a traditional PI controller to manipulate the value of dp/di in order to produce the adequate amount of PV power.

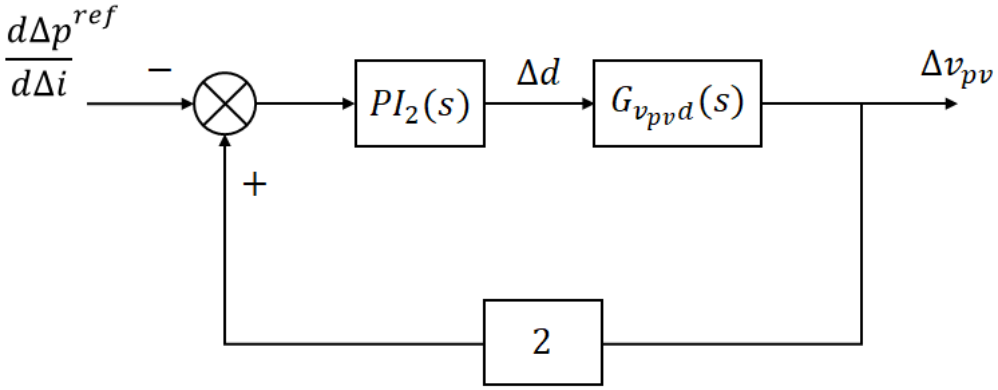

Figure 5.9 Control block diagram of the inner dp/di loop.

As shown in Figure 5.9, the control framework of the inner dp/di loop is introduced. It is critical to bear in mind that the latter one is a positive feedback loop, which differs from the negative feedback loop in the conventional V-dp/dv control. To compute the closed-loop system with a positive feedback, the formula can be expressed as

$$G_2(s) = \frac{\Delta v_{pv}(s)}{\frac{d\Delta p^{ref}}{d\Delta i}(s)} = \frac{G_{v_{pv}d}(s)PI_2(s)}{2G_{v_{pv}d}(s)PI_2(s) - 1} \tag{5.27}$$

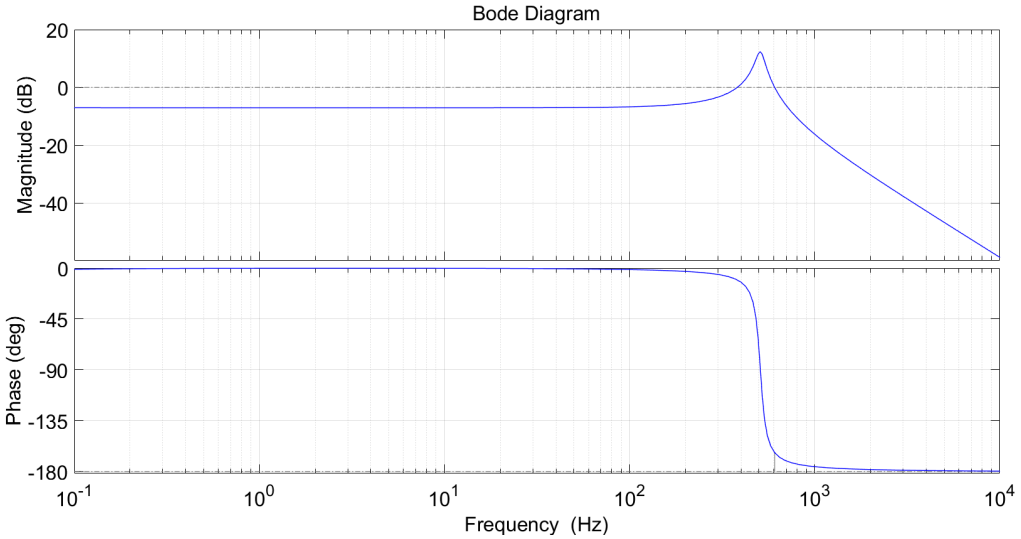

Figure 5.10 Bode plots of inner dp/di regulator of proposed method in MPPT mode.

It can be observed in Figure 5.10 that the closed-loop system of inner loop of proposed V-dp/di control is stable, in contrast to the dp/dv regulator in the conventional control. The nominal switching frequency of the proposed method is 20 kHz, which stays the same as previous analysis. The proportional and integral terms of the PI controller implemented in MATLAB are set to 0.01 and 0.001, respectively. The dc MG system is operating in either grid-connected or islanded mode, where the control strategy is maximising the PV output power at standard test conditions. The bandwidth obtained in Figure 5.10 is 607 Hz and hence the proposed method takes advantage of high bandwidth. There is a 43.8% increase in the bandwidth, compared to conventional strategy, which turns out a higher speed of steady-state response. The phase margin of the inner dp/di regulator is 16.7 °, instead of the negative phase margin shown in the dp/dv control loop. This system can be considered as stable when measured phase margin is positive in the graph of frequency response of the system. This stability analysis is based on a boost converter, in which the RHP zero adds complexity to the closed-loop system [85]. The term dp/di is used to increase the accuracy of power measurement. These bode plots in Figure 5.10 present a stable closed-loop system of a PV-based dc MG. Therefore, it can be concluded that the proposed V-dp/di control algorithm is applicable for both buck and boost converters in a PV-based dc MG system.

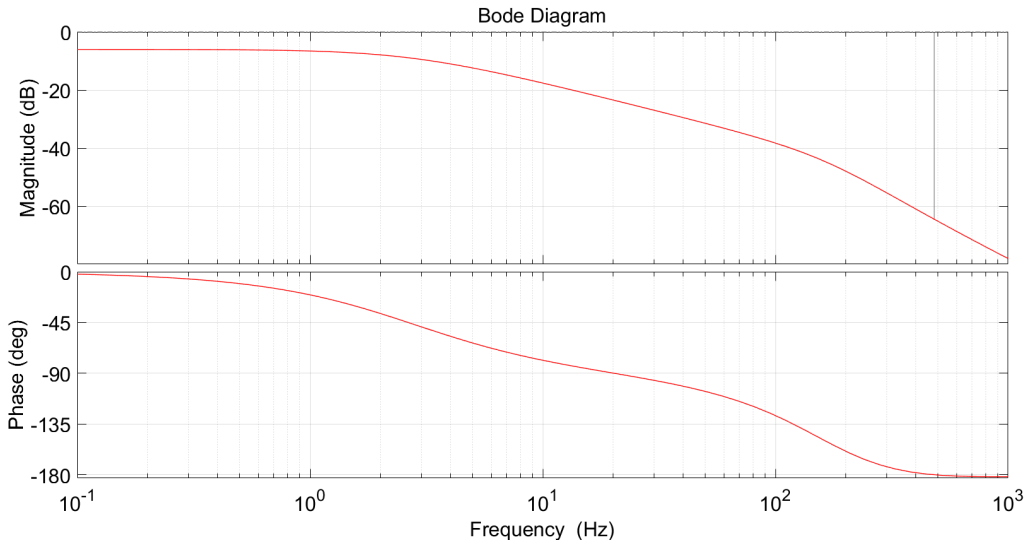

Figure 5.11 Bode plots of inner loop of proposed control algorithm in PV standalone mode.

In a PV standalone operation, Figure 5.11 presents the steady-state characteristics of the inner dp/di regulator. A load power of 1.5 kW is drawn from the PV arrays via the dc bus. The PI settings defined in Section 5.2 are deployed to ensure the consistency. The gain margin on the magnitude plot is 64.4 dB. A positive value of gain margin implies that the closed-loop system is stable. In terms of phase margin, this cannot be measured on the phase plot due to no zero dB crossing of the gain. In MATLAB, the measured phase margin is infinity which is much greater than the gain margin. The bandwidth of the inner loop of the proposed V-dp/di control scheme is found to be 481 Hz. Compared with the outcomes in MPPT mode, the bandwidth in stand-alone operation is slightly lower. In a PV standalone mode, it is always more challenging for a droop control system to reach a steady state. The desired dc bus voltage and value of dp/di have to be re-calculated to meet the local load demand. To sum up, the inner loop of the proposed V-dp/di control strategy in both battery islanded and PV standalone modes is always stable, regardless of the normal PI settings and/or load conditions.

Plus, the small-signal duty cycle of PI controller in the proposed inner loop can be derived as

$$\Delta d(s) = \Delta d_p(s) + \Delta d_i(s)$$
$$\Delta d_p(s) = \left(2\Delta v_{pv} - \frac{d\Delta p^{ref}}{d\Delta i}\right) K_{p2} \tag{5.28}$$
$$\Delta d_i(s) = \left(2\Delta v_{pv} - \frac{d\Delta p^{ref}}{d\Delta i}\right) \frac{K_{i2}}{s}$$

where Δd_p and Δd_i are the ac variations of proportional and integral parts of the small-signal model, respectively. Substituting (5.28) into (5.2) and (5.3), and taking Laplace transformation, this yields

$$\overset{LT}{\Rightarrow} sL\Delta i_L = V_{dc}\left[\left(2\Delta v_{pv} - \frac{d\Delta p^{ref}}{d\Delta i}\right)K_{p2} + \Delta d_i\right] + \Delta v_{pv} - D'\Delta v_{dc} \tag{5.29}$$

$$\overset{LT}{\Rightarrow} sC\Delta v_{dc} = D'\Delta i_L - \frac{\Delta v_{dc}}{R_o} - I_L\left[\left(2\Delta v_{pv} - \frac{d\Delta p^{ref}}{d\Delta i}\right)K_{p2} + \Delta d_i\right] \tag{5.30}$$

$$\overset{LT}{\Rightarrow} sC_{pv}\Delta v_{pv} = K_{pv2}\Delta v_{pv} - \Delta i_L \tag{5.31}$$

Equations (5.29)-(5.31) are representing an overall closed-loop control system, in which the impacts of energy source and load are taken into account. A classical PI controller is used to control the dc bus voltage by regulating dp/di. This can reassure the type of controller in proposed V-dp/di and conventional control methods is consistent, so that the dynamic and steady-state performance of the dc MG system can be assessed and compared with each other. Rearranging (5.30), it can be rewritten as

$$\Delta i_L = \frac{sC\Delta v_{dc}}{D'} + \frac{\Delta v_{dc}}{D'R_o} + \frac{I_L}{D'}\left[\left(2\Delta v_{pv} - \frac{d\Delta p^{ref}}{d\Delta i}\right)K_{p2} + \Delta d_i\right] \tag{5.32}$$

The formula (5.32) is an expression of ac variations of inductor current in the equivalent circuit. The small-signal ac variations of dc-link voltage, PV voltage and dp/di are involved in (5.32) to define the relationship between these key terms. Substituting (5.32) into (5.29), one obtains

$$sL\left\{\frac{sC\Delta v_{dc}}{D'} + \frac{\Delta v_{dc}}{D'R_o} + \frac{I_L}{D'}\left[\left(2\Delta v_{pv} - \frac{d\Delta p^{ref}}{d\Delta i}\right)K_{p2} + \Delta d_i\right]\right\}$$
$$= V_{dc}\left[\left(2\Delta v_{pv} - \frac{d\Delta p^{ref}}{d\Delta i}\right)K_{p2} + \Delta d_i\right] + \Delta v_{pv} - D'\Delta v_{dc}$$
$$\Delta v_{dc}\left[s^2LC + s\frac{L}{R_o} + (D')^2\right]$$
$$= (V_{dc}D' - sLI_L)\left[\left(2\Delta v_{pv} - \frac{d\Delta p^{ref}}{d\Delta i}\right)K_{p2} + \Delta d_i\right] + D'\Delta v_{pv} \tag{5.33}$$

The equation can be rearranged by extracting the small-signal ac variations of PV voltage and substituting (5.28) into (5.33). The equation can be derived as

$$\Delta v_{dc}\left[s^2LC + s\frac{L}{R_o} + (D')^2\right] = (V_{dc}D' - sLI_L)\left[\left(2\Delta v_{pv} - \frac{d\Delta p^{ref}}{d\Delta i}\right)K_{p2} + \left(2\Delta v_{pv} - \frac{d\Delta p^{ref}}{d\Delta i}\right)\frac{K_{i2}}{s}\right] + D'\Delta v_{pv}$$

$$\Delta v_{dc}\left[s^2LC + s\frac{L}{R_o} + (D')^2\right] = \Delta v_{pv}\left(D' + 2D'V_{dc}K_{p2} + 2D'V_{dc}\frac{K_{i2}}{s} - s2LI_LK_{p2} - 2LI_LK_{i2}\right) + \frac{d\Delta p^{ref}}{d\Delta i}\left(sLI_LK_{p2} + LI_LK_{i2} - D'V_{dc}K_{p2} - D'V_{dc}\frac{K_{i2}}{s}\right) \quad (5.34)$$

To eliminate the small-signal PV voltage, (5.32) can be substituted into (5.31). The formula for describing small ac variations in PV output voltage is written as

$$sC_{pv}\Delta v_{pv} = K_{pv2}\Delta v_{pv} - \frac{sC\Delta v_{dc}}{D'} - \frac{\Delta v_{dc}}{D'R_o} - \frac{I_L}{D'}\left[\left(2\Delta v_{pv} - \frac{d\Delta p^{ref}}{d\Delta i}\right)K_{p2} + \left(2\Delta v_{pv} - \frac{d\Delta p^{ref}}{d\Delta i}\right)\frac{K_{i2}}{s}\right]$$

$$\Delta v_{pv} = \frac{sC\Delta v_{dc} + \frac{\Delta v_{dc}}{R_o} - I_LK_{p2}\frac{d\Delta p^{ref}}{d\Delta i} + I_L\frac{K_{i1}}{s}\frac{d\Delta p^{ref}}{d\Delta i}}{K_{pv2}D' - 2I_LK_{p2} - 2I_L\frac{K_{i2}}{s} - sC_{pv}D'} \quad (5.35)$$

Multiplying both sides of the equation (5.34) by sR_o, all of the fractions in (5.34) can easily be removed by the elimination method. It is rewritten as

$$\Delta v_{dc}[s^3LCR_o + s^2L + s(D')^2R_o] = \Delta v_{pv}\left(sD'R_o + sV_{dc}D'R_o2K_{p2} + V_{dc}D'R_o2K_{i2} - s^2LR_oI_L2K_{p2} - sLR_oI_L2K_{i2}\right) + \frac{d\Delta p^{ref}}{d\Delta i}\left(s^2LR_oI_LK_{p2} + sLR_oI_LK_{i2} - sV_{dc}D'R_oK_{p2} - V_{dc}D'R_oK_{i2}\right) \quad (5.36)$$

Substituting (5.35) into (5.36), the equation for expressing the overall closed-loop transfer function can be derived as

$$\Delta v_{dc}F_1 = \Delta v_{dc}F_2 - \frac{d\Delta p^{ref}}{d\Delta i}F_3 + \frac{d\Delta p^{ref}}{d\Delta i}F_4 \quad (5.37)$$

$$F_1 = (s^3LCR_o + s^2L + s(D')^2R_o)\left(K_{pv2}D' - I_L2K_{p2} - I_L2\frac{K_{i2}}{s} - sC_{pv}D'\right)$$

$$= s^3LCR_oK_{pv2}D' - s^32LCR_oI_LK_{p2} - s^22LCR_oI_LK_{i2} - s^4LCR_oC_{pv}D'$$

$$+s^2LK_{pv2}D' - s^22LI_LK_{p2} - s2LI_LK_{i2} - s^3LC_{pv}D'$$

$$+sR_oK_{pv2}(D')^3 - s2R_oI_LK_{p2}(D')^2 - 2R_oI_LK_{i2}(D')^2 - s^2R_oC_{pv}(D')^3$$

$$F_2 = \left(sC + \frac{1}{R_o}\right)\left(sD'R_o + sV_{dc}D'R_o2K_{p2} + V_{dc}D'R_o2K_{i2}\right.$$
$$\left.-s^2LR_oI_L2K_{p2} - sLR_oI_L2K_{i2}\right)$$
$$= s^2CR_oD' + s^2CV_{dc}R_o2K_{p2}D' + sCV_{dc}R_o2K_{i2}D' - s^3LCR_oI_L2K_{p2} - s^2LCR_oI_L2K_{i2}$$
$$+sD' + sV_{dc}2K_{p2}D' + V_{dc}2K_{i2}D' - s^2LI_L2K_{p2} - sLI_L2K_{i2}$$

$$F_3 = \left(I_LK_{p2} + I_L\frac{K_{i2}}{s}\right)\left(sD'R_o + sV_{dc}D'R_o2K_{p2} + V_{dc}D'R_o2K_{i2}\right.$$
$$\left.-s^2LR_oI_L2K_{p2} - sLR_oI_L2K_{i2}\right)$$
$$= sR_oI_LK_{p2}D' + sV_{dc}R_oI_L2{K_{p2}}^2D' + V_{dc}R_oI_L2K_{p2}K_{i2}D' - s^2LR_o{I_L}^2{2K_{p2}}^2$$
$$-sLR_o{I_L}^2K_{p2}K_{i2} + R_oI_LK_{i2}D' + V_{dc}R_oI_L2K_{p2}K_{i2}D' + V_{dc}R_oI_L2\frac{{K_{i2}}^2}{s}D'$$
$$-sLR_o{I_L}^2K_{p2}K_{i2} - LR_o{I_L}^2{2K_{i2}}^2$$

$$F_4 = \left(s^2LR_oI_LK_{p2} + sLR_oI_LK_{i2} - sV_{dc}D'R_oK_{p2} - V_{dc}D'R_oK_{i2}\right)\left(K_{pv}D' - I_L2K_{p2} - I_L2\frac{K_{i2}}{s}\right.$$
$$\left.-sC_{pv}D'\right)$$
$$= s^2LR_oI_LK_{p2}K_{pv2}D' + sLR_oI_LK_{i2}K_{pv2}D' - sV_{dc}R_oK_{pv2}K_{p2}(D')^2 - V_{dc}R_oK_{pv2}K_{i2}(D')^2$$
$$-s^2LR_o{I_L}^2{2K_{p2}}^2 - sLR_o{I_L}^2K_{p2}K_{i2} + sV_{dc}R_oI_L2{K_{p2}}^2D' + V_{dc}R_oI_L2K_{p2}K_{i2}D'$$
$$-sLR_o{I_L}^2K_{p2}K_{i2} - LR_o{I_L}^2{2K_{i2}}^2 + V_{dc}R_oI_L2K_{p2}K_{i2}D' + V_{dc}R_oI_L2\frac{{K_{i2}}^2}{s}D'$$
$$-s^3LR_oC_{pv}I_LK_{p2}D' - s^2LR_oC_{pv}I_LK_{i2}D' + s^2V_{dc}R_oC_{pv}K_{p2}(D')^2 + sV_{dc}R_oC_{pv}K_{i2}(D')^2$$

There are two key signals in (5.37), including small ac variations of dc-link voltage and dp/di. One of them is the output of the closed-loop transfer function of dp/di regulator and the latter is the input signal of the transfer function. Most of the parameters existed in the dc MG and control system are taken into consideration, except for parasitic circuit elements such as internal resistances. When it comes to the final outcome of closed-loop transfer function, this ensures that similar behaviour of the system is present in the simulation for comparison. By rearranging (5.37), the small-signal $V_{dc} - \frac{dP}{dI}$ transfer function of the closed-loop control system is derived as

$$\frac{\Delta v_{dc}}{\frac{d\Delta p^{ref}}{d\Delta i}} = \frac{F_4 - F_3}{F_1 - F_2}$$

where

$$F_4 - F_3 = -s^3\left(LR_oC_{pv}I_LK_{p2}\right) - s^2(LR_oC_{pv}I_LK_{i2} - V_{dc}R_oC_{pv}K_{p2}D'$$
$$-LR_oI_LK_{p2}K_{pv2}) - s(R_oI_LK_{p2} + V_{dc}R_oK_{p2}K_{pv2}D' - LR_oI_LK_{i2}K_{pv2}$$
$$-V_{dc}R_oC_{pv}K_{i2}D') - R_oI_LK_{i2} - V_{dc}R_oK_{i2}K_{pv2}D'$$

$$F_1 - F_2 = -s^4\left(LR_oCC_{pv}\right) - s^3\left(LC_{pv} - LR_oCK_{pv2}\right) - s^2(R_oC + R_oC_{pv}(D')^2$$
$$-LK_{pv2} + 2V_{dc}R_oCK_{p2}) - s(1 + 2V_{dc}K_{p2} + 2V_{dc}R_oCK_{i2}$$
$$-R_oK_{pv2}(D')^2 + 2R_oI_LK_{p2}D') - (2V_{dc}K_{i2} + 2R_oI_LK_{i2}D')$$

The small-signal $\frac{dp}{di}$ − output transfer function of inner control loop is written as

$$H_2(s) = \frac{\Delta v_{dc}}{\frac{d\Delta p^{ref}}{d\Delta i}} = \frac{b_0s^3 + b_1s^2 + b_2s + b_3}{a_0s^4 + a_1s^3 + a_2s^2 + a_3s + a_4} \tag{5.38}$$

where

$$b_0 = LR_oC_{pv}I_LK_{p2}$$
$$b_1 = LR_oC_{pv}I_LK_{i2} - V_{dc}R_oC_{pv}K_{p2}D' - LR_oI_LK_{p2}K_{pv2}$$
$$b_2 = R_oI_LK_{p2} + V_{dc}R_oK_{p2}K_{pv2}D' - V_{dc}R_oC_{pv}K_{i2}D' - LR_oI_LK_{i2}K_{pv2}$$
$$b_3 = R_oI_LK_{i2} + V_{dc}R_oK_{i2}K_{pv2}D'$$
$$a_0 = LR_oCC_{pv}$$
$$a_1 = LC_{pv} - LR_oCK_{pv2}$$
$$a_2 = R_oC + R_oC_{pv}(D')^2 + 2V_{dc}R_oCK_{p2} - LK_{pv2}$$
$$a_3 = 1 + 2V_{dc}K_{p2} + 2V_{dc}R_oCK_{i2} + 2R_oI_LK_{p2}D' - R_oK_{pv2}(D')^2$$
$$a_4 = 2V_{dc}K_{i2} + 2R_oI_LK_{i2}D'$$

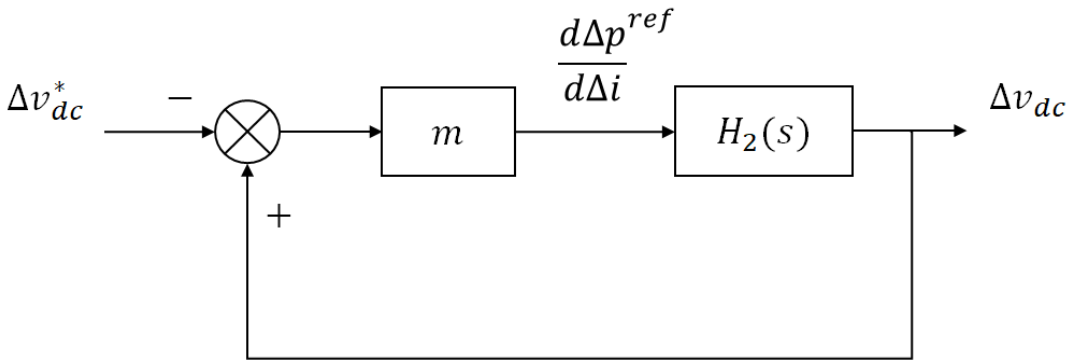

Figure 5.12 Block diagram of the proposed control system.

In MATLAB simulation, it is vital to calculate the inductor current of the boost converter to derive the small-signal transfer function. By substituting (5.21) into (5.38), as well as the parameters, the results of the inner loop transfer function can be obtained. The stability of the cascade control can be determined by bode plots, which is the main objective of deriving the closed-loop transfer function of the dc MG. To finalise the overall transfer function of the proposed control system, the droop coefficient is involved in the calculations for a comprehensive analysis of the stability. It can be seen from Figure 5.12 that the open-loop transfer function is defined as the product of the droop coefficient and small-signal $v_{dc} - \frac{dp}{di}$ transfer function. Last but not least, this is a positive feedback loop which is exactly the same as the skeleton of primary loop. In other words, the general feedback equation cannot be applied to the proposed V-dp/di control system. Considering Figure 5.12, the overall transfer function of the system with proposed V-dp/di method can be written as

$$\frac{\Delta v_{dc}}{\Delta v_{dc}^{ref}} = \frac{m \cdot H_2(s)}{m \cdot H_2(s) - 1} \tag{5.39}$$

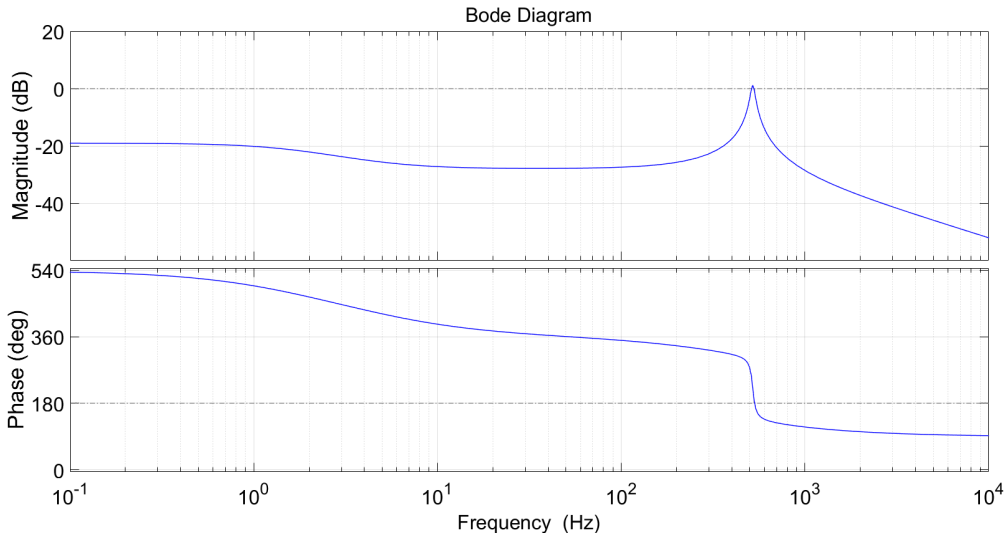

Figure 5.13 Bode plots of outer feedback loop of proposed control method in MPPT mode.

It is shown in Figure 5.13 that the outer loop of proposed V-dp/di control method is stable. The stability of the PV-based dc MG system with proposed control scheme has been improved, since the system in MPPT mode is stable with a lower bandwidth in Section 5.2. The phase margin obtained in the phase plot is 11.3 °. And the measured gain margin is 1.17 dB. As can be observed in Figure 5.13, the bandwidth of the closed-loop system is approximately 528 Hz. The bandwidth of conventional V-dp/dv method is 45% less than the new value of bandwidth. Therefore, the proposed V-dp/di control algorithm takes advantage of novel term dp/di to boost the speed of steady-state response. In MPPT mode, surprisingly, the bandwidth difference between inner and outer loops is insignificant for droop control methods. This is due to the fact that the desired dc bus voltage is the same as the reference value. The functionality of droop coefficient is disabled in MPPT mode, in which the control system behaves as a single dp/di regulator. This is the main benefit of a droop control scheme for a PV source. The maximum PV power can thus be rapidly extracted from PV arrays to operate in grid-connected/islanded mode.

A droop controller is implemented in the outer loop of decentralized coordination control, which is simply a fixed constant. In [70], Cai et al. established the conventional cascade control with dp/dv to autonomously manipulate PV output power according to the status of dc MG system. However, in [10], the authors suggested that the outer voltage PI controller can be removed from the control system. A comprehensive analysis of two droop control configurations is provided in [50]. They validated the droop control with a single loop controller and summarised that the single PI controller offers better dynamic characteristics

than the classical cascade control with two independent controllers. In [50], the pole shifting trajectories of the classical cascaded loop show that two poles are near the imaginary axis, in which the system takes longer to reach the steady state. Meanwhile, these two poles are unaffected by two control settings of the outer voltage PI circuit. The improvement of dynamic performance of droop controller is therefore necessary to increase the overall stability of a dc MG .The lack of outer PI controller has a positive impact on the overall speed of steady-state response of proposed V-dp/di control. The control system of a PV generator in a dc MG remains stable in the absence of outer voltage PI controller.

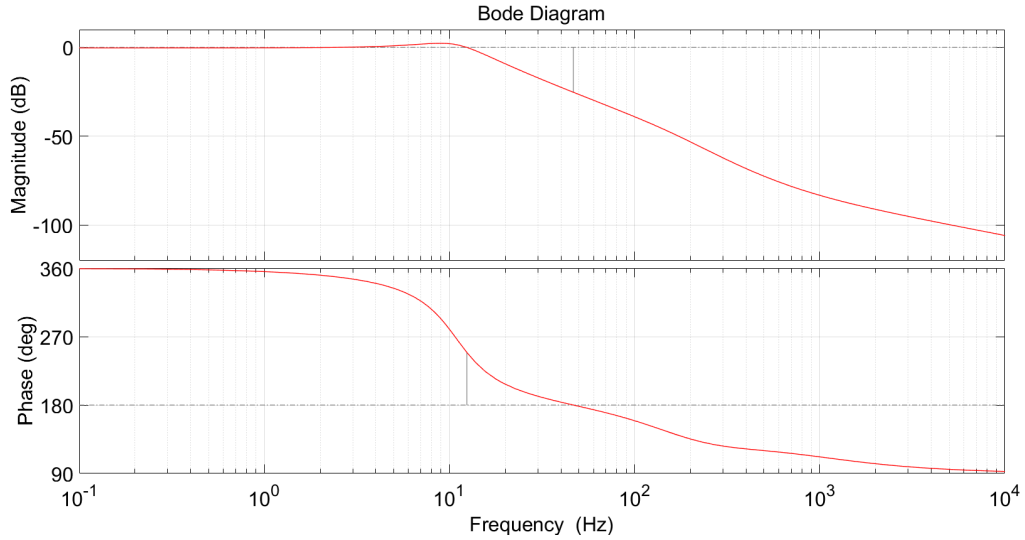

Figure 5.14 Bode plots of outer loop of proposed control method in stand-alone operation.

It can be seen from Figure 5.14 that the outer loop of proposed V-dp/di control system is stable, given the gain margin and phase margin are both positive. To make a comparison between two control algorithms, the same set of parameters is implemented in this analysis to assess the steady-state performance of the proposed V-dp/di control system. The droop coefficient of the system is set to 5, which means the maximum dc bus voltage fluctuation is about 27 V. This is similar to the simulation study. The PV standalone mode is activated, at which the available PV production is higher than the load consumption. The outer loop of the cascade control system generates a desired dc bus voltage with the help of droop coefficient. A reference dp/di value is fed into the inner loop for producing a sufficient PV power to meet the load demand. Therefore, the PV standalone mode is crucial to validate the functionality of the proposed V-dp/di droop control method. As shown in Figure 5.14, the phase margin is 69.3 ° in which the proposed system has greater stability than classical method. Moreover, the gain margin of the novel control strategy is 25.2 dB. The measured gain is higher than the

original value, which implies better static characteristics of the dc MG system. The bandwidth of the outer loop is found to be 46.7 Hz. In literature, most of the studies suggested a minimum of five to ten times difference in cascaded loop is critical to the overall performance of the system. Eventually, the proposed V-dp/di control method satisfies all the basic requirements, while optimising the control system. The proposed method takes advantage of accurate inner variable. The feasibility of the system has been verified in the stability analysis.

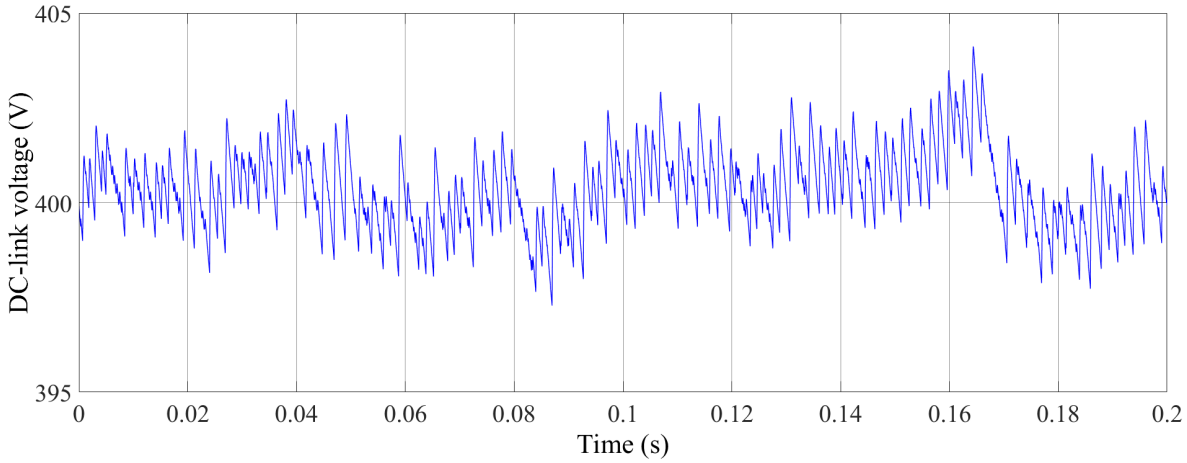

Figure 5.15 Steady-state response of the dc bus voltage with critical gain.

A simulation model is used to validate the results obtained in the stability analysis. By gradually increasing the proportional gain of the controller, the static response of the output voltage begins to indefinitely oscillate. This is referred to as critical gain. All the integral and derivative terms are set to zero, in order to measure the critical gain. As a result, the critical gain of the closed-loop system in Simulink is 0.00625. As shown in Figure 5.15, the steady-state characteristic of the dc bus voltage can be observed. The output voltage is fluctuating around the reference value. It is concluded that the system is marginally stable. The load power is set to 1.5 kW in this part, which implies that the desired dc bus voltage has to be greater than 400 V in the proposed V-dp/di droop control.

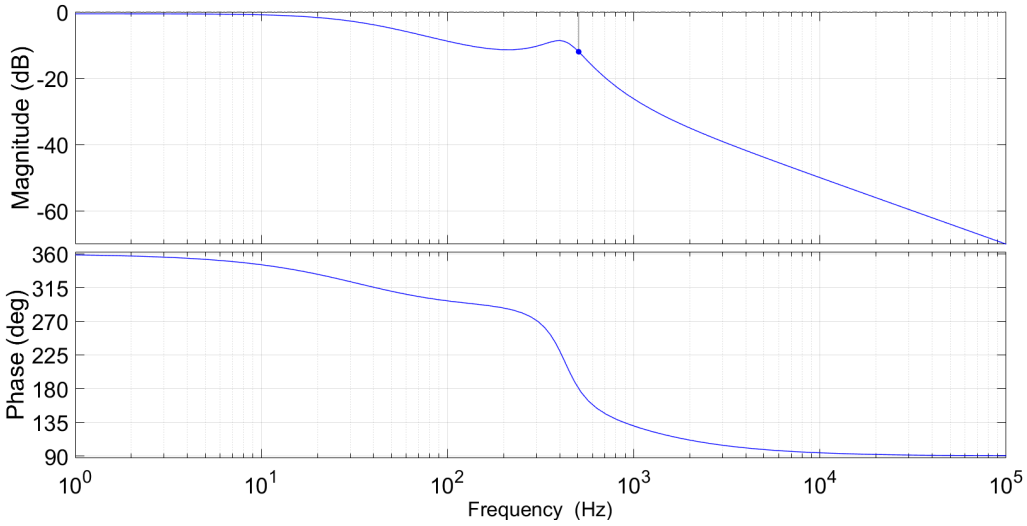

Figure 5.16 Bode plot of the closed-loop transfer function with critical gain.

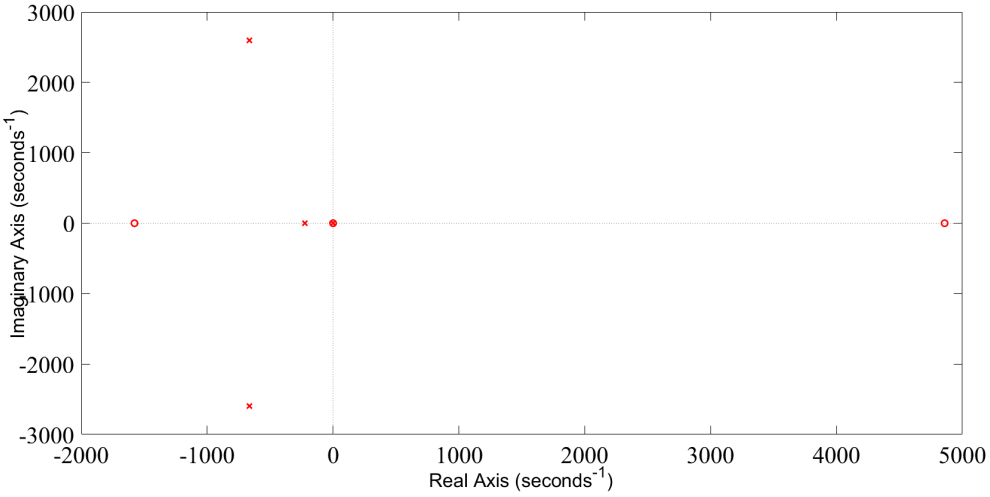

Figure 5.17 Pole-zero map of the overall closed-loop transfer function.

The critical gain is applied to the closed-loop transfer function calculated in Section 5.3. It can be seen from Figure 5.16 that the bandwidth is 506 Hz and gain margin is 3.98 dB. There is a RHP zero observed in Figure 5.17, which is the key drawback of a classical boost converter. It leads to a non-minimum phase characteristic, in which the output response becomes negative before changing the direction back to positive. Eventually, control engineers may consider selecting a lower bandwidth to make the system stable. The results in simulation model validate the outcomes of the stability analysis, in which a critical gain is used to make a comparison between two independent methods.

5.4 Chapter Summary

In this chapter, a comparison of conventional V-dp/dv and proposed V-dp/di control systems in the form of mathematical analysis is present to evaluate the steady-state response performance of a PV-based dc MG. The overall closed-loop transfer function of the conventional V-dp/dv method is derived in Section 5.2. The results in MATLAB show that the inner loop system is unstable in a PV-based dc MG with a boost converter, regardless of the PI settings. The main issue of implementing the conventional method is low accuracy of dp/dv.

The overall closed-loop transfer function of the proposed V-dp/di control algorithm is thus derived in Section 5.3. This is a detailed mathematical analysis to fully understand the limitations of conventional V-dp/dv control method. The specifications of the dc MG system in proposed control are exactly the same as the one in conventional method. The stability analysis is based on a simplified dc MG system that involves a single PV source. The results of stability analysis for inner loop and outer loop demonstrate that the proposed control variable dp/di easily stabilises the dc MG system with the help of PI controller. The importance of dp/di has a crucial effect on the stability of the control system. The term dp/di is the variable that can accurately represent the correct amount of PV power, which is validated in Chapter 4. Compared to conventional dp/dv, dp/di is more appropriate to be chosen as the inner control variable to perform PV power balancing. The outer voltage loop of proposed V-dp/di control system is stable in Section 5.3, according to the outcomes in MATLAB. Furthermore, recent literature has reported that the droop control strategy with a single PI controller is always reacting faster than the generic cascade control system with two individual controllers. The key advantage of the proposed V-dp/di control algorithm is simple tuning process, which requires only one PI controller to be tuned. A simulation model is presented to validate the results of the stability analysis. This can simply be undertaken by looking for the critical gain of the closed-loop transfer function in the simulation model. The critical gain can be substituted into the transfer function calculated in stability analysis. The results show that the gain margin is almost zero which is close to the outcomes in simulation.

Chapter 6. Simulation Results of Proposed V-dp/di and Conventional Control Algorithms

6.1 Introduction

In this chapter, the improved dynamic performance of the proposed V-dp/di droop control method is examined, following the assessment of the conventional V-dp/dv control strategy. The system dynamics of the conventional control technique is demonstrated to replicate the dynamic behaviour in literature. Simulation results of two different control schemes are presented to fully understand the impact of dp/di, as well as the effect of introducing second differential of current approach. This provides a platform to identify the key challenges of the conventional method and to assess the effectiveness of the proposed control system. The proposed V-dp/di control is implemented in the dc MG system to yield an improved dynamic and steady-state performance. Taking standard test conditions into account, the impacts of step load change and fast irradiance change are investigated to simulate abrupt dynamic characteristics of the system. A significant variation in solar irradiance and step load change are implemented to validate the robustness of the proposed method.

To validate the proposed control method, the dc MG system with multiple PV sources is established in MATLAB/Simulink® using MATLAB R2017a. The Simulink model consists of two sets of PV arrays with basic step-up converters, a Lithium-ion battery with a bi-directional dc/dc converter, and a variable dc load with a step-down converter. The overview of the control framework can be reviewed in Chapter 4. A droop coefficient is used to equally distribute the load demand to each PV array for the purpose of proportional power balancing. It is noted that a classical PI controller is employed in the BESS, load system, and single-phase grid-connected inverter to perform the basic functions for simulation, respectively.

The rest of this chapter is organised in the following sections. Section 6.2 introduces the simulation model in detail and fundamental preparations during the phase of a simulation study. The remaining sections present the simulation results of the conventional and proposed V-dp/di control methods, and a comparison of two different control schemes. The parameters for performance evaluation include settling time, voltage deviation, voltage overshoot, voltage ripple, and power fluctuations. Last but not least, the impacts of the novel 2nd differential term are discussed in Subsection 6.4.4.

6.2 Simulation Model

The model of the dc MG system with PV arrays is implemented in Simulink® using the MATLAB® based Simscape™ for power electronic components such as capacitor and inductor. All of the dc/dc converters in this thesis are based on the classical topologies to ensure that the fundamental functions of each of them can be performed. To realise proportional power sharing, two independent PV systems are used to share the load demand among solar panels without any communication agent. A detailed description of the mathematical model of PV arrays is present in Chapter 3. The main benefit of customising a PV model is high flexibility. The specifications of the PV module are obtained from the datasheet provided by the manufacturer to simulate the PV characteristics, taking the intrinsic elements into consideration, which should be almost the same as practical model.

In an islanded mode, where grid-connected inverter is unavailable, the BESS has become the dominant energy source to maintain the single bus voltage at 400 V. To behave as a dominant source, it is compulsory to restore the dc-link voltage and to feed power through the dc bus to the consumer load. As previously stated, in [47], a thorough control framework of the bi-directional dc/dc converter for BESS is provided in Chapter 3. It comprises two modes of operation, charging and discharging. The battery is usually discharged in an islanded mode unless the solar power is adequate for supporting the load demand. The battery discharge mode is the most commonly used operation mode in an islanded dc MG. Figure 3.7 shows the control diagram for the discharge mode, which is simply a classical cascaded loop. It is made up of an outer dc-link voltage loop and inner battery current loop. Each of them is associated with an independent PI controller to manipulate the variable, respectively.

The load system is composed of a step-down converter, two resistive loads, and a classical voltage loop. The specifications of the converter can be observed in Chapter 3. To evaluate the performance of the dc MG, a step load change is included in the simulation. This can be accomplished by implementing a single switch connected to the 2nd resistor. A pulse generator is employed to produce a signal to activate the second load during the simulation. The resistance at the load side is significantly varied to simulate step load changes. A traditional PI controller is used to process the error signal and output a duty cycle.

There are some basic settings and configurations of the islanded dc MG system with two PV arrays. The controlled current source in Simulink is directly connected to the output side of the PV model, which is used to generate a corresponding current to behave as a PV array.

PV1 is made up of 6 SunPower® X-Series Residential Solar Panels (X21-335-BLK) with 2 in series and 3 in parallel. The nominal power of the PV1 is 2 kW. The open-circuit voltage and short-circuit current of the PV1 are 135.8 V and 18.69 A, respectively. The rated power of PV2 is set to 1.368 kW. As a result, the performance of power balancing among PV generators in the proposed V-dp/dv control method can be evaluated. The open-circuit voltage remains unchanged, however, the short-circuit current of PV2 is 12.46 A. All of the power converters are modelled in MATLAB/Simulink using Simscape™ Library blocks. A dc-link capacitor is implemented in the single dc bus to initialise the nominal dc-link voltage of 400 V. The specifications of the simulation model can be reviewed in Chapter 3 and Section 4.4.4.

6.3 Simulation Results of Conventional V-dp/dv Droop Control

The conventional droop control method is implemented in the dc MG system to obtain simulation results. The dc MG operates in a battery islanded mode, where the grid-connected inverter is disconnected, which means the bi-directional dc/dc converter in BESS participates in the dc-link voltage restoration. The dominant energy source always keeps the dc bus voltage at the desired value of 400 V, regardless of how the PV outputs and load demand vary. In other words, the deviation of dc bus voltage is approximately zero, assuming the PI controller for BESS works properly. This means two PV systems play a critical role in harvesting the maximum available energy from the PV arrays.

To assess the system dynamics of the conventional V-dp/dv control, the SoC of BESS is assumed to be high for the battery system to be disabled. Therefore, the SoC of a battery is set to 80 per cent. In this scenario, the BESS is forced to be deactivated until the SoC drops below 80 percent. It is said to be PV standalone mode. PV sources and consumer load have become the key elements of the dc MG, without the support of BESS and single-phase grid-connected inverter. Both PV1 and PV2 take part in the dc bus voltage regulation, and proportional power sharing among PV arrays. The droop coefficient is capable of linearizing the PV characteristics, and hence the power ratio between PV1 and PV2 can usually be kept constant. This thesis assumes that both PV arrays are installed in a rural area, in which the standard test conditions are consistent throughout the simulation. The step load changes and significant change in irradiance are implemented in Simulink to identify the key issues of the conventional V-dp/dv control technique. Table 6.1 shows the controller parameters for the simulation of conventional control based on Table 2.1 and manual tuning. The proportional term is first tuned to obtain a steady-state response, which has SSE and reduced settling time.

Afterwards, the integral term is introduced to eliminate the SSE and stabilise the closed-loop system. Eventually, the derivative term is increased to suppress the voltage overshoot. The dc load may vary over time to demonstrate the working principle of the conventional PV droop control system.

Table 6.1 Simulation parameters for conventional V-dp/dv control method

Parameter	Value
Outer Proportional gain for BESS $K_{p\_OutBESS}$	7
Outer Integral gain for BESS $K_{i\_OutBESS}$	0.06
Inner proportional gain for BESS K_{p_InBESS}	0.007
Inner integral gain for BESS K_{i_InBESS}	0.0008
Proportional term for load K_{p_load}	0.00025
Integral term for load K_{i_load}	0.00013
Proportional gain for PV1 controller K_{p_PV1}	6
Integral gain for PV1 controller K_{i_PV1}	0.05
Derivative gain for PV1 controller K_{d_PV1}	20
Proportional term for PV2 controller K_{p_PV2}	3
Integral term for PV2 controller K_{i_PV2}	0.012
Derivative term for PV2 controller K_{d_PV2}	18
Droop coefficient for PV1	5
Droop coefficient for PV2	4.25
Sampling frequency f_s	20 kHz
Switching frequency f_{sw}	20 kHz

6.3.1 Islanded Mode

In the islanded operation, the voltage regulation of the dc MG is handled by the bi-directional dc/dc converter in BESS. The nominal dc-link voltage would be 400 V during the phase of

simulation work. The standard test conditions of the irradiance and temperature for both PV sources are set to 1000 W/m^2 and 25 ℃, respectively. As can be seen from Table 6.2, the solar insolation of PV1 and PV2 drops to 800 W/m^2 at 0.05 s, and then 500 W/m^2 at 0.15 s. A step changing irradiance is implemented in the signal builder to create disturbance to the PV systems, as well as the single dc bus. This provides an opportunity to observe the transient response of the dc MG, in order to have a better understanding of system dynamics of BESS. The operating temperature keeps constant in the simulation. Moreover, a step load change is developed in the simulation model to validate the classical control for BESS and PV arrays. To start with, Load 1 is set to 500 W (4.608 Ω) with a typical load voltage of 48 V. The load system is composed of two resistive loads. The switch for step change is driven by the pulse generator, which allows Load 2 of 1.5 kW (1.536 Ω) to be in working order after a time delay of 0.1 s. The reference load voltage remains the same in a parallel circuit during transients. Table 6.3 presents the step changes in output load resistance for the simulation study. Furthermore, the initial SoC of battery is set to 50%. This is to ensure that the Lithium-ion battery model is capable of storing excessive power from the dc bus, and generating adequate energy to supply the consumer loads.

Table 6.2 Simulated irradiance changes for PV systems

Period	Time (s)	Irradiance (W/m^2)
I	0 – 0.05	1000
II	0.05 – 0.15	800
III	0.15 – 0.2	500

Table 6.3 Step load changes in islanded mode

Time (s)	Resistive load (Ω)	Load power (kW)
0 – 0.1	4.608	0.5
0.1 – 0.2	1.152	2

Figure 6.1 shows the dynamic performance of the BESS in islanded operating state. The blue curve represents the battery voltage under significant change in irradiance and step changing

load. The maximum overshoot/undershoot of the battery current are found to be less than 0.058%. The measured voltage ripple is ±0.03%. On the other hand, the red curve refers to the current signal of the battery. The overall current ripple of the battery is around ±11.11%. The averaged settling time of the current is 15 ms, which is within an acceptable range. The inner current loop always responds much quicker to the step changes, compared with outer voltage loop, which in turn experiences severe overshoots and fluctuations during transients.

A step change in load resistance and step-changed insolation are implemented in the system to understand the dynamic behaviour of the BESS. In period I, the maximum PV power is extracted under full irradiance and hence the Li-ion battery starts charging. It is crucial to bear in mind that the PV arrays are always operating in MPPT mode for an islanded dc MG. Next, the reduction in irradiance, in period II, leads to a decrease in charging current. But the PV array power is adequate to supply the resistive load. A significant change in load resistance is occurred at 0.01 s, which dramatically increases the load demand to a total of 2 kW. As shown in Figure 6.1(b), the current is approaching zero value as a result of the rise in load resistance. In period III, halving the full solar insolation results in a battery discharging mode to support the load. The dc-link voltage is the indicator to represent the present status of the MG. According to the multi-loop in BESS, the voltage deviation is processed by the outer PI controller to calculate the correct amount of battery current for keeping the reference voltage constant.

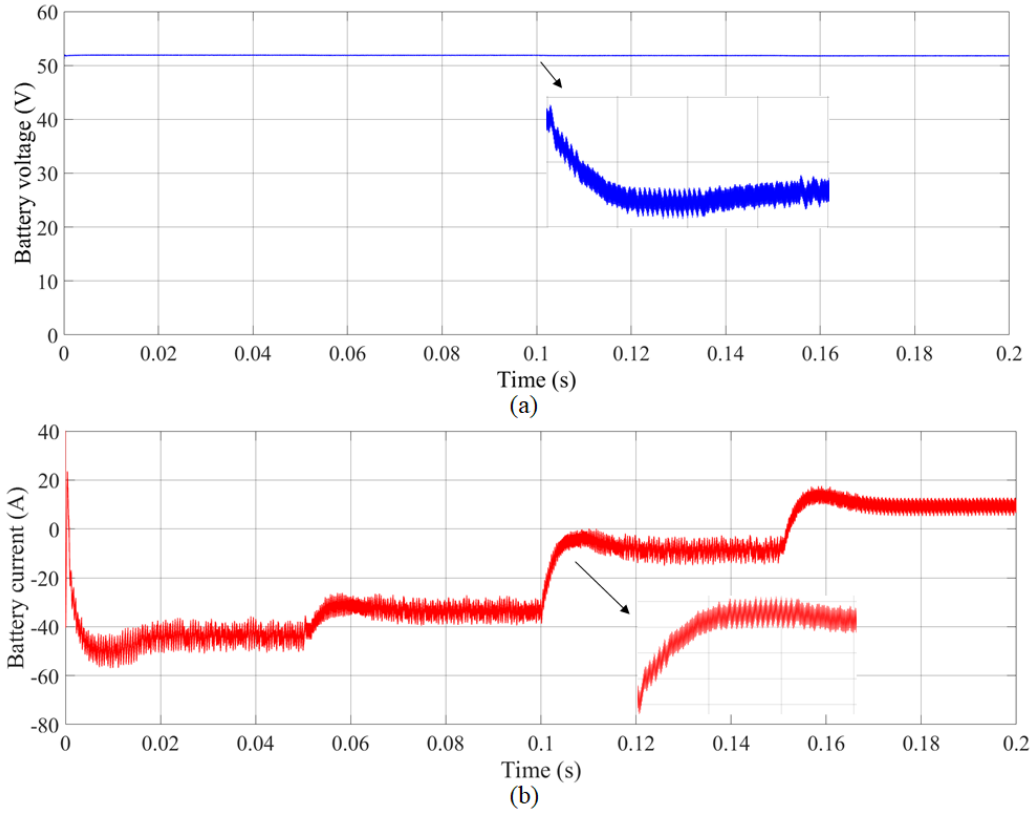

Figure 6.1 System dynamics under different irradiance and step load changes. (a) Battery voltage. (b) Battery current.

Given the dc MG continues its operation in an islanded form, the nominal dc-link voltage has to be maintained which is simply a classical power system. The PV array is maximising its power at the beginning, and therefore a 1% of maximum voltage overshoot can be observed in Figure 6.2. There are three voltage undershoots due to the drop in solar insolation and increase in load resistance. However, the settling time of the dc bus voltage is approximately 10 ms in which the BESS accommodates with those abrupt conditions. The voltage ripple of the dc bus is around 0.375% which greatly supports the idea of establishing a dc MG to integrate renewable energy sources alongside BESS and electrical loads. The oscillations of dc-link voltage are particularly small under half irradiance. This can be linked to the voltage fluctuations in solar panels. Considering a PV array voltage with high ripple, it has an adverse effect on the output of the dc/dc converter which turns out poor dynamics of the dc bus voltage. This is the key reason to devise the proposed V-dp/di method to significantly improve the PV power oscillations and reduce the voltage ripple.

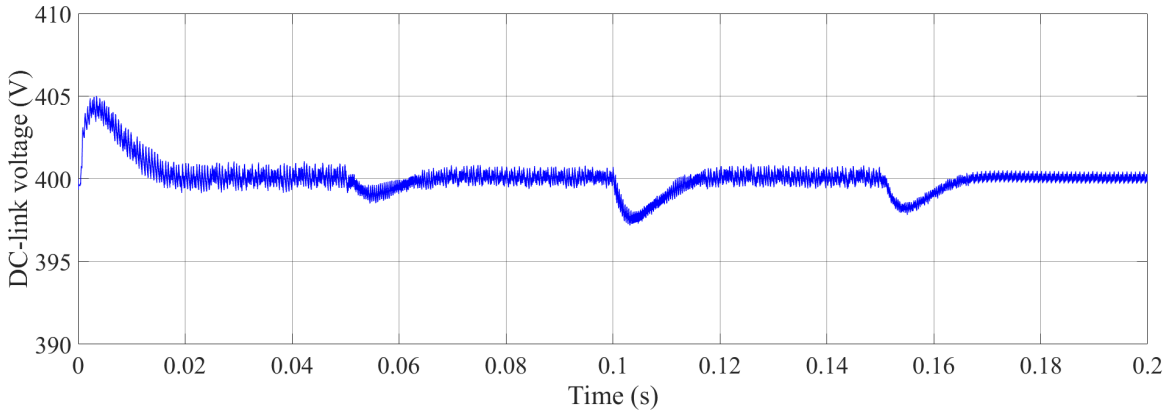

Figure 6.2 DC bus voltage of an islanded dc MG.

It can be seen from Figure 6.3 that the output power of two individual PV sources is present. The blue line represents the array power of PV1, and the red line represents the output power of PV2. Compared to the conventional control algorithm, in [10], the power oscillations in this thesis are eliminated by the PID controller. The power ripple is ±0.63%. However, the implementation of PI controller in [10] results in power oscillations of over ±5%. The overshoots in Figure 6.3 are mainly suppressed by the derivative term, which shows a promising dynamic response performance. In an islanded operation, two PV sources always work in the MPPT mode under different irradiance. An argument to the decentralized coordination control method is how to ensure the BESS is the dominant energy source in an islanded mode. There may be a contradiction between PV arrays and BESS, if both of the energy supplies work in voltage restoration mode. Indeed, the BESS is always the dominant energy supply in an islanded dc MG unless the maximum charge/discharge limit has attained. When it comes to the cascade control in BESS, the value of reference current relies on the voltage deviation of the outer loop. But the PV source requires a searching algorithm to reach the steady state under atmospheric conditions. The MPPT technique takes a significant amount of time to search for new MPP. Instead, the multi-loop in BESS is capable of calculating an instantaneous current reference to restore the dc-link voltage. The outcomes in Figure 6.1 and Figure 6.3 clearly illustrate the modes of operation for BESS and PV systems, and their own responsibilities for an islanded dc MG.

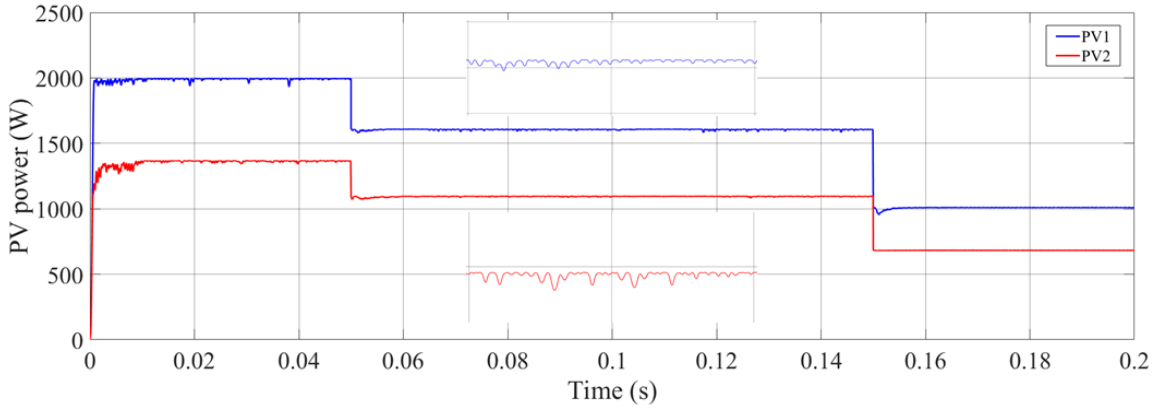

Figure 6.3 Step response of output power of PV1 and PV2 in an islanded mode.

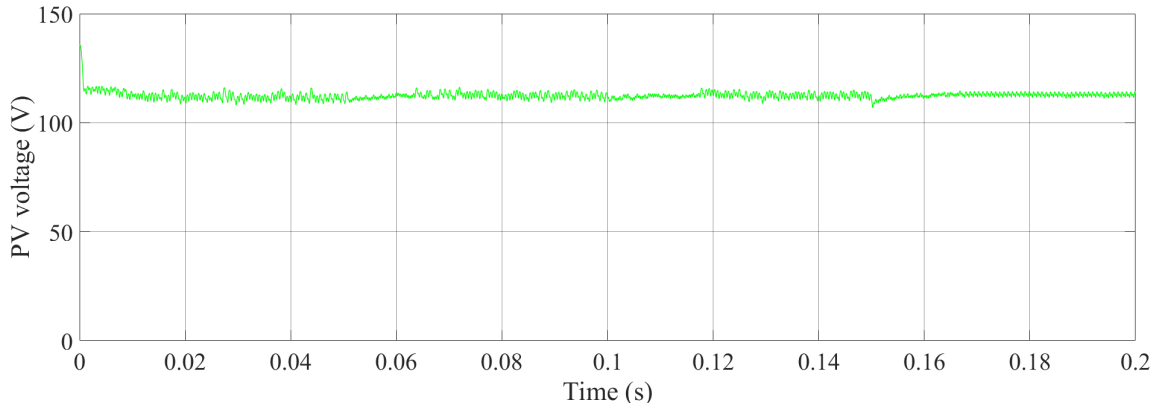

Figure 6.4 Simulation result for voltage of PV1 in islanded operation.

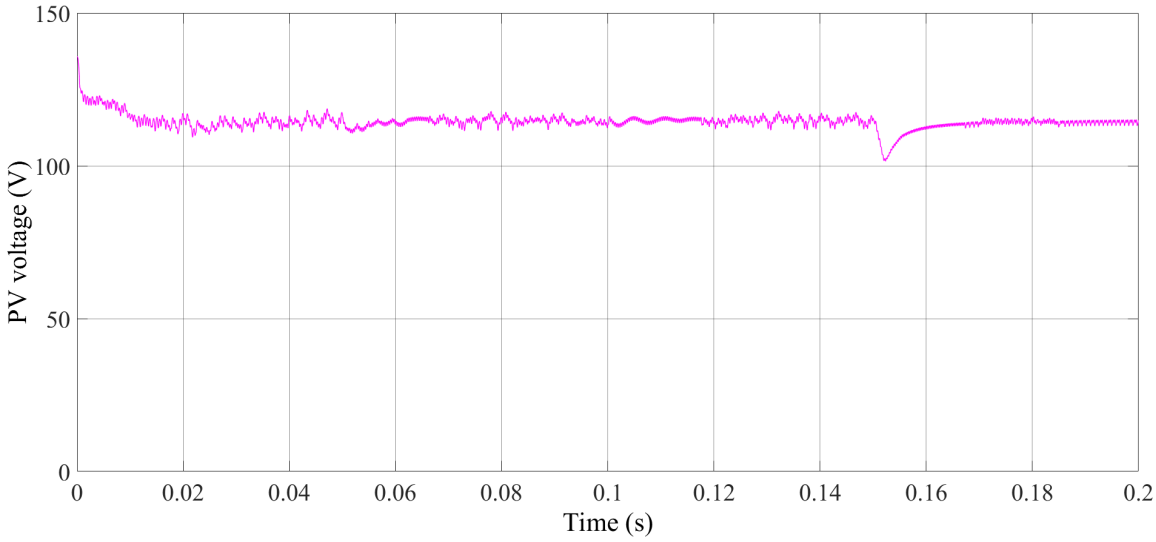

Figure 6.5 Simulation result for voltage of PV2 in islanded operation.

The voltage signals of PV1 and PV2 in an islanded mode are shown in Figure 6.4 and Figure 6.5, respectively. The PV1 and PV2 voltages are kept constant at MPP, regardless of how the weather conditions and load demand vary. The output voltage of PV1 ranges from 112 V to

113 V. The most significant undershoot occurs at 0.15 s when the solar insolation is reduced to 500 W/m^2. The percentage overshoot is about 4.5% which is within a safe operating range. The settling time of PV1 voltage is 5 ms. In terms of PV2, the maximum overshoot is approximately 10.5% which is acceptable. The settling time of PV2 voltage is about 10 ms. The averaged settling time of PV voltages is less than the BESS, but the key function of two PV sources in an islanded dc MG is to maximise their outputs without the need for voltage restoration. As aforementioned, the response speed of a searching MPPT algorithm is always lower than the cascade control of BESS. Overall, the conventional V-dp/dv control presents a better dynamic performance using a PID controller instead of classical PI controller. When it comes to the traditional PI control, this dc MG system may experience severe voltage overshoot and in the worst case it might collapse. Therefore, it would be highly recommended to implement a PID controller in the decentralized coordination method.

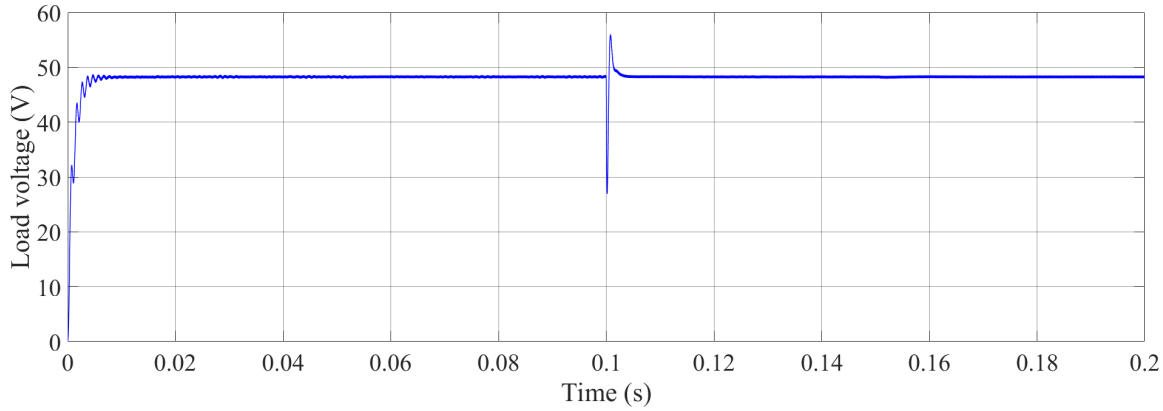

Figure 6.6 Load voltage of the islanded dc MG system.

The load voltage of the dc MG in islanded mode remains unchanged during the dynamic process, as shown in Figure 6.6. The PI controller in the load system has suppressed the voltage overshoot. There is a notable voltage overshoot occurred at 0.1 s as a result of the sudden load change. However, it takes about 2 ms to stabilise the load voltage of 48 V. This can be summarised as a normal condition. To improve the transient response of the load system, a robust controller can be used to avoid unexpected overshoots/undershoots but it is beyond the scope of this thesis. The load voltage is unaffected by the changes in atmospheric conditions, given the BESS immediately responds to compensate for the lack of electrical energy.

6.3.2 PV Standalone Mode

In standalone operation, PV arrays have become the dominant sources of energy to participate in voltage regulation with the help of decentralized coordination control. The solar irradiance of 600 $\mathrm{W/m^2}$ and operating temperature of 25 ℃ are initial test conditions of two PV sources. The solar insolation is scheduled to rise to 800 $\mathrm{W/m^2}$ at 0.05 s, and to full irradiance (1000 $\mathrm{W/m^2}$) at 0.15 s. The step changing irradiance in the PV standalone mode can be observed in Table 6.4. These settings are used to simulate the event, in which the PV power exceeds the load demand. The dynamic performance of the dc MG can thus be assessed. Plus, a step change in load is deployed to understand the properties of the existing control strategy. The initial load resistance is set to 4.608 Ω with a nominal voltage of 48 V. The consumer load is increased to 1.536 Ω at 0.1 s to draw 1.5 kW power from the dc MG. The simulation events for step changing load are presented in Table 6.5. On the other hand, the battery is assumed to be fully charged at SoC of over 80% and is therefore disconnected from the dc MG.

Table 6.4 Different step-changed irradiances for PV arrays

Period	Time (s)	Irradiance (W/m^2)
I	0 – 0.05	600
II	0.05 – 0.15	800
III	0.15 – 0.2	1000

Table 6.5 Step changing load in PV standalone mode

Time (s)	Load resistance (Ω)	Load power (kW)
0 – 0.1	4.608	0.5
0.1 – 0.2	1.536	1.5

Figure 6.7 shows the transient performance of the dc-link voltage waveform in PV standalone mode. It can be summarised that the dc bus voltage is within an acceptable range, since the maximum allowable voltage of the conventional V-dp/dv control method is about 435V. The voltage deviation in Figure 6.7 can be utilised to curtail the PV output power, so that the PV-

based dc MG system is stable. The settling time of the dc-link voltage in average is approximately 20 ms. The feedback voltage is greater than the nominal value, which implies that curtailing the excess solar energy is the best way to stabilise the dc MG. At 0.1 s, the sudden increase in load demand results in a drop in dc-link voltage. Surprisingly, the voltage ripple is proportional to the solar insolation. The results in Figure 6.7 demonstrate that voltage fluctuations occur when the PV system is under full irradiance. The step response of the single bus voltage depends on the quality of PV power. In Chapter 4, the key issues of the accuracy of primary control variable in conventional V-dp/dv method have been discussed. To tackle the challenges, the V-dp/di control strategy is proposed to yield an improved PV power quality. The voltage ripple is found to be 0.25% during simulation. In case of step-changed irradiance, the dynamic characteristics of PV curve are varied accordingly. Therefore, the PV system is required to search for the new point of output power. This has led to an increase in dc bus voltage, but the maximum voltage of the common bus is strictly limited by the droop coefficient.

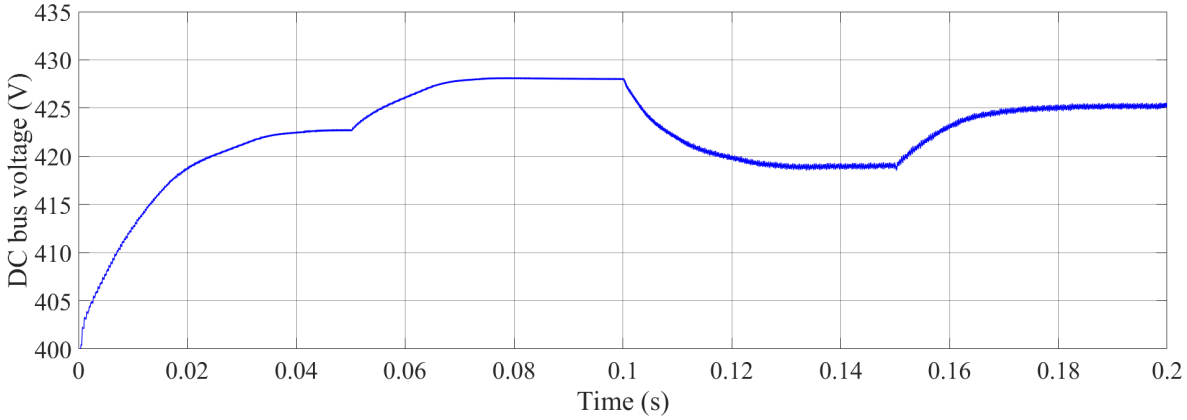

Figure 6.7 Step response of dc bus voltage under step changing load and irradiance.

It is shown in Figure 6.8 that the PV power takes roughly 20 ms to reach the steady-state value. The voltage swells are expected to occur in the event of abrupt change in irradiance. The voltage swell only appears in a short period of time, which is not harmful to the switching device. However, under full irradiance, with the conventional V-dp/dv control method, the measured power oscillation is about $\pm 5\%$. Compared with the power ripple in MPPT mode in Figure 6.3, the present ripple in PV standalone operation is almost ten times larger than the previous percentage. A PID controller has been implemented in the conventional control method to achieve better outputs, but the inaccurate inner variable dp/dv is a serious problem to the overall performance of the dc MG. Hence, the focus of this thesis. The results in Figure 6.8 demonstrate how the PV arrays can share the power in proportion. The initial power ratio

of two PV generators is 1:0.68. In the mode of voltage regulation, the power ratio in average is about 1:0.6 which is close to the theoretical value. This validates the decentralized droop control algorithm for a PV-based dc MG in a PV standalone mode.

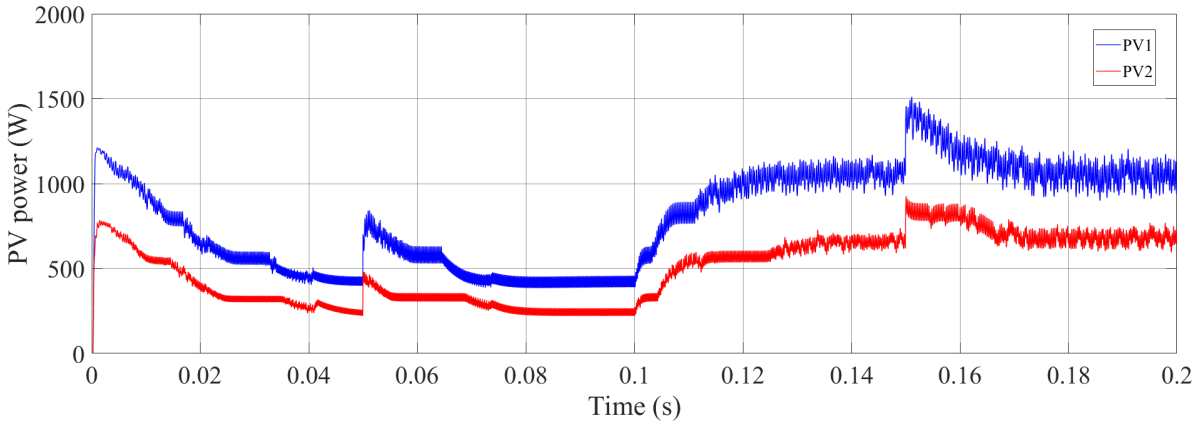

Figure 6.8 Dynamic responses of two PV power curves under step changes.

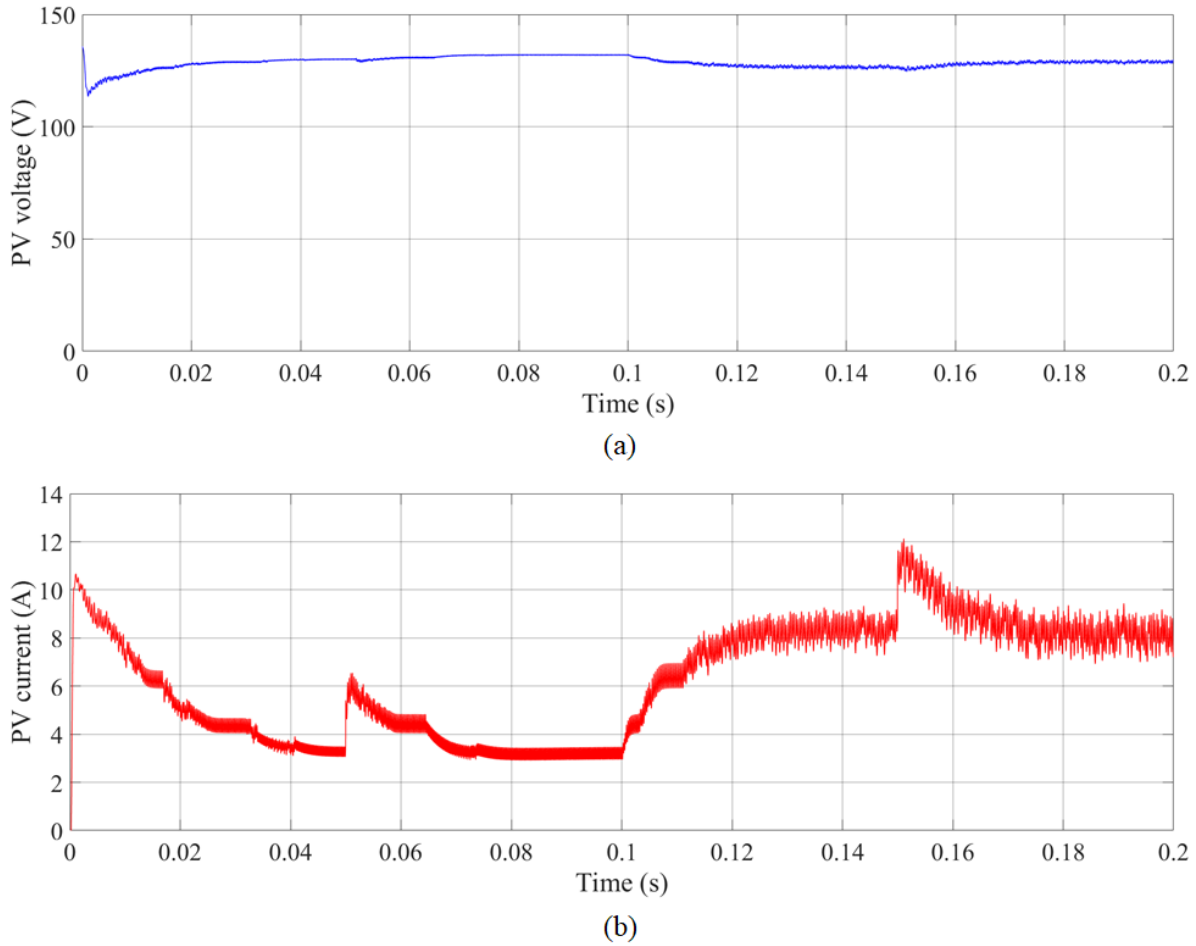

Figure 6.9 System dynamics of PV1 under step changes. (a) PV voltage. (b) PV current.

As shown in Figure 6.9, voltage and current waveforms of PV1 under step load change and fast changing irradiance are presented, respectively. Overall, the voltage signal of the PV1 is

performing well during simulation. These values are all located on the right side of the MPP in the P-V characteristic curve, which is in between voltage at MPP and open-circuit voltage. This is the designated operating region for the PV arrays to produce solar power, in order to prevent short-circuit issues. The measured voltage ripple in Figure 6.9(a) is $\pm 0.8\%$, where the conventional V-dp/dv control algorithm is able to reduce the voltage fluctuations. However, the maximum PV current ripple in Figure 6.9(b) is found to be $\pm 9.375\%$ under full irradiance. It can be concluded that current variations in MPP cannot be suppressed by the conventional control method under high irradiance, resulting in poor PV power fluctuations. This is one of the drawbacks of the conventional voltage-based control. The lack of precision in control variable dp/dv and slow inner loop response are summarised to be the key challenges of the conventional V-dp/dv control system.

In PV standalone mode, the step response of the resistive load is exactly the same as the one in islanded operation. As shown in Table 6.5, there is a step load change occurred at 0.1 s. Figure 6.6 presents a 14.6% voltage overshoot to indicate the large variation in resistance, where two PV sources are increasingly generating solar power to meet the load demand. It takes about 20 ms to reach the new operating point for providing sufficient power to the dc MG. This simulates the worst scenario when the local load demand is growing rapidly. PV arrays play a critical role in regulating the single bus voltage and generating correct amount of solar energy. It is therefore crucial to propose a novel droop control strategy to yield an improved dynamic performance of a dc MG system, regardless of the operation mode.

6.4 Simulation Results of Proposed V-dp/di Droop Control

The V-dp/di droop control method is implemented in the simulation model to evaluate the dynamic response performance of the islanded dc MG, and to compare with the conventional control strategy. The framework of the system is exactly the same as the one in Section 6.3. The dc MG operates in an islanded mode to understand if the proposed method can behave as a MPPT algorithm to extract the maximum solar power. The BESS is in a leading position in a PV-based dc MG to perform voltage restoration. In this case, the main objective of the PV arrays is to maximise their output power. The dc bus voltage remains constant at its rated value in the islanded operation.

The dc MG system works in the PV standalone mode, when the BESS is unavailable. The SoC of battery is set to 80%, which means the upper charging limit is attained. For safety reason, the BESS is temporarily disconnected from the dc MG. The fundamental functions of

the PV arrays are voltage regulation and proportional power balancing among solar panels. It is noted that there is no communication agent between PV arrays to ensure a fully decentralized control. Basically, the dc bus voltage is the key parameter for PV systems to estimate the amount of power required for the resistive loads. The concept of droop control from the conventional V-dp/dv method is applied to linearize the P-I characteristics of the PV panel and compute dp/di, which in turn outputs power in proportion according to the energy consumption. As usual, the standard and abrupt test conditions can be used for assessing the robust performance of the proposed V-dp/di control system. The step changed load and fast irradiance change with the use of Simulink are deployed to observe the system dynamics of the simulation model. Therefore, some key results can be produced to validate the feasibility of proposed V-dp/di method.

Table 6.6 Simulation parameters for proposed V-dp/di control scheme

Parameter	Value
Proportional gain for PV systems (K_{p_PV})	2
Integral gain for PV systems (K_{i_PV})	0.1
Derivative gain for PV systems (K_{d_PV})	7.5
Droop coefficient for PV1 (m_1)	5
Droop coefficient for PV2 (m_2)	5.03
Sampling frequency (f_s)	20 kHz
Switching frequency (f_{sw})	20 kHz

Table 6.6 provides the system parameters for the dc MG with the proposed V-dp/di control algorithm. There is no difference for BESS and load system in this simulation. The discrete PID controllers for PV1 and PV2 are the same, provided that the results show a promising performance. In theory, the initial droop coefficient for a PV source can be calculated. However, manual tuning method is carried out to enhance the accuracy of proportional power sharing. The switching and sampling frequencies remain unchanged to make a comparison between two control methods. Moreover, the test conditions for two modes of operation are

consistent with Section 6.3. Compared with the outcomes obtained in Section 6.3, this should provide a solid understanding of the proposed V-dp/di control algorithm.

6.4.1 Islanded Mode with BESS

The simulation model of the dc MG with proposed V-dp/di method has identical test conditions to the one in Subsection 6.3.1. In islanded mode, the BESS behaves as the dominant source to keep the dc bus voltage constant, while two PV arrays are performing MPPT function under ambient conditions. As shown in Table 6.2, the step-changed irradiance over time is illustrated. The initial value is set to full irradiance, followed by 800 $\mathrm{W/m^2}$ and 500 $\mathrm{W/m^2}$. The PV generators run at a standard operating temperature of 25 ℃ throughout the simulation events. In principle, the dynamic performance of the proposed control scheme in MPPT mode can be assessed. As shown in Table 6.3, the step change in load is present to observe the step response of the dc MG with proposed V-dp/di control algorithm. An additional load power of 1.5 kW is drawn from the common dc bus at 0.1 s, which is a dramatic change in load resistance. The preliminary SoC of BESS is at a half charged state (50%). It offers the battery the best position to charge/discharge battery's current, so that it can manage the unbalanced energy in a MG. The typical common bus voltage is set to 400 V, which is one of the most widely used voltage values in literature.

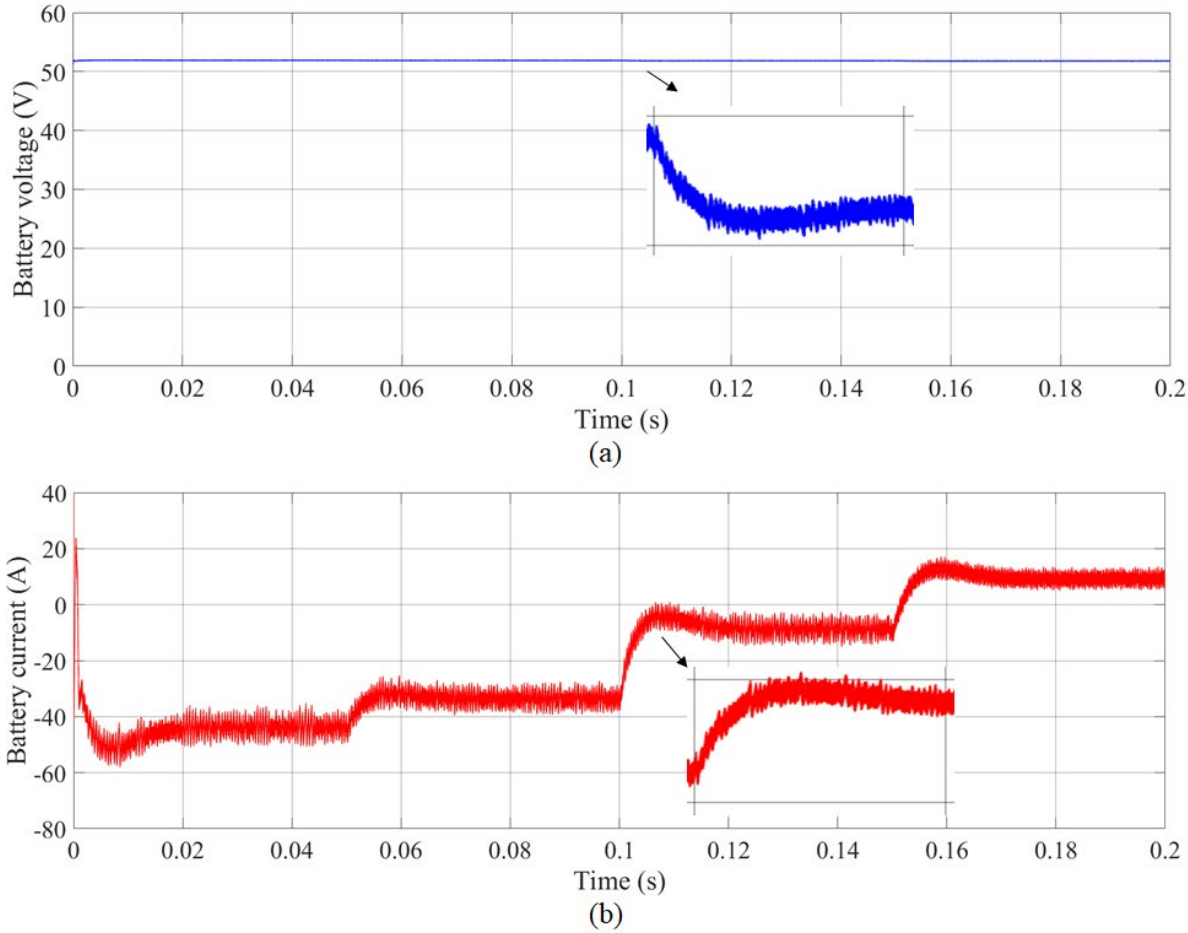

Figure 6.10 System dynamics of an islanded dc MG. (a) Battery voltage. (b) Battery current.

As can be seen from Figure 6.10, the transient response of the BESS is demonstrated. Figure 6.10(a) refers to the voltage signal of the Li-ion battery in blue. Figure 6.10(b) represents the battery's current, where positive sign means the battery is discharging and vice versa. The maximum current overshoot of the BESS is about 1.54%, which is slightly greater than previous value (1.21%) in 6.3.1. Similar to previous simulation in 6.3.1, there is no voltage ripple since the BESS has massive capacity of 250 Ah. The battery voltage remains constant at 51.9 V during transients. It makes no difference to the proposed V-dp/di control in an islanded operation. In addition, the ripple current of the BESS is $\pm$7.32%. The settling time of the battery voltage is around 15 ms. Compared with the results in 6.3.1, the overall battery performance in this test is almost identical to the previous one but the BESS is experiencing more fluctuations and higher overshoot. Besides, the significant change in load demand at 0.01 s brings a negligible impact to the battery's voltage. The BESS is the leading energy supply in this scenario, since the PV arrays are harvesting the maximum available power. It can thus be described as a robust control system due to the abrupt condition. The details of the

step-changed load and fast irradiance change are illustrated in Subsection 6.3.1. There is no major divergence between two simulation models.

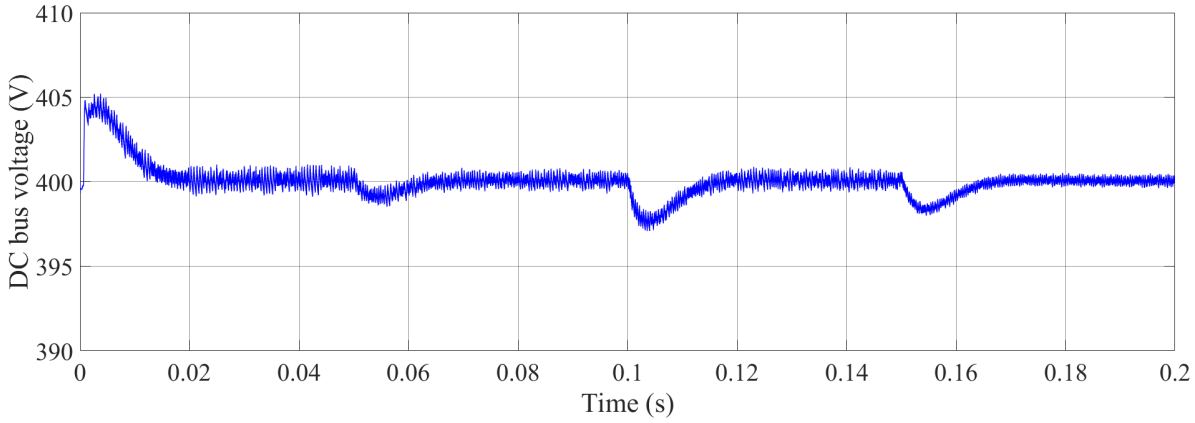

Figure 6.11 Common bus voltage of the dc MG in islanded operation.

Figure 6.11 shows the dynamic response of the dc bus voltage in the islanded dc MG system. There is a 1.13% of voltage overshoot at the beginning, which is consistent with the test in 6.3.1. The surplus PV power results in an overshoot of the dc bus voltage and thus the BESS is responsible for restoring the voltage by charging the battery. The settling time of the single bus voltage is 10 ms, considering 0.5% of steady-state value. Besides, the ripple voltage of common dc bus is found to be 0.375% under full irradiance. It is critical to bear in mind that the proposed V-dp/di control method is designated for the PV arrays. In theory, the transient performance of the islanded dc MG is unaffected. The main point is that the voltage ripple grows with the solar insolation, in which the fluctuations of PV power have a huge impact on the load side of PV system.

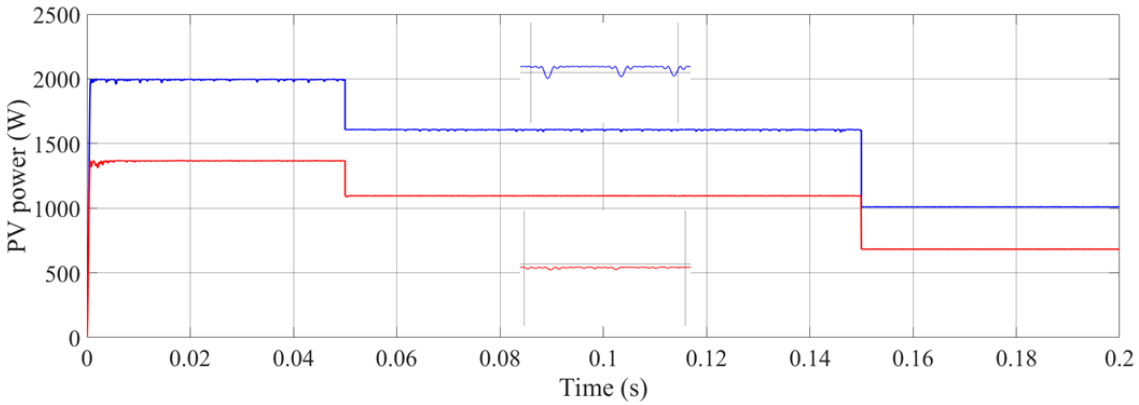

Figure 6.12 System dynamics of array power for PV1 and PV2 in the islanded mode.

As shown in Figure 6.12, the dynamic characteristics of the PV1 and PV2 are presented. In terms of the transient response, the PV power in the above figure experiences less fluctuations and shorter settling time. The power ripple of the PV1 is $\pm 0.5\%$. The performance is greatly improved by 20%, compared with the ripple measured in Figure 6.3. Furthermore, the proposed V-dp/di control algorithm significantly increases the transient response speed of the PV arrays. The settling time is dropped from 10 to 5 ms which in turn shortens the settling time by half. When it comes to a reduction in irradiance at 0.05 s and 0.15 s respectively, notable undershoots can be observed in the power curves shown in Figure 6.3. However, in Figure 6.12, no overshoot/undershoot is demonstrated in two PV power signals where the robust tracking performance has been achieved in the proposed control algorithm. The proposed controller takes full advantage of precise dp/di. The common argument for a MPPT algorithm is that MPPT method based on current usually suffers from fast irradiance change, which results in short-circuit and stability issues. For the proposed control system, the dp/di is utilised to harvest maximum power from the PV arrays. The operating point of power is usually located at the zero slope of tangent line in MPPT mode. This turns out the active region is on the left side of the P-I characteristics. Plus, there is no current reference value directly fed into the PI/PID controller in order to prevent the issue of short-circuits. To sum up, the proposed V-dp/di control strategy demonstrates an improved dynamic performance of the PV systems in an islanded operation.

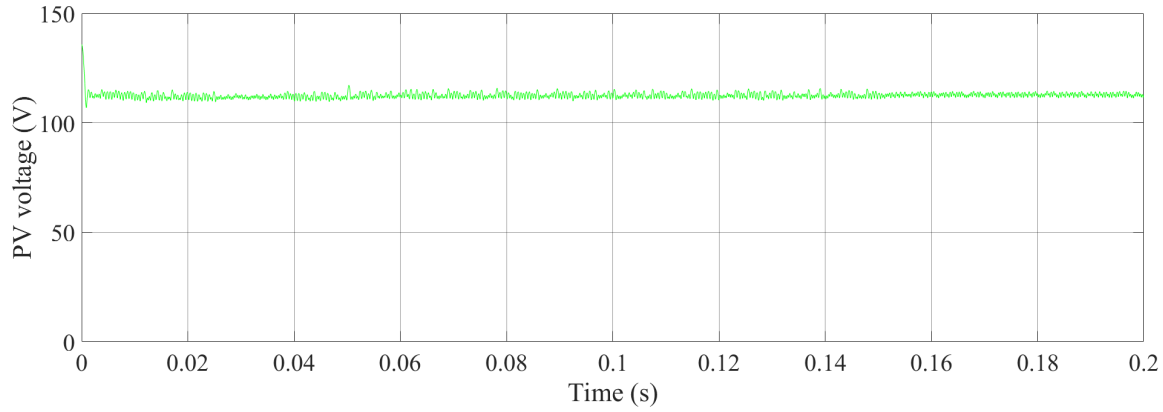

Figure 6.13 Simulated voltage of PV1 under step load change and rapid varying irradiance.

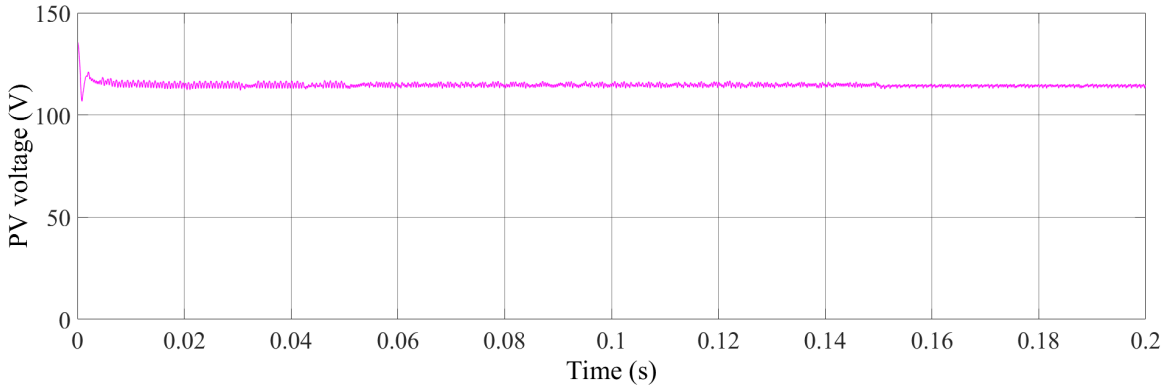

Figure 6.14 Simulated voltage of PV2 under step change and rapid varying irradiance.

The results in Figure 6.13 and Figure 6.14 clearly show that fixed voltage values of PV1 and PV2 are manipulated by proposed V-dp/di control to realise MPPT. A constant voltage of PV1, in a range from 112 to 113 V, is observed. The voltage ripple of PV1 is $\pm 0.9\%$, however, the ripple with conventional V-dp/dv in Figure 6.4 is almost $\pm 1.8\%$. The voltage ripple of PV2 is $\pm 1.09\%$ which is slightly larger than PV1. It has validated the assumptions illustrated in Chapter 4 that the accuracy of conventional control term dp/dv is particularly low, if it is compared to the proposed variable dp/di. The MPPT algorithm in the decentralized coordination method contains only the inner control loop. With no variation in common bus voltage, the zero slope of tangent of P-I characteristic curve is the reference value for the PID controller to achieve. Given dp/di represents the correct amount of PV output power, it is effortless for the PV arrays to reach a specific point of power. The maximum voltage overshoot of 3.08% occurs at 0.05 s, when a step irradiance change is applied to the PV systems. The overshoots are suppressed by the proposed V-dp/di control strategy with a minimum of 31.6% improvement in the transient performance. Indeed, the

expected overshoots at 0.1 s and 0.15 s are absent from the voltage curve in Figure 6.13. This has shown a promising performance of the proposed controller.

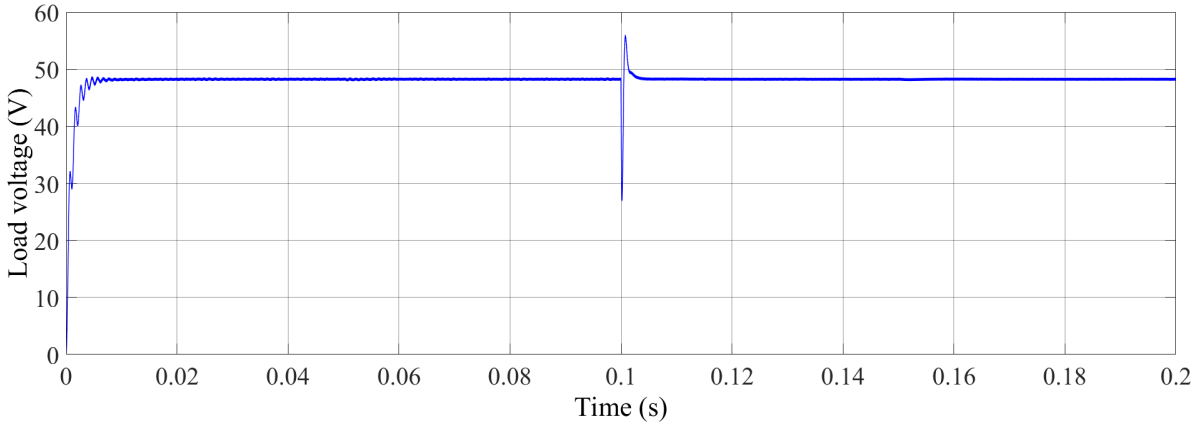

Figure 6.15 Simulation result of load voltage in islanded dc MG.

It can be seen from Figure 6.15 that the load voltage is kept at a constant value of 48.2 V, which implies a SSE of 0.2 V. There is an unusual voltage spike arising from the step-changed load. The signal first experiences a voltage dip at 0.1 s that is absolutely normal to the load system, due to the sudden reduction in load resistance. This in turn means that a huge amount of power is drawn from the common dc bus and hence the voltage dramatically falls to a very low level. There is a 16.18% of voltage overshoot following the voltage sag. The classical PI compensator takes an approach to reduce the error by maximising the duty ratio. The load voltage starts to drop, at which the controller identifies the voltage overshoot. The settling time of the output voltage is 2 ms during transient. Taking the short duration event into consideration, the percentage overshoot will not cause any damage to the device. Afterwards, a static voltage of 48.2 V is attained. It can be summarised that the rapid varying solar insolation in an islanded dc MG has no impact on the resistive load, if the BESS instantaneously reacts to the step changes.

6.4.2 PV Standalone Mode

PV sources are responsible for regulating the single bus voltage of the dc MG system within a safe operating range in the PV stand-alone mode. The PV arrays are constantly providing clean energy to the load, when the BESS and grid-connected inverter are disconnected. The key assumption of the simulation model is that the total solar power is always greater than the local power consumption. Otherwise, the dc MG system may require a load shedding scheme which is beyond the scope of this thesis. To show a promising performance of the proposed V-dp/di control algorithm, the standard test conditions and step changes are applied in

Subsection 6.4.2 to provide a comparative analysis of two control strategies. Table 6.4 presents scheduled step changes in solar irradiance at various times to determine the stability of the dc MG. Basically, the insolation is raised from 600 W/m^2 to 1000 W/m^2 with a step of 200 W/m^2. It can be observed in Table 6.5 that the initial load power is 500 W, followed by an additional load demand of 1 kW. The operating temperature of PV arrays is fixed at 25 ℃. The SoC of the battery is set to 80%, so that the BESS is assumed to be fully charged up. The remaining part of the dc MG system is also known as PV standalone system. These conditions are referring to the simulation events recommended in Section 6.3 for performance evaluation.

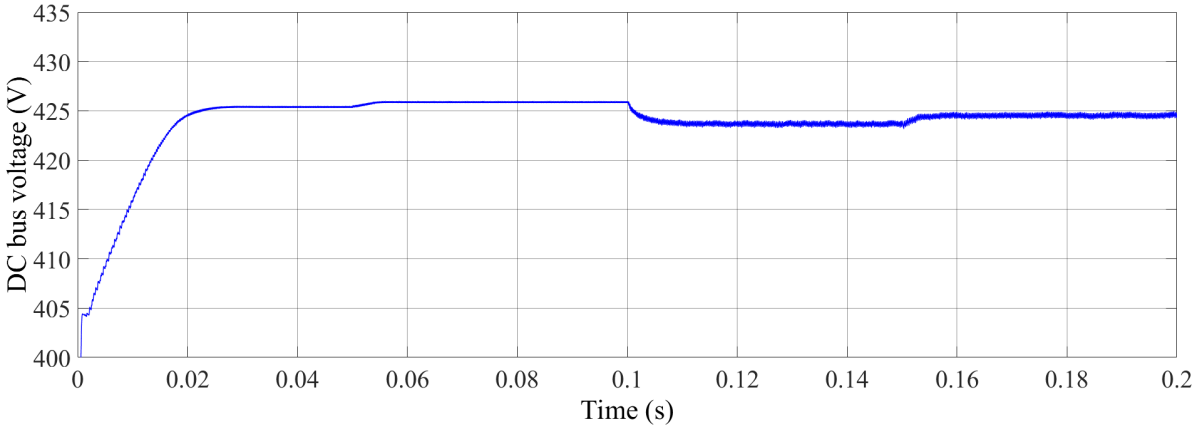

Figure 6.16 Dynamic behaviour of the dc bus voltage in PV standalone mode.

It is shown in Figure 6.16 that the common bus voltage under step changes in load and irradiance, in stand-alone operation, is stable without any overshoot. The upper limit of the dc bus voltage depends on the settings of droop coefficient. In the proposed V-dp/di control strategy, the maximum allowable voltage is dp/di at open-circuit voltage divided by the droop coefficient. Compared to conventional V-dp/dv method, the dp/di at open-circuit voltage is simple to calculate where it is exactly the value of PV open-circuit voltage. In this case, the default upper limit of single bus voltage in the dc MG would be 427 V. As shown in Figure 6.16, it can be confirmed that the voltage has never reached the limit during simulation. Meanwhile, neither overshoot nor undershoot can be observed in Figure 6.16. The averaged settling time of the dc bus voltage is about 5 ms, when the conventional technique takes twice as long to stabilise the system. The voltage ripple of the dc bus is obtained as $\pm 0.07\%$. The voltage fluctuations are dramatically reduced by the proposed method, since the feedback loop is controlling dp/di with a high degree of precision. This is one of the key benefits of the proposed control algorithm. It is concluded the reference voltage is an indicator to represent the energy distribution of a dc MG. However, the proposed feedback loop takes advantage of

small voltage variations to maintain closed-loop stability. The rapid irradiance change has a minor impact on the computation of dc bus voltage under step changes. It is observed in Figure 6.16 that full irradiance can potentially cause voltage oscillations. Therefore, a comprehensive solution to this issue is present in Subsection 6.4.4.

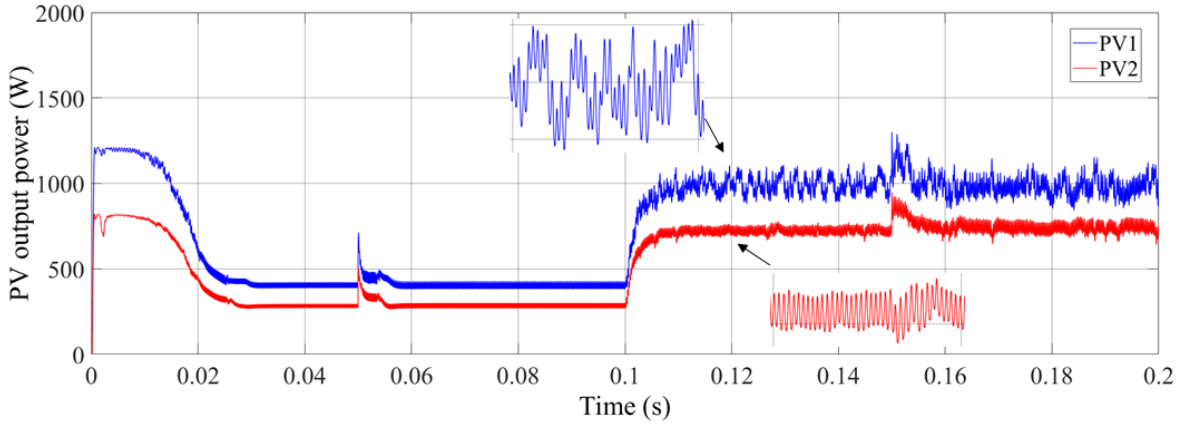

Figure 6.17 Output characteristics of the PV power curves in PV standalone mode.

Simulation results showing the output power signals of PV1 and PV2 in PV standalone operation can be observed in Figure 6.17. Apart from the first transient response, the settling time is 10 ms in average, where the proposed V-dp/di control scheme yields an enhanced dynamic performance of the PV array power. The most striking result to emerge from the data is that the control system with dp/di reaches the steady state in half the time. Similar to Subsection 6.3.2, voltage swells can be seen from the graph. This is mainly caused by the significant change in solar insolation. Nevertheless, the proposed method is capable of generating constant PV output power during transients. The measured power oscillations under full irradiance are $\pm 2.5\%$, where this is 50% less than the power ripple obtained in Section 6.3.2. A PID compensator is implemented in the proposed V-dp/di control strategy to provide a detailed analysis of two decentralized coordination methods. Accordingly, the application of dp/di has a positive impact on the dc MG. It is proved to offer 50% improvement in settling time. Moreover, the typical ratio of two PV power levels is 1:0.68. It can be analysed in Figure 6.17 that the measured power ratio is ranged from 1:0.7 to 1:0.73, which is very close to the nominal value. It is crucial to bear in mind that this is a proportional energy balancing and hence it may differ slightly from the initialised PV power ratio.

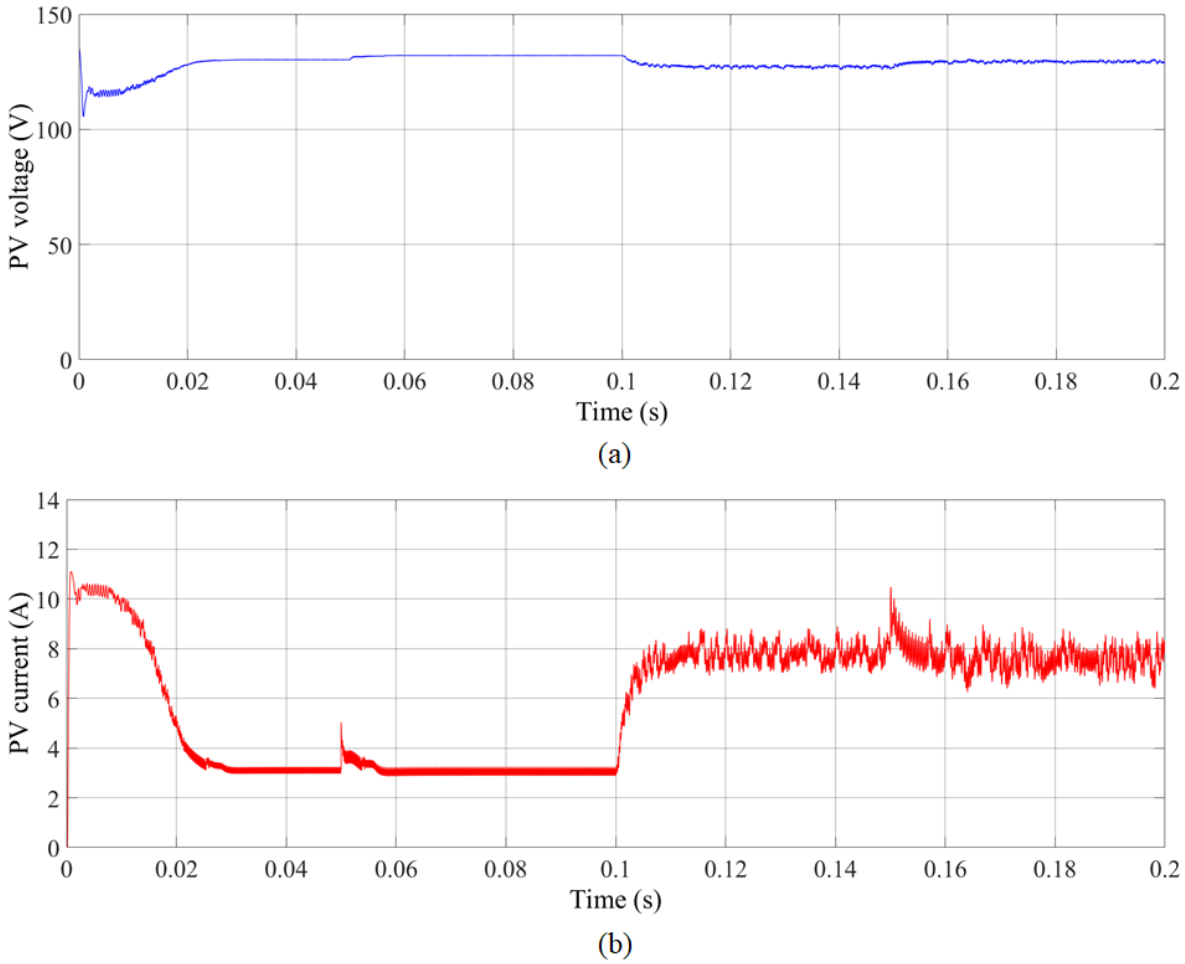

Figure 6.18 Simulation results for transient response of PV1 in stand-alone mode. (a) PV voltage. (b) PV current.

The simulation results in Figure 6.18(a) display the voltage signal of the PV1 in a PV standalone mode. As expected, the voltage ripple in proposed V-dp/di control algorithm is found to be $\pm 0.4\%$. In case of inaccurate dp/di, the PID controller is unable to reduce the SSE, leading to the rise in voltage fluctuations and thus poor quality of PV power. In simple words, the term dp/di is capable of representing the corresponding level of PV power, which turns out a robust performance of the PV system. Furthermore, in the proposed control scheme, the P-I characteristic curve of the PV arrays is used to search for the PV operating point which is based on dp/di. The safe operating range is therefore on the left side of the P-I characteristics. Compared with conventional method, the left side of the P-I curve is gradually varying where a gentle slope can be obtained. Overall, the dp/di is always either positive or zero. The negative slope, on the right side of the MPP, is limited by the saturator at the output of the outer voltage loop. The main benefit of neglecting the negative slopes is short circuit protection. In addition, the traditional MPPT algorithms such as P&O and INC suffer from

fluctuations around the MPP. But the proposed V-dp/di control method allows the PV system to work in a limited operating range, which turns out fewer fluctuations.

The simulation result for output current of the PV1 is shown in Figure 6.18(b). The maximum ripple current during the simulation is $\pm 6.45\%$. There is a 30% improvement of current ripple, compared with conventional control strategy. It validates the working principle of a differential based on current approach. The application of a complete PID compensator results in no overshoot/undershoot of the output signal. A promising performance of the dc MG system in PV standalone operation can be achieved, only if the inner variable is precisely representing the PV array power. The load voltage of the dc MG in the PV standalone mode is displayed in Figure 6.15. When it comes to the step change in load resistance, both PV arrays begin to generate more solar power to meet the load demand and hence the load voltage experiences an overshoot due to searching MPPT algorithm. To conclude, the overall performance of the dc MG system is notably enhanced by the proposed V-dp/di droop control scheme.

6.4.3 Partially Shaded PV Modules in Standalone Mode

It is important to evaluate the dynamic performance of the PV array under partial shading conditions. The term refers to a number of PV modules in a PV generator at different solar irradiance levels, which implies a reduction in PV power generation and power imbalance. As shown in Figure 6.19, the schematic diagram of the PV modules under partially shaded condition is demonstrated. Two of the PV modules on the left are at 800 $\mathrm{W/m^2}$, two of them at the centre are under full irradiance, and the remaining column is at 600 $\mathrm{W/m^2}$. This is one of the most commonly used patterns to assess the P-V and I-V characteristics of the PV generator under partial shading condition [87]. The proposed V-dp/di method with second differential term is implemented in the PV system to produce sufficient solar power and regulate dc-link voltage. The load power is initialised as 800 W, and increased to 1300 W at 0.05 s. The step load change is used to obtain the transient response of the dc MG. The reference value of the dc bus voltage remains unchanged at 400 V. The parameters such as settling time, overshoot, steady-state error, and rise time are utilised to evaluate the dynamic response performance of the proposed control algorithm under partially shaded condition. The outcomes show the robustness and feasibility of the proposed control strategy.

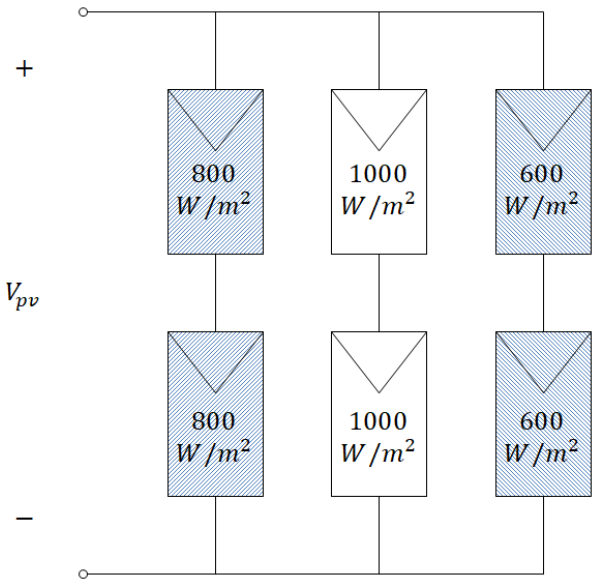

Figure 6.19 PV modules under partially shaded condition.

As can be seen from Figure 6.20, the I-V and P-V characteristics of the PV array under partial shading condition are presented. The first and third columns are under lower irradiances, in which the overall generated power is dropped to 1.6 kW. This shaded pattern has no impact on the operating voltage, which results in similar behaviour of a normal PV generator. However, the rated current is significantly reduced by the shading condition. This is because of the series-parallel configuration. To calculate the PV current, it is crucial to consider the effect of the solar insolation. Therefore, under lower irradiance, the PV output current is less than its maximum rated value. It is measured as 14.95 A, which is slightly less than the maximum PV current. It is expected that the shape of the I-V characteristic curve has no difference, except for the values. Overall, the I-V and P-V characteristic curves are demonstrated in this subsection to understand the properties of the partial shading pattern, in order to investigate the feasibility of the proposed V-dp/di control method with 2nd derivative.

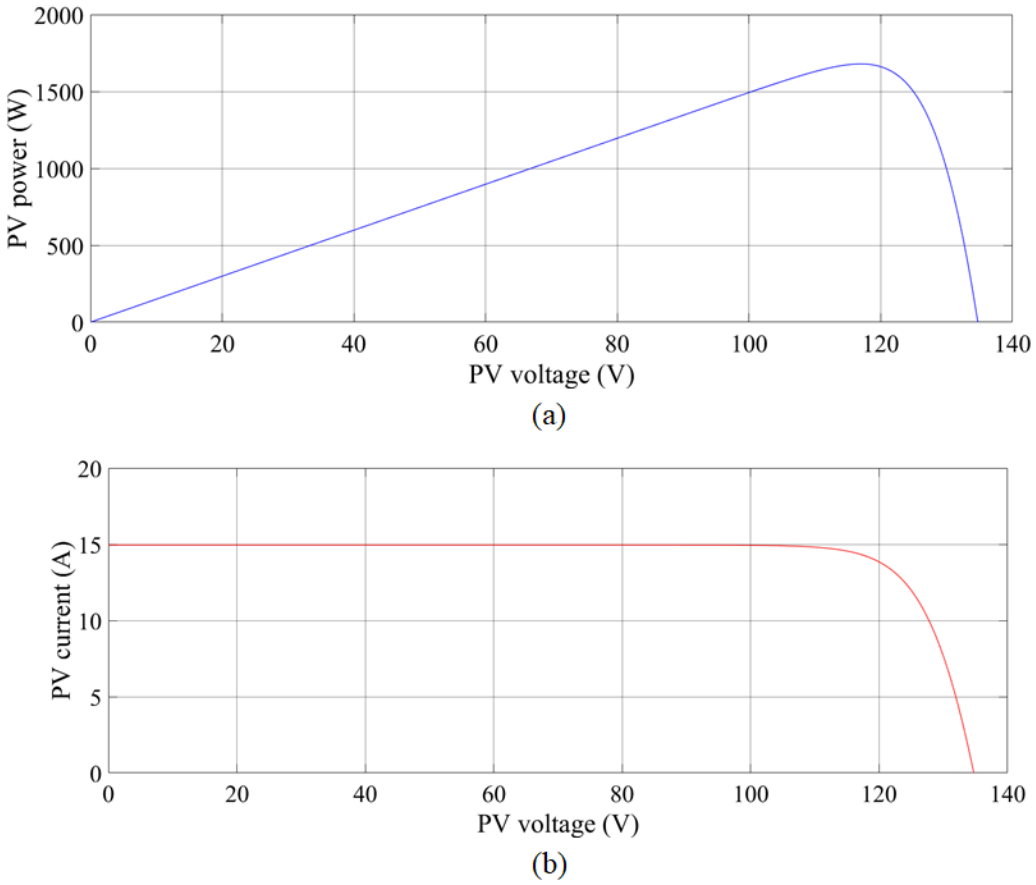

Figure 6.20 Behaviours of PV array under partially shaded condition. (a) P-V curve. (b) I-V curve.

It is shown in Figure 6.21 that the dc MG system is stable without any overshoots/undershoots. The settling time of the step response is about 30 ms. There is a step load change at 0.05 s to increase the load power. Hence the dc bus voltage is slightly dropped to accommodate with the step change. The decrease in voltage can be used to generate more PV output power to stabilise the MG system. As expected, there is no voltage overshoot occurred during transients. This is mainly due to a classical PID controller to eliminate the voltage overshoot and reach the steady-state value in a short period of time. The voltage ripple is ±0.08%, which is approximately the same as the PV standalone operation. No steady-state error is observed in the graph. The proposed V-dp/di method with second differential term is implemented to significantly mitigate the voltage fluctuations in a steady state, in which a promising static response performance has been achieved.

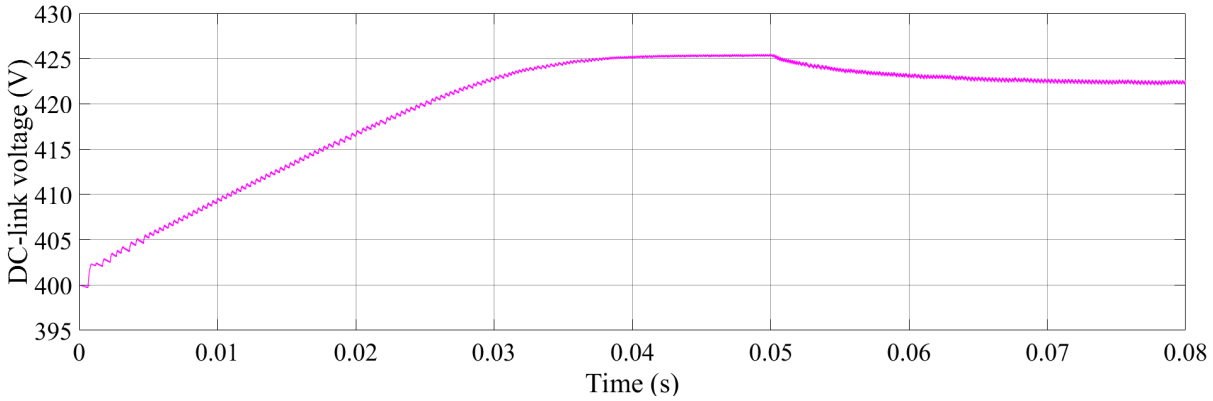

Figure 6.21 Dynamic response of the dc bus voltage under partially shaded condition.

One of the focuses of the partially shaded condition is on PV output power. As shown in Figure 6.22, all three columns of the PV generator reach the steady-state value in 30 ms. The averaged power oscillation is ±3.33%, which implies the robustness of the proposed V-dp/di method with 2nd differential term. The second derivative of power to current is introduced, at which the step response is identified to be stable. Therefore, it is obvious that the power fluctuations are significantly minimised during steady state. According to the graph, there is no overshoot in transient response. Power sharing among PV modules can be maintained under partially shaded condition. This has shown a superior dynamic performance of the proposed control strategy.

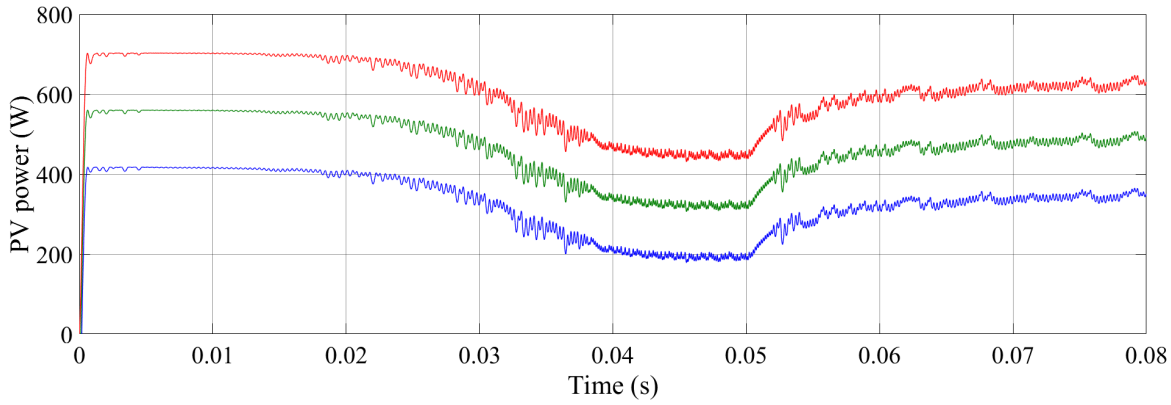

Figure 6.22 Dynamic response of PV output power for three columns under partial shading condition at three irradiance levels.

6.4.4 Impact of Second Differential of Current Approach

In this subsection, the effect of utilising the second derivative of power to current is investigated. As mentioned earlier, the implementation of second differential of current approach is designated for steady-state conditions to further minimise the power fluctuations.

In particular, the proposed V-dp/di control algorithm with second derivative term yields an enhanced static performance in a PV stand-alone operation. In spite of this, the proposed control method is first implemented in an islanded dc MG system to obtain the maximum PV output power of two solar generators. This thesis focuses on the steady-state response of the PV-based dc MG in the standalone mode. The solar irradiance and operating temperature are initialised as 600 $\mathrm{W/m^2}$ and 25 ℃, respectively. There is a significant change in solar insolation at 0.1 s with a step of 400 $\mathrm{W/m^2}$ under abrupt weather condition, as can be seen from Table 6.7. A full irradiance of 1000 $\mathrm{W/m^2}$ means that the PV arrays are directly absorbing the sunlight during periods of high insolation. Afterwards, the irradiance is dropped to 800 $\mathrm{W/m^2}$ to observe the transient response of the system, as well as the steady-state characteristics. In terms of the load transient, a step-changed load is applied to the dc MG at 0.05 s. As shown in Table 6.8, the total resistance of the load is presented to understand the dynamic behaviour of the dc MG. The load is intended to draw part of the maximum available power from the PV arrays, so that the performance of voltage regulation and proportional power sharing can be assessed during the simulation. The power ratio of two PV arrays is constantly measured to validate the feasibility of the proposed V-dp/di droop control algorithm with 2nd differential term for multiple PV generators.

Table 6.7 Simulation events for different irradiance levels and temperature

Period	Time (s)	Irradiance ($\mathrm{W/m^2}$)
I	0 – 0.1	600
II	0.1 – 0.15	1000
III	0.15 – 0.2	800

Table 6.8 Load transient event for the PV stand-alone system

Time (s)	Load resistance (Ω)	Load power (kW)
0 – 0.05	2.88	0.8
0.05 – 0.2	1.772	1.3

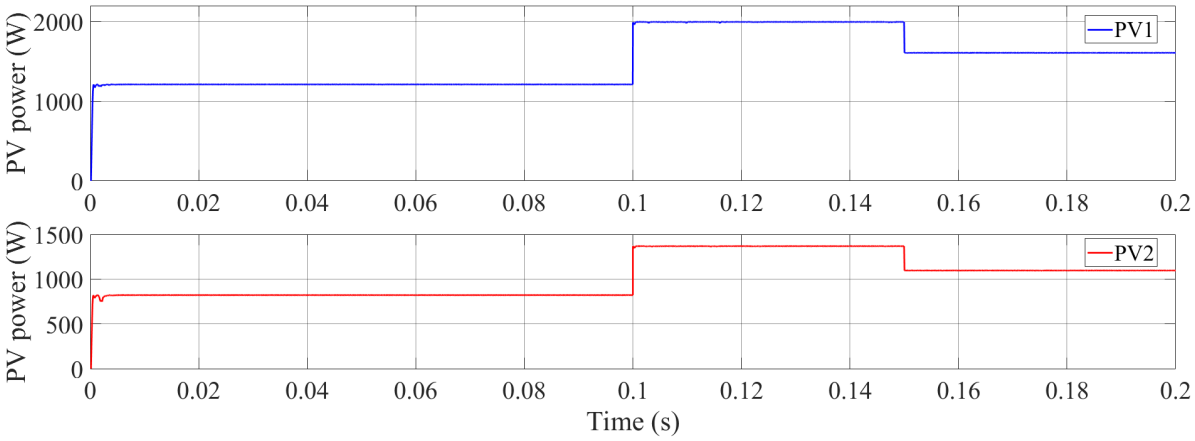

Figure 6.23 Dynamic response of output power for PV1 and PV2 in an islanded mode.

To perform the basic MPPT operation of the proposed V-dp/di control method with second differential term, the dc MG system works in the islanded mode where the decentralized controller harvests maximum power from the PV array. In case of step-changed irradiance, the next available MPP is reached by the PV arrays instantaneously. There is no overshoot or undershoot observed in Figure 6.23. Meanwhile, the averaged settling time of less than 1 ms for a PV source has demonstrated the robust performance of the proposed control scheme. When it comes to the PV power quality, the measured power ripple is $\pm 0.375\%$ in which the 2nd derivative of power to current has minor impact on the steady-state response of the PV power in islanded operation. However, the number of oscillations has been reduced by the 2nd differential term. A smooth power signal is achieved in this simulation, in comparison with the conventional V-dp/dv approach.

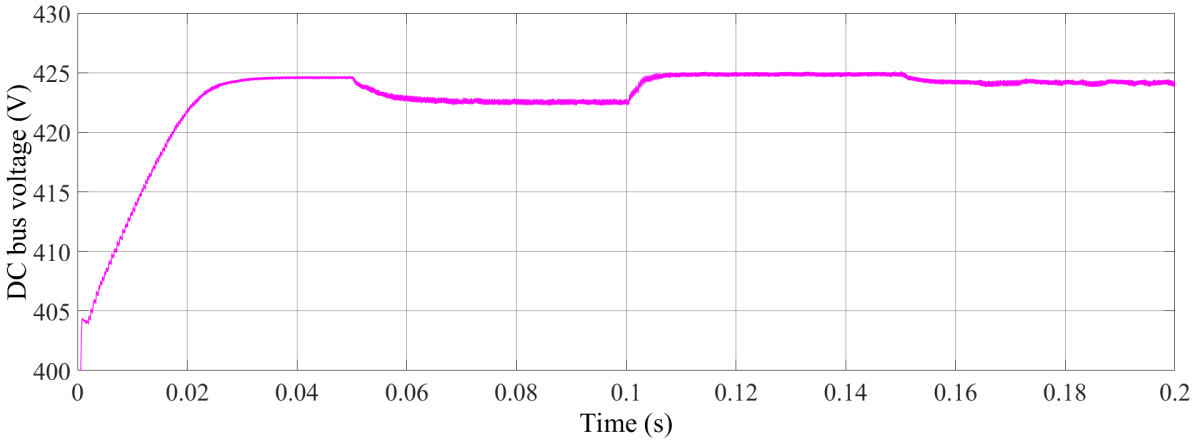

Figure 6.24 System dynamics of dc bus voltage under step-changed load and irradiance.

The proposed control algorithm with 2nd differential approach is implemented in the PV standalone mode to provide a comprehensive analysis of the effect of 2nd derivative. As

shown in Figure 6.24, the dynamic characteristics of common bus voltage are present. It is summarised that no overshoot or undershoot can be observed in the graph. The settling time of the dynamical dc MG is 10 ms in average, since the control method for transient response remains unchanged. The main concern of this subsection is the steady-state performance of the proposed control system, given the conditional signal for enabling the 2nd derivative control (d^2p/di^2) is only TRUE when the system is in a steady state. The details for setting up the conditional signal are illustrated in Chapter 4 for reference. The ripple of the dc bus voltage, with the 2nd differential control, is reduced by 15%, compared to the measured ripple in Figure 6.16. None of these differences are statistically significant. However, it is noted that the initial proposed method with dp/di has successfully addressed the voltage ripple issue caused by the instability of conventional dp/dv. Eventually, the measured voltage ripple in the simulation is $\pm 0.06\%$. This clearly indicates that the 2nd differential of current approach has no effect on the dynamic behaviour of a dc MG system. A common argument to the 2nd differential approach is the possibility of deploying the variable permanently without any conditional signal. In the research, it is concluded that the 2nd derivative term can only be applied to a steady-state response. Otherwise, the unusual error is simply enlarged by the droop coefficient deployed in the outer loop. In simple words, new reference value for the primary loop could be higher than the expected tangent slope, leading to the undesired power collapse in a PV-based dc MG system.

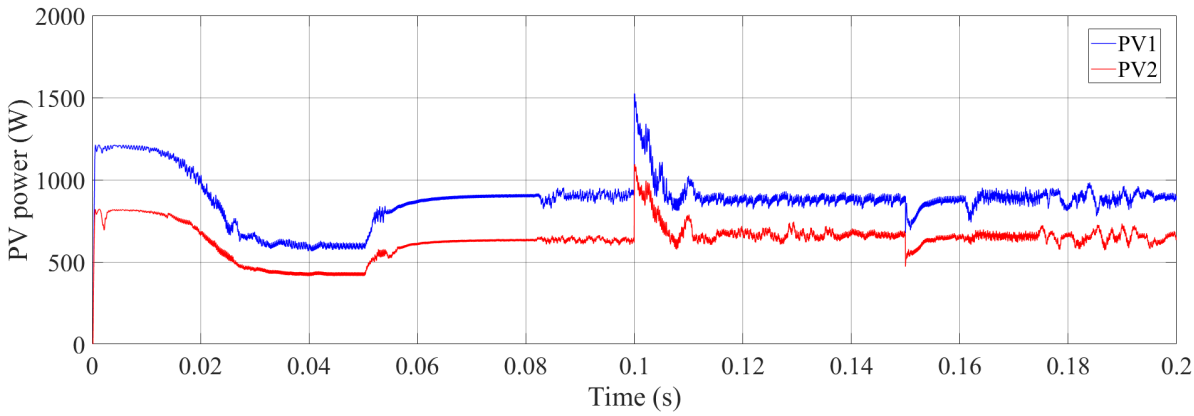

Figure 6.25 Dynamic characteristics of PV1 and PV2 with 2nd differential term under step changes in load and irradiance.

Regarding the PV systems, the system dynamics of two PV arrays are shown in Figure 6.25. The blue line represents the PV1 and hence the red line refers to the response of PV2. Compared to Figure 6.17, the dynamic behaviour of two curves in Figure 6.25 are almost identical. The averaged settling time of the PV power is approximately 10 ms. Last but not

least, there is no severe overshoot or undershoot shown in the graph. The power swell occurred at 0.1 s is due to significant change in irradiance, as can be seen from Table 6.7. It is deployed to verify the robustness of the proposed control algorithm under step-changed irradiance. The voltage sag at 0.15 s can be observed in Figure 6.25, since the solar insolation suddenly drops to 800 $\mathrm{W/m^2}$.

In terms of steady-state performance, it can be concluded that the 2nd derivative of power to current performs outstandingly in a PV standalone mode. As shown in Figure 6.25, the measured power ripple under full irradiance is $\pm 1.75\%$ in average. There is a 30% improvement in PV power fluctuations with the support of 2nd differential term. A common argument to the proposed V-dp/di control method is stability. When it comes to the smoothness of power signal, it can be argued that there are a lot of fluctuations in a steady state which seems to be unstable. Indeed, the steady-state response in Figure 6.17 shows that the power oscillations of PV1 are worse than the results in Figure 6.25. The 2nd differential approach is included in the inner loop to minimise the power fluctuations. During simulation, the common bus voltage is the principle variable for PV sources to generate a solar power in proportion. Small changes of the manipulated variable are often found in a decentralized coordination control, since two PV arrays are always adjusting their outputs to maintain a constant power ratio. The range of power ratio is from 1:0.7 to 1:0.74, in which the ratio is unaffected by the proposed 2nd differential term.

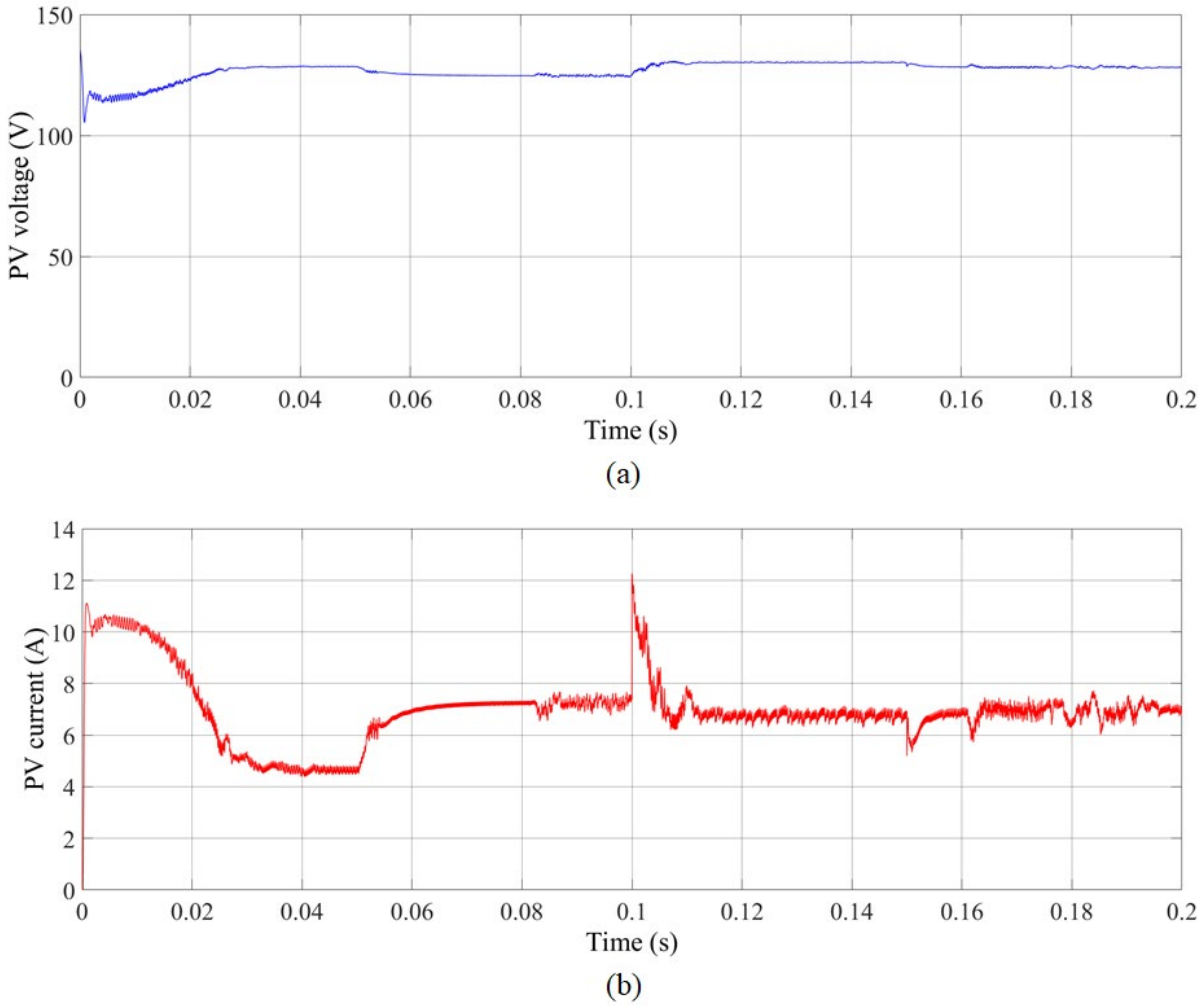

Figure 6.26 Dynamic characteristics of PV1 in 2nd differential approach. (a) PV voltage. (b) PV current.

The simulation results for the voltage of PV1 are displayed in Figure 6.26(a). The measured ripple voltage of PV1 is $\pm$0.19% which is reduced to one half, compared with the outcomes in Figure 6.18. This has shown a promising steady-state performance of the proposed control algorithm with 2nd derivative control. No major differences in transient response can be observed in the proposed control method with 2nd differential term. Besides, neither overshoot nor undershoot is obtainable in the graph. This is mainly due to the fact that the derivative term of a classical PID controller is used to reduce the overshoot of the feedback signal. It can be confirmed that the implementation of second differential term has no impact on the dynamic characteristics. It is important to bear in mind that the conditional signal must always be executed to activate the 2nd differential control only if the system has reached a steady state and disabled the function during transients.

As shown in Figure 6.26(b), the system dynamics of the current of PV1 are presented to understand the effects of utilising the 2nd order derivative term in a PV-based dc MG system. When it comes to a steady state, the simulation result of PV current shows that there are less oscillations around the operating point in comparison with Figure 6.18(b). The maximum ripple current measured in the graph is ±4.48%. The simulation data is recorded, at which the PV generator is under full irradiance. As a result, the steady-state performance of the PV current of PV1 is improved by over 30%. It is critical to implement the proposed 2nd differential term in a decentralized controller in order to enhance the steady-state performance. Furthermore, some fluctuations are observed during steady state after the decrease in solar insolation. The PV system is in the process of proportional power sharing. The proposed V-dp/di control scheme is a droop control which linearizes the tangent slope of P-I characteristics. The decentralized coordination control method in a dc MG is incapable of performing accurate power sharing among PV arrays. Consequently, it is completely normal to notice these power oscillations particularly in the PV stand-alone operation.

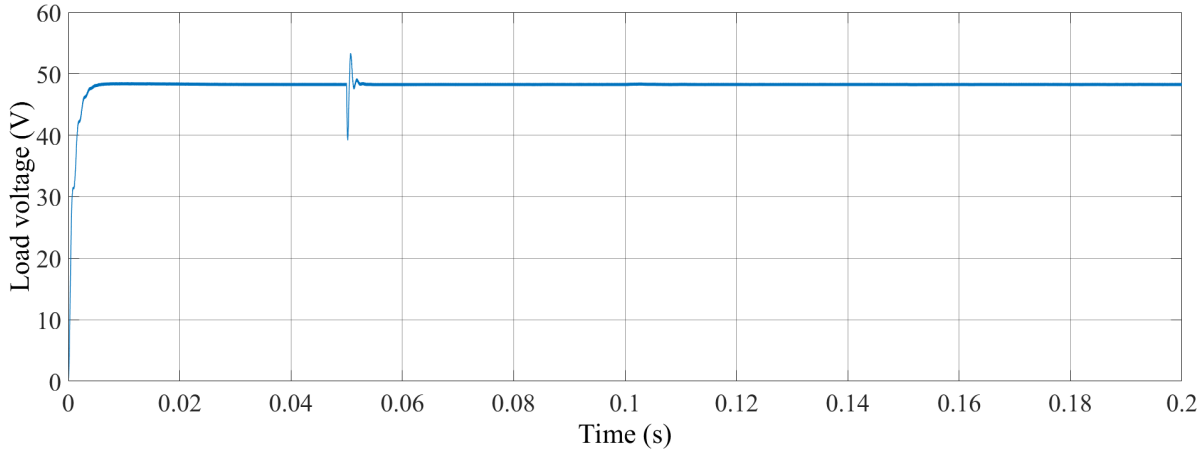

Figure 6.27 System dynamics of load voltage in 2nd differential of current approach.

The dynamic response of the load voltage in a PV-based dc MG system is shown in Figure 6.27. At the beginning of the dynamic process, there is no voltage overshoot found in the graph. This is because of the PID controller deployed in the proposed V-dp/di control. Compared with Figure 6.15, the load voltage in islanded mode experiences some minor oscillations and slightly underdamping. The reason behind the scene might be cascade control system of the battery. A traditional PI controller is employed in two nested loops, respectively. As a result, the oscillations occurred in battery voltage are directly transmitted to the output load voltage. In Figure 6.27, during transients, it is undoubted that the resulting voltage oscillation is addressed. No overshoot can be observed in the transient response. The averaged

settling time of the load voltage is about 5 ms. Therefore, it is crucial to optimise the control algorithm so as to obtain a satisfactory response.

Table 6.9 Overall performance comparisons among two decentralized control algorithms

Method	Operation Mode	Averaged Settling Time (ms)	DC Bus Voltage Overshoot (%)	DC Bus Voltage Ripple (%)	PV Power Fluctuations (%)	MAX DC Bus Voltage Deviation (V)
V-dp/dv	Islanded	10	1	0.375	±0.63	No deviation
Proposed V-dp/di	Islanded	10	1.13	0.375	±0.5	No deviation
V-dp/dv	PV Standalone	20	No overshoot	0.25	±5	9
Proposed V-dp/di	PV Standalone	10	No overshoot	0.14	±2.5	2
Proposed V-dp/di with 2nd derivative	PV Standalone	10	No overshoot	0.12	±1.75	2

The transient response performance of the proposed V-dp/di control is excellent, in comparison to conventional V-dp/dv algorithm. The proposed droop control strategy is capable of regulating the bus voltage and sharing the PV power instantaneously. In a steady state, the error between desired value and feedback voltage is around 0.25 V. The voltage ripple measured in Figure 6.27 is $\pm 0.52\%$. The step-changed load starts to operate at 0.05 s, where the voltage overshoot is 10.7%. The overshoot issue can be resolved by the load voltage loop, but it is beyond the scope of this thesis. In summary, the proposed V-dp/di control algorithm with 2nd differential term leads to better dynamic performance of the load voltage. The full performance comparison of the conventional and proposed control algorithms is presented in Table 6.9. This has shown the dynamic and steady-state performance improvement of the proposed droop control method, in terms of ripples, settling time and voltage deviation. The proposed V-dp/di control with 2nd differential term further reduces the voltage ripple and PV power fluctuations, which are the main benefits of the proposed control system.

6.5 Chapter Summary

In this chapter, the proposed V-dp/di and conventional control algorithms of the PV-based dc MG system have been presented. The key challenges of the conventional V-dp/dv method are poor dynamic characteristics and severe PV power oscillations. The proposed droop control scheme based on 2nd differential of current approach is proposed in this thesis. The tangent slope of P-I characteristics is used as an inner variable to represent the output power of the PV array. Given the dp/di controller is highly accurate, it is the best available option to participate in the primary control loop. This ensures that the control output of the outer voltage loop corresponds to the linear approximation of PV power. Furthermore, the implementation of the 2nd derivative of power to current yields an improved steady-state performance of the dc MG with multiple solar arrays. A conditional signal is utilised to identify the state of dc MG and to enable the 2nd differential term if applicable. The proposed V-dp/di control strategy is a fully decentralized coordination control that allows the PV sources to work in grid-connected, battery islanded, and PV standalone modes. Section 6.4.3 introduces the effect of partially shaded PV modules in PV standalone mode with the implementation of proposed V-dp/di method. It takes about 30 ms to reach the steady-state value, which is 20 ms longer than the settling time under normal conditions.

The proposed V-dp/di control algorithms are implemented in the simulation model of a PV-based dc MG system to assess both the dynamic and steady-state performance. The simulation results show that the proposed solution leads to better dynamic response performance and higher PV power quality. The proposed control system has some advantages over the existing control scheme, including precise control variable, easy to implement, and high stability. Overall performance comparisons among the proposed and conventional droop control methods are presented to summarise the simulation results in terms of operation mode, settling time, voltage overshoot, voltage ripple, power oscillations, and voltage deviation. It has achieved at least 50% improvement in settling time, no voltage overshoot, 48% reduction in voltage ripple, and 65% improvement in steady-state power ripple, which is the key motivation to devise the proposed control strategy.

Chapter 7. Thesis Conclusions and Future Work

7.1 Conclusions

This thesis presents a thorough literature review on three main categories of coordination control strategies implemented in a PV-based dc MG system, namely centralized, distributed and decentralized control. A detailed description of a PV-based dc MG is provided to demonstrate how the simulation model can be developed to assess the control algorithms. A comparison of the proposed V-dp/di and conventional control methods is presented to identify the differences between them, for instance, high accuracy of proposed inner control variable and working principle. The V-dp/di droop control strategy with 2^{nd} differential term has been proposed in the thesis. The stability analysis and simulation results of the proposed control algorithm are presented in the thesis to yield a 50% improvement in settling time and 30% improvement in PV power fluctuations. The main contributions and conclusions of this research are presented as follows.

7.1.1 Literature Review on Three Main Coordinated Control Methods

Coordination control methods of a dc MG system can be classified into three main categories, including centralized, distributed, and decentralized control methods. Generally speaking, centralized control suffers from single point of failure which is the most unreliable control strategy. However, it is the simplest control among three major schemes. Distributed coordination control is the most commonly used algorithm in the field of dc MG, due to its robustness and high stability. The control framework is difficult to design, compared with the other two main control strategies. Decentralized control refers to an independent control of an energy source in a dc MG without any neighbour's information. The key advantages of a decentralized method are the absence of communication agent, plug-and-play capability, and easy to implement. Hence, the focus of this research.

7.1.2 Limitations of Conventional Decentralized Control Method

An analysis of conventional droop control strategies was carried out. The classical droop method with inner current control is definitely inapplicable for a PV-based dc MG, due to short-circuit issues under fast irradiance change. In terms of conventional V-dp/dv control, it is established that a voltage regulator is integrated with MPPT controller. The term dp/dv represents the PV output power and acts as an inner control variable. However, it falls into the category of a voltage control which results in long settling time of the transient response. A

part of study in this thesis investigates the accuracy of the inner control variables dp/dv and dp/di. The percentage error of dp/dv is about 2-4%, which significantly affects the settling time and PV power ripple. The conventional dp/dv is incompetent to behave as an inner loop parameter due to precision issue. The averaged percentage error of dp/di is about 1.1%. In literature, an INR (dv/di) MPPT has an improved dynamic response performance in short settling time, low power ripple and wider operating range than INC (di/dv) MPPT. This implies that the proposed V-dp/di droop control method is crucial for an islanded dc MG with multiple PV generators.

7.1.3 Analysis of Proposed V-dp/di Control Strategy

The proposed V-dp/di droop control scheme is presented in Chapter 4 to yield 50% performance improvements in settling time and PV power oscillations, compared with conventional V-dp/dv method. The stability analysis of both conventional and proposed control methods is conducted in Chapter 5. An ideal boost converter is used in the stability analysis to simulate robustness to system variations, in contrast to a basic buck converter in literature. The magnitude and phase margin of proposed V-dp/di control are higher than the values obtained in conventional V-dp/dv method. The overall percentage error of dp/di is usually less than 1%. As a result, the proposed variable dp/di is capable of representing the correct amount of PV power. This is the key advantage of the proposed control algorithm. Moreover, the proposed method benefits from high quality of PV power, which in turn means the measured power ripple is lower than its rated value. The proposed V/dp/di control scheme takes advantage of fast response speed, regardless of rapid changes in solar insolation. It is noted that the proposed control method becomes a single loop control in grid-connected or battery islanded mode. In the stability analysis, the bandwidth of the inner loop is 1.2 times greater than the one in outer loop. This is the main reason why the proposed control algorithm is a one-off solution to the present challenges of PV-based dc MG. The characteristics of the cascade control are presented in PV standalone mode, where the value of inner loop bandwidth is ten times larger. Overall, the proposed V-dp/di control achieves promising dynamic performance in both islanded and standalone operations.

7.1.4 Second Differential of Current Approach

To enhance the steady-state performance of a dc MG system with multiple PV arrays, the proposed second derivative of PV power to current is established to help minimise the PV power oscillations. The adaptive control is commonly used in literature. However, the

mechanism of such control is always challenging to develop in practice. This is the reason why the establishment of second differential term is one of the contributions of this thesis. The variable focuses on the intrinsic oscillations of PV output power. The most important benefit of the proposed control algorithm is easy to use. There is a conditional signal to enable the controller of second differential term during steady state. The steady state of an islanded dc MG system is determined by dc bus voltage fluctuations and steady-state error. The error of dp/di is assumed to be almost zero in a steady state. Therefore the PI controller can be used to manipulate the second differential term, which refers to the rate of change of dp/di.

7.2 Suggestions for Future Research

This thesis proposed a novel droop control V-dp/di method with a second differential approach to yield an enhanced dynamic and steady-state performance. There are some works that can be carried out in the near future. First, the experimental study was not complete in this thesis due to the unprecedented situation in 2020. A test rig has been developed to validate the concept of a dc MG system, however, preliminary outcomes related to the proposed V-dp/di control algorithm are yet to obtain. This is the reason why the experimental results could be an extra piece of work to support this thesis. A hardware-in-the-loop test would be suggested for a dc MG system with multiple energy sources. The main advantage of this kind of test is that the plant can easily be built up with the help of software. In practice, it is summarised that performing an experiment on a complex dc MG system can take a significant amount of time in developing the test rig due to the needs for several power electronic converters. Given the number of safety devices depends on the complexity of the system, it is mandatory to design a safety circuit diagram. It is thus recommended that a practical test rig is challenging to be developed for this kind of research.

Regarding the control method, an adaptive control can further be established in the proposed strategy to improve the transient response performance of the system. An adaptive droop was attempted to be built throughout the study, but the results show that it is inappropriate to vary the droop coefficient in the control process. This is due to the fact that the droop coefficient is a linear term, in which the control system heavily depends on the linear P-I characteristics of the PV arrays. This in turn means the maximum allowable voltage should stay the same. Therefore, it is recommended to implement an adaptive proportional term in a classical PI controller which can become an advantageous feature of the control system. The adaptive proportional gain can be maximised when the error reaches a high level, and minimised when

the dc MG reaches a steady state. In literature, this is proved to be an effective method for enhancing the overall performance of the control method. However, in this thesis, a novel second differential term of current approach is proposed to make some fruitful contributions.

References

[1] "Renewables 2022 Global Status Report (GSR 2022)," 2022. [Online]. Available: https://www.ren21.net/reports/global-status-report/

[2] "Renewables 2020 Global Status Report (GSR 2020)," 2020. [Online]. Available: https://www.ren21.net/reports/global-status-report/

[3] W. C. Chan, M. Armstrong, D. Atkinson, and V. Pickert, "V-dP/dI droop control technique with d2P/dI2 to improve steady state performance for multiple PV modules in a dc microgrid," in *2019 21st European Conference on Power Electronics and Applications (EPE '19 ECCE Europe)*, 3-5 Sept. 2019 2019, pp. P.1-P.10, doi: 10.23919/EPE.2019.8915405.

[4] S. Anand, B. G. Fernandes, and J. Guerrero, "Distributed Control to Ensure Proportional Load Sharing and Improve Voltage Regulation in Low-Voltage DC Microgrids," *IEEE Transactions on Power Electronics,* vol. 28, no. 4, pp. 1900-1913, 2013, doi: 10.1109/TPEL.2012.2215055.

[5] P. Karlsson and J. Svensson, "DC bus voltage control for a distributed power system," *IEEE Transactions on Power Electronics,* vol. 18, no. 6, pp. 1405-1412, 2003, doi: 10.1109/TPEL.2003.818872.

[6] D. Kumar, F. Zare, and A. Ghosh, "DC Microgrid Technology: System Architectures, AC Grid Interfaces, Grounding Schemes, Power Quality, Communication Networks, Applications, and Standardizations Aspects," *IEEE Access,* vol. 5, pp. 12230-12256, 2017, doi: 10.1109/ACCESS.2017.2705914.

[7] H. Kakigano, Y. Miura, and T. Ise, "Distribution Voltage Control for DC Microgrids Using Fuzzy Control and Gain-Scheduling Technique," *IEEE Transactions on Power Electronics,* vol. 28, no. 5, pp. 2246-2258, 2013, doi: 10.1109/TPEL.2012.2217353.

[8] T. Dragičević, X. Lu, J. C. Vasquez, and J. M. Guerrero, "DC Microgrids—Part I: A Review of Control Strategies and Stabilization Techniques," *IEEE Transactions on Power Electronics,* vol. 31, no. 7, pp. 4876-4891, 2016, doi: 10.1109/TPEL.2015.2478859.

[9] H. Lotfi and A. Khodaei, "AC Versus DC Microgrid Planning," *IEEE Transactions on Smart Grid,* vol. 8, no. 1, pp. 296-304, 2017, doi: 10.1109/TSG.2015.2457910.

[10] H. Cai, J. Xiang, W. Wei, and M. Z. Q. Chen, "V-dp/dv Droop Control for PV Sources in DC Microgrids," *IEEE Transactions on Power Electronics,* vol. 33, no. 9, pp. 7708-7720, 2018, doi: 10.1109/tpel.2017.2771803.

[11] M. Wang, S. Tan, C. Lee, and S. Y. Hui, "A Configuration of Storage System for DC Microgrids," *IEEE Transactions on Power Electronics,* vol. 33, no. 5, pp. 3722-3733, 2018, doi: 10.1109/TPEL.2017.2723909.

[12] Y. Chen, Y. Wu, C. Song, and Y. Chen, "Design and Implementation of Energy Management System With Fuzzy Control for DC Microgrid Systems," *IEEE Transactions on Power Electronics,* vol. 28, no. 4, pp. 1563-1570, 2013, doi: 10.1109/TPEL.2012.2210446.

[13] X. Lu, K. Sun, J. M. Guerrero, J. C. Vasquez, and L. Huang, "State-of-Charge Balance Using Adaptive Droop Control for Distributed Energy Storage Systems in DC Microgrid Applications," *IEEE Transactions on Industrial Electronics,* vol. 61, no. 6, pp. 2804-2815, 2014, doi: 10.1109/TIE.2013.2279374.

[14] T. Dragičević, X. Lu, J. C. Vasquez, and J. M. Guerrero, "DC Microgrids—Part II: A Review of Power Architectures, Applications, and Standardization Issues," *IEEE Transactions on Power Electronics,* vol. 31, no. 5, pp. 3528-3549, 2016, doi: 10.1109/TPEL.2015.2464277.

[15] K. Hu and C. Liaw, "Incorporated Operation Control of DC Microgrid and Electric Vehicle," *IEEE Transactions on Industrial Electronics,* vol. 63, no. 1, pp. 202-215, 2016, doi: 10.1109/TIE.2015.2480750.

[16] H. S. Goh, M. Armstrong, and B. Zahawi, "The effect of grid operating conditions on the current controller performance of grid connected photovoltaic inverters," in *2009 13th European Conference on Power Electronics and Applications*, 8-10 Sept. 2009 2009, pp. 1-8.

[17] F. Mulolani, "Performance of direct power controlled grid-connected voltage source converters," Thesis (Ph. D.)--Newcastle University, 2017., Newcastle upon Tyne, England, 2017.

[18] H. Kakigano, Y. Miura, and T. Ise, "Low-Voltage Bipolar-Type DC Microgrid for Super High Quality Distribution," *IEEE Transactions on Power Electronics,* vol. 25, no. 12, pp. 3066-3075, 2010, doi: 10.1109/TPEL.2010.2077682.

[19] L. Meng *et al.*, "Review on Control of DC Microgrids and Multiple Microgrid Clusters," *IEEE Journal of Emerging and Selected Topics in Power Electronics,* vol. 5, no. 3, pp. 928-948, 2017, doi: 10.1109/JESTPE.2017.2690219.

[20] Y. Shan, J. Hu, M. Liu, J. Zhu, and J. M. Guerrero, "Model Predictive Voltage and Power Control of Islanded PV-Battery Microgrids With Washout-Filter-Based Power Sharing Strategy," *IEEE Transactions on Power Electronics,* vol. 35, no. 2, pp. 1227-1238, 2020, doi: 10.1109/TPEL.2019.2930182.

[21] Q. Shafiee, T. Dragičević, J. C. Vasquez, and J. M. Guerrero, "Hierarchical Control for Multiple DC-Microgrids Clusters," *IEEE Transactions on Energy Conversion,* vol. 29, no. 4, pp. 922-933, 2014, doi: 10.1109/TEC.2014.2362191.

[22] J. Park, J. Candelaria, L. Ma, and K. Dunn, "DC Ring-Bus Microgrid Fault Protection and Identification of Fault Location," *IEEE Transactions on Power Delivery,* vol. 28, no. 4, pp. 2574-2584, 2013, doi: 10.1109/TPWRD.2013.2267750.

[23] R. M. Cuzner and G. Venkataramanan, "The Status of DC Micro-Grid Protection," in *2008 IEEE Industry Applications Society Annual Meeting*, 5-9 Oct. 2008 2008, pp. 1-8, doi: 10.1109/08IAS.2008.382.

[24] P. Li *et al.*, "Reduced-Order Modeling and Comparative Dynamic Analysis of DC Voltage Control in DC Microgrids Under Different Droop Methods," *IEEE Transactions on Energy Conversion,* vol. 36, no. 4, pp. 3317-3333, 2021, doi: 10.1109/TEC.2021.3076438.

[25] M. M. Mardani, M. H. Khooban, A. Masoudian, and T. Dragičević, "Model Predictive Control of DC–DC Converters to Mitigate the Effects of Pulsed Power Loads in Naval DC Microgrids," *IEEE Transactions on Industrial Electronics,* vol. 66, no. 7, pp. 5676-5685, 2019, doi: 10.1109/TIE.2018.2877191.

[26] R. F. Bastos, T. Dragičević, J. M. Guerrero, and R. Q. Machado, "Decentralized control for renewable DC Microgrid with composite energy storage system and UC voltage restoration connected to the grid," in *IECON 2016 - 42nd Annual Conference of the IEEE Industrial Electronics Society*, 23-26 Oct. 2016 2016, pp. 2016-2021, doi: 10.1109/IECON.2016.7793249.

[27] T. R. Oliveira, W. W. A. G. Silva, and P. F. Donoso-Garcia, "Distributed Secondary Level Control for Energy Storage Management in DC Microgrids," *IEEE Transactions on Smart Grid,* vol. 8, no. 6, pp. 2597-2607, 2017, doi: 10.1109/TSG.2016.2531503.

[28] Z. Wang, W. Wu, and B. Zhang, "A Distributed Control Method With Minimum Generation Cost for DC Microgrids," *IEEE Transactions on Energy Conversion,* vol. 31, no. 4, pp. 1462-1470, 2016, doi: 10.1109/TEC.2016.2584649.

[29] Y. Wang, M. Yu, and Y. Li, "Self-adaptive inertia control of DC microgrid based on fast predictive converter regulation," *IET Renewable Power Generation,* vol. 11, no. 8, pp. 1295-1303, 2017, doi: 10.1049/iet-rpg.2016.0463.

[30] N. L. Diaz, T. Dragičević, J. C. Vasquez, and J. M. Guerrero, "Intelligent Distributed Generation and Storage Units for DC Microgrids—A New Concept on Cooperative Control Without Communications Beyond Droop Control," *IEEE Transactions on Smart Grid,* vol. 5, no. 5, pp. 2476-2485, 2014, doi: 10.1109/TSG.2014.2341740.

[31] K. D. Hoang and H. Lee, "Accurate Power Sharing With Balanced Battery State of Charge in Distributed DC Microgrid," *IEEE Transactions on Industrial Electronics,* vol. 66, no. 3, pp. 1883-1893, 2019, doi: 10.1109/TIE.2018.2838107.

[32] C. Li, J. C. Vasquez, and J. M. Guerrero, "Multiagent-based distributed control for operation cost minimization of droop controlled DC microgrid using incremental cost consensus," in *IECON 2015 - 41st Annual Conference of the IEEE Industrial Electronics Society*, 9-12 Nov. 2015 2015, pp. 005202-005205, doi: 10.1109/IECON.2015.7392917.

[33] T. V. Vu, S. Paran, F. Diaz-Franco, T. El-Mezyani, and C. S. Edrington, "An Alternative Distributed Control Architecture for Improvement in the Transient Response of DC Microgrids," *IEEE Transactions on Industrial Electronics,* vol. 64, no. 1, pp. 574-584, 2017, doi: 10.1109/TIE.2016.2607681.

[34] A. Küçüker, T. Kamal, S. Z. Hassan, H. Li, G. M. Mufti, and M. Waseem, "Design and control of photovoltaic/wind/battery based microgrid system," in *2017 International Conference on Electrical Engineering (ICEE)*, 2-4 March 2017 2017, pp. 1-6, doi: 10.1109/ICEE.2017.7893445.

[35] J. Hu, J. Duan, H. Ma, and M. Chow, "Distributed Adaptive Droop Control for Optimal Power Dispatch in DC Microgrid," *IEEE Transactions on Industrial Electronics,* vol. 65, no. 1, pp. 778-789, 2018, doi: 10.1109/TIE.2017.2698425.

[36] M. Baranwal, A. Askarian, S. Salapaka, and M. Salapaka, "A Distributed Architecture for Robust and Optimal Control of DC Microgrids," *IEEE Transactions on Industrial Electronics,* vol. 66, no. 4, pp. 3082-3092, 2019, doi: 10.1109/TIE.2018.2840506.

[37] D. Dam and H. Lee, "A Power Distributed Control Method for Proportional Load Power Sharing and Bus Voltage Restoration in a DC Microgrid," *IEEE Transactions on Industry Applications,* vol. 54, no. 4, pp. 3616-3625, 2018, doi: 10.1109/TIA.2018.2815661.

[38] X. Lu, J. M. Guerrero, K. Sun, and J. C. Vasquez, "An Improved Droop Control Method for DC Microgrids Based on Low Bandwidth Communication With DC Bus Voltage Restoration and Enhanced Current Sharing Accuracy," *IEEE Transactions on Power Electronics,* vol. 29, no. 4, pp. 1800-1812, 2014, doi: 10.1109/TPEL.2013.2266419.

[39] T. Dragičević, J. M. Guerrero, and J. C. Vasquez, "A Distributed Control Strategy for Coordination of an Autonomous LVDC Microgrid Based on Power-Line Signaling," *IEEE Transactions on Industrial Electronics,* vol. 61, no. 7, pp. 3313-3326, 2014, doi: 10.1109/TIE.2013.2282597.

[40] H. Huang, C. Hsieh, J. Liao, and K. Chen, "Adaptive Droop Resistance Technique for Adaptive Voltage Positioning in Boost DC–DC Converters," *IEEE Transactions on Power Electronics,* vol. 26, no. 7, pp. 1920-1932, 2011, doi: 10.1109/TPEL.2010.2095508.

[41] J. M. Guerrero, J. C. Vasquez, J. Matas, L. G. d. Vicuna, and M. Castilla, "Hierarchical Control of Droop-Controlled AC and DC Microgrids—A General Approach Toward Standardization," *IEEE Transactions on Industrial Electronics,* vol. 58, no. 1, pp. 158-172, 2011, doi: 10.1109/TIE.2010.2066534.

[42] V. Nasirian, A. Davoudi, F. L. Lewis, and J. M. Guerrero, "Distributed Adaptive Droop Control for DC Distribution Systems," *IEEE Transactions on Energy Conversion,* vol. 29, no. 4, pp. 944-956, 2014, doi: 10.1109/TEC.2014.2350458.

[43] S. Augustine, M. K. Mishra, and N. Lakshminarasamma, "Adaptive Droop Control Strategy for Load Sharing and Circulating Current Minimization in Low-Voltage Standalone DC Microgrid," *IEEE Transactions on Sustainable Energy,* vol. 6, no. 1, pp. 132-141, 2015, doi: 10.1109/TSTE.2014.2360628.

[44] A. Iovine, S. B. Siad, G. Damm, E. D. Santis, and M. D. D. Benedetto, "Nonlinear Control of a DC MicroGrid for the Integration of Photovoltaic Panels," *IEEE Transactions on Automation Science and Engineering,* vol. 14, no. 2, pp. 524-535, 2017, doi: 10.1109/TASE.2017.2662742.

[45] H. Liu, P. C. Loh, X. Wang, Y. Yang, W. Wang, and D. Xu, "Droop Control With Improved Disturbance Adaption for a PV System With Two Power Conversion Stages," *IEEE Transactions on Industrial Electronics,* vol. 63, no. 10, pp. 6073-6085, 2016, doi: 10.1109/TIE.2016.2580525.

[46] A. Khorsandi, M. Ashourloo, and H. Mokhtari, "A Decentralized Control Method for a Low-Voltage DC Microgrid," *IEEE Transactions on Energy Conversion,* vol. 29, no. 4, pp. 793-801, 2014, doi: 10.1109/TEC.2014.2329236.

[47] K. Sun, L. Zhang, Y. Xing, and J. M. Guerrero, "A Distributed Control Strategy Based on DC Bus Signaling for Modular Photovoltaic Generation Systems With Battery Energy Storage," *IEEE Transactions on Power Electronics,* vol. 26, no. 10, pp. 3032-3045, 2011, doi: 10.1109/TPEL.2011.2127488.

[48] K. Strunz, E. Abbasi, and D. N. Huu, "DC Microgrid for Wind and Solar Power Integration," *IEEE Journal of Emerging and Selected Topics in Power Electronics,* vol. 2, no. 1, pp. 115-126, 2014, doi: 10.1109/JESTPE.2013.2294738.

[49] Y. Gu, X. Xiang, W. Li, and X. He, "Mode-Adaptive Decentralized Control for Renewable DC Microgrid With Enhanced Reliability and Flexibility," *IEEE Transactions on Power Electronics,* vol. 29, no. 9, pp. 5072-5080, 2014, doi: 10.1109/TPEL.2013.2294204.

[50] H. Wang, M. Han, R. Han, J. M. Guerrero, and J. C. Vasquez, "A Decentralized Current-Sharing Controller Endows Fast Transient Response to Parallel DC–DC Converters," *IEEE Transactions on Power Electronics,* vol. 33, no. 5, pp. 4362-4372, 2018, doi: 10.1109/TPEL.2017.2714342.

[51] A. Althobaiti, M. Armstrong, and M. A. Elgendy, "Space vector modulation current control of a three-phase PV grid-connected inverter," in *2016 Saudi Arabia Smart Grid (SASG)*, 6-8 Dec. 2016 2016, pp. 1-6, doi: 10.1109/SASG.2016.7849673.

[52] N. Pandiarajan and R. Muthu, "Mathematical modeling of photovoltaic module with Simulink," in *2011 1st International Conference on Electrical Energy Systems*, 3-5 Jan. 2011 2011, pp. 258-263, doi: 10.1109/ICEES.2011.5725339.

[53] R. A. Messenger, *Photovoltaic systems engineering*, 2nd ed.. ed. Boca Raton: Boca Raton : CRC Press, 2004.

[54] J. A. Gow and C. D. Manning, "Development of a model for photovoltaic arrays suitable for use in simulation studies of solar energy conversion systems," in *1996 Sixth International Conference on Power Electronics and Variable Speed Drives (Conf. Publ. No. 429)*, 23-25 Sept. 1996 1996, pp. 69-74, doi: 10.1049/cp:19960890.

[55] M. G. Villalva, J. R. Gazoli, and E. R. Filho, "Comprehensive Approach to Modeling and Simulation of Photovoltaic Arrays," *IEEE Transactions on Power Electronics,* vol. 24, no. 5, pp. 1198-1208, 2009, doi: 10.1109/TPEL.2009.2013862.

[56] M. K. KAZIMIERCZUK, *Pulse-width Modulated DC–DC Power Converters*. United States: A John Wiley and Sons, Ltd, Publication, 2008.

[57] J. L. Agorreta, L. Reinaldos, R. Gonzalez, M. Borrega, J. Balda, and L. Marroyo, "Fuzzy Switching Technique Applied to PWM Boost Converter Operating in Mixed Conduction Mode for PV Systems," *IEEE Transactions on Industrial Electronics,* vol. 56, no. 11, pp. 4363-4373, 2009, doi: 10.1109/TIE.2009.2019567.

[58] M. Elshaer, A. Mohamed, and O. Mohammed, "Smart optimal control of DC-DC boost converter in PV systems," in *2010 IEEE/PES Transmission and Distribution Conference and Exposition: Latin America (T&D-LA)*, 8-10 Nov. 2010 2010, pp. 403-410, doi: 10.1109/TDC-LA.2010.5762913.

[59] Q. Xu *et al.*, "A Decentralized Dynamic Power Sharing Strategy for Hybrid Energy Storage System in Autonomous DC Microgrid," *IEEE Transactions on Industrial Electronics,* vol. 64, no. 7, pp. 5930-5941, 2017, doi: 10.1109/TIE.2016.2608880.

[60] W. Choi *et al.*, "Reviews on grid-connected inverter, utility-scaled battery energy storage system, and vehicle-to-grid application - challenges and opportunities," in *2017 IEEE Transportation Electrification Conference and Expo (ITEC)*, 22-24 June 2017 2017, pp. 203-210, doi: 10.1109/ITEC.2017.7993272.

[61] Y. Xia, M. Yu, P. Yang, Y. Peng, and W. Wei, "Generation-Storage Coordination for Islanded DC Microgrids Dominated by PV Generators," *IEEE Transactions on Energy Conversion,* vol. 34, no. 1, pp. 130-138, 2019, doi: 10.1109/TEC.2018.2860247.

[62] N. Saxena, I. Hussain, B. Singh, and A. L. Vyas, "Implementation of a Grid-Integrated PV-Battery System for Residential and Electrical Vehicle Applications," *IEEE Transactions on Industrial Electronics,* vol. 65, no. 8, pp. 6592-6601, 2018, doi: 10.1109/TIE.2017.2739712.

[63] X. Jia, D. Xu, S. Du, C. Hu, M. Chen, and P. Lin, "A high power density and efficiency bi-directional DC/DC converter for electric vehicles," in *2015 9th International Conference on Power Electronics and ECCE Asia (ICPE-ECCE Asia)*, 1-5 June 2015 2015, pp. 874-880, doi: 10.1109/ICPE.2015.7167885.

[64] S. Almazrouei, A. Hamid, and M. Shamsuzzaman, "Predictive energy management in large-scale grid connected PV-batteries system," in *2018 5th International Conference on Renewable Energy: Generation and Applications (ICREGA)*, 25-28 Feb. 2018 2018, pp. 315-318, doi: 10.1109/ICREGA.2018.8337601.

[65] H. Juan, L. Jianlin, and H. Dong, "Research on Bi-directional converter for lithium battery energy storage system," in *Proceedings of 2011 International Conference on Electronic & Mechanical Engineering and Information Technology*, 12-14 Aug. 2011 2011, vol. 4, pp. 1897-1900, doi: 10.1109/EMEIT.2011.6023409.

[66] R. Sabzehgar, "A review of AC/DC microgrid-developments, technologies, and challenges," in *2015 IEEE Green Energy and Systems Conference (IGESC)*, 9-9 Nov. 2015 2015, pp. 11-17, doi: 10.1109/IGESC.2015.7359384.

[67] M. H. F. Ahamed, U. D. S. D. Dissanayake, H. M. P. D. Silva, H. R. C. G. P. Pradeep, and N. W. A. Lidula, "Modelling and simulation of a solar PV and battery based DC microgrid system," in *2016 International Conference on Electrical, Electronics, and Optimization Techniques (ICEEOT)*, 3-5 March 2016 2016, pp. 1706-1711, doi: 10.1109/ICEEOT.2016.7754977.

[68] M. Mao, C. Qian, and Y. Ding, "Decentralized coordination power control for islanding microgrid based on PV/BES-VSG," *CPSS Transactions on Power Electronics and Applications,* vol. 3, no. 1, pp. 14-24, 2018, doi: 10.24295/CPSSTPEA.2018.00002.

[69] K. M. S. Y. Konara and M. L. Kolhe, "Charging management of grid integrated battery for overcoming the intermittency of RE sources," in *2016 IEEE International Conference on Information and Automation for Sustainability (ICIAfS)*, 16-19 Dec. 2016 2016, pp. 1-6, doi: 10.1109/ICIAFS.2016.7946554.

[70] H. Cai, J. Xiang, and W. Wei, "Decentralized Coordination Control of Multiple Photovoltaic Sources for DC Bus Voltage Regulating and Power Sharing," *IEEE Transactions on Industrial Electronics,* vol. 65, no. 7, pp. 5601-5610, 2018, doi: 10.1109/TIE.2017.2779412.

[71] A. Sangwongwanich, Y. Yang, F. Blaabjerg, and H. Wang, "Benchmarking of Constant Power Generation Strategies for Single-Phase Grid-Connected Photovoltaic Systems," *IEEE Transactions on Industry Applications,* vol. 54, no. 1, pp. 447-457, 2018, doi: 10.1109/TIA.2017.2740380.

[72] A. Sangwongwanich, Y. Yang, and F. Blaabjerg, "A Sensorless Power Reserve Control Strategy for Two-Stage Grid-Connected PV Systems," *IEEE Transactions on Power Electronics,* vol. 32, no. 11, pp. 8559-8569, 2017, doi: 10.1109/TPEL.2017.2648890.

[73] F. E. Aamri, H. Maker, D. Sera, S. V. Spataru, J. M. Guerrero, and A. Mouhsen, "A Direct Maximum Power Point Tracking Method for Single-Phase Grid-Connected PV Inverters," *IEEE Transactions on Power Electronics,* vol. 33, no. 10, pp. 8961-8971, 2018, doi: 10.1109/TPEL.2017.2780858.

[74] M. A. Elgendy, B. Zahawi, and D. J. Atkinson, "Assessment of Perturb and Observe MPPT Algorithm Implementation Techniques for PV Pumping Applications," *IEEE Transactions on Sustainable Energy,* vol. 3, no. 1, pp. 21-33, 2012, doi: 10.1109/TSTE.2011.2168245.

[75] A. Sangwongwanich, Y. Yang, and F. Blaabjerg, "High-Performance Constant Power Generation in Grid-Connected PV Systems," *IEEE Transactions on Power Electronics,* vol. 31, no. 3, pp. 1822-1825, 2016, doi: 10.1109/TPEL.2015.2465151.

[76] M. A. Elgendy, B. Zahawi, and D. J. Atkinson, "Assessment of the Incremental Conductance Maximum Power Point Tracking Algorithm," *IEEE Transactions on Sustainable Energy,* vol. 4, no. 1, pp. 108-117, 2013, doi: 10.1109/TSTE.2012.2202698.

[77] H. Cai, X. Ji, and W. Wei, "Decentralized autonomous operation for islanded photovoltaic-based DC microgrids," in *2017 36th Chinese Control Conference (CCC)*, 26-28 July 2017 2017, pp. 10570-10575, doi: 10.23919/ChiCC.2017.8029041.

[78] H. Cai, J. Xiang, M. Z. Q. Chen, and W. Wei, "A decentralized control strategy for photovoltaic sources to unify MPPT and DC-bus voltage regulation," in *2017 American Control Conference (ACC)*, 24-26 May 2017 2017, pp. 2066-2071, doi: 10.23919/ACC.2017.7963257.

[79] E. Mojica-Nava, J. M. Rey, J. Torres-Martinez, and M. Castilla, "Decentralized Switched Current Control for DC Microgrids," *IEEE Transactions on Industrial Electronics,* vol. 66, no. 2, pp. 1182-1191, 2019, doi: 10.1109/TIE.2018.2833020.

[80] A. Lashab, D. Sera, and J. M. Guerrero, "A Dual-Discrete Model Predictive Control-Based MPPT for PV Systems," *IEEE Transactions on Power Electronics,* vol. 34, no. 10, pp. 9686-9697, 2019, doi: 10.1109/TPEL.2019.2892809.

[81] F. Liu, S. Duan, F. Liu, B. Liu, and Y. Kang, "A Variable Step Size INC MPPT Method for PV Systems," *IEEE Transactions on Industrial Electronics,* vol. 55, no. 7, pp. 2622-2628, 2008, doi: 10.1109/TIE.2008.920550.

[82] Q. Mei, M. Shan, L. Liu, and J. M. Guerrero, "A Novel Improved Variable Step-Size Incremental-Resistance MPPT Method for PV Systems," *IEEE Transactions on Industrial Electronics,* vol. 58, no. 6, pp. 2427-2434, 2011, doi: 10.1109/TIE.2010.2064275.

[83] T. M. Chung, H. Daniyal, M. H. Sulaiman, and M. S. Bakar, "Comparative study of P&O and modified incremental conductance algorithm in solar maximum power point tracking," in *4th IET Clean Energy and Technology Conference (CEAT 2016)*, 14-15 Nov. 2016 2016, pp. 1-6, doi: 10.1049/cp.2016.1300.

[84] R. W. Erickson, *Fundamentals of Power Electronics*, 3rd ed. 2020.. ed. Cham : Springer International Publishing : Imprint: Springer, 2020.

[85] L. Ruisheng, M. Armstrong, S. Gadoue, and W. Chen, "On-line parameter estimation of non-minimum phase switch mode power DC-DC boost converters," in *8th IET International Conference on Power Electronics, Machines and Drives (PEMD 2016)*, 19-21 April 2016 2016, pp. 1-6, doi: 10.1049/cp.2016.0172.

[86] C. Wang, "System identification and adaptive current balancing ON/OFF control of DC-DC switch mode power converter," Thesis (Ph. D.)--Newcastle University, 2018., Newcastle upon Tyne, England, 2018.

[87] S. M. Maharana, A. Mohapatra, C. Saiprakash, and A. Kundu, "Comparative Analysis of different PV Array Configurations under Partial Shading Conditions," in *2020 3rd International Conference on Energy, Power and Environment: Towards Clean Energy Technologies*, 5-7 March 2021 2021, pp. 1-5, doi: 10.1109/ICEPE50861.2021.9404378.

[88] S. Liu, L. Luowei, and W. Lu, "Simple analytical approach to predict large-signal stability region of a closed-loop boost DC–DC converter," *Power Electronics, IET,* vol. 6, pp. 488-494, 03/01 2013, doi: 10.1049/iet-pel.2012.0323.

[89] T. Pavlovic, T. Bjazic, and Z. Ban, "Simplified Averaged Models of DC–DC Power Converters Suitable for Controller Design and Microgrid Simulation," *IEEE Transactions on Power Electronics,* vol. 28, no. 7, pp. 3266-3275, 2013, doi: 10.1109/TPEL.2012.2224889.

Appendix A

A.1 Introduction

This appendix presents the nomenclature and fundamental equations of a PV array. There are four equations to simulate the characteristics of a solar panel in such a way to fully design a non-linear PV model. As a result, the mathematical modelling of a PV generator offers an opportunity to vary the size of PV model at any time with high flexibility.

A.2 General Nomenclature for a PV Model

Charge of electron (C)	$q = 1.602 \times 10^{-19}$
Boltzmann constant (J/k)	$k = 1.3806 \times 10^{-23}$
Cell operating temperature (K)	$T = 298$
Module operating temperature (℃)	$T_{ak} = 25$
Reference temperature (℃)	$T_{rk} = 25$
Cell saturation current (A)	I_o
Reverse saturation current (A)	I_{rs}
Light generated current/photocurrent (A)	I_{ph}
Diode saturation current (A)	I_D
PV output current (A)	I_{pv}
PV output voltage (V)	V_{pv}
Cell series resistance (Ω)	R_s
Cell shunt resistance (Ω)	R_{sh}
Ideal factor	$A = 0.96065$
Number of cells in parallel	N_p

Number of cells in series	N_s
Short-circuit current (A)	I_{scr}
Open-circuit voltage (V)	V_{oc}
Band gap energy for semiconductor (eV)	$E_G = 1.1$
Short-circuit temperature coefficient (A/°C)	$k_i = 0.0029$
Solar irradiance (W/m^2)	$G = 1000$

A.3 PV Characteristic Equations

The photocurrent of a PV array can be expressed as

$$\mathrm{I_{ph}} = [\mathrm{I_{scr}} + \mathrm{k_i}(\mathrm{T} - 298)] * \frac{\mathrm{G}}{1000} \tag{A.1}$$

where I_{scr} is the short-circuit current, k_i is the short-circuit temperature coefficient, T is the cell operating temperature, and G is solar insolation.

To calculate the reverse saturation current of a PV generator, the formula is written as

$$\mathrm{I_{rs}} = \mathrm{I_{scr}}/(\mathrm{e}^{\frac{\mathrm{qV_{oc}}}{\mathrm{N_s AkT_{ak}}}} - 1) \tag{A.2}$$

where V_{oc} is the open-circuit voltage, N_s is the number of cells connected in series, A is the ideal factor, k is Boltzmann constant, T_{ak} is the module operating temperature.

In theory, the module saturation current mainly depends on the operating temperature of those cells which can be derived as

$$\mathrm{I_o} = \mathrm{I_{rs}}\left(\frac{\mathrm{T_{ak}}}{\mathrm{T_{rk}}}\right)^3 \mathrm{e}^{\frac{\mathrm{qE_g}\left(\frac{1}{\mathrm{T_{rk}}} - \frac{1}{\mathrm{T}}\right)}{\mathrm{Ak}}} \tag{A.3}$$

where I_o is the cell saturation current, T_{rk} is the reference temperature, q is the charge of electron, and E_g is the band gap for silicon.

Appendix B

B.1 Introduction

State-space averaged model is widely used in system identification to describe the dynamic behaviour of a power converter. The physical system can be expressed as a mathematical model to observe the transient response, and to design a feedback controller to further enhance the performance of the overall system. In other words, a state space model can be converted to an open-loop transfer function which is adopted to represent the plant in practice. The state-space model is employed to obtain the preliminary results before building up to a test rig. In this appendix, a detailed description of the state-space averaged model of a boost converter is presented.

B.2 State-space Average Modelling of DC-DC Boost Converter

Mode 1: Switch Closed

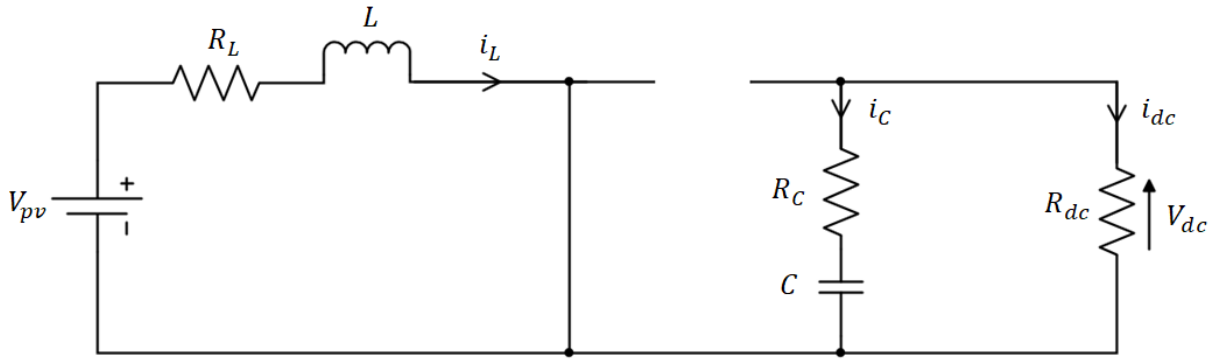

Figure B.1 Boost converter schematic for the switch closed.

$$V_{dc} = V_C \frac{R_{dc}}{R_{dc} + R_C} \tag{B.1}$$

$$I_C = C\frac{dV_C}{dt} = -\frac{V_C}{R_{dc} + R_C}$$

$$\frac{dV_C}{dt} = -\frac{1}{C(R_{dc} + R_C)} V_C \tag{B.2}$$

$$V_{pv} = I_L R_L + V_L = I_L R_L + L\frac{dI_L}{dt} \quad (Kirchhoff's\ Voltage\ Law)$$

$$\frac{dI_L}{dt} = \frac{1}{L}V_{pv} - \frac{R_L}{L}I_L \tag{B.3}$$

By substituting (D.1)-(D.3), the state space model in mode 1 can be defined as

$$A_1 = \begin{bmatrix} -\frac{R_L}{L} & 0 \\ 0 & -\frac{1}{C(R_{dc}+R_C)} \end{bmatrix}$$

$$B_1 = \begin{bmatrix} \frac{1}{L} \\ 0 \end{bmatrix}$$

$$C_1 = \begin{bmatrix} 0 & \frac{R_{dc}}{R_{dc}+R_C} \end{bmatrix} \quad \text{(B.4)}$$

$$D_1 = 0$$

$$x = \begin{bmatrix} I_L \\ V_C \end{bmatrix}$$

$$u = [V_{pv}]$$

Mode 2: Switch Open

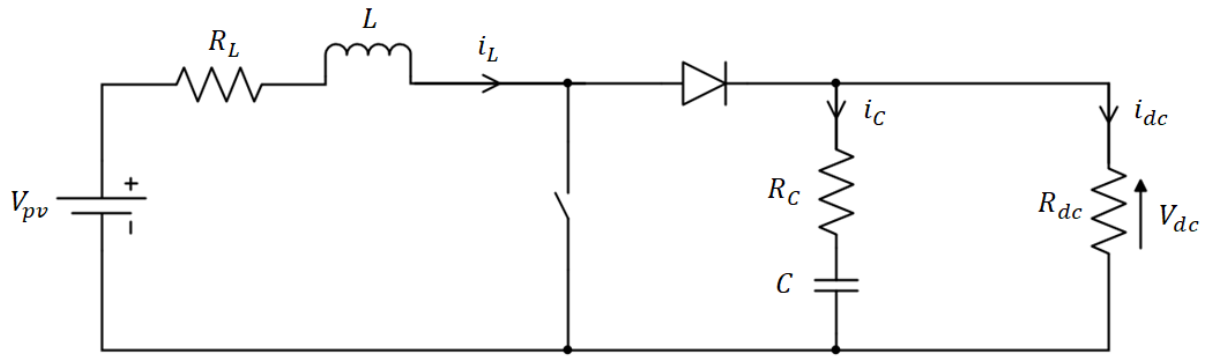

Figure B.2 Circuit diagram of boost converter for the switch open.

$$I_C = I_L - I_{dc} \quad (Kirchoff's\ Current\ Law)$$

$$C\frac{dV_C}{dt} = I_L - \frac{V_{dc}}{R_{dc}} \quad \text{(B.5)}$$

$$V_{dc} = V_C + (I_L - \frac{V_{dc}}{R_{dc}})R_C \quad \text{(B.6)}$$

$$V_{pv} = I_L R_L + V_L + V_{dc} \quad (Kirchhoff's\ Voltage\ Law) \quad \text{(B.7)}$$

(D.6) can be rearranged as follows

$$V_{dc} = \frac{V_C + I_L R_C}{1 + \frac{R_C}{R_{dc}}} \quad \text{(B.8)}$$

Substitute (D.8) into (D.5), the equation can be written as

$$C\frac{dV_C}{dt} = I_L - \frac{\frac{V_C + I_L R_C}{1 + \frac{R_C}{R_{dc}}}}{R_{dc}}$$

$$\therefore \frac{dV_C}{dt} = \frac{R_{dc}}{C(R_{dc} + R_C)} I_L - \frac{1}{C(R_{dc} + R_C)} V_C \tag{B.9}$$

Substitute (D.8) into (D.7), it is rearranged in the following

$$V_{pv} = I_L R_L + L\frac{dI_L}{dt} + \frac{V_C + I_L R_C}{1 + \frac{R_C}{R_{dc}}}$$

$$\frac{dI_L}{dt} = \frac{1}{L} V_{pv} - \frac{R_{dc}}{L(R_{dc} + R_C)} V_C - \frac{(R_L R_{dc} + R_L R_C + R_C R_{dc})}{L(R_{dc} + R_C)} I_L \tag{B.10}$$

By substituting (D.5-D.10), the state space model in mode 2 is expressed as

$$A_2 = \begin{bmatrix} -\frac{(R_L R_{dc} + R_L R_C + R_C R_{dc})}{L(R_{dc} + R_C)} & -\frac{R_{dc}}{L(R_{dc} + R_C)} \\ \frac{R_{dc}}{C(R_{dc} + R_C)} & -\frac{1}{C(R_{dc} + R_C)} \end{bmatrix}$$

$$B_2 = \begin{bmatrix} \frac{1}{L} \\ 0 \end{bmatrix} \tag{B.11}$$

$$C_2 = \begin{bmatrix} \frac{R_{dc} R_C}{R_{dc} + R_C} & \frac{R_{dc}}{R_{dc} + R_C} \end{bmatrix}$$

$$D_2 = 0$$

State-space Averaged Model

A state equation and output equation can be implemented to describe the behaviour of the 2nd order system. Taking all the substructures into consideration, it is crucial to apply state-space averaging method to ensure that both turn-on and turn-off cases have contributed to this mathematical model [88]. This provides a platform to observe the steady-state response of the boost converter, as well as the dynamic performance.

$$\dot{x}_{avg} = A_{avg} x + B_{avg} u = d(A_1 x + B_1 u) + (1 - d)(A_2 x + B_2 u)$$

Therefore, the general form of a state-space averaged model can be defined as

$$\dot{x}_{avg} = [dA_1 + (1-d)A_2]x + [dB_1 + (1-d)B_2]u$$
$$y_{avg} = [dC_1 + (1-d)C_2]x + [dD_1 + (1-d)D_2]u \quad \text{(B.12)}$$

Compared mode 1 with mode 2, the matrix equations are summarised as follows

$$A_1 \neq A_2, B_1 = B_2 = B_{avg}, C_1 \neq C_2, D_1 = D_2 = D_{avg} = 0$$

The state-space averaged model is derived as

$$\dot{x}_{avg} = \begin{bmatrix} \frac{dR_CR_{dc} - (R_CR_{dc} + R_LR_{dc} + R_LR_C)}{L(R_{dc} + R_C)} & -\frac{(1-d)R_{dc}}{L(R_{dc} + R_C)} \\ \frac{(1-d)R_{dc}}{C(R_{dc} + R_C)} & -\frac{1}{C(R_{dc} + R_C)} \end{bmatrix} \begin{bmatrix} I_L \\ V_C \end{bmatrix} + \begin{bmatrix} \frac{1}{L} \\ 0 \end{bmatrix} [V_{pv}]$$
$$y_{avg} = \begin{bmatrix} \frac{(1-d)R_{dc}R_C}{R_{dc} + R_C} & \frac{R_{dc}}{R_{dc} + R_C} \end{bmatrix} \begin{bmatrix} I_L \\ V_C \end{bmatrix} \quad \text{(B.13)}$$

All the matrix equations can be given by

$$A_{avg} = \begin{bmatrix} \frac{dR_CR_{dc} - (R_CR_{dc} + R_LR_{dc} + R_LR_C)}{L(R_{dc} + R_C)} & -\frac{(1-d)R_{dc}}{L(R_{dc} + R_C)} \\ \frac{(1-d)R_{dc}}{C(R_{dc} + R_C)} & -\frac{1}{C(R_{dc} + R_C)} \end{bmatrix}$$
$$B_{avg} = \begin{bmatrix} \frac{1}{L} \\ 0 \end{bmatrix}$$
$$C_{avg} = \begin{bmatrix} \frac{(1-d)R_{dc}R_C}{R_{dc} + R_C} & \frac{R_{dc}}{R_{dc} + R_C} \end{bmatrix} \quad \text{(B.14)}$$
$$D_{avg} = 0$$
$$x = \begin{bmatrix} I_L \\ V_C \end{bmatrix} \qquad u = [V_{pv}]$$

B.3 Continuous Transfer Function of Boost Converter with ESR

As previously mentioned, the state-space averaged model can be converted to a continuous transfer function for the purpose of simulation. The general form of the equation is defined as

$$G(s) = \frac{\begin{vmatrix} sI - A & B \\ C & D \end{vmatrix}}{|sI - A|}$$

$$sI - A = \begin{bmatrix} s - \dfrac{dR_C R_{dc} - (R_C R_{dc} + R_L R_{dc} + R_L R_C)}{L(R_{dc} + R_C)} & \dfrac{(1-d)R_{dc}}{L(R_{dc} + R_C)} \\ -\dfrac{(1-d)R_{dc}}{C(R_{dc} + R_C)} & s + \dfrac{1}{C(R_{dc} + R_C)} \end{bmatrix}$$

$$|sI - A| = s^2 + \frac{L - dCR_C R_{dc} + C(R_C R_{dc} + R_L R_{dc} + R_L R_C)}{LC(R_{dc} + R_C)} s + \frac{(1-d)^2 R_{dc}^2 - dR_C R_{dc} + (R_C R_{dc} + R_L R_{dc} + R_L R_C)}{LC(R_{dc} + R_C)^2}$$

$$G(s) = \frac{V_{out}(s)}{d(s)} = \frac{-\frac{1}{L}\left[\frac{(1-d)R_C R_{dc} - (1-d)R_{dc}^2}{C(R_{dc} + R_C)^2} - \frac{(1-d)R_C R_{dc}}{(R_{dc} + R_C)} s\right]}{|sI - A|}$$

$$\therefore Numerator\ of\ G(s) = C(R_{dc} + R_C)(1-d)R_{dc}R_C s - (1-d)R_{dc}R_C + (1-d)R_{dc}^2$$

$$Denominator\ of\ G(s) = LC(R_{dc} + R_C)^2 s^2 + (R_{dc} + R_C)[L - dCR_{dc}R_C + C(R_{dc}R_C + R_{dc}R_L + R_L R_C)]s + (1-d)^2 R_{dc}^2 - dR_{dc}R_C + (R_{dc}R_C + R_{dc}R_L + R_L R_C) \quad \text{(B.14)}$$

The above mathematical expression is the continuous transfer function of a boost converter with ESR. This formula can be implemented in MATLAB/Simulink for the simulation of dynamic behaviour of a boost converter. There is a transfer function block in Simulink for engineers to specify an open-loop transfer function of a physical system. This can be used to develop a closed-loop control system with the help of a PI controller. As a result, the overall control feedback system of a boost converter with a proper controller can be simulated in MATLAB/Simulink. The parameters of the PI controller can be tuned prior to experimental study, which can be a reference value for the manual tuning in practice. A linear small-signal model of a boost converter without ESR can be reviewed in [89] for dc MG systems.

Appendix C

C.1 Introduction

In this appendix, the experimental study is presented to validate the proposed V-dp/di droop control of a PV-based dc MG. It begins with the description of the experimental setup. This includes the design of the small-scale test rig, introduction to the H-bridge dc/dc converter, technical specifications of the system, a description of the general control board and gate drive circuit, as well as the application of the dc electronic load. Furthermore, the dc-link and protection wiring diagrams are demonstrated to show the mechanism of the protection scheme in this project. Basic experimental results are presented to investigate the influence of the dc bus voltage deviation of the PV-based dc MG, and to observe the dynamic response under step load change.

C.2 Experimental Setup

A low-powered test rig is developed to verify the decentralized control algorithm. The schematic diagram of the power system is shown in Figure C.1. The experimental system is capable of delivering 1.34 kW, i.e. rated power of PV2, to the resistive load with a nominal dc bus voltage of 48 V. Basically, it consists of a general control board, H-bridge dc/dc converter, gate drive board, protection devices, LC-filter, auxiliary power supply unit, voltage and current sensors, recovery rectifier diode, and a resistor for pre-charging input capacitor.

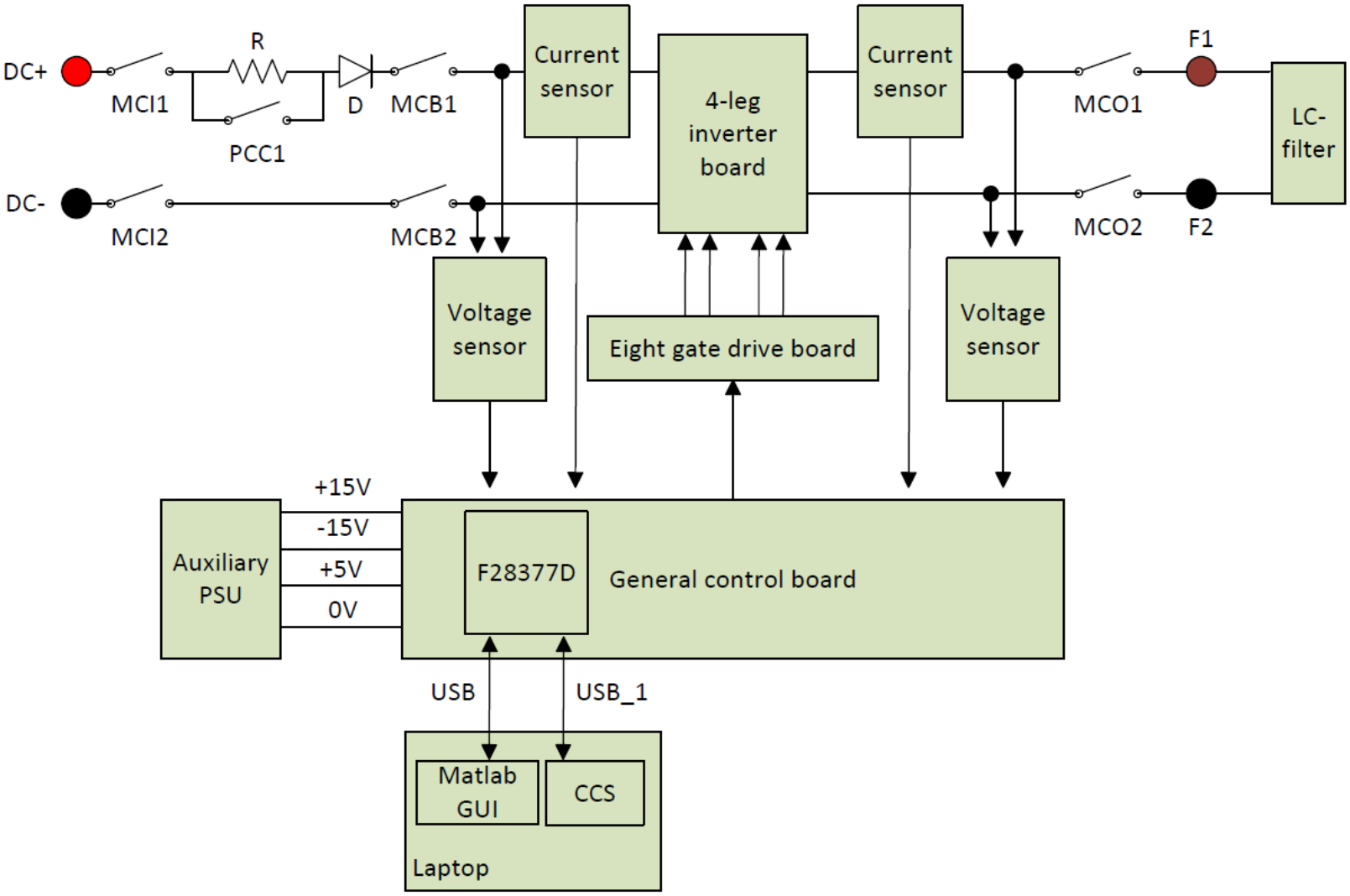

Figure C.1 Block diagram of the test rig.

The schematic diagram of the test rig can be observed in Figure C.1. The circuit is powered by the Thurlby Thandar EX354RD dc power supply with a maximum dc voltage of 35 V and a maximum current of 4 A. Two sets of the Schneider Electric (LC1D125P7 and LC1D096P7) normally open main contactors are used for switching the input and output circuits on or off, respectively. There is a resistor of 22 Ω for pre-charging the dc capacitor of 500 μF with a maximum voltage of 800 V. The timer for pre-charging the input electrolytic capacitor is set to 2 s. The pre-charge contactor (LC1D128P7) is closed once the input dc capacitor is fully charged up. The Vishay (VS-20ETF06-M3) fast recovery rectifier diode is used to prevent reverse power flow to a PV array. The Schneider Electric (A9F53210) 10 A miniature circuit breaker (MCB) provides a full protection against overloads and short-circuits.

The 4-leg inverter board developed by Dr Dave Atkinson at Newcastle University is implemented in the test rig to behave as an H-bridge dc/dc converter. It is used to step the dc source voltage down, in order to attain the nominal dc bus voltage. The converter board comprises 4 transistor switches in 2 legs, which turns out the other two legs are redundant. The input side of the H-bridge converter is composed of two electrolytic capacitors of 1000 μF/400 V connected in series and a 150 nF ceramic capacitor to eliminate low-frequency and high-frequency oscillations, respectively. Infineon (IPW60R099C6FKSA1) MOSFETs are deployed in the converter board as power transistors for switching. These power MOSFETs are driven by the eight gate drive board. Avago Technologies (ACPL-332J) gate drivers are used to produce 15V switching signals to drive the power MOSFETs. The Chroma (63210) dc electronic load is used to simulate step load change during transients. A LC-filter is fitted between H-bridge dc/dc converter and electronic load, where it is placed in a separated plastic enclosure. It is employed to act as a low-pass filter to filter out high frequency noise, resulting in pure dc signal at the output. The values of the inductor and capacitor can be determined by the buck equations, since this H-bridge converter is theoretically the same as a classical dc-dc chopper.

The general control board (GCB) designed by Dr Dave Atkinson is an evaluation tool for the Texas Instruments TMS320F28377D dual-core Delfino™ microcontroller. The DSP is a 32-bit floating point microcontroller, operating at 200 MHz for advanced control applications. There are two independent 32-bit central processing units (CPUs), mainly focusing on the communication and diagnostics. Moreover, the microcontroller unit features two programmable control law accelerators (CLA) which are the same 200 MHz, 32-bit processor

as the main CPU. The CLA is capable of performing complex mathematical tasks such as trigonometric operations and closed-loop control operations, which is associated with each main CPU in parallel. The GCB has four 12-bit analogue-to-digital converters (ADC) with up to 24-channels, including a sample-and-hold unit for each ADC. The code is written in C/C++ language running in Texas Instruments Code Composer Studio™ (CCS) integrated development environment version 6.4.12. Texas Instruments XDS100 v2 emulator is a USB probe to download and run the code from CCS. The serial communication interface B (SCI-B) is implemented for communication with a host PC and a MATLAB graphical user interface (GUI). The GUI acts as a control panel for users to observe the parameters in real-time and to control the PWM signals of the converter. The photograph of the components inside the enclosure is presented in Figure C.2. The parameters for the preliminary experiments are provided in Table C.1.

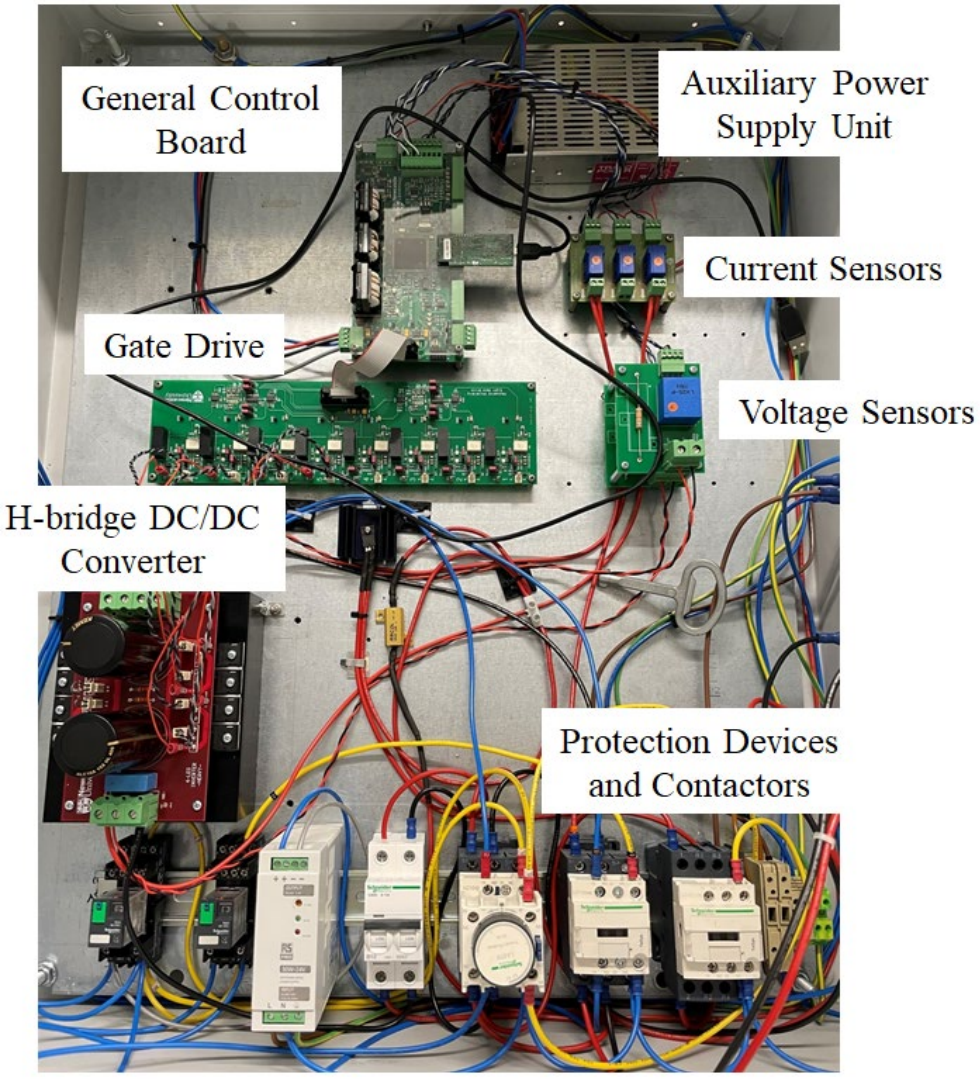

Figure C.2 Photograph of the experimental rig.

$$Inductor\ L = \frac{1}{f_{sw}} \times \frac{(V_{pv} - V_{dc}) \times V_{dc}}{\Delta I_L \times V_{pv}} = \frac{1}{20000} \times \frac{48 \times (114.6 - 48)}{27.934 \times 10\% \times 114.6} = 0.5\ mH$$

$$Filter\ capacitor\ C_{out} = \frac{27.934 \times 10\%}{8 \times 20000 \times 48 \times 0.5\%} = 72.7\ \mu F \approx 80\ uF$$

Table C.1 System parameters of the test rig

Parameter	Value
DC bus voltage V_{DC}	48 V
Nominal power	1.34 kW
DC capacitor C_{in}	500 µF
Inductor L	0.5 mH
Filter capacitor C_{out}	80 µF
Proportional term K_p	0.0004
Integral term K_i	0.0002
Switching frequency f_{sw}	20 kHz
Sampling frequency f_s	20 kHz

C.3 Design of Protection Scheme

Basically, the protection wiring system is composed of two independent circuits, namely high voltage switchgear and low voltage switchgear. As shown in Figure C.3, a single-phase 230 V AC supply is used to energize the auxiliary power supply unit, RS PRO (136-8308) 24 V power supply, pneumatic timer, and high voltage contactors. The Traco Power AC/DC power supply is employed to mainly power up the GCB and eight gate drive board. The AC/DC power supply provides 4 voltage levels in total, including +/-15 V, 5 V and 0 V. The Schneider Electric (LC1D125P7) contactor is the main input contactor for isolating the power circuit, unless the input switch button is pressed in the 24 V circuit. If so, this first energizes the Schneider Electric (RXZE2M114M) input pilot socket and thus the main contactor. There is a pre-charge process for the input dc capacitor on the H-bridge converter, resulting in an ON delay of the main input contactor. The Schneider Electric (LADT0) timer relay and (LC1D128P7) contactor are used to delay the on-time of the main input contactor for 2 s. This short interval should be enough for charging up the dc capacitor. Similarly, the output switch button is pressed to energize the output pilot socket and thus the Schneider Electric

(LC1D096P7) main output contactor. This configuration can be used to disconnect the link between H-bridge converter and electronic load at the beginning. To conclude, the main input and output contactors provide double protection against electric shock.

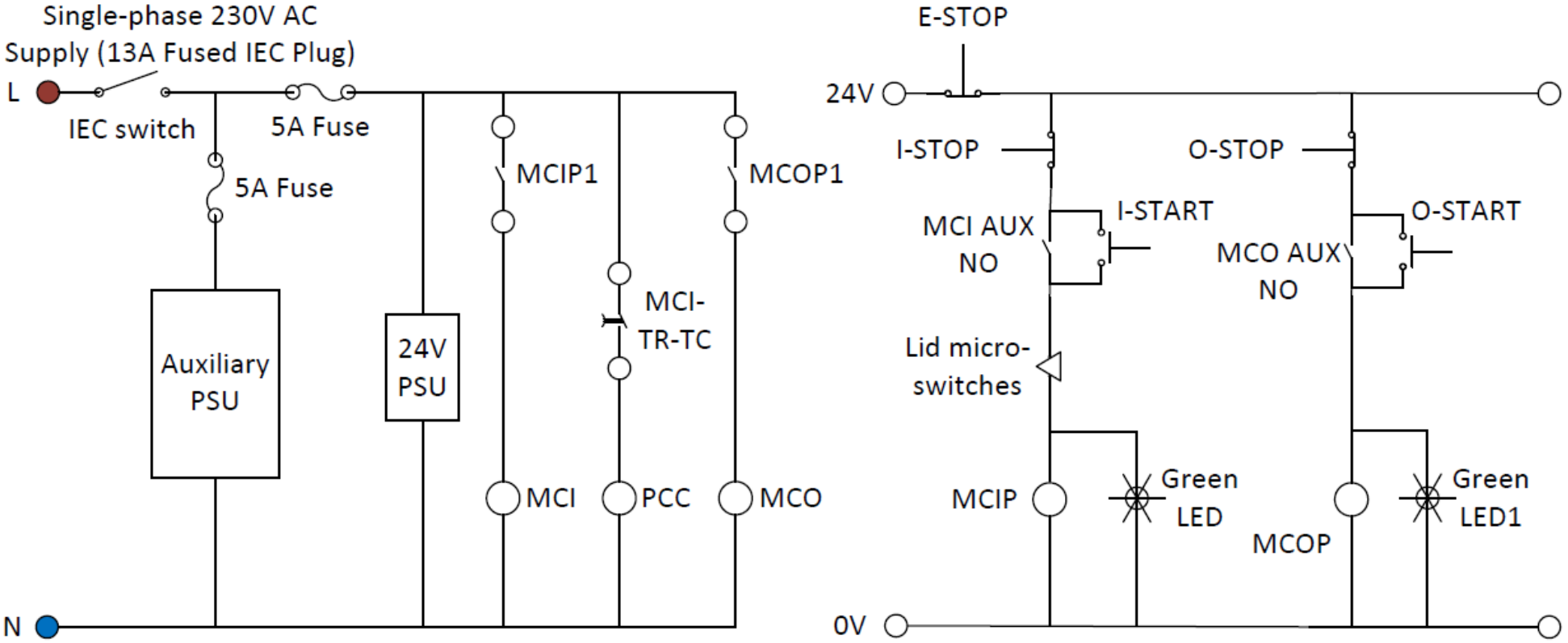

Figure C.3 Protection wiring diagram of the test rig.

On the other hand, the 24 V power supply is deployed to power up the low voltage contactors, green pilot lights, contactor auxiliary switches, lid micro-switches, emergency stop button, and input and output stop buttons. In the first place, Allen-Bradley (800FP-MT44) emergency stop button is utilised to allow users to stop the entire power circuit immediately in case of electrical failure. Basically, the input and output stop operators are used to control the input and output connections of the H-bridge converter, respectively. The input and output start buttons are normally-open, which can be pressed to energize the input and output pilots in the low voltage circuit, respectively. There are two lid micro-switches for preventing the lid open accidentally during the experiments. The input and output contactor pilots can thus be energized. This controls the input and output auxiliary switches in the next cycle to be closed, which energizes the green pilot lights to indicate that the test rig is working as expected.

C.4 Operating Instructions for Test Rig

1. Connect 240 Vac supply to the mains on the side panel.
2. Connect the DC input leads to the power supply unit.
3. Connect the DC output leads to the LC filter box.
4. Connect the micro-switches leads to the LC filter box with lid closed.
5. Run the program ‘microgrid_cpu1.c’ on CCS TI v6.4.12. Press the ‘resume’ button on CCS to start the program when it is ready.
6. Run the graphical user interface ‘gui10’ on MATLAB. PWM should first be switched off.
7. Press the green start button under the label ‘Input DC’ on the front panel. Wait 2 seconds for the DC input capacitor to be charged up. Once the click sound is heard, i.e. pre-charge process finished, the DC input power source will automatically be connected to the H-bridge DC/DC converter.
8. Press the green start button under label ‘Load’ on the front panel. This activates the connection between H-bridge converter and load.
9. Press the ‘PWM ON’ button on the MATLAB GUI panel to turn on PWM signals.
10. Before disconnecting the PSU and load, please ensure ‘PWM OFF’ button is pressed on MATLAB GUI panel.
11. Press red stop button under the ‘Load’ label on the front panel.
12. Press red stop button under the ‘Input DC’ label on the front panel.

Should any of the supplies fail, the lid be opened, either of the emergency stops be pressed, then power will be disconnected from the PSU immediately.

C.5 Experimental Results

The dynamic and steady-state characteristics of the dc bus voltage are assessed in the experimental section to validate the fundamental mechanism of the proposed V-dp/di droop control method. This includes voltage ripple, voltage overshoots, and settling time. First, the gate drive signals of two high-side MOSFETs are demonstrated to verify the feasibility of a full-bridge dc/dc converter. Unipolar switching is utilised to achieve higher conversion efficiency and reduce harmonic distortion. Indeed, it allows the zero voltage level of the output to be used and the switching frequency of the output voltage can thus be doubled. Zero value is usually maintained for a short period of time, at which both high-side power devices are switched on. Afterwards, the closed voltage and current loops of the H-bridge converter with the dc electronic load are presented in this section. Given the input voltage of the power supply is always fixed, the experimental results show how the classical PI controller can regulate the output voltage or current of the variable electronic load. Last but not least, the dynamic and static behaviours of the dc bus voltage are investigated. This can be accomplished by introducing a step change in reference voltage. The experiment clearly demonstrates the feasibility of a voltage droop control, which is the main feature of a decentralized control in an islanded dc MG.

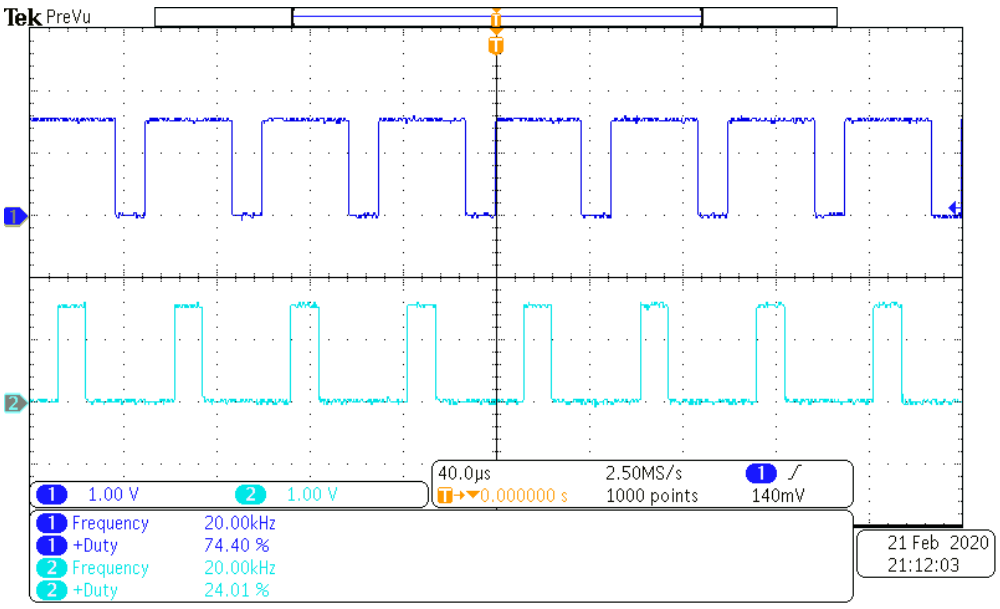

Figure C.4 Gate drive signals of two high-side MOSFETs in an H-bridge converter.

To verify the design of a full-bridge dc/dc converter, a preliminary test was undertaken to observe the gate drive signals of the power switches. The sampling and switching frequencies are set to 20 kHz. The execution timer of the microcontroller shows that it takes 10 µs to

process one complete cycle of the control loop and display the sensor data on MATLAB GUI. This is about 20 per cent of a PWM period which is found to be appropriate for this application. The duty ratio for the high-side gate drive signal of leg A is set to 75%. As shown in Figure C.4, the resulting duty cycle of high-side MOSFET in leg A is obtained as 74.4%. This is due to the fact that both power MOSFETs in the same leg cannot be turned on simultaneously. Therefore, the high-side power device must entirely be switched off before turning on the low-side MOSFET. This is referred to as deadband. The dead time is set to 500 ns which is 1% of the switching period, according to the datasheet of the power MOSFET. The duty ratio for the low-side gate drive signal is measured as 24%. The variation can be due to the deadband and measurement errors. The voltage attenuation ratio of the Tektronix probe is 2x, in which the peak voltage of the gate-source signal is 15 V. This ensures the power MOSFETs to be fully turned on, which exceeds the threshold gate-source voltage.

C.5.1 Closed Voltage and Current Loops

A closed-loop control system is implemented in the DSP to observe the transient and steady-state response. The dc electronic load is used as a variable resistor to perform single voltage/current loop control. The current reference value is set to 0.5 or 1 A, in order to develop a step change in current. The resistance is initialised as 24 Ω, and dropped to 19 Ω at 1 A after 1 s. The step change is repeated every 2 s. The closed-loop current control is maintaining the feedback current at certain levels during step changes. As can be seen from Figure C.5, the dc-link voltage can be obtained. There is no voltage overshoot/undershoot in the graph, given the passive elements contain ESRs. A traditional PI controller is used to minimise the steady-state error and suppress the voltage overshoot. The averaged voltage ripple is measured as ±1.64%. The settling time of the step response is approximately 33 ms which shows an excellent dynamic performance.

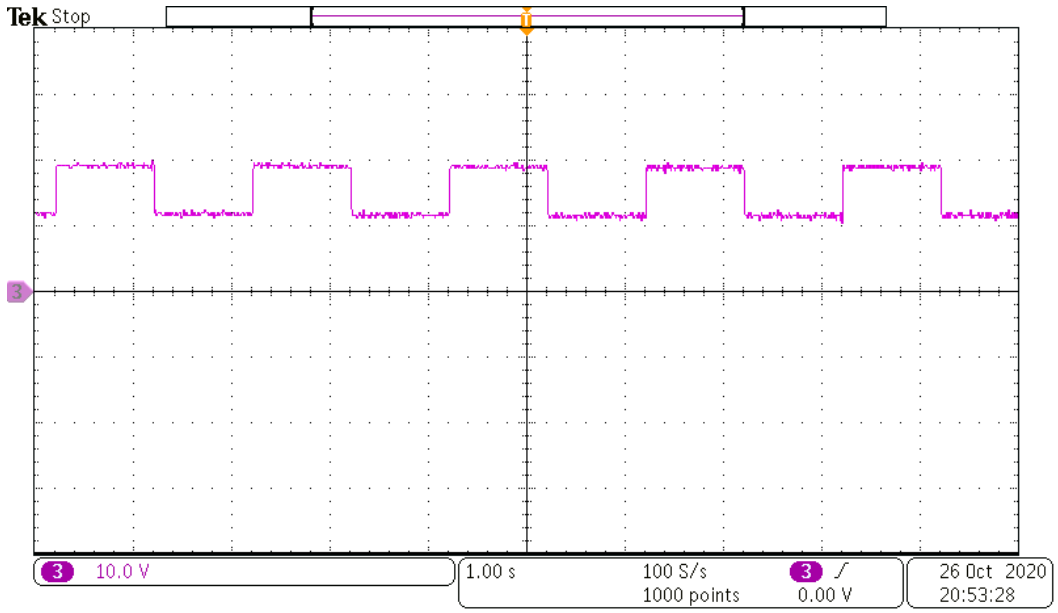

Figure C.5 Output load voltage under step change in reference current.

The closed-loop voltage control is implemented in the DSP to assess the dynamic response performance of a dc MG system. The resistance of the electronic load is set to 20 Ω. The voltage reference value is initialised as 25 V, followed by 15 V. This process is repeated again. The time interval of the step change is set to 1 s, in order to record the transient and steady-state response of the dc bus voltage. Nevertheless, a classical PI compensator is used to regulate the dc bus voltage and generate a duty ratio to control the power devices of an H-bridge dc/dc converter. Similar to closed-loop current control, there is no significant voltage overshoot/undershoot obtained in the step response. It is noted some voltages drop across the inductor and capacitor in practice, resulting in a critically damped response with no overshoot. The averaged settling time of the dc bus voltage is about 40 ms, which takes longer time than the current control to reach the steady state. This is due to the fact that the current of the inductor is controlled. The output voltage is measured at the dc-link capacitor which usually takes time to charge or discharge. The overall voltage ripple is measured as ±1.77%. The voltage fluctuations are within the acceptable operating range and considered to be stable.

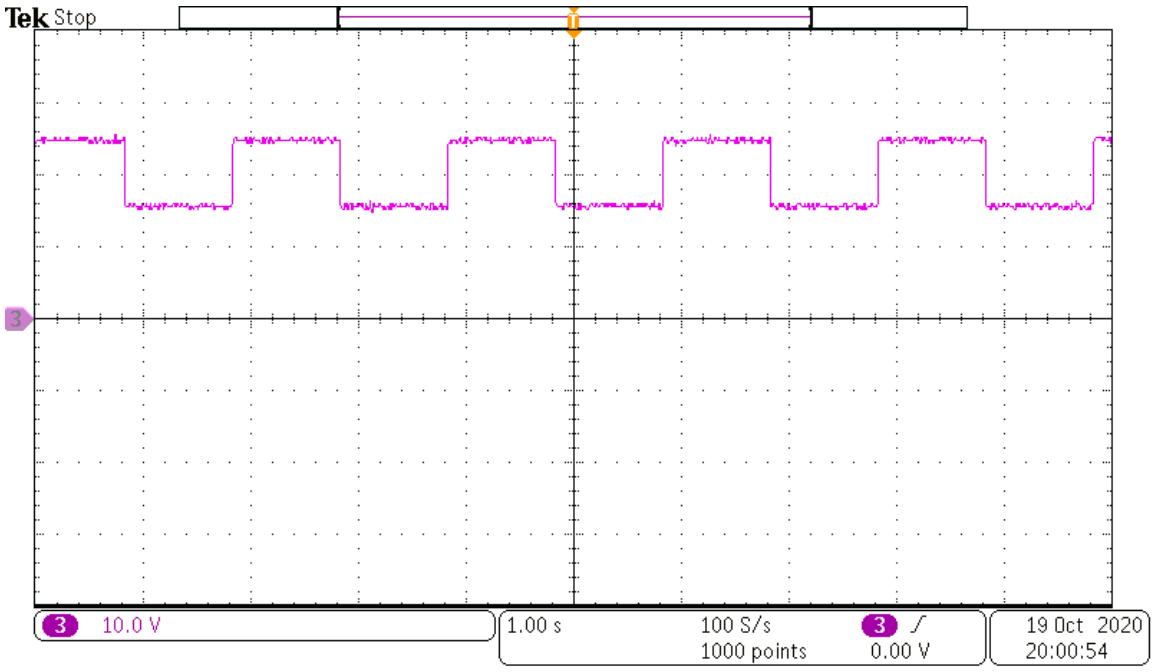

Figure C.6 Dynamic response of the dc bus voltage under step change in reference value.

C.5.2 Voltage Droop Control

The dynamic and steady-state performance of the dc bus voltage can be validated experimentally in a standalone mode, where the dc input source is responsible for voltage regulation. The deviation of the dc bus voltage is utilised as an indicator to produce a new voltage reference value, and to reduce the power generation. The dc bus voltage reference is initialised as 10 V. The deviation of the dc bus voltage is assumed to be 5 V. In other words, the calculated voltage set-point is changed to 15 V. This can replicate the conditions of a dc MG system in standalone operation, in which the droop control determines a dc bus voltage reference to stabilise the overall dc MG. As shown in Figure C.7, the dynamic response of the dc bus voltage under step change in voltage reference is presented. The averaged settling time is 40 ms, which is considered to be a robust control system. No voltage overshoot/undershoot is observed in the graph. The averaged voltage ripple is ±1.5%. This has validated the concept of dc bus signalling, in which the dc bus voltage can be used as an indicator to generate or reduce input power, in order to maintain the stability of a dc MG. Moreover, the screenshot of the MATLAB GUI used in the experiments is shown. The control panel clearly presents the data in real-time with the help of universal asynchronous receiver-transmitter connection. The control loop takes less than 10 µs to calculate the duty ratio for PWM generation, which is one fifth of a PWM period. To conclude, the microprocessor has the capability to further

increase the switching frequency and/or implement advanced control system to achieve multiple objectives such as proportional power sharing and dc bus voltage regulation.

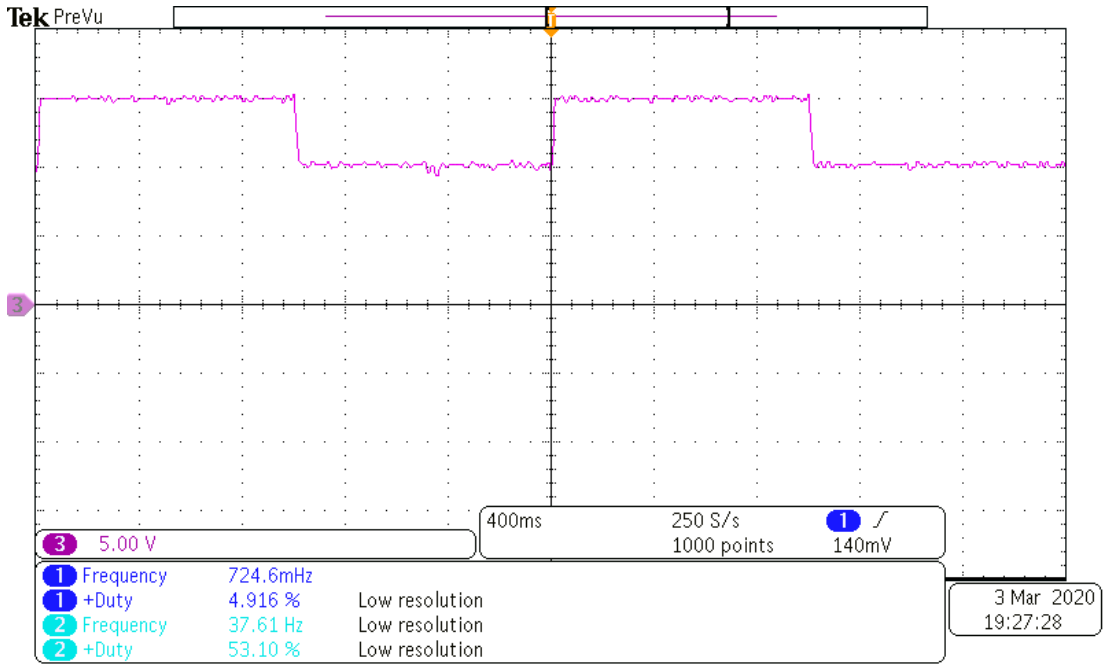

Figure C.7 Transient response of dc bus voltage under step change in voltage reference.

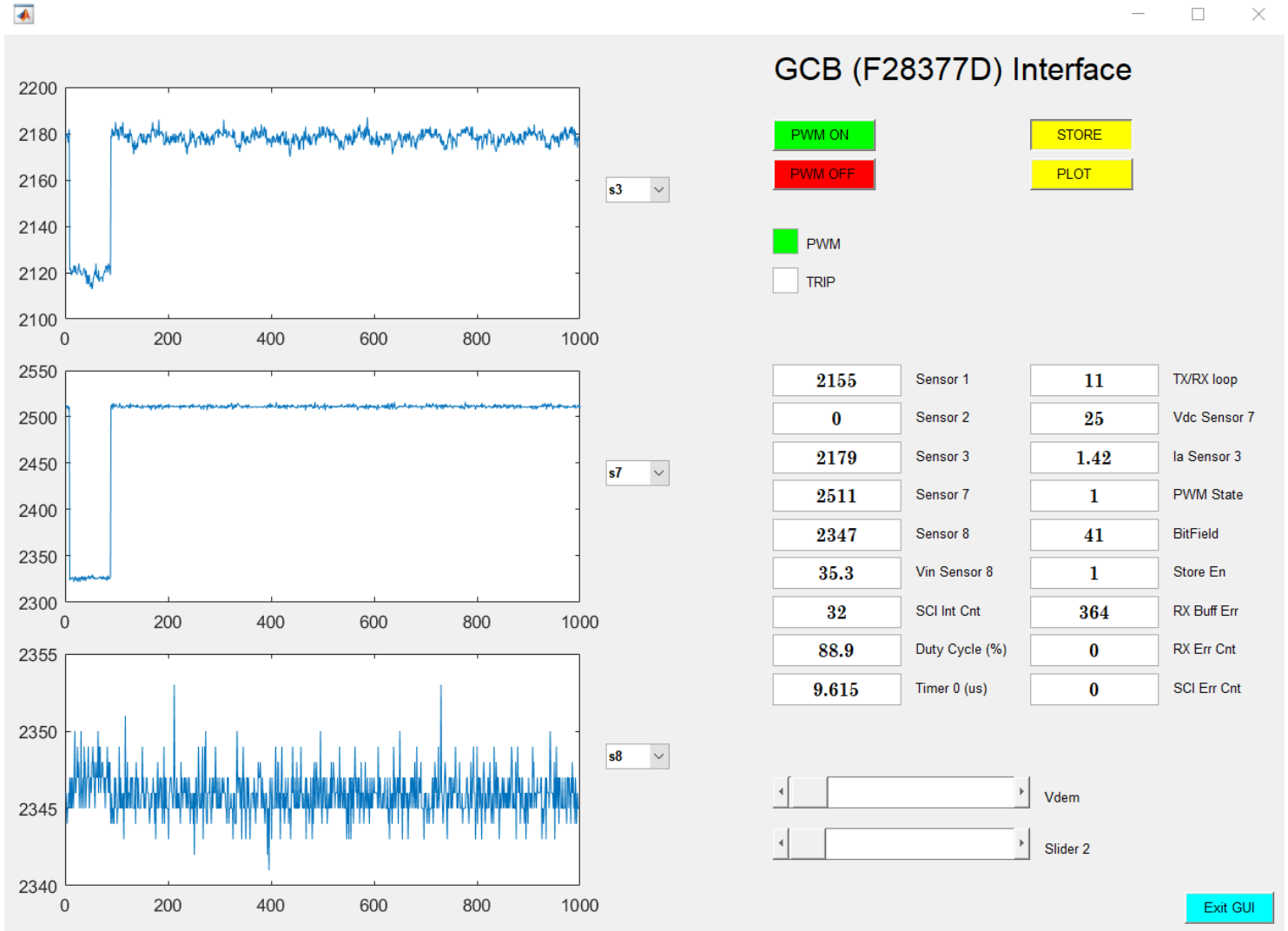

Figure C.8 Screenshot of the GUI control panel developed in MATLAB.